SIDELOBE CANCELLING AND ADAPTIVE ARRAY PROCESSING

DR. ELI BROOKNER
Raytheon Company
M/S 3-1-162
528 Boston Post Road
Sudbury, MA 01776
Telephone: 978-440-4007
Fax: 978-440-4040
E-mail: Eli_Brookner@ raytheon.com

PRACTICAL PHASED ARRAY ANTENNA SYSTEMS and
ADAPTIVE ARRAYS for RADAR and COMMUNICATION SYSTEMS
WINTER/SPRING 2004 LECTURE SERIES

BOSTON IEEE AESS

Sidelobe Cancelling and Adaptive Array Processing

Dr. Eli Brookner*

Vugraphs 1 and 2 give the outline for this lecture.

1.0 Sidelobe Canceller

1.1 Single Loop Sidelobe Canceller

1.1.1 Basics of Sidelobe Cancelling

Vugraph 3 illustrates the jamming problem. If we could some how generate an exact replica of the jamming signal, E_J, coming in through the main beam sidelobes and subtract it from the mainbeam as illustrated in Vugraph 4, then we could get rid of the jammer. This is the basis for jammer cancellation. The question is: How do we obtain a copy of the jammer signal E_J. This is done with the use of an auxiliary antenna as shown in Vugraph 5. The jammer signal received by the auxiliary antenna has a value which is 1/W times the value of the jammer seen in the main channel. This is due to the difference in the gain of the auxiliary antenna at the angle where the jammer is located versus the gain that the jammer sees coming through the main antenna sidelobes at this same angle; see Vugraph 5. Generally we do not know the gain of the main antenna at the angle where the jammer is coming through. However, if we some how had a clairvoyant in the auxiliary channel, as shown in Vugraph 6, who knew what W was, he could make the proper adjustment. Not having a clairvoyant we shall show how W is estimated in real time from the signals in the main and auxiliary channels.

1.1.2 Open-Loop Sidelobe Canceller

Vugraph 7 shows an open-loop circuit obtaining the estimate $\hat{W}$ of W. The optimality of $\hat{W}$ is demonstrated in Vugraph 8. When $JNR_a >> 1$ in the auxiliary channel then $\hat{W} \doteq W$. The larger JNR_a, the better this approximation. This is as it should be. The larger the jammer, the more accurate the estimate $\hat{W}$ and hence the better the jammer cancellation. When the jammer is not present, $\hat{W}$ on the average is zero; see numerator of $\hat{W}$ in Vugraph 8.

Vugraph 9 gives a simulation carried out for Vugraph 7 when $N=N_{AVG}=4$. Initially the jammer plus noise is at the 120 dB level before the cancellation part of the circuit in Vugraph 7 is hooked in. When the weighted auxiliary jammer signal estimate is subtracted from the mainlobe channel as done in Vugraph 7, the total interference becomes 50 dB, the value of the receiver noise level. Thus the open-loop circuit has effectively cancelled out the jammer within a few pulses.

If $\hat{W} = W$, then the jammer signal in the main channel is cancelled out. However, there is still a degradation in the signal-to-noise ratio in the main channel over and above that obtained if there was no jammer present. This is due to what is called the carry over noise from the auxiliary channel. The auxiliary channel in addition to having the jammer signal J_A, has its own receiver noise N_A. This

* Raytheon Comp., Wayland, MA 01778, U.S.A;

noise is also weighted by $\hat{W}$ and subtracted from the main channel. Because it is independent of the noise in the main channel, it adds to it as illustrated in Vugraph 10 which gives the magnitude of the increase of the noise and signal-to-interference ratio in the main channel.

1.1.3 Effects of Errors

So far we have assumed no errors in the amplitude or phase in the estimate of $\hat{W}$. Such errors can occur due to differences in the gain of the auxiliary and main channel receivers after the point at which the correlation signals are obtained in Vugraph 7. Vugraph 11 shows the cancellation achievable when either only an amplitude or only a phase error is present in one channel relative to the other. Vugraph 12 gives the cancellation limit due to the simultaneous presence of amplitude and phase errors.

Usually the jammer signal arrives at different times at the main antenna and auxiliary antenna, as shown in Vugraph 13. If the jammer bandwidth is zero, that is, the jammer consists of a CW signal, then the fact that the jammer signals arrive at different times at the main and auxiliary antennas does not matter. However, if it has a non-zero bandwidth, the weight W can only be set up for one frequency of the jammer, the optimum weight W being dependent on the carrier frequency because the relative phases of the jammer signal in the main channel and auxiliary channel depend on frequency. Vugraph 14 illustrates how the main channel residual interference to receiver noise level varies as the carrier frequency changes when the weight is set to perfectly cancel out the signal for a carrier frequency of 300 MHz. Also given in this figure is a normalized scale which applies for the case where the weight W is set to perfectly cancel out a signal at a carrier frequency f_o.

For the non-zero bandwidth case there is an optimum weight W_{OPT}, different from W for the zero bandwidth jammer. W_{OPT} is given in Vugraph 15 (for the assumption that W = 1 for the zero bandwidth jammer). Also given in this vugraph is the main channel jammer cancellation achieved as a function of the jammer bandwidth, B, times the difference of time of arrival, τ, between the main and auxiliary channel for the jammer signal. The figure indicates that for $B\tau = 0.001$ the jammer cancellation is 55 dB. However, if $B\tau = 0.1$ the maximum cancellation achievable is about 15 dB, a decrease of 40 dB in the cancellation achieved. What do you do if you cannot live with just 15 dB of cancellation. One thing you could do is narrow the signal bandwidth. This requires a narrowing of the signal bandwidth by a factor of 100. If this is not a feasible option, then one of the three options listed in Vugraph 16 could be used.

The first option consists of breaking the signal up into M narrower bands by passing the signal through a bank of M filters each having a bandwidth of B/M. This is done for both the main and auxiliary channels. Vugraph 17 illustrates this for the case where a M = 8. From Vugraph 15 it follows that the cancellation ratio achievable is proportional to $1/(B\tau)^2$. One can apply a sidelobe canceller to the ith narrow band filter output of the main channel by using the ith narrow band filter output of the auxiliary channel, this filter being centered at the same frequency. Similarly one can apply an open-loop canceller to the seven other narrow band main channel outputs. Because the bandwidths of these signals is 1/8th of the original signal, the maximum jammer cancellation achievable

increases by 8^2 = 18 dB. Thus instead of achieving a cancellation ratio of only 15 dB the cancellation ratio achievable now becomes 33 dB.

The bank of filters can be synthesized digitally by using a Fast Fourier Transform (FFT) algorithm as indicated in Vugraph 18. The use of frequency channelization into narrow bands, as illustrated in Vugraphs 17 and 18, not only eliminates the degradation in the cancellation achievable due to the difference of time arrivals of the jammer signal at the main and auxiliary channels, it also compensates for the nontracking of the amplitude and phase characteristics with frequency of the main and auxiliary channel amplifiers as illustrated in Vugraph 17.

The second way for compensating for the difference in the time of arrival between the main and auxiliary channels of the jammer signal is to use an equalizer circuit in either the main or auxiliary channel. Vugraph 19 illustrates how an equalizer placed in the auxiliary channel can compensate for the nontracking of the amplitude and phase errors of the auxiliary channel relative to the main channel. Vugraph 20 shows an example equalizer circuit placed in the auxiliary channel. Such a circuit in addition to compensating for the difference in the time of arrival between the two channels, also compensates for amplitude and phase nontracking between the two channels as illustrated in Vugraph 19.

The final method listed in Vugraph 16 for compensating for the diffference in arrival times between the main and auxiliary channels is the use of multiple loop cancellers. Vugraph 21 illustrates a multiple loop canceller. It consists of M auxiliary antennas instead of just one auxiliary antenna. The determination of the weights for a multiple loop canceller will be discussed later.

A physical motivation of why a multiple loop canceller improves the jammer cancellation achievable when a non-zero bandwidth jammer is present is now given. The solid curve of Vugraph 22 gives the antenna pattern when the signal jammer carrier frequency is $f = f_1$. At this carrier frequency the antenna is seen to have a null at the off-boresite angle $\theta = \theta_1$. Now let the jammer frequency be f_2, then the antenna null moves from θ_1 to θ_2; see Vugraph 22. There is no longer a null at the angle θ_1 for the carrier frequency f_2. Thus if a non-zero bandwidth jammer at the angle θ_1 having carrier frequencies f_1 and f_2 is to be nulled out, it is necessary to have two sidelobe cancellers with two auxiliary antenna which would produce a null at θ_1 at the carrier frequencies f_1 and f_2. Vugraph 22 gives an estimate of the number of sidelobe cancellers needed as a function of the signal bandwidth $B = \Delta f$, the antenna 3 dB beamwidth θ_3 and the off-boresite angle θ_1.

1.1.4 Feedback Sidelobe Canceller (SLC)

Now we will cover the estimation of the weight W through the use of the linear single-loop feedback sidelobe canceller circuit shown in Vugraph 23. This circuit was invented by Paul Howells; see Vugraph 24. This seminal patent represents the starting point for sidelobe cancelling. The paper is still worth reading. The feedback sidelobe canceller circuit has been the one most commonly used up till now. The feedback sidelobe canceller circuit has the advantage over the open-loop circuit of not being degraded by an amplitude and/or phase error between the auxiliary and main channel

(for the case of a narrow-band jammer). It has the disadvantage, however, of a poorer settling time, that is, the time between when the jammer is turned on and when it is finally cancelled by the sidelobe canceller. It is important to keep this settling time small when coping with a blinking jammer.

1.1.4.1 Cancellation Ratio (CR)

Vugraph 25 gives an approximate derivation of the jammer cancellation achieved with the feedback sidelobe cancelling circuit. Specifically, it gives the ratio, CR, defined as the ratio of the mainlobe interference before cancellation to the residual interference after cancellation. Vugraph 25 indicates that this ratio is proportional to the feedback loop gain G_L^2 when $G_L >> 1$. As a result if G_L = 30 dB, then the cancellation ratio CR = 30 dB, G_L being a voltage gain. An exact derivation will be given shortly.

The weight W is shown as being generated at the input to the mixer. Actually it should include the conversion factor, k, of the mixer. For the open-loop canceller of Vugraphs 6 through 8, the factor k was included in the weight W, or equivalently, it was implicitly assumed that k = 1. For the feedbback circuit of Vugraph 25 the factor k is kept separate so that the auxiliary signal here has to be multiplied by kW.

1.1.4.2 Transient Response

Vugraph 26 derives the transient response for the feedback linear single-loop SLC (SSLC). It shows that the closed loop time constant τ_L is approximately equal to the open loop time constant τ_o = RC divided by the loop gain G_L when $G_L >> 1$; see Vugraph 26. Thus the higher the loop gain, the smaller the loop time constant and the better the jammer cancellation ratio (CR); see Vugraph 25, Equation 4. It is interesting to note that the feedback linear SSLC (L/SSLC) is equivalent to the ordinary Type O follower servo shown in Vugraph 26a [17].

1.1.4.3 Exact Derivation of Cancellation Ratio (CR)

Vugraph 27 gives an exact derivation of a more complete expression for the cancellation ratio (CR). This expression, Equation 5 of Vugraph 27, includes the degradation in the CR due to decorrelation of the signals in the main and auxiliary channels. This decorrelation could result from the independent thermal receiver noise in the main and auxiliary channels. It also can result from the different times of arrivals of the jammer signals in the main and auxiliary antennas when the jammer has a non-zero bandwidth.

Vugraph 28 gives the CR for special cases. The first expression, Equation 1, gives the CR for when the correlation coefficient ρ between the signals in the main and auxiliary channel is one. It is seen that this exact expression is identical to the expression derived in Vugraph 25 using an approximate derivation. Equation 2 of Vugraph 28 gives the CR for when the loop gain is infinite. Equation 3 gives the CR for when the decorrelation is due to the independent thermal noise in the main and auxiliary channels.

Vugraph 28a gives the CR limits due to the differences in times of arrival of the jammer signal at the main and auxiliary

channels for the case of a non-zero bandwidth jammer. The plot also applies as well for when the decorrelation is simply due to the thermal noise because Vugraph 28a gives a plot of Equation 2 of Vugraph 28 which applies in general as long as the loop gain is very large. Vugraphs 29 through 31 derive the relationship for the correlation coefficient for when it is limited by the main and auxiliary channel thermal noise. From Equation 1 of Vugraph 31 and Equation 2 of Vugraph 28, Equation 3 of Vugraph 28 follows:

Vugraph 32 proves the optimality of the steady state weight W_S of Vugraph 26 and 27 (Equation 3b) for $G_L >> 1$ or more exactly $G_L = \infty$.

1.1.4.4 Loop Noise

In Vugraph 33 the equation for the feedback single-loop SLC closed-loop time constant τ_L is repeated for convenience. Vugraph 34 gives the equation for the residual feedback SLC signal V_r transient response; Equation 4. The second term on the right of Equation 4 disappears when steady state conditions are reached. Plots of the transient response will be given shortly. It is apparent from Vugraphs 33 and 34 that the higher the loop gain the shorter the transient response will be. It is desirable to have the loop transient response be as short as possible in order to best cope with a blinking jammer. There is a limit however as to how short the close-loop time constant τ_L can be made. When it gets too small not enough averaging takes place in the estimate of the weight W of Vugraph 25. As a result the estimate of W will have a large variance. When the estimate of W gets too poor it fluctuates by large amounts and as a result one achieves a poor cancellation. Vugraph 35 gives the conditions on the closed loop bandwidth ω_L (and equivalently τ_L because $\tau_L = 1/\omega_L$; see Equation 2) that must be met in order to achieve good averaging for the estimate of W. Specifically it indicates that the two sided closed loop bandwidth should be less than or equal to 1/10th of the signal bandwidth B_S, or equivalently, jammer bandwidth (which is made equal to the signal bandwidth by properly selecting the RF or IF amplifier bandwidths .

The constraint given by Equation 1 of Vugraph 35 results in the constraint on τ_o of Equation 1 of Vugraph 36. An example is also given in Vugraph 36. For this example the loop gain when no jammer is present, G_o, is set equal to unity, the signal bandwidth was assumed to be B_S = 5 MHz and the jammer-to-noise ratio in the auxiliary channel $JNR_a = 10^4 = 40$ dB. Based on these assumptions the loop noise constraint given by Equation 1 of Vugraph 36 requires that the open-loop time constant τ_o be at least 6370 μs. From Equation 4 of Vugraph 36 it then follows that the loop gain G_L (given as a voltage in Equation 4) is 80 dB. In turn from Equation 1 of Vugraph 33 it follows that τ_L = 0.637 μs. The loop noise constraint given by Equation 1 of Vugraph 35, which leads to Equation 1 of Vugraph 36, results in at least H = 10 noise samples being averaged in estimating the weight W of Vugraph 25.

From Equation 4 of Vugraph 36 it follows that the loop gain G_L varies as JNR_a varies. Let us fix τ_o at the value 6370 μs of the example of Vugraph 36 (obtained for a JNR_a = 40 dB . If now JNR_a is different, G_L will be different and in turn τ_L will be different. Vugraph 37 gives the variation of τ_L and G_L with JNR_a. Vugraph 37 also gives the cancellation CR_o of the jammer in the main channel. Finally the vugraph gives the time $t_A = t_4$ at which the

jammer power is a factor A=4 below the main channel thermal noise level N_M. Assume that the thermal noise level in the auxiliary channel, N_A, equals that in the main channel, that is, $N_M = N_A$. Assume also that in the direction of the jammer the gain of the main channel sidelobe is equal to the gain of the auxiliary antenna. With these assumptions, $JNR_m = JNR_a$. Also the carry over noise, that is, the thermal noise carried over from the auxiliary channel into the main channel is equal to the noise level of the auxiliary channel, that is, it is equal to N_A. Thus when the jammer signal becomes a factor of 4 below N_M, it will be a factor of 8 (9 dB) below the total main channel thermal noise of $N_M + N_A$.

The table of Vugraph 37 indicates that τ_L and t_4 increase with decreasing JNR_a, t_4 going from 3.38 μs when JNR_a = 40 dB to 979 μs for when JNR_a = 10 dB. Vugraph 38 gives plots of the mainlobe transient response for the cases where $JNR_a = JNR_m$ = 40, 30, 20, and 10 dB.

The transient time of t_4 = 979 μs for JNR_a = 10 dB is undesirably long. (Even $t_{0.5}$ is large, it being 427 μs). It is desirable to decrease the SLC transient response for when the jammer signal is weak. One way around this predicament is to use the open-loop canceller presented in Vugraph 7. An alternate way however is to use hard limiting in the feedback SLC as will be discussed in the next section.

Another problem with the linear single-loop SLC (L/SSCL) is the very large dynamic range it requires. Specifically, in order that the noise from the mixer before the feedback amplifier of gain G (see Vugraph 39) not be larger than the receiver front end noise level, it is necessary that Equation 1 of Vugraph 39 be met. If the mixer conversion factor is 0.1 then the RF amplifier gain must be at least 60 dB. This problem is also eliminated by the use of a hard limiter in the feedback SLC described in the next section.

1.1.4.5 Hard-Limited (HL) Single-Loop SLL (SSLL)

Vugraph 40 shows the feedback SLC with a hard limiter in the auxiliary channel. Vugraph 41 gives an approximate derivation of the CR achieved with the hard-limited single-loop SLC (HL/SSLC). The CR is seen to be identical to that obtained with the linear single-loop SLL (L/SSLC) of Vugraph 25. The HL/SSLC weight W transient response is derived in Vugraph 42. On comparing the equations of Vugraph 42 for W and the loop time constant τ_L with those of Vugraph 26 for the L/SSLC, one sees that they are identical. However the equations for G_L are different; compare Equation 2a of Vugraph 42 and Equation 2a of Vugraph 25 which define G_L for these two cases. Vugraph 43 gives the transient response of the main channel residue voltage V_r. Equation 1 of Vugraph 44 gives the loop noise constraint for the HL/SSLC which is equivalent to Equation 1 given in Vugraph 36 for the L/SSLC. Vugraph 44 also gives an example for the HL/SSLC that is equivalant to that given in Vugraph 36 for the L/SSLC. It is seen that for the hard-limited SSLC τ_o = 637 μs with τ_L = 0.636 μs, essentially the same τ_L as obtained for the linear loop.

Vugraphs 45 through 47 compare the HL/SSLC with the L/SSLC.

Using the design obtained in the example of Vugraph 44, that is, τ_o = 637 μs and G_o = 10, the variation of the HL/SSLC closed loop gain (G_L), closed loop time constant τ_L and t_4 were obtained as a function of the jammer-to-noise level in Vugraph 48. As in Vugraph 37 for the linear SSLC, τ_L and t_4 increase with decreasing jammer level. However the increase is not as large as it was for the linear loop, it now being roughly proportional to $\sqrt{JNR_a}$ instead of JNR_a. Specifically, for the hard-limited loop when JNR_a = 10 dB, t_4 = 34.3 μs instead of 979 μs, a factor of almost 30 smaller t_4. Vugraph 49 shows the transient responses for the HL/SSLC for $JNR_a = JNR_m$ = 40, 30, 20 and 10 dB.

1.1.5 Further Discussions on Loop Noise

Vugraph 35 indicates that the number of noise samples, H, that should be averaged in order to obtain a good estimate of W is H = 10 at least. An estimate of W which is accurate is needed in order not to degrade the steady state achievable CR given in Vugraphs 25, 27 and 41. This constraint was first given in the work of Reference 1 (see also Ref. 17). Simulations [1] carried out at the Syracuse University Research Corp. (SURC; now SRC) support this constraint as do other simulations: [11] (see Vugraph 49a) and [22a]. It can be shown that Reference 7, a classic paper on the subject, agrees with this constraint for the case of a single CW jammer. However, it is worth pointing out that there are references in the literature which indicate a more stringent larger H is needed: [14](see Vugraphs 50 and 51) and [4](see Vugraphs 52 and 53).

The more stringent requirement indicates that the number of samples H required is roughly equal to two times the CR desired. These references giving the more stringent requirement claim to use a more exact analysis. Specifically they do not assume that the weight estimate W and interference are independent. However, a similar more stringent exact analysis ([18,19], see Vugraphs 54, 54a and 54b) yields a result similar to the weaker constraint on H of Vugraph 35. Why these differences is not altogether clear. They appear to be partly due to the different assumptions in the different analyses.

In fact, the more stringent larger H requirement can be obtained from Reference 7, the classic paper, if the assumptions of Reference 14 are used, specifically if it is assumed that a nonzero bandwidth jammer is present without any receiver thermal noise. A simple analysis carried out by this author also yields the more stringent result when the assumptions of Reference 14 are used. The same type analysis yields the less stringent requirement if a CW jammer is assumed with receiver thermal noise present. It remains for someone to clarify the differences between the work of Reference 4 and of References 18 and 19.

1.1.6 More On Effects of Non-Zero Bandwidth Jammer and SLC Errors

Vugraph 55 show the CR achieved for a L/SSLC as a function of the jammer direction for different IF filter shapes for a non-zero bandwidth jammer. Vugraph 56 shows the CR achieved versus the JNR_m for different IF filter shapes for a non-zero bandwidth jammer. Vugraph 57 shows the effect of IF filter mismatch between the main and auxiliary channels.

1.2 Double-Loop SLC

When more than one jammer is present it is necessary to use a sidelobe canceller consisting of more than one loop. Specifically if there are two jammers present a double-loop SLC (DSLC) is needed. Vugraph 58 shows a linear DSLC (L/DSLC). The multiple-loop SLC is also needed when the jammer bandwidth is large and there is a difference in the time of arrival of the signal to the main and auxiliary antennas as was the case for Vugraphs 55 through 57; see also Vugraphs 21 and 22.

Vugraph 59 gives the closed-loop time constants for the L/DSLC. This vugraph shows that there are now two loop time constants τ_{L1} and τ_{L2}. This is because there are two loops involved. These two loops can be made independent of each other by the use of a transformation (to be presented later). The time constant for one of these loops, τ_{L1}, is much larger than the other, τ_{L2}. For Example No. 1 in Vugraph 59 one of the time constants is 16.2 μs while the other is 0.325 μs versus the value of 0.637 μs obtained in the example of Vugraph 36. For the second example of Vugraph 59, the difference in the time constants is even larger, one being 1593 μs while the other is 0.319 μs, the ratio of the time constants being roughly 5000. It is the longer of the two time constants that determines the settling time of the L/DSLC because both loops must reach steady state before the jammer (or jammers) are cancelled out. Thus although the double-loop sidelobe canceller can provide a better CR than the single-loop sidelobe canceller, its transient response can be much worse.

Vugraph 60 gives the equation for the CR achievable with the L/DSLC. The example in Vugraph 60 indicates that the dual-loop provides a CR of 57 dB versus 27 dB for the single-loop canceller.

Vugraph 61 provides a plot of the CR achievable as a function of the difference in the time of arrival of the signal between the main and auxiliary channels. This vugraph actually also plots the equation for CR given in Vugraph 60 and hence also represents a plot of CR versus the correlation coefficient ρ by using the lower abscissa axis in the figure. These results are for the case when a single jammer is present.

Vugraph 62 gives a plot of CR versus the bandwidth ratio α which is equal to 0.833/H. This figure is the equivalent figure to that of Vugraph 51 for the single-loop canceller. On comparing these figures one notes that a better cancellation ratio is achievable with the double-loop canceller for a given correlation coefficient and bandwidth ratio. However, as indicated above, the price one pays is a poorer transient response. It is not always true that the cancellation ratio for the dual canceller is better than that for the single loop canceller. Vugraph 63 shows the regions where the single loop canceller is better and vice versa.

1.3 Multi-Loop SLC (MLSC)

Vugraph 64 shows a multi-loop configuration. Each of the auxiliary antennas has a loop as indicated in Vugraph 58 for the dual-loop SLC. Vugraph 65 shows how the CR of the multi-loop sidelobe canceller (MLSC) system increases as the number of loops increases. The figure indicates that for the case simulated there is

a point beyond which it does not pay to increase the number of auxiliary loops. A single jammer was assumed for the plot of Vugraph 65.

2.0 Adaptive Array Processing

2.1 Fully Adpative Array

Vugraph 66 shows the fully adaptive array configuration for a phased array consisting of K elements. For the fully adaptive array, the weights W_1, W_2, etc. are to be chosen such that the main beam of the array points at the target. At the same time nulls in the sidelobes of the antenna are placed in the direction of the jammers. With such weights the maximum possible signal-to-interference ratio at the summer output point of the array is achieved. The optimum weight $W_{OPT} = W_o$ is given by Equation 1 of Vugraph 66. The covariance matrix M is defined in Vugraph 67. The column matrix S* is also defined in Vugraph 67. Physically S* represents the optimum weights W_o that would be used if there was no jammer inteference present, just the thermal receiver noise at each antenna element, with these being independent and having equal stength. Physically the ith element of S* represents the phase shift to be placed on the ith element of the array so as to steer the main beam of the array onto the target. The "*" here means "complex conjugate of" so that S with an * is the complex conjugate of the column matrix S. In turn physically the phase of the ith element of S, S_i, represents the phase of the target signal received at the ith element of the array.

If we assume that the target is in the far field of the antenna array then the signals received by each of the array elements have equal amplitude and if we ignore the actual value of this amplitude and make it unity then the signal received on the ith element is given by $S_i = \exp(j\theta_i)$, where θ_i is the phase of the target signal received by the ith element.

If there is no jammer present then the matrices M and M^{-1} can be replaced by the identity matrix I; see Vugraph 68 (the constant shown in Vugraph 68 in front of the identity matrix I has been ignored here for simplicity because it is of no consequence in this discussion). Vugraph 68 gives an equation for the optimum weight column matrix, W_{OPT}, for the case where no jammer is present. Leaving out the constant shown there W_o can be written as S* . Furthermore, the target receiver output signal is then given by

$$S_o = S^T S^* = \sum_{i=1}^{K} \exp(j\theta_i)|^2 = K \qquad (2.1)$$

where "T" stands for the "transpose of". This is the maximum value S_o can have. The receiver noise terms from the various antenna elements are independent and hence add up with random phases relative to each other. As a result the rms of the output noise voltage N_o is $\sqrt{K}$ times the rms of the noise at each element, these being assumed to have equal rms values. This results in a maximum signal-to-interference ratio at the output summing point for the case when there is no jammer interference present. For this case the weight vector S* takes out the phase differences of the received target echoes at each of the array elements and adds them in phase so as to

maximize the receiver output signal-to-interference ratio, just like a matched filter does in a pulse compression system.

For the case where an arbitrary interference is present from one or more directions, the matrix M is no longer an identity matrix and the value of the weight given by Equation 1 of Vugraph 66 represents the optimum weight, that is, the one that maximizes the output signal-to-interference ratio. That this weight is indeed optimum is shown through a simple derivation using the Schwartz Inequality in Vugraphs 69 and 70.

2.2 Methods for Estimating M

Ordinarily M will not be known a priori. The question is how do we determine M. There are a number of ways for estimating M or M^{-1} in real time. Vugraph 71 lists some of these methods. These will be discussed in the following sections.

2.2.1 Sample Matrix Inversion (SMI) Method

Vugraph 72 shows how M is estimated using the simple SMI algorithm. R here represents the number of independent time samples used in the estimate. Because Equation 1 of Vugraph 72 provides only an estimate of M and not the true value, it will not provide the maximum signal-to-interference ratio achievable with the fully adaptive array, there will be some degradation. Vugraph 73 gives the degradation as a function of R. In Vugraph 73 SIR_A represents the maximum signal-to-interference ratio obtainable when using the exact M, that is, it represents the maximum SIR achievable using the optimum weight of Vugraph 66. The ratio ρ in Vugraph 73 represents the ratio of the SIR achieved using the SMI estimate for M, SIR_{SMI}, over the optimum SIR, SIR_A. Vugraph 73 indicates that for SIR_{SMI} to be 3 dB below that achievable with the optimum weights, R should be equal to about two times the number of radiating elements in the array, that is, R = 2K.

A more recent reference, No. 37, indicates that because the fully adaptive array antenna output interference plus thermal noise does not have a Gaussian distribution, the degradation can be larger than indicated by Equation 4 of Vugraph 73 when the loss is measured in terms of the detection loss rather than SIR loss. This loss is larger the smaller the false alarm probability desired and the smaller K; see Vugraph 74. Vugraph 74 shows that instead of the 3 dB loss indicated in the example of Vugraph 73, the loss can be 4.7 dB when the false alarm probability $P_{fa} = 10^{-6}$ and K = 8.

2.2.2 Applebaum Adaptive Array Technique

Vugraph 75 shows the Applebaum-Howells adaptive loop array configuration for estimating M in real time. In this configuration each element has its own single-loop sidelobe canceller. Because there are K elements there are K such loops. Vugraph 76 shows that when the loop gain G for each of these loops is large then the weights generated are indeed the optimum ones specified in Vugraph 66. The disadvantage of this method for estimating the weights is that it has a longer transient time than the SMI algorithm. This shall be illustrated shortly.

2.2.3 Recursive Update Estimate of M

Vugraph 77 summarizes the recursive algorithm. This vugraph shows how the Jth estimate of M and M_J^{-1} are obtained recursively using the estimate for these at time J-1. The first estimate of M_J, that is, for J = 1, is obtained using Equation 1 of Vugraph 72 with R = 1. The estimate for M_1^{-1} is then obtained by the direct inverse of the matrix $\hat{M}$ for R = 1. Successive estimates of M and M^{-1} are then obtained using Equations 1 and 2 of Vugraph 77. To obtain the updates of M_J^{-1} does not require any further matrix inversions to be carried out.

An advantage of the recursive technique for updating the matrix M^{-1} is that the weights will change with a changing environment. Specifically, if the jammers are moving, the weights will adjust so as to have the nulls track the jammers. The parameter α determines how fast the weights change. The closer α is to unity the faster the weights will change. Alternately the closer α is to zero the slower the weights will change or alternatively the larger the number of past data samples used in forming the estimate of M or equivalently W.

A comparison is now made of the recursive procedure with the Applebaum and SMI procedures. This is done for an airborne look-down radar designed to see low flying aircraft or moving ground targets in the background of ground clutter. For this application it is necessary to not only null out potential jammers but also at the same time the ground clutter. This was done in Reference 6 using an adaptive airborne moving target indicator (AMTI) in conjuction with a fully adaptive array. Vugraph 78 shows the block diagram of the system. The antenna array consists of N elements. In turn each element effectively consists of a three pulse canceller which is adaptively controlled as indicated in the figure. The AMTI is used to eliminate the ground clutter. The incorporation of these adaptive AMTI loops in a fully adaptive array provides the jammer cancellation. In Reference 6 the performance of this system was simulated for the three algorithms discussed above -- the SMI, Applebaum and recursive algorithms. Vugraph 79 shows the transient response of the adaptive AMTI system of Vugraph 78 for each of the three algorithms. The results are given in this vugraph for the case where the mainlobe is pointed broadside to the aircraft flight path, that is, at a scan angle of 90°. The figure indicates that the settling time when using the Applebaum algorithm is very large, steady state conditions not being reached even after a 1000 samples have been processed. In contrast both the SMI and recursive algorithms settle very rapidly, almost at the same time, both after about 16 time samples which is equal to 2 times the number of array elements of 8.

Vugraph 80 gives the results obtained when the mainbeam is pointed in the direction of the flight path of the aircraft. Similar results are obtained here with the SMI algorithm having a slightly faster time constant than the recursive algorithm as expected.

The open-loop canceller of Vugraphs 7 and 8 is essentially a fully adaptive two-element array using the SMI algorithm and as a result also has a very fast settling time as indicated in Vugraph 9.

It is desirable to digress for a moment in order to explain the basis by which the adaptive AMTI circuit of Vugraph 78 works. To understand how it works we have to explain how the well known Displaced Phase Center Antenna (DPCA) achieves its clutter rejection. Assume an aircraft going at a velocity v_s as indicated in Vugraph 81 with an antenna placed along the side of the aircraft. Assume that the beam is pointing broadside as indicated in Vugraph 81. Assume that the target of interest is abeam of the aircraft velocity vector, and at the peak of the beam as shown in Vugraph 81. In the upper right hand corner of the vugraph is shown the antenna pattern as a function of the off axis angle θ. The target is shown at $\theta = 0°$. The antenna pattern also represents the shape of the clutter return in the same range cell as the target, the clutter being assumed homogeneous. In the lower right hand corner of Vugraph 81 is shown the doppler spectrum of the target and mainlobe clutter echoes. The mainlobe clutter has a spectrum shape which is the same as the antenna pattern given in the figure above. The ground clutter which forms the mainlobe clutter spectrum is stationary. However the aircraft is moving. As a result the ground clutter echo has a spectral width and shape given by the antenna pattern. Some of the ground clutter scatterers in the same range cell as the target will have a positive doppler velocity, those for which θ_i is positive, while others, those with a negative θ_i, will have a negative doppler velocity. The clutter scatterer located at the peak of the beam will have a zero doppler velocity, θ_i equalling zero for this scatterer. If the target is moving at a high velocity towards the aircraft then its doppler velocity will be high and far from the mainlobe clutter as indicated by the return at the far right in the lower right hand figure of Vugraph 81. Such a target is out of the mainlobe clutter and easily detected. On the other hand if the target had a low doppler velocity so as to be within the mainlobe clutter as indicated by the dashed line in the lower right hand figure of Vugraph 81, it could be masked by the mainlobe clutter probably.

One wants to see these slow moving or low doppler velocity targets. The question is how do we get rid of the mainlobe clutter? Well, you can get rid of the mainlobe clutter if you could stop the aircraft so as to force the width of the mainlobe clutter to be zero, the mainlobe clutter scatterers now having zero doppler velocity at all angles θ_i. The target having a nonzero doppler velocity would then not be in the mainlobe clutter. One can stop the aircraft by making it a helicopter. A helicopter however is limited by the size of the radar it can handle and the altitude it can fly. As a result it will have a limited range capability. One would really like to place the radar on an aircraft which can fly high and as a result of necessity moves at a relatively fast velocity.

There is another solution to this problem. That solution is to electronically stop the forward motion of the antenna between two successive pulses. Once this is done the mainlobe clutter becomes truly stationary for all θ and has a zero spread (except for internal motion of the clutter scatterers themselves) and consequently the standard two-pulse canceller moving target indicator shown in Vugraph 82 can be used. The clutter being stationary will be cancelled out by the two-pulse canceller while the moving target being non-stationary will not be cancelled out.

Vugraph 83 shows how the antenna can be electronically stopped. Shown in this vugraph is the antenna at time $t = 0$ and time $t = T$.

The antenna is shown to be made up of 3 parts a center part C and a back and front Part A and B, respectively. At time t = 0 only parts C and B of the antenna are used. At a time T later, where T is the pulse-to-pulse period of the radar, the aircraft has moved forward a distance Δ which is equal to the length of parts A and B of the antenna; see Vugraph 83. At time t = T only parts A and C of the antenna are used. From Vugraph 83 it is seen that although the aircraft has moved forward an amount Δ between the first and second pulse transmitted, the part of the antenna being used during the first and second pulse has not changed. Consequently the antenna has not moved electronically for these two pulses and for their clutter echoes. This is in effect what is taking place with the adaptive AMTI circuit of Vugraph 78. This is what the DPCA technique for removing ground clutter in an airborne platform involves.

It is possible to implement the AMTI (or DPCA) without changing the active part of the transmit antenna that is used from pulse-to-pulse. Instead only the receive antenna active part is moved backward electronically. This is actually what was done in the Reference 6 simulations of Vugraphs 79 and 80. For this case the receive antenna has to roll back electronically a distance 2Δ if the aircraft moves forward a distance Δ. Vugraph 84 shows the transmit antenna pattern while Vugraphs 85 and 86 show the receive antenna patterns for pulses 1 and 2 obtained for the simulations like those of Vugraphs 79 and 80. These last two vugraphs show that the receive antenna patterns are nearly the same for the two successive pulses which is what is necessary in order to have stopped the antenna forward motion. The circuit of Vugraph 78 adaptively stops the antenna forward motion. For the simulations which led to Vugraphs 85 and 86 three interferers at 35°, 45° and 55° were assumed, hence the nulls in the receive patterns at these angles.

2.2.4 Use of Orthogonal Transformation in Estimating W

In this procedure before applying the Applebaum loops as indicated in Vugraph 75, an orthogonal transformation is first applied to the antenna array as shown in Vugraph 87. This transformation causes the signals Y_1, Y_2, etc. to be independent. As a consequence of this each of the Applebaum loops have become independent. Vugraph 88 shows the orthogonal transformation. Vugraphs 89 and 90 give the transient response for each of the independent loops. The development for each independent loop is essentially the same as to that of the single feedback SLC of Vugraph 26. From Vugraph 90 it is seen that the closed loop time constant for the ith orthogonal loop is proportional to one over the power of the ith jammer. Thus, as was the case in the table of Vugraph 37, if a weak jammer is present then the loop time constant for this jammer will be large. Furthermore, the time constant for the whole fully adaptive array will be determined by the time constant for the weakest jammer present.

One would like to reduce the time constant for the weaker jammers. This is done by using an AGC circuit at the output of the orthogonal transformation network of Vugraph 87; see Vugraphs 91 and 91a. These AGC networks are set to make the power levels identical at the output of each of the terminals of the orthogonal transformation network. The AGC networks thus represent a whitening filter; see Vugraphs 91a and 92. As a result of this whitening filter now all the loops will have the same time constant; see

Vugraph 92. Vugraph 92 indicates that the output power levels are set equal to that of the largest expected jammers and as a result all the loops have a time constant identical to that expected for the largest jammer, this resulting in all the loops having the shortest time constant.

The approach of Vugraph 92 can run into difficulties if the jammer varies its strength with time. For example, assume initially the jammer in a specific orthogonal channel is weak and the AGC is set high to achieve a short time constant in this channel. If the jammer abruptly increases its strength this channel could saturate with little jammer cancellation being achieved until the AGC adjusted to the new jammer level.

Vugraph 93 shows mathematically how the orthogonalization and whitening transformations are carried out. Vugraph 94 shows the transformations in block diagram form.

The orthogonal transformation can be carried out using the well known Gram-Schmidt algorithm shown in Vugraph 94a. Vugraph 95 shows an implementation of the Gram-Schmidt orthogonalization using Applebaum-Howells loops. The implementation shown in Vugraph 95 is almost systolic in structure. A systolic implementation has been developed in References 21, 32, 33, 33a, 42, 43 and 43a for doing adaptive nulling. It will be described in Section 2.3.

Let us digress for a moment and explain how the fully adaptive array physically works. What it does is first places the mainbeam in the direction where the targets should be or is being looked for. Next it locates the interferer (jammer) and places an auxiliary beam pointed in the direction of the jammer; see Vugraph 96. The gain of the auxiliary beam in the direction of the jammer is adjusted so that it is equal to the gain of the mainbeam sidelobe in the direction of the jammer. Now by subtracting the auxiliary beam signal from the mainbeam signal, the jammer is cancelled out from the mainbeam as was done for the simple open-loop SLC of Vugraph 7. When there are two jammers present at two different angles, then two auxiliary beams are formed, each pointing at each of the jammers. By appropriately subtracting the signals of these two beams from the mainbeam, these two jammers can be cancelled out. The maximum number of auxiliary beams that can be formed with a phased array having K elements is K-1. Vugraph 97 illustrates this process mathematically. Each auxiliary beam pointed at a jammer is called an eigenvector beam. These eigenvector beams are formed from the eigenvectors of the covariance matrix M. Specifically, if the elements of the eigenvectors of M are used as the weights W_i of the array of Vugraph 66 they form beams in the direction of the jammers. Vugraphs 98 and 99 illustrate this process for the case of a single jammer whose location is indicated by the arrow on the abscissa. Vugraph 98 shows the antenna pattern before and after the eigenvector beam has been subtracted out from the mainbeam pattern. Vugraph 99 shows the eigenvector beam and the mainbeam antenna sidelobes (the dotted curve) in the region where the jammer is located.

Vugraphs 100 and 101 show similar results for the case of two closely spaced jammers. Vugraph 100 shows the two eigenvector beams. In this case, because the jammers are very closely spaced, closer than a sidelobe width, the second eigenvector beam is given by a difference pattern while the first is given by the standard sum beam pattern. Vugraph 101 shows the unadapted and adapted patterns.

Let us now return to the issue of orthogonalization. Another method that can be used for achieving orthogonalization is the use of the lattice matrix. Vugraph 102 shows a lattice filter orthogonalization network.

2.3 Methods That Do Not Require Estimating M [21,32,33,33a,37a,42,43,43a]

The algorithms described above which require the estimation of the covariance matrix M, designated as $\hat{M}$, followed by the calculation of $\hat{M}^{-1}$ to determine W, have the disadvantage of requiring high computation precision. Such methods are called "power methods" because the terms of $\hat{M}$ are voltage-squared. In contrast there are algorithms which do not require the computation of $\hat{M}$ or $\hat{M}^{-1}$ which require about half the precision required using the "power methods". These are called "voltage methods" because they obtain the adapted array output directly from the array voltage outputs through orthonormal transformations. (These methods are also referred to as "square-root" methods because in some sense they are dealing with the square root of $\hat{M}$ [37a].) For the "voltage methods" the wordlength w_v required for the computations is about half the wordlength (w_p) required using the "power methods" [33a,37a,43a]. Specifically [37a].

$$w_v \doteq 1/2\ w_p \geq 1/2\ [\log_2 (\lambda_{max}/\lambda_{min})] + 1 \text{ (for sign)} \qquad (2.1)$$

where λ_{min} and λ_{max} are respectively the minimum and maximum eigenvalues of M.

Vugraph 102a gives the results of a simulation comparing the array output signal-to-interference (S/I) ratio loss versus the wordlength size. The simulation was carried out for a MSLC (see Vugraph 64) consisting of 14 antennas. The eigenvalue spread $\lambda_{max}/\lambda_{min}$ was about 73 dB = 2^{24} which implies that it is necessary to use $\geq$25 bits with the "power methods". This is indeed the result obtained in the simulation using the "power method" (with the Cholesky algorithm for doing the inversion of $\hat{M}$). The "voltage methods" are seen to require about half the wordlength. The "voltage methods" were carried out using the Givens, Householder and Gram-Schmidt orthonormal transformations. (This Gram-Schmidt transformation is different from that of Vugraph 94a). The "voltage method" saves in wordlength at an expense in computation operations count (complex multiplications and adds, CMADs). For example, with the Householder transform, which is the most efficient computationwise of the voltage methods of Vugraph 102a, the CMADs are a factor 1.4 greater when R, the number of time samples used in estimating the weights, is two times the number of array elements, K. For R>>K, the expense in computation is a factor of 2. With the Givens the expense in computation is about twice that of the Householder while the Gram-Schmidt is in between the two [41a].

The systolic implementation [21,32,33,33a,42,43,43a] mentioned in Section 2.2.4 uses a "voltage method". Specifically it uses the Givens orthonormal transformation. Vugraph 102b shows this systolic implementation. Although shown for a MSLC it applies just as well to the fully adaptive array of Vugraph 66. (References 33a and 33b show that the fully adaptive array can be thought of as a MSLC when using an appropriate constraint equation.) The systolic implementatuon of Vugraph 102b obtains the adapted array output without ever calculating W as well as $\hat{M}$ or $\hat{M}^{-1}$. This systolic array type of

adaptive nulling processor is being developed in a test-bed system at the Standard Telecommunications Laboratory in Harlow, Britain [33a].

A simulation of an 8 element adaptive array using the systolic architecture (a "voltage method") was carried out and compared to one using the SMI algorithm (a "power method") to see the difference in sensitivity to arithmetic precision [43a]. Vugraph 102c shows the results. For this simulation a 24 bit floating point wordlength (16 bit mantissa and 8 bit exponent) was used for the computation. This vugraph shows the significantly poorer results obtained using the SMI algorithm even with a 24 bit floating point wordlength. This is believed due to the need for a large enough number of bits in the mantissa. The number of bits being required in the mantissa is believed to be equal to that specified by Equation 2.1 above which for this simulation is estimated to be about 21 bits for the "power method" versus about 11 bits for the "voltage method" [41a]. There has to be enough bits in the mantissa to handle the dynamic range of having a weak (the thermal noise) and strong signal (the jammer) simultaneously. Having the floating point exponent does not help with respect to the handling simultaneously of a strong and weak signal here.

The systolic implementation of Vugraph 102b is for a fading memory or growing memory. It can be made to be a fading memory filter by having $0<\beta<1$ in Vugraph 102b. For $\beta=1$ it is a growing memory filter. Reference 37a presents a nonorthonormal transformation for the "voltage method" which results in a sliding window filter. It is the hyperbolic Householder transform also called Rader transform after its originator.

2.4 Widrow, Steepest Descent and Other Fully Adaptive Array Techniques

Vugraph 103 shows the Widrow minimum mean square error (MSE) adaptive array configuration. This figure shows that this technique requires the use in the receiver of a reference signal s(t) which is a replica of the target signal that one desires to detect. Generally in a radar one does not have such a reference signal, the target range and doppler velocity being unknown. Hence this algorithm is not used for radar. It does find application in communication systems where such a reference signal can be available. The reference signal can be obtained by using a pilot tone in conjunction with the transmitted signal containing the information in the form of a modulation on a carrier. Alternately sometimes the carrier signal itself can be extracted for use as the reference signal. It turns out that the optimum weights for the Widrow system are identical to those given in Vugraph 66; see Vugraph 104. Vugraph 105 derives the equation for the optimum Widrow weight.

Vugraph 106 illustrates the least mean square steepest descent algorithm [46,34]. Vugraph 107 gives an analog realization of this algorithm [34]. The Newton gradient algorithm is given in Vugraph 107a [46].

2.5 Fully Adaptive Array as a Multi-Loop SLC (MSLC)

It is educational to point out that the multi-loop sidelobe canceller of Vugraph 64 can be thought of as a special case of the fully adaptive array of Vugraph 66 when the appropriate vector S*

is used. Assume for Vugraph 66 that the first element, element number "1", is the mainbeam element for Vugraph 64, with the rest of the elements being the auxiliary elements. Then the appropriate S* to be used is one that causes the array to place only the mainbeam antenna element, element number one of Vugraph 66, in the circuit when there is no interference present. The S* which does this is given by Equation 2 in Vugraph 108. When there is no jammer interference present M^{-1} in effect becomes an identity matrix and W_o thus becomes S* from Equation 2 of Vugraph 108, as desired. This says that the weight for antenna element one is unity while for all the auxiliary antenna elements it is zero. This thus forces only the mainbeam antenna element to be in the circuit of Vugraph 66 when there is no jammer interference present. Physically the above $W_o = S^*$ can be thought of as the optimum antenna weight for when no jammer is present. Vugraph 109 completes the development for the fully adaptive array as a MSLC. The method for estimating the covariance matrix M_a, which is the covariance matrix for the auxiliary array of Vugraph 64, is the same as described above for the fully adaptive array; see Vugraph 110.

2.6 Additional Subjects

2.6.1 Digital Gram-Schmidt MSLC

Vugraphs 111 and 112 present a MSLC consisting of one main antenna and two auxiliary antennas. For this configuration the Gram-Schmidt orthogonalization is used. Furthermore the orthogonalization is carried out digitally. The reference indicates that the hardware for this digital implementation is well within the present state-of-the-art. Vugraphs 113 and 114 give simulation results obtained for the Gram-Schmidt two loop canceller of Vugraph 111 and for the case where a Howells-Applebaum canceller was used instead. The Gram-Schmidt implementation is seen to have a better transient response, as at is expected to have. Vugraph 115 gives the cancellation loss versus the number of bits for the digital Gram-Schmidt canceller.

2.6.2 Kalman MSLC Weight Prediction

It is possible to use a Kalman predicter to update the weights for a MSLC. Vugraph 116 shows such an implementation; Vugraph 117, the Kalman update equation for the weights; Vugraph 118 the all pole filter for generating the interference model used; in Vugraph 119 are examples of the transient response characteristics obtained.

2.6.3 Number of Bits Required for MSLC Weights

Vugraphs 120 and 121 indicate the number of bits required for the weights of a linear MSLC (L/MSLC) as a function of the cancellation ratio desired and the number of auxiliary elements used. Vugraphs 122 and 123 give the number of bits required to do the matrix inversion when using the SMI algorithm (a "power method") as a function of the cancellation ratio desired and the number of auxiliary elements used. These results are in reasonable agreement with the bound of Equation 2.1.

2.6.4 Anechoic Chamber Test Results

Vugraphs 124 and 125 show some scaled geosynchronous communication antenna tested in an anechoic chamber for a sidelobe canceller

[31]. Vugraph 126 gives the antenna patterns for the seven auxiliary antennas. The mainbeam pattern is centered on this cluster and has a mainbeam width of 18°. Thus mainlobe cancelling is actually being carried out here with the auxiliary elements. Vugraph 127 shows the excellent results obtained. Vugraph 127 indicates that for a signal bandwidth of 1 MHz a cancellation ratio of 59 dB was obtained; for a bandwidth of 2.5 MHz a cancellation ratio of 56 dB was achieved. These results indicate what one may be able to expect for a radar in the future.

2.7 Adaptive-Adaptive Array Processing [8-10]

Appendix A (Vugraphs A-1 to A-16) and Appendix B give a new way for achieving the performance of a fully adaptive array without its many penalties. Two penalties are the computation complexity and poorer transient response of the fully adaptive array versus the adaptive-adaptive array processing; see Vugraph A-10. The fully adaptive array also has the problem of very poor sidelobes in regions other than where the jammer interference sources exist; see Vugraphs A-5 through A-7. This last problem is true even when the number of independent samples for estimating the covariance matrix M is much much larger than two times the number of radiating elements in the array; see Vugraph A-5 which gives an example where 3000 samples were used for an array consisting of only 14 elements. The figure still shows very poor sidelobes.

2.8 Adaptive Array Processing and Spectral Estimation

2.8.1 Maximum Entropy Spectral Analysis (MESA)

Reference 17a relates spectral estimation via maximum entropy spectral analysis (MESA), also referred to as the maximum entropy method (MEM), to the fully adaptive array processing of Vugraph 66 and the MSLC of Vugraph 64. MESA is in turn related to prediction theory [25a].

Appendix C summarizes in vugraph form the essentials of prediction theory with its relationship to the maximum entropy method (MEM) for spectrum estimation. Specifically, Vugraph C-2 gives the all pole model for the random process $\tilde{X} = X_1, X_2 \ldots, X_{n-1}$ whose value X_n is to be predicted from $X_{n-1}, X_{n-2}, \ldots, X_{n-p}$. In this Vugraph $Hp(Z)$ (which is the Z transform of the tapped delay line filter frequency transfer characteristic $Hp(f)$ produces the white noise sequence e_n at its output when $\tilde{X}$ is applied at its input. Alternately if the white noise sequence e_n is applied to the inverse of this filter, $H_I(Z) = 1/Hp(Z)$, then $\tilde{X}$ is generated at the output; see Vugraph C-3. Thus the inverse filter frequency transfer characteristic $H_I(f)$ represents the frequency spectrum of the process $\tilde{X}$. Hence if $H_I(f)$ can be estimated then an estimate of the frequency spectrum for $\tilde{X}$ would be had. Physically the locations of the poles of $H_I(f)$ (which are the poles of the all pole model for $\tilde{X}$) can be thought of as the frequency locations of the sinusoidal components making up the $\tilde{X}$ process.

Vugraph C-4 relates the parameters ap_i of the filter $Hp(Z)$ to the covariance matrix M of $\tilde{X}$. It is clear from Vugraph C-4 that obtaining an estimate of the covariance matrix M would permit the obtaining of an estimate of the ap_i weights which in turn define $Hp(f)$ and $H_I(f)$. Vugraph C-5 gives the filter which predicts X_{n-1} from $X_n, X_{n-1}, \ldots, X_{n-P+1}$. It contains a tape delay line filters

having the ap_i weights. This filter minimizes the mean square value of the prediction error e_n; see Vugraphs C-5 and C-6. It is clear that having an estimate of the ap_i weights defines the prediction filter.

Vugraph 129 repeats the fully adaptive array of Vugraph 66 in a form where it is essentially equivalent to the predictor of Vugraph C-5. Vugraph 130 similarly repeats the MSLC of Vugraph 64 in a form equivalent to the predictor of Vugraph C-5. The MSLC of Vugraph 130 minimizes the mean square value of the output error e_n. When this is achieved the output is a white noise process just as it is for the predictor of Vugraph C-5. The adapted antenna then acts like a whitening filter. The adapted antenna gain $G_A(\theta)$ versus the angle θ is the whitening filter. Physically the adapted pattern $G_A(\theta)$ has nulls at the jammer locations and hence its inverse $G_I(\theta) = 1/G_A(\theta)$ will have peaks (poles) at these locations thus indicating where the jammers are located. Accordingly the inverse $G_I(\theta)$ provides the all pole model for the location of the interferers. The amplitudes of these peaks are not in general proportional to the interference strength because of the nonlinear processing used in obtaining the estimate. This is especially true when many interferers are present which are closely spaced. When the interferers are far apart the peaks are proportional to the square of the interference strength.

This will all be clearer with an example. Reference 17a gives a simulation demonstrating the ability of the system of Vugraph 129 to locate jammers. The simulation was carried out for an array of eight identical elements with two jammers located at 18° and 22°. Vugraph 131 shows the adapted pattern with two nulls at the angles the jammers are located at (see the arrows). Also shown is the single-element unadapted pattern. Vugraph 132 shows the two eigenvector beams. Vugraph 133 plots $G_I(\theta)$, that is, one over the adapted gain plot of Vugraph 131. Also shown is the conventional 8 element antenna output obtained as if it is scanned in angle. This vugraph illustrates the superresolution capability of the MESA technique.

2.8.2 Spectral Analysis Using Applebaum-Howells Loops

Reference 17a gives a simulation of the fully adaptive Applebaum-Howells array of Vugraph 75. This algorithm (together with others) gave the superresolution results of Vugraph 134. This vugraph gives the resolution achievable versus the signal-to-interference ratio per source.

2.8.3 Maximum-Likelihood Method (MLM)

Reference 17a points out that the minimization of the output power of Vugraph 129 subject to the contraint $S^TW = 1$ yields the maximum-likelihood method (MLM) estimate of the locations of the interferers. $S = S(\theta)$ here is the signal that would be received from a direction θ (see Vugraph 67). The output of the adapted array versus S as a function of θ gives the jammer spectrum in angle space. Vugraph 134a gives the MEM estimate obtained for the example of Vugraphs 131 to 133. Vugraph 135 gives the equation for the MLM estimate of the jammer locations. The MLM estimate has the advantage that the peaks of the spectral lines are proportional to the strength of the interferers producing them. Also there are

fewer and lower amplitude false spikes than obtained with the MESA technique.

Reference 38a gives the multiple signal classification (MUSIC) algorithm for estimating the locations of the interferers. Vugraph 136 gives the MUSIC algorithm. Vugraphs 137 and 138 compare its performance to other algorithms indicating the advantages of the MUSIC algorithm.

1. Applebaum, S. and R. Davis, Private Communication, Syracuse University Research Com. (SURC, Now SRC), Syracuse, N.Y.

2. Applebaum, S.P., "Adaptive Arrays," IEEE Trans. on Antennas and Propagation Vol. AP-24, No. 5, September 1976, pp. 585-598.

3. Baird, C.A. Jr. et al, "Adaptive Processing for Antenna Arrays," Harris Corp. Report, RADC-TR-72-174, June 1972.

4. Berni, A.J., "Weight Jitter Phenomena in Adaptive Array Control Loops," IEEE Transactions on Aerospace and Electronic Systems, Vol. AES-13, No. 4, July 1977, pp. 355-361.

5. Brennan, L.E. and I.S. Reed, "Theory of Adaptive Radar," IEEE Trans. Aerosp. Electron. Syst. AES-9, 237-252 (March 1973).

6. Brennan, L.E., Mallett, J.D. and I.S. Reed. "Adaptive Arrays in Airborne MTI Radar," IEEE Trans. on Antennas and Propagation, Vol. AP-24, No. 5, September 1976, pp 607-615.

7. Brennan, L.E., E.L. Pugh and I.S. Reed, "Control-Loop Noise in Adaptive Array Antennas," IEEE Transactions on Aerospace and Electronic Systems, Vol. AES-7, No. 2, March 1971, pp. 254-262.

8. Brookner, E. and J.M. Howell, "Adaptive-Adaptive Array Processing," Phased Arrays 1985 Symposium Proceedings, October 15-18, 1985, The Mitre Corp. Bedford, MA, pp. 133-146; Also RADC Rept. RADC-TR-85-171 August 1985, Electromagnetics Science Div., RADC, Hanscom AFB, Bedford, MA 01731, Air Force Systems Command; see also IEE 1987 International Radar Conf.

9. Brookner, Eli, "Radar of the '80s and Beyond--An Update," IEEE see Electro/86, May 13-15, 1986, Session 25; also Brookner, E., "Array Radars: An Update," Microwave J., Vol. 30, No. 3, pp. 107-174.

10. Brookner, E. and J.M. Howell, "Adaptive-Adaptive Array Processing," IEEE Proc., Vol. 74, No. 4, April 1986, pp. 602-604.

11. Bucciarelli, T., M. Esposito, A. Farina and G. Losquadro, "The Gram-Schmidt Sidelobe Canceller," IEE Radar-82, October, 1982, pp. 486-490.

12. Chapman, D.J., "Partial Adaptivity for the Large Array," IEEE Trans. on Antennas and Propagation, Vol AP-24, No. 5, September 1976, pp. 685-696.

13. Farina, A., "Single Sidelobe Canceller: Theory and Evaluation," IEEE Transactions on Aerospace and Electronic Systems, Vol. AES-13, No. 6, November 1977, pp. 690-699.

14. Farina, A. and S.A. Studer, "Evaluation of Sidelobe-Canceller Performance," IEE Proc., Vol. 129, Pt. F, No. 1, February 1982, pp. 52-58.

15. Farina, A. and F.A. Studer, "Application of Gram-Schmidt Algorithm to Optimum Radar Signal Processing," IEE Proc., Vol. 131, Part F, No. 2, April 1984, pp. 139-145.

16. Farina, A. and F.A. Studer, "Adaptive Implementation of the Optimum Radar Signal Processor," Int. Conf. on Radar, May 21-24, 1984, Paris, France, pp. 93-102.

17. Gabriel, W.F., "Adaptive Arrays - An Introduction," Proc. IEEE, Vol. 64, No. 2, February 1976, pp 239-272.

17a. Gabriel, W.F., "Nonlinear Spectral Analysis and Adaptive Array Superresolution Techniques," NRL Report 8345, Feb. 1980; or Gabriel, W.F., "Spectral Analysis and Adaptive Array Superresolution Techniques," IEEE Proc., Vol. 68, No. 6, June 1980, pp. 654-666.

18. Gerlach, K. and K.H. Lang, "Exact Solution for Control Loop Adaptive Antenna Weights in Band-Limited Noise," IEEE Trans. on Antennas and Propagation, Vol. AP-34, No. 3, March 1986, pp. 395-403.

19. Gerlach, K.R., "Application of Probabilistic Methods in Adaptive Arrays," The School of Engineering and Applied Science of the George Washington University, Doctor of Science dissertation, February 1981.

20. Giraudon, C., "Optimum Antenna Processing: A Modular Approach," Proceedings of NATO Advanced Study Institute on Signal Processing and Underwater Acoustics, Porto Venere, Italy, 1976 (Reidel, 1977).

21. Griffiths, J.W.R., "Adaptive Array Processing--A Tutorial," IEE Proc., Vol 130, Pts. F and H, No. 1, February 1983, pp. 3-10.

22. Griffiths, J.W.R. and J.E. Hudson, "Adaptive Processing in a Passive Sonar System," Proceedings of NATO Advanced Study Institute on Signal Processing and Underwater Acoustics, Proto Venere, Italy, 1976, (Reidel, 1977).

22a. Howell, J.M, Raytheon Comp., Private Communication.

23. Howells, Paul W., "Explorations in Fixed and Adaptive Resolution at GE and SURC," IEEE Transactions on Antennas and Propagation, Vol. AP-24, No. 5, September 1976, pp. 575-583.

24. Hudson, J.E., "A Kalman Filter Algorithm for Adaptive Radar Arrays and Modelling of Non-Stationary Weights," IEE Conf. Publ. 180, 1979, pp. 198-202.

25. Hudson T.E., "Adaptive Array Principles," P. Peregrinis, 1981.

25a. Kay, S. and L. Marple, "Spectrum Analysis -- A Modern Perspective," Proc. IEEE, Nov., 1981.

26. Kretschmer, F.F., Jr. and B.L. Lewis, "Digital Open-Loop Sidelobe Canceler Techniques," NRL Report 8100, April 6, 1977; see also IEEE AES Trans. 1/78.

27. Kretschmer, F.F., Jr. and B.L. Lewis, "An Improved Algorithm for Adaptive Processing," IEEE Transactions on Aerospace and Electronic Systems, Vol. AES-14, No. 1, January 1978, pp. 172-176.

28. Krucker, K., "Rapid Interference Suppression Using a Kalman Filter Technique," IEE Proc., Vol. 130, Pts. F and H, No. 1, February 1983, pp. 36-40.

29. Krucker, K., "Rapid Interference Suppression Using a Kalman Filter Approach," Electron, Lett., 1981, 17, (2) pp. 65-67.

29a. B.L. Lewis, F.F. Kretschmer, Jr., and W.W. Shelton, "Aspects of Radar Signal Processing" Artech House, Norwood, MA, 1986.

30. Marr, J.D., "A Survey of Adaptive Antenna Arrays," IEEE 15th Southeastern Sym. on Systems Theory, Huntsville, Alabama, March 28-29, 1983, pp. 298-301.

31. Mayhan, J.T., "Bandwidth Limitations on Achievable Cancellation for Adaptive Nulling Systems," MIT Lincoln Lab Technical Note 1978-1, 17 February 1978.

32. McWhirter, J.G., and T.J. Shepherd, "Adaptive Algorithms in the Space and Time Domains," IEE Proc., Vol. 130, Pts. F and H, No. 1., February 1983, pp. 17-21.

33. McWhirter, J.G., "Recursive Least-Squares Minimization Using a Systolic Array," Proc. SPIE, Vol. 431, Real Time Signal Processing, Vol. 1, 1983, pp. 105-112.

33a. McWhirter, J.G., "A Brief Review of Adaptive Null Steering Techniques," Royal Signals and Radar Establishment, RSRE Memorandum No. 3939, February, 1986.

33b. McWhirter, J.G., "Systolic Array for Recursive Least Squares Minimization," Electronic Letters, Vol. 19, No. 18, Sept. 1983, p. 729.

34. Monzingo, R.A. and T.W. Miller, "Introduction to Adaptive Arrays," Wiley-Interscience, 1980.

35. Nitzberg, R., "Effect of Errors in Adaptive Weights," IEEE Transactions on Aerospace and Electronic Systems, Vol. AES-12, No. 3, May 1976, pp 369-373.

36. Nitzberg,R., "Computational Precision Requirements for Optimal Weights in Adaptive Processing," IEEE Transactions on Aerospace and Electronic Systems, Vol. AES-16, No. 4, July 1980, pp. 418-425.

37. Nitzberg, Ramond, "Detection Loss of the Sample Matrix Inversion Technique," IEEE Transactions on Aerospace and Electronic Systems, Vol AES-20, No. 6, November 1984, pp.824-827.

37a. Rader, C.M. and A.O. Steinhardt, "Hyperbolic Householder Transformation," IEEE Trans. on Acoustics, Speech and Signal Processing, Vol. ASSP-34, No. 6, Dec. 1986, pp. 1589-1602.

38. Reed, I.S., J.D. Mallett, and L.E., Brennan, "Rapid Convergence Rate in Adaptive Arrays," IEEE Transactions on Aerospace and Electronic Systems, Vol. AES-10, No. 6, November 1974, pp. 853-863

38a. Schmidt, R.O., "Multiple Emitter Location and Signal Parameter Estimation," IEEE Trans. on Antennas and Propagation, Vol. AP-34, No.3, March 1986, pp. 276-280.

39. "Special Issue on Adaptive Arrays," IEE Proceedings-F, Communications, Radar and Signal Processing, Vol. 130, Pt. F, No. 1, February 1983.

40. "Special Issue on Adaptive Antennas," Trans on Antennas and Propagation, Vol. AP-24, No. 5, September, 1976.

41. "Special Issue on Adaptive Processing Antenna Systems," Trans on Antennas and Propagation Vol AP-34, No 3, March 1986.

41a. Allan O. Steinhardt, Private Communication, Formerly Lincoln Laboratory, MIT, Lexington, MA, now with Cornell University, Electrical Eng. Dept., Ithica, N.Y.

42. Ward, C.R., A.J. Robson, and P.J. Hargrave, "The Application of a Systolic Least Squares Processing Array to Adaptive Beamforming," IEEE/ICASSP 1984 Conference, pp. 34A.3.1-4.

43. Ward, C.R., and P.J. Hargrave, "A Systolic Array for High Performance Adaptive Beamforming," AGARD Conf. Proc. No. 380, "The Impact of Very High Performance Integrated Circuits on Radar, Guidance and Avionics Systems," May, 1985 Paper No. 19.

43a. Ward, C.R., P.J. Hargrave and J.G. McWhirter, "A Novel Algorithm and Architecture for Adaptive Digital Beamforming," IEEE Trans. on Antennas and Propagation, Vol. AP-34, No. 3, March, 1986, pp. 338-346

44. White, W.D., "Cascade Preprocessors for Adaptive Antennas," IEEE Trans. on Antennas and Propagation, Vol. AP-24, No. 5, Sept. 1976, pp. 670-684.

45. White, W.D., "Adaptive Algorithms," AIL Report 77-51, September 1977.

46. Widrow, B. and S.D. Stearns, "Adaptive Signal Processing," Prentice-Hall., 1985.

SIDELOBE CANCELLING AND ADAPTIVE
ARRAY PROCESSING

(1)

1.0 SIDELOBE CANCELLER
- 1.1 SINGLE LOOP SIDELOBE CANCELLER
  - 1.1.1 BASICS OF SIDELOBE CANCELLING
  - 1.1.2 OPEN-LOOP SIDELOBE CANCELLER
  - 1.1.3 EFFECTS OF ERRORS
  - 1.1.4 FEEDBACK SIDELOBE CANCELLER (SLC)
    - 1.1.4.1 CANCELLATION RATIO (CR)
    - 1.1.4.2 TRANSIENT RESPONSE
    - 1.1.4.3 EXACT DERIVATION OF CANCELLATION RATIO (CR)
    - 1.1.4.4 LOOP NOISE
    - 1.1.4.5 HARD-LIMITED (HL) SINGLE-LOOP SLL (SSLL)
  - 1.1.6 MORE ON EFFECTS OF NON-ZERO BANDWIDTH JAMMER AND SLC ERRORS
- 1.2 DOUBLE-LOOP SLC
- 1.3 MULTI-LOOP SLC (MLSC)

(2)

2.0 ADAPTIVE ARRAY PROCESSING
- 2.1 FULLY ADAPTIVE ARRAY
- 2.2 METHODS FOR ESTIMATING
  - 2.2.1 SAMPLE MATRIX INVERSION (SMI) METHOD
  - 2.2.2 APPLEBAUM ADAPTIVE ARRAY TECHNIQUE
  - 2.2.3 RECURSIVE UPDATE ESTIMATE OF M
  - 2.2.4 USE OF ORTHOGONAL TRANSFORMATION IN ESTIMATING W
- 2.3 OTHER FULLY ADAPTIVE ARRAY TECHNIQUES
  - 2.3.1 WIDROW MEAN SQUARE ERROR (MSE) ADAPTIVE ARRAY TECHNIQUE
- 2.4 FULLY ADAPTIVE ARRAY AS A MULTI-LOOP SLC (MSLC)
- 2.5 ADDITIONAL SUBJECTS
- 2.6 ADAPTIVE-ADAPTIVE ARRAY PROCESSING [8-19]
- 2.7 PREDICTION THEORY AND MAX. ENTROPY METHOD
- 2.8 UBIQUITOUS ORTHONORMAL TRANSFORMATION

JAMMING PROBLEM

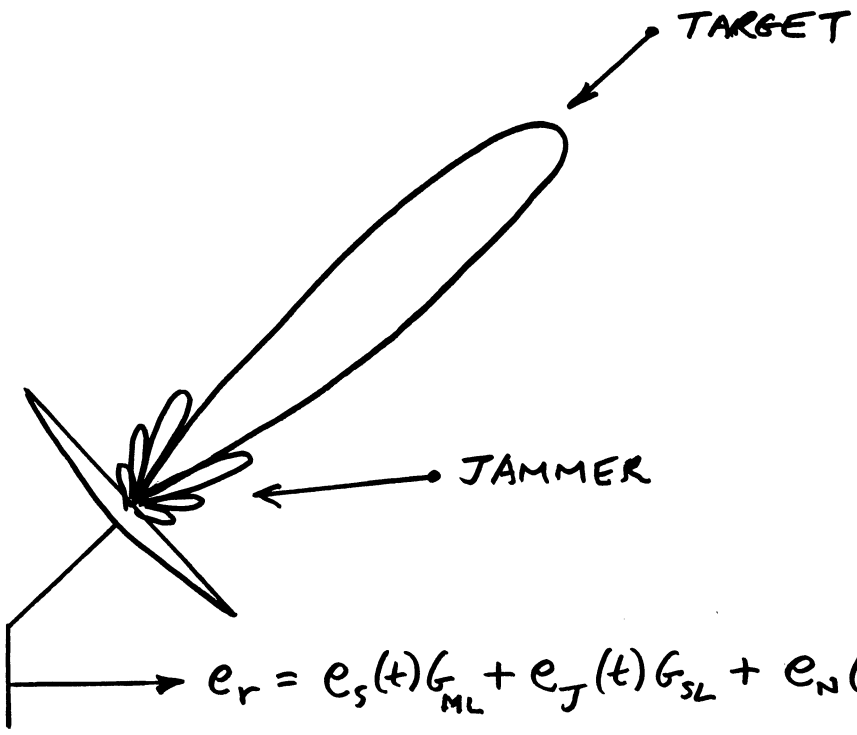

$$e_r = e_s(t) G_{ML} + e_J(t) G_{SL} + e_N(t) \quad \text{(REAL NOT.)}$$

$$E_R = E_S + E_J + E_N \quad \text{(COMPLEX NOT.)}$$

BASIS FOR JAMMER CANCELLATION

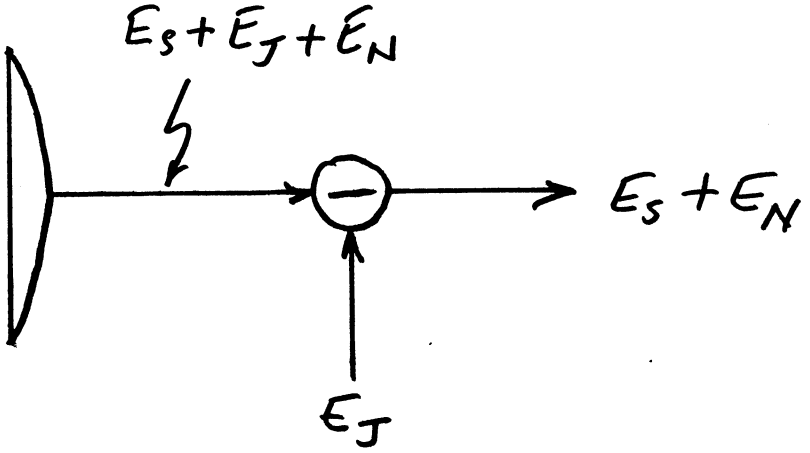

JAMMER CANCELLATION SIGNAL

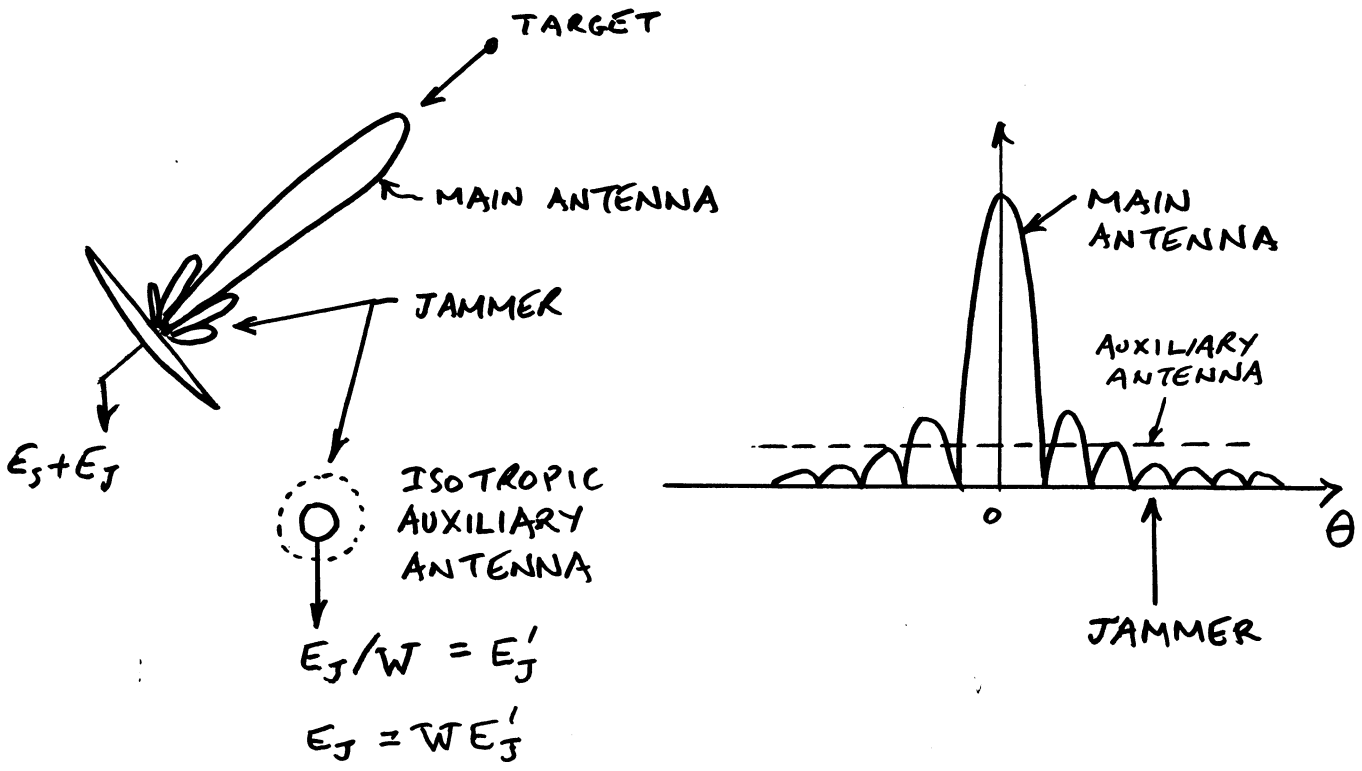

JAMMER CANCELLATION CLAIRVOYANT

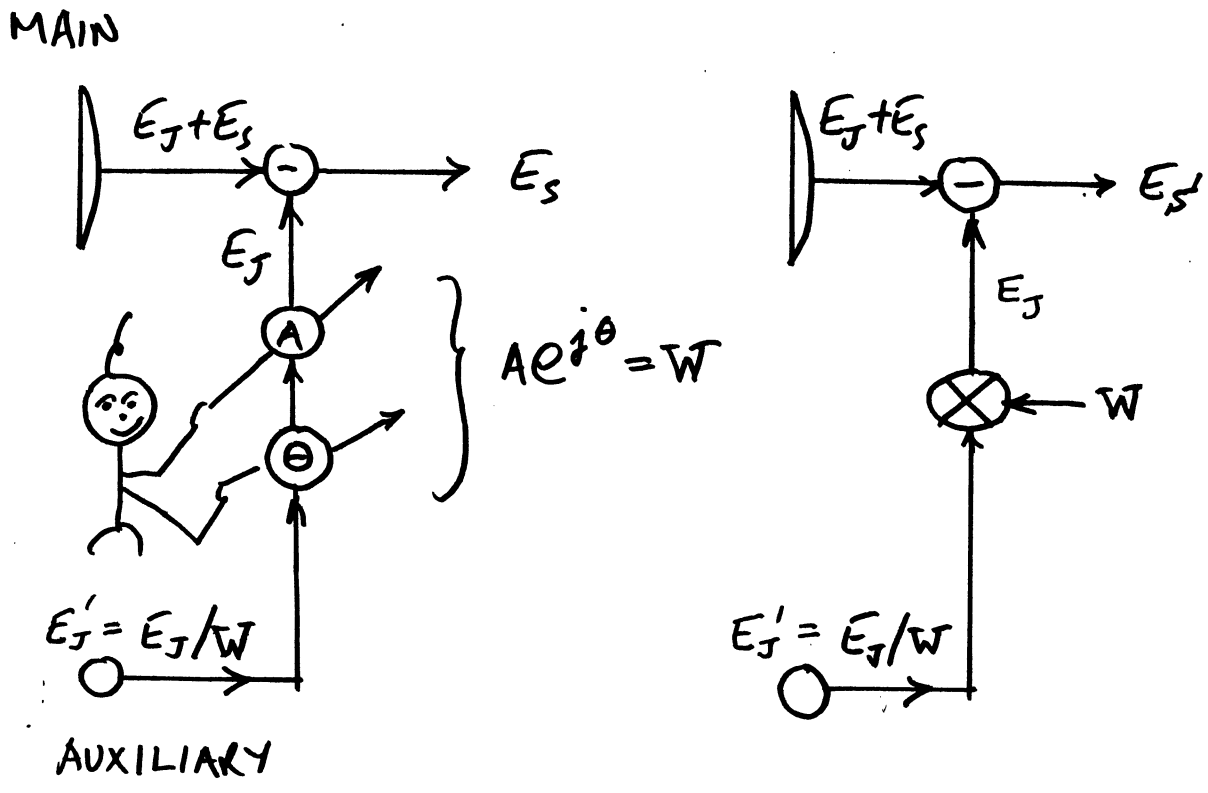

OPEN-LOOP JAMMER CANCELLER

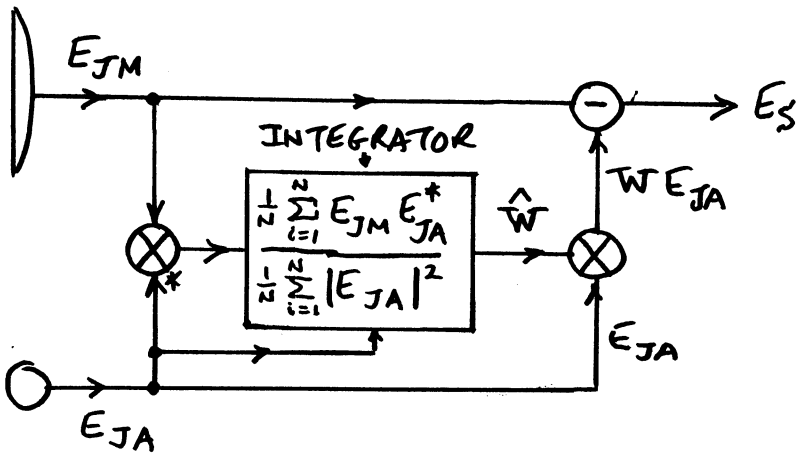

$$\hat{W} = \frac{\overline{E_{JM} E_{JA}^*}}{\overline{E_{JA} E_{JA}^*}}$$

$$E_{JM} = W E_{JA}$$

NOTE "*" INDICATES COMPLEX CONJUGATE.

OPTIMALITY OF OPEN-LOOP WEIGHTING

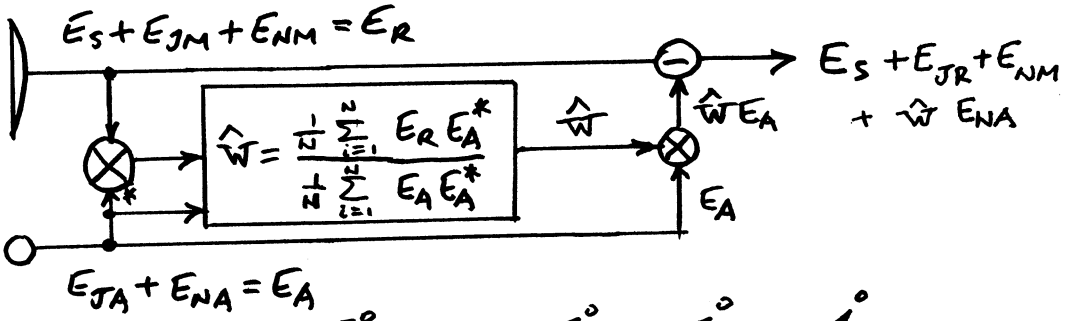

$$\hat{W} = \lim_{M\to\infty} \frac{\sum_{i=1}^{N} \left[\overset{\to 0}{E_S E_{JA}^*} + \overset{\to 0}{E_S E_{NA}^*} + E_{JM} E_{JA}^* + \overset{\to 0}{E_{JM} E_{NA}^*} + \overset{\to 0}{E_{NM} E_{JA}^*} + \overset{\to 0}{E_{NM} E_{NA}^*} \right]}{\sum_{i=1}^{N} \left[E_{JA} E_{JA}^* + \underset{\to 0}{E_{JA} E_{NA}^*} + \underset{\to 0}{E_{JA}^* E_{NA}} + E_{NA} E_{NA}^* \right]}$$

$$= \frac{\overline{E_{JM} E_{JA}^*}}{\overline{|E_{JA}|^2} + \overline{|E_{NA}|^2}} = \frac{\overline{E_{JM} E_{JM}^* / W^*}}{\overline{|E_{JM} E_{JM}^* / W|^2} + \overline{|E_{JA}|^2}} = W \frac{1}{\left[1 + \frac{1}{JNR_A}\right]}$$

$\uparrow$ $E_{JA} = E_{JM} / W$

$\hat{W} \doteq W$ FOR $JNR_A \gg 1$

(8a)

JAMMER CANCELLATION RATIO CR_o FOR OPEN-LOOP CANCELLER

FROM (8)

$$\hat{W} = W \frac{1}{\left[1 + \frac{1}{JNR_A}\right]} \doteq W\left[1 - \frac{1}{JNR_A}\right] \qquad (1)$$

E_{JR} = RESIDUAL JAMMER SIGNAL AFTER CANCELLATIO

$$= E_{JM} - \hat{W} E_{JA} = E_{JM} - W E_{JA} + \frac{E_{JM}}{JNR_A} \qquad (2)$$

$$= E_{JM} / JNR_A \quad \text{BECAUSE} \quad E_{JM} = W E_{JA}$$

$$\therefore \; CR_o = \frac{\overline{|E_{JM}|^2}}{\overline{|E_{JR}|^2}} = (JNR_A)^2 \qquad (3)$$

EX. $JNR_A = 40dB$

$CR_o = 80\,dB$

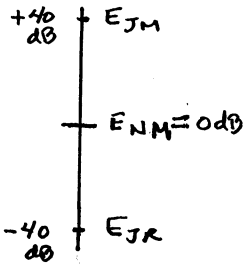

(9)

DIGITAL OPEN-LOOP CANCELLER PERFORMANCE

[NAVG = 4, (J_m/N) = 50 dB, (J_m/S_m) = 20 dB, $J_a = J_m, S_a = 0$]

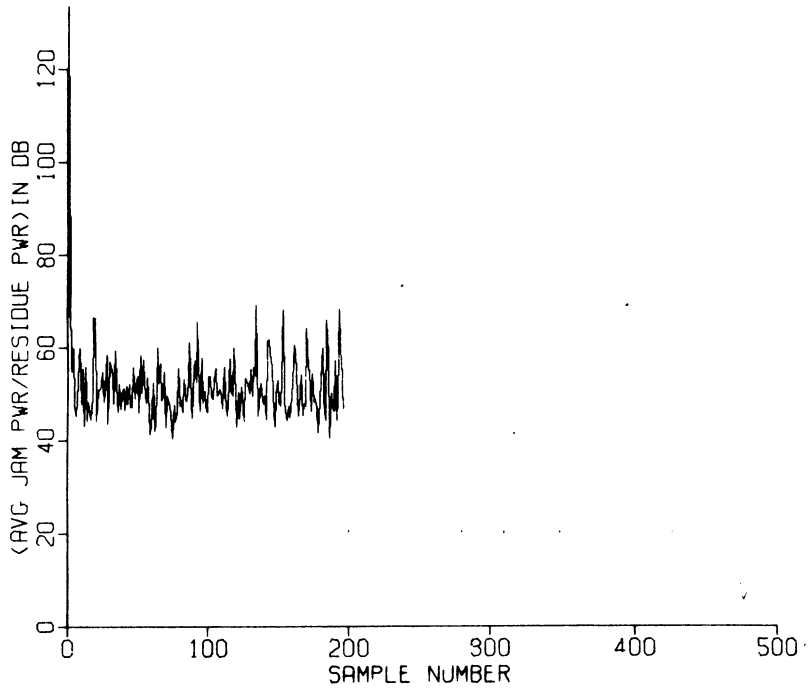

(KRETSCHMER AND LEWIS, IEEE AES, 1/78.)

CARRY OVER NOISE

(10)

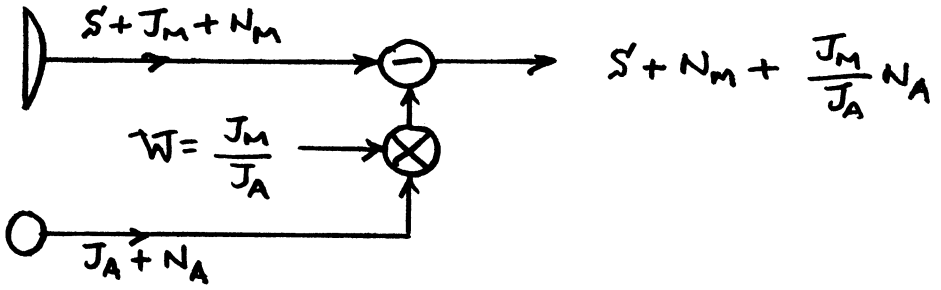

$$SIR_o = \frac{\overline{|S|^2}}{\overline{|N_M|^2} + \left|\frac{J_M}{J_A}\right|^2 \overline{|N_A|^2}} = \frac{\overline{|S|^2}}{\overline{|N_M|^2}\left[1 + \left|\frac{J_M}{J_A}\right|^2\right]} = \frac{SNR_M}{1 + \left|\frac{J_M}{J_A}\right|^2}$$

(FOR $\overline{|N_M|^2} = \overline{|N_A|^2}$)

EX. 1. $J_M = J_A \Rightarrow SIR_o = SNR_M/2 \Rightarrow$ 3dB LOSS.

2. $J_A = \frac{1}{10} J_M \Rightarrow SIR_o = SNR_M/11 \Rightarrow$ 10.4dB LOSS.

3. $J_A = 10 J_M \Rightarrow SIR_o = SNR_M/1.1 \Rightarrow$ 0.4dB LOSS.

EFFECT OF AMPLITUDE AND PHASE ERRORS ON JAMMER CANCELLATION

(11)

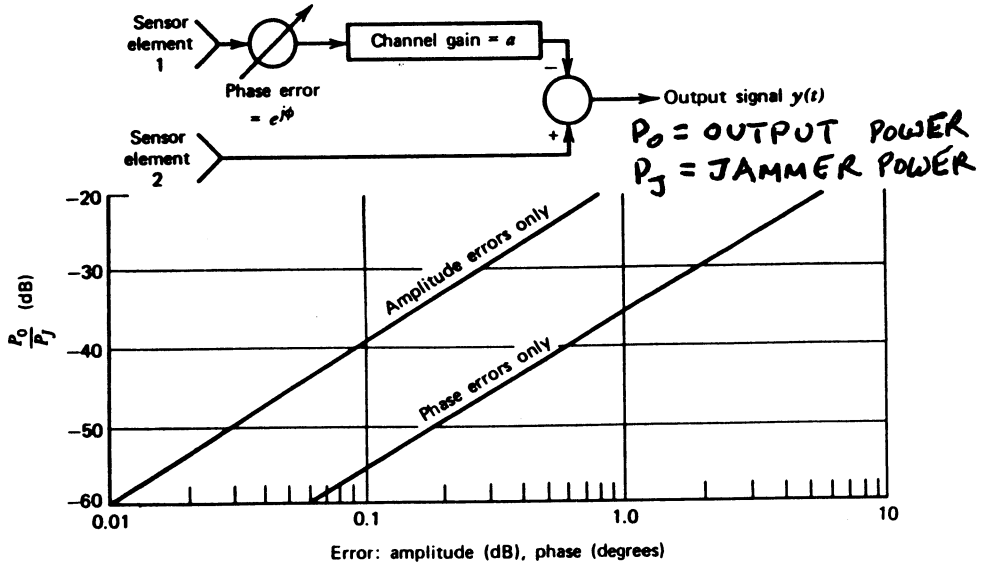

(FROM MONZINGO AND MILLER)

TRACKING ERROR LIMITATION ON CANCELLATION C

(12)

$C = \sigma^2$ IN dB

$\sigma^2 = \sigma_A^2 + \sigma_\phi^2$

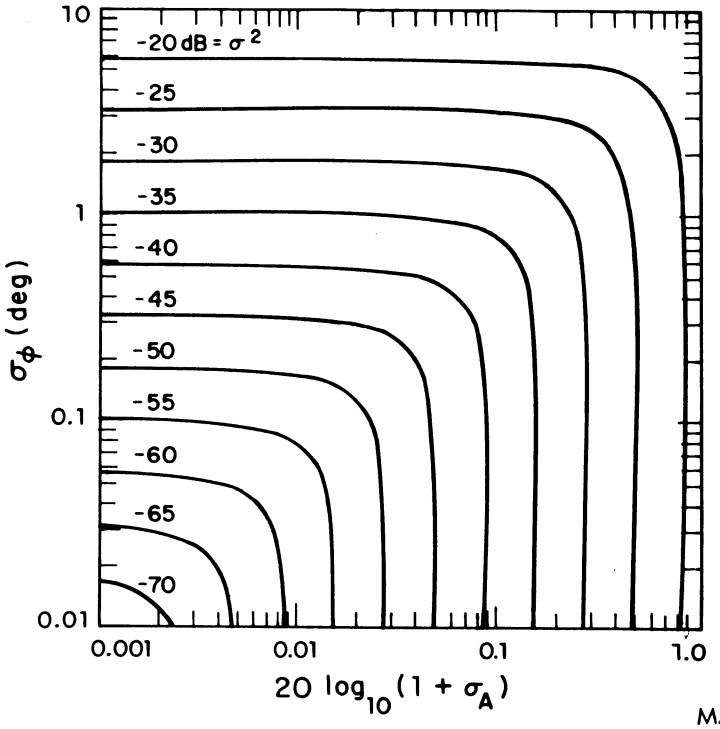

FOR $CR_0 = 40dB$

ϕ	A
0.6°	0.0 dB
0.0°	0.09 dB
0.4°	0.06 dB

MAYHAN, LINCOLN LAB.
REPORT 1978-1
FEB. 17, 1978

$CR_0 = 20 \log_{10} \sigma^2$

(13)

CASE OF DIFFERENT TIMES OF ARRIVAL, τ, FOR MAIN AND AUXILIARY SIGNALS

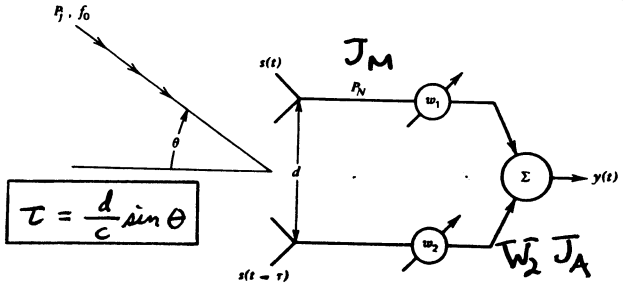

(AFTER MONZINGO AND MILLER)

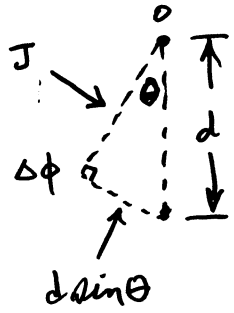

$$\Delta\phi = 2\pi \frac{d \sin\theta}{\lambda_0}$$

$$\Delta\phi = \frac{2\pi\tau}{\tau_0} = 2\pi\tau f_0$$

EFFECT OF DIFFERENT TIMES, τ, OF ARRIVAL ON JAMMER CANCELLATION

(14)

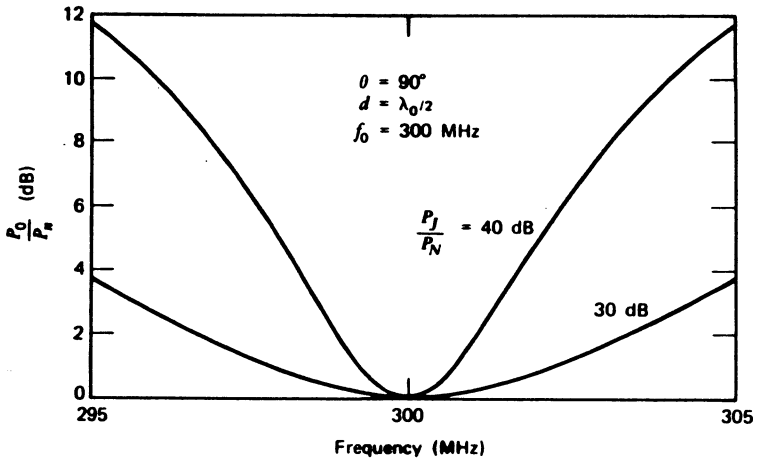

P_O = OUTPUT POWER

P_N = THERMAL NOISE POWER

NORMALIZED FREQ. $= \frac{2\pi d \sin\theta}{\lambda} \cdot \frac{f - f_0}{f}$

(AFTER MONZINGO AND MILLER)

CANCELLATION VS (JAMMER BW, B)$\cdot\tau$ FOR OPTIMUM WEIGHT

(15)

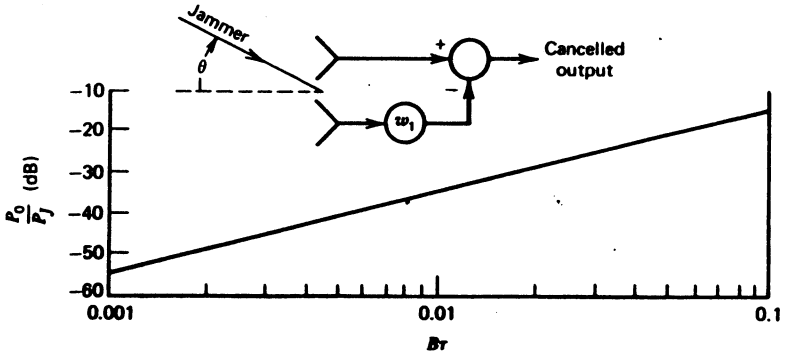

$$W_1 = W_{OPT} = \frac{\sin \pi B \tau}{\pi B \tau}$$

(AFTER MONZINGO AND MILLER)

METHODS FOR COPING WITH WIDEBAND JAMMERS

(16)

- FREQUENCY CHANNELIZATION INTO NARROW BANDS
- EQUAZIZATION
- MULTIPLE LOOP CANCELLER

FREQUENCY CHANNELIZATION

(17)

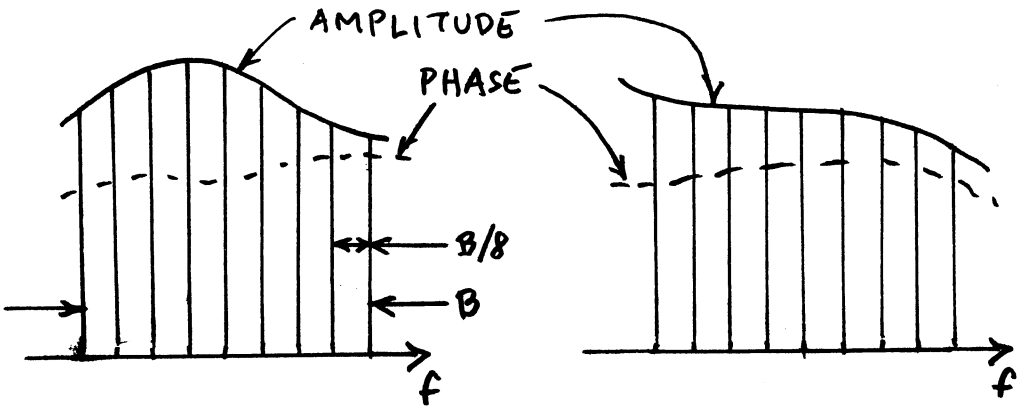

MAIN CHANNEL

AUXILIARY CHANNEL

FREQUENCY CHANNELIZATION USING FFT

(18)

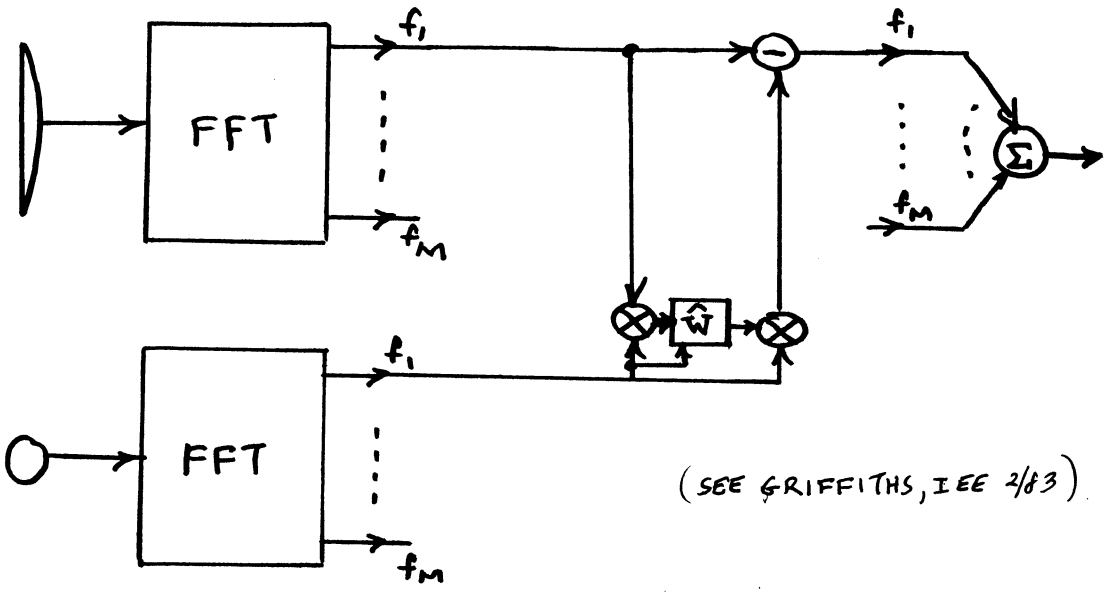

(SEE GRIFFITHS, IEE 2/83)

(19)

EQUALIZATION FILTER TO CORRECT DIFFERENCE BETWEEN MAIN AND AUXILIARY CHANNEL

MAIN CHANNEL

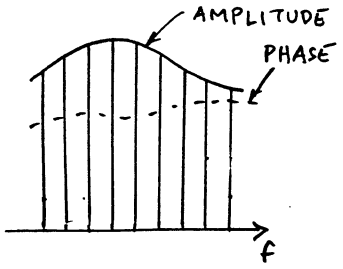

AUXILIARY CHANNEL

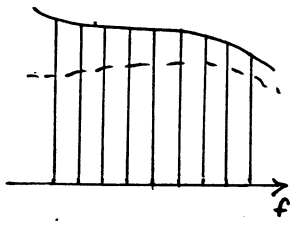

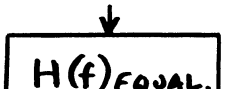

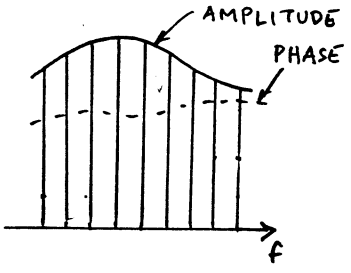

USE OF EQUALIZER TO HANDLE WIDEBAND SIGNAL CASE

(20)

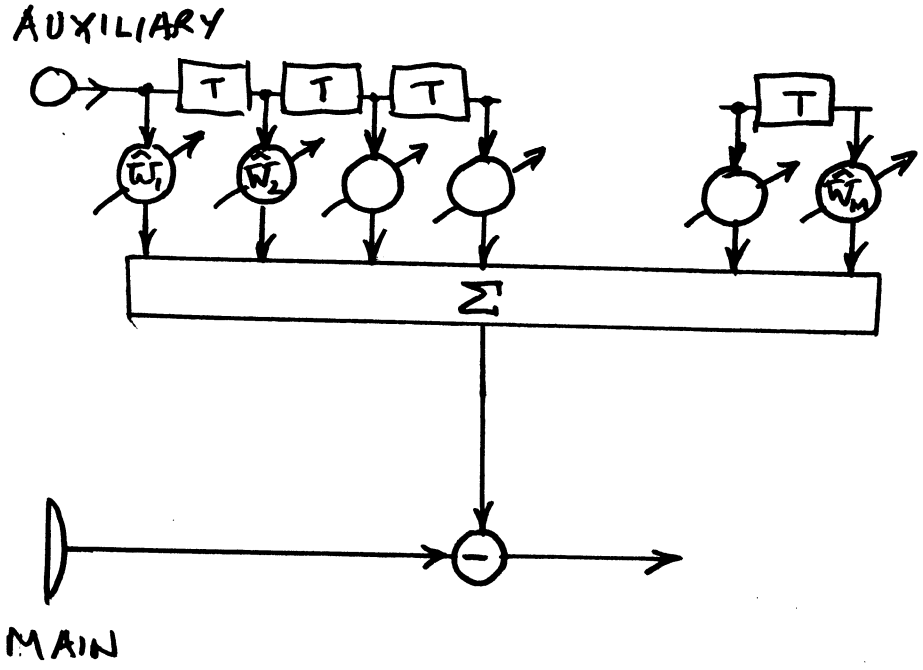

MULTIPLE LOOP CANCELLER

(21)

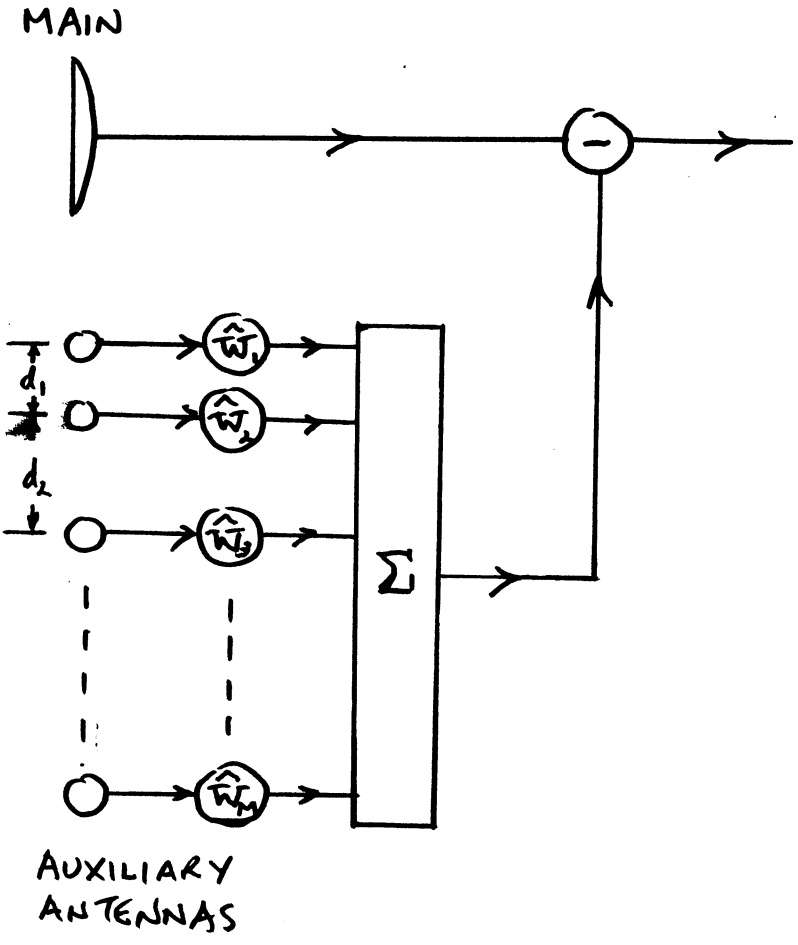

MOVEMENT OF SIDELOBE NULL WITH CARRIER FREQUENCY

(22)

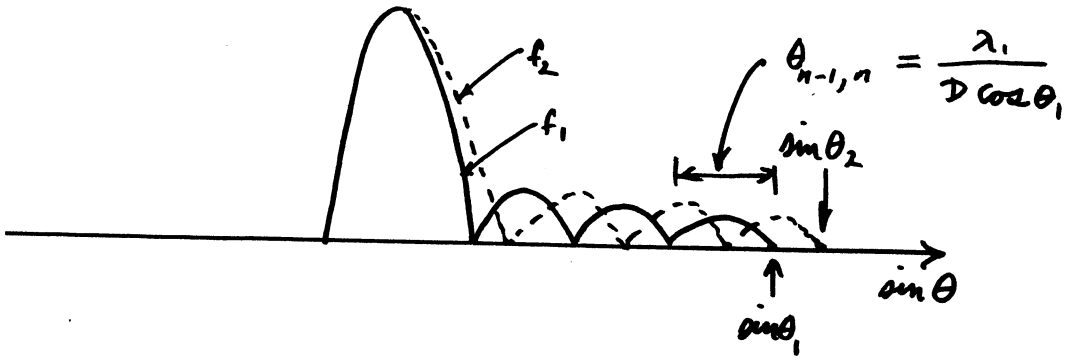

$$\sin\theta_1 = \frac{n\lambda_1}{D}$$

$$\sin\theta_2 = \frac{n\lambda_2}{D} = \frac{n(\lambda_1+\Delta\lambda)}{D} = \frac{n\lambda_1}{D} + \frac{n\Delta\lambda}{D} = \sin\theta_1 + \frac{n\Delta\lambda}{D}$$

$$\sin\theta_2 - \sin\theta_1 = \frac{n\Delta\lambda}{D} \qquad \Delta\theta\cos\theta_1 = \frac{n\Delta\lambda}{D}$$

$$\frac{\Delta\theta}{\theta_{n-1,n}} = \frac{n\Delta\lambda}{D\cos\theta_1}\,\frac{D\cos\theta_1}{\lambda_1} = \frac{n\Delta\lambda}{\lambda_1} = \frac{\Delta\lambda}{\lambda_1}\,\frac{D\sin\theta_1}{\lambda_1} = \frac{\Delta f}{f_1}\,\frac{\sin\theta_1}{\theta_3}$$

WHERE $\theta_3 \doteq \lambda/D \equiv$ 3dB BEAMWIDTH AT BORESIGHT.

N_L = NO. OF SLC LOOPS REQUIRED

$$\boxed{N_L \doteq 2\,\frac{\Delta f}{f_1}\,\frac{\sin\theta_1}{\theta_3}}$$

Ex. $\Delta f = 100\,MHz$, $f_1 = 1GHz$, $\theta_1 = 30°$, $\theta_3 = 20\,mrad$.
$\Rightarrow N_L \doteq 5$.

(23)

LINEAR SINGLE-LOOP FEEDBACK SIDELOBE CANCELLER (SLC)

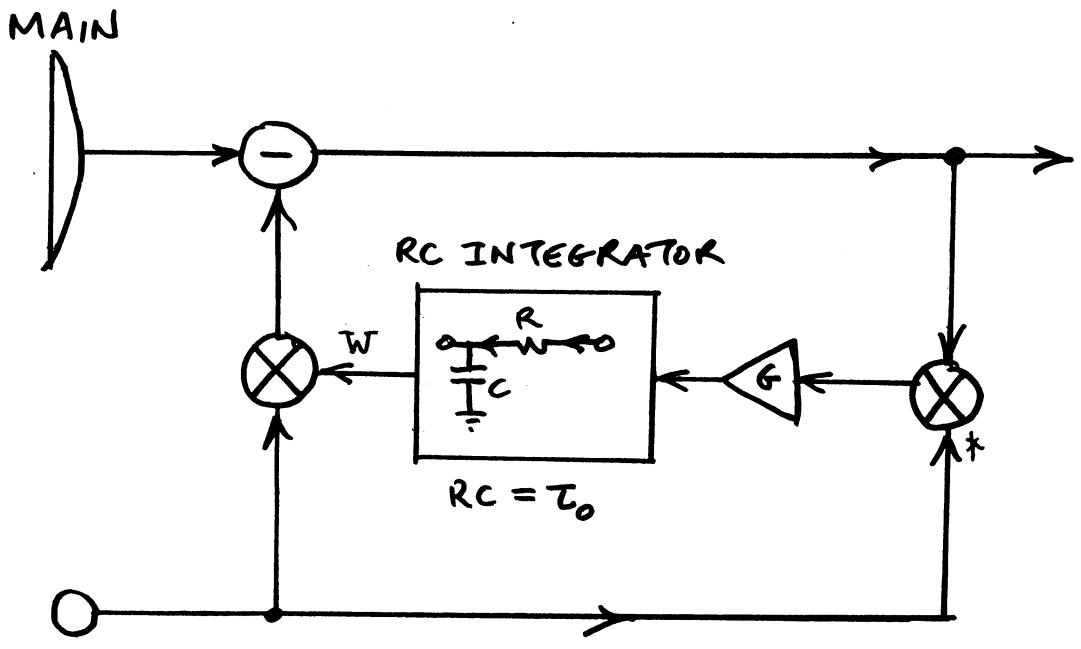

SEMINAL HOWELLS' SLC PATENT

(24)

Aug. 24, 1965 P. W. HOWELLS 3,202,990

INTERMEDIATE FREQUENCY SIDE-LOBE CANCELLER

Filed May 4, 1959 2 Sheets-Sheet 1

FIG. 1a.

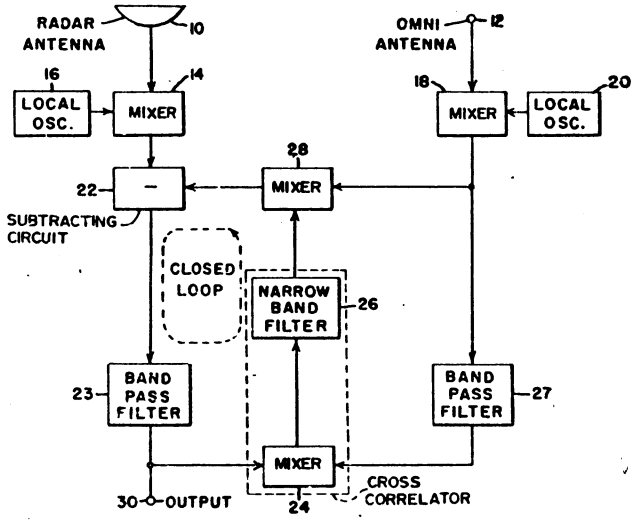

(25)

APPROXIMATE DERIVATION OF CANCELLATION FOR SINGLE-LOOP FEEDBACK SLC

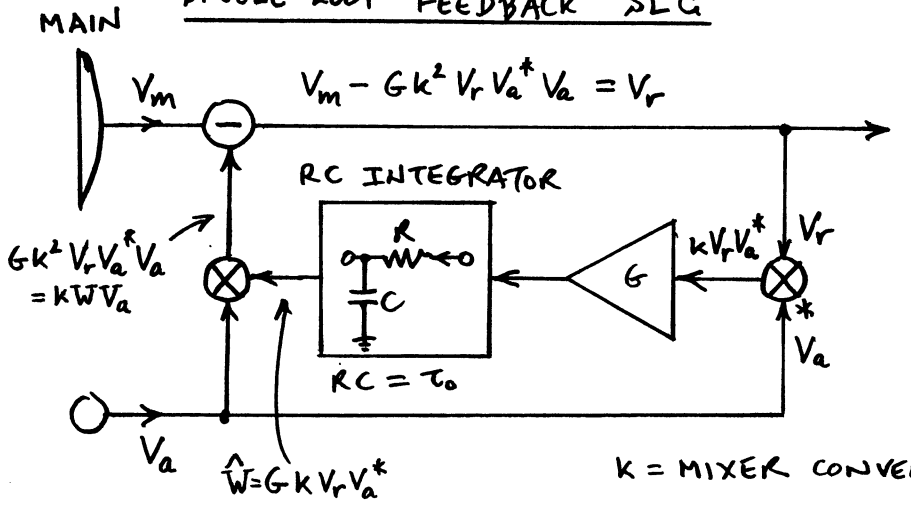

K = MIXER CONVERSION FACTOR

$$V_r = V_m - Gk^2 V_r V_a^* V_a \quad (1)$$

$$V_m = V_r + Gk^2 V_r V_a^* V_a = V_r\left[1 + \underbrace{Gk^2|V_a|^2}\right] \quad (2)$$

$$\boxed{V_m/V_r = [1 + G_L] \doteq G_L} \quad \text{FOR } G_L \gg 1 \quad (3)$$

G_L = LOOP GAIN $= Gk^2|V_a|^2$ (2a)

CR = CANCELLATION RATIO

$$\boxed{CR = |V_m|^2/|V_r|^2 = [1 + G_L]^2 \doteq G_L^2} \quad (4)$$

EX. FOR G_L = 30dB CR = 30dB.

TRANSIENT ANALYSIS FOR SINGLE-LOOP SLC

(26)

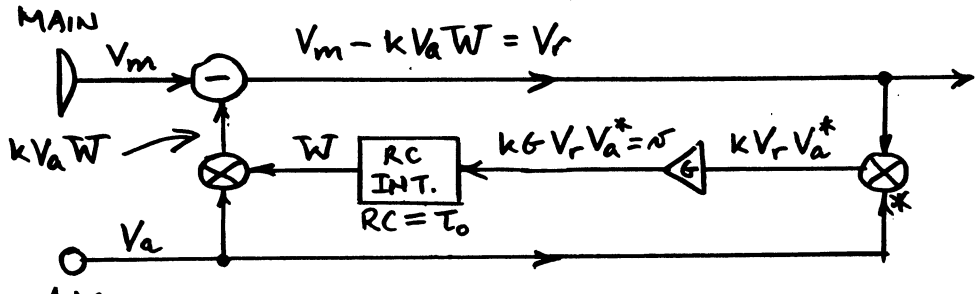

$$\tau_0 \frac{dW}{dt} + W = \bar{\nu} = kG\overline{V_rV_a^*} = kG\overline{(V_m - kV_aW)V_a^*} = kG\overline{V_mV_a^*} - \underbrace{k^2G|V_a|^2}_{G_L}W \quad (1)$$

$$\tau_0 \frac{dW}{dt} + W(1+G_L) = \underbrace{kG\overline{V_mV_a^*}}_{h}$$

$$\frac{dW}{dt} + W\underbrace{\left(\frac{1+G_L}{\tau_0}\right)}_{\alpha} = \frac{h}{\tau_0}$$

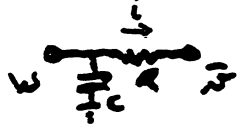

$$\bar{\nu} = iR + \frac{\int i\,dt}{C}$$

$$= iR + W$$

$$\frac{\int i\,dt}{C} = W \Rightarrow i = \frac{C\,dW}{dt} = RC\frac{dW}{dt} + W$$

$$\frac{dW}{dt} + \alpha W = h/\tau_0 \quad \text{WHERE} \quad \alpha = \frac{1+G_L}{\tau_0}, \quad h = kG\overline{V_mV_a^*}$$

$$\boxed{W = W_S\left(1 - e^{-t/\tau_L}\right)}$$

W_S = STEADY STATE WEIGHT
$= h/\alpha\tau_0 = h/(1+G_L)$

$$\boxed{W_S = kG\overline{V_mV_a^*}/(1+G_L)}$$

τ_L = LOOP TIME CONSTANT

$$\boxed{\tau_L = \frac{\tau_0}{1+G_L} = \frac{1}{\alpha}}$$

(26a)

SINGLE LOOP FEEDBACK SLC WITH RC INTEGRATOR EQUIVALENT TO TYPE 0 FOLLOWER SERVO

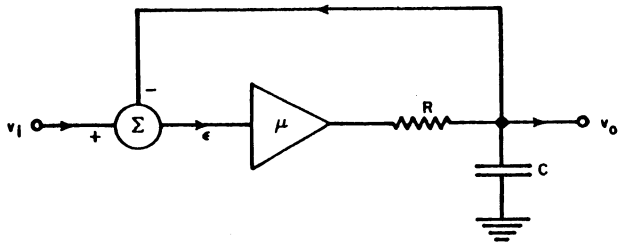

(SEE GABRIEL, PROC. IEEE, FEB. '76, pp239-272)

MORE EXACT DERIVATION FOR STEADY STATE CR (27)

STEADY STATE RESIDUE $\overline{|V_r|^2}$ GIVEN BY:

$$\overline{|V_r|^2} = \overline{|V_{rs}|^2} = \overline{|V_m - k W_s V_a|^2} = \overline{|V_m|^2} + k^2 |W_s|^2 \overline{|V_A|^2} - 2Re\left[k\overline{V_m V_a^*} W_s^*\right] \quad (1)$$

BUT $W_s = \dfrac{kG\overline{V_m V_a^*}}{1+G_L} = \dfrac{kG\overline{|V_a|^2}}{1+G_L}\dfrac{\overline{V_m V_a^*}}{\overline{|V_a|^2}} = \dfrac{k^2 G\overline{|V_a|^2}}{k(1+G_L)}\dfrac{\overline{V_m V_a^*}}{\overline{|V_a|^2}} = \dfrac{G_L}{1+G_L}\dfrac{\rho\sqrt{\overline{|V_m|^2}\,\overline{|V_a|^2}}}{k}\dfrac{1}{\overline{|V_a|^2}}$

WHERE ρ = CORRELATION COEFFICIENT BETWEEN V_m AND V_a

$$= \overline{V_m V_a^*} \Big/ \sqrt{\overline{|V_m|^2}\,\overline{|V_a|^2}} \quad (2) \qquad (3b)$$

$$\therefore |W_s|^2 = \frac{\rho^2|\rho|^2}{k^2}\frac{\overline{|V_m|^2}\overline{|V_a|^2}}{(\overline{|V_a|^2})^2} \quad (3) \quad \text{and} \quad W_s = \frac{\rho}{k}\frac{\overline{V_m V_a^*}}{\overline{|V_a|^2}} \quad \text{WHERE} \quad \rho = \frac{G_L}{1+G_L}$$

$$\therefore \overline{|V_{rs}|^2} = \overline{|V_m|^2} + \rho^2|\rho|^2\overline{|V_m|^2} - 2k\,Re\left[\overline{V_m V_a^*}\frac{\rho}{k}\frac{\overline{V_m^* V_a}}{\overline{|V_a|^2}\,\overline{|V_m|^2}}\right]\overline{|V_m|^2} \quad (3a)$$

$$= \overline{|V_m|^2} + \rho^2|\rho|^2\overline{|V_m|^2} - 2\rho|\rho|^2\overline{|V_m|^2}$$

$$\boxed{\overline{|V_{rs}|^2} = \overline{|V_m|^2}\left[1 + \rho^2|\rho|^2 - 2\rho|\rho|^2\right]} \quad (4)$$

$$\boxed{CR = \frac{\overline{|V_m|^2}}{\overline{|V_{rs}|^2}} = \left[1 + \rho^2|\rho|^2 - 2\rho|\rho|^2\right]^{-1}} \quad (5)$$

CR FOR SPECIAL CASES: (L/SSLC) (28)

- FOR $\rho = 1$

$$\boxed{CR = (1+G_L)^2} \quad (1)$$ EX. FOR $G_L = 27\,dB$, $CR \doteq 27\,dB$.

- FOR $G_L = \infty$

$$\boxed{CR = \left[1 - |\rho|^2\right]^{-1}} \quad (2)$$ EX. FOR $\rho = 0.999$, $CR \doteq 27\,dB$

- FOR $G_L = \infty$ AND $JNR_m \gg 1$ AND $JNR_a \gg 1$ (SEE 29-1 to 29-5b)

$$CR \doteq JNR_E \quad (3)$$

WHERE $$\boxed{JNR_E = \frac{1}{\frac{1}{JNR_m} + \frac{1}{JNR_a}}} \quad (3a)$$

EX. $JNR_m = JNR_a = 30dB$
$JNR_E = 27dB$
$CR = 27dB$

- FOR $G_L \gg 1$, $JNR_m \gg 1$, $JNR_a \gg 1$

$$\boxed{CR \doteq \left[\frac{1}{JNR_E} + \frac{1}{G_L^2}\right]^{-1}} \quad (4)$$

EX. $JNR_E = 27dB$ $G_L = 27dB$
$CR = 24dB$

(4) FOLLOWS FROM (28-5), (28-3a) and (31-1).

CR VS ρ FOR $G_L = \infty$

(28a)

L/SSLC CASE

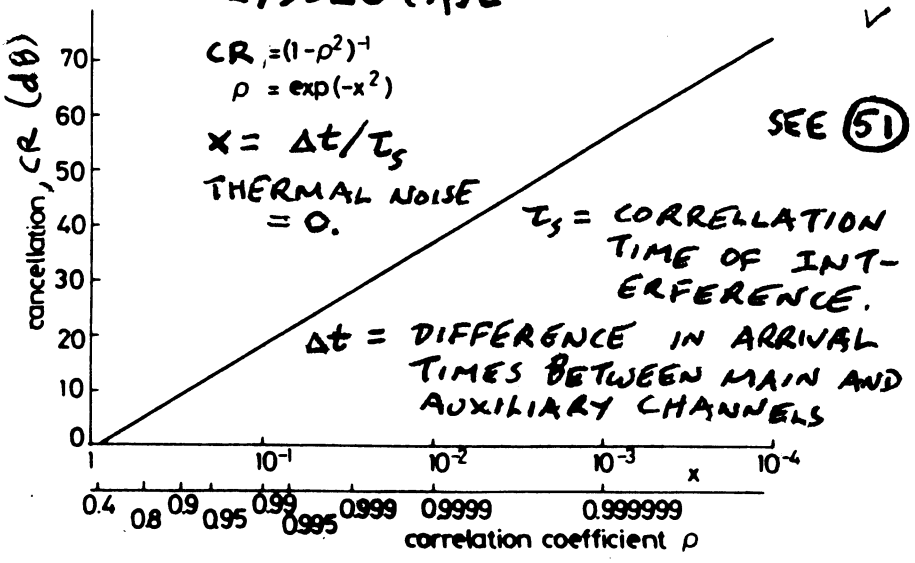

(AFTER FARINA AND STUDER, IEE PROC., PT. F, 2/82)

(28aa)

LINEAR SINGLE-LOOP SLC (L/SSLC)

FROM (27-5)

$$CR = \frac{\overline{|V_m|^2}}{\overline{|V_{rs}|^2}} = \left[1 + \rho^2|\rho|^2 - 2\rho|\rho|^2\right]^{-1} = \left[1 + |\rho|^2\rho(\rho-2)\right]^{-1} \qquad (1)$$

FROM (31-1)

$$|\rho|^2 \doteq 1 - \frac{1}{JNR_E} \qquad (2)$$

FROM (27)

$$\rho(\rho-2) = \frac{G_L}{1+G_L}\left(\frac{G_L}{1+G_L} - 2\right) = \left(\frac{1}{1+\frac{1}{G_L}}\right)\left(\frac{1}{1+\frac{1}{G_L}} - 2\right) \doteq \left(1 - \frac{1}{G_L} + \frac{1}{G_L^2}\right)\left(1 - \frac{1}{G_L} + \frac{1}{G_L^2} - 2\right)$$

$$= \left(1 - \frac{1}{G_L} + \frac{1}{G_L^2}\right)\left(-1 - \frac{1}{G_L} + \frac{1}{G_L^2}\right) = -1 + \cancel{\frac{1}{G_L}} - \cancel{\frac{1}{G_L^2}} - \cancel{\frac{1}{G_L}} + \cancel{\frac{1}{G_L^2}} - \frac{1}{G_L^3} + \frac{1}{G_L^3} - \frac{1}{G_L^4} + \frac{1}{G_L^4}$$

$$\doteq -1 + \frac{1}{G_L^2} = -\left(1 - \frac{1}{G_L^2}\right) \qquad (3)$$

$$\therefore \quad CR^{-1} = 1 - \left(1 - \frac{1}{JNR_E}\right)\left(1 - \frac{1}{G_L^2}\right) \doteq 1 - 1 + \frac{1}{JNR_E} + \frac{1}{G_L^2} = \frac{1}{JNR_E} \quad \frac{1}{G_L^2} \qquad (4)$$

$$CR = \left[\frac{1}{JNR_E} + \frac{1}{G_L^2}\right]^{-1} \qquad (5)$$

BUT FROM (36-4)

$$G_L = G_o(1 + JNR_a) \qquad (1)$$

WHERE G_o = CLOSED LOOP GAIN WHEN NO JAMMER PRESENT (SEE (36-2))

LET $G_o = 1 \qquad (2)$

THEN

$$G_L = (1 + JNR_a) \qquad (3)$$

$$G_L \doteq JNR_a \quad \text{FOR } JNR_a >> 1 \qquad (4)$$

LET $JNR_m = JNR_a \qquad (5)$

THEN FROM (31-2)

$$JNR_E = JNR_a/2 \qquad (6)$$

AND

$$\boxed{CR \doteq \left[\frac{2}{JNR_a} + \frac{1}{(JNR_a)^2}\right]^{-1}} \qquad (7)$$

FOR $JNR_m = JNR_a >> 1$, $G_o = 1$

OR

$$\boxed{CR \doteq \frac{JNR_a}{2}} \qquad (8)$$

EX. $JNR_a = 40dB$, $CR = 37dB$

LIMITING CASE FOR $|\rho|^2$ (29)

LET

$$V_a = V_{Ja} + V_{na} \qquad (1)$$

$$V_m = V_{Jm} + V_{nm} \qquad (2)$$

WHERE V_{nm} AND V_{na} ARE THERMAL NOISE IN MAIN AND AUXILIARY WHILE V_{Jm} AND V_{Ja} ARE JAMMER SIGNALS IN MAIN AND AUXILIARY CHANNELS

THEN

$$\rho = \frac{\overline{V_m V_a^*}}{\sqrt{|V_m|^2 |V_a|^2}} = \frac{\overline{(V_{Jm} + V_{nm})(V_{Ja}^* + V_{na}^*)}}{\sqrt{(|V_{Jm}|^2 + |V_{nm}|^2)(|V_{Ja}|^2 + |V_{na}|^2)}} \qquad (3)$$

$$= \frac{\overline{V_{Jm} V_{Ja}^*} + 0}{\sqrt{|V_{Jm}|^2 |V_{Ja}|^2}\sqrt{\left(1 + \frac{1}{JNR_m}\right)\left(1 + \frac{1}{JNR_a}\right)}} \qquad (4)$$

WHERE

$$JNR_m = \overline{|V_{Jm}|^2}/\overline{|V_{nm}|^2} \qquad (5a)$$

$$JNR_a = \overline{|V_{Ja}|^2}/\overline{|V_{na}|^2} \qquad (5b)$$

LET $V_{Ja} = J_a$ AND $V_{Jm} = WJ_a \qquad (6)$

LIMITING CASE FOR $|\rho|^2$ (CONT.)

LET $\rho_\infty = \rho$ FOR $JNR_m = JNR_a = \infty$

$$\rho_\infty = \frac{\overline{V_{JM} V_{Ja}^*}}{\sqrt{\overline{|V_{JM}|^2}\,\overline{|V_{Ja}|^2}}}$$

$$\rho_\infty = \frac{\overline{W J_a J_a^*}}{\sqrt{\overline{|W|^2}\,\overline{|J_a|^2}\,\overline{|J_a|^2}}} = \frac{W}{\sqrt{\overline{|W|^2}}}$$

$\therefore |\rho_\infty|^2 = 1$

$$\therefore |\rho|^2 = \frac{1}{\left(1+\frac{1}{JNR_m}\right)\left(1+\frac{1}{JNR_a}\right)} \doteq \frac{1}{1+\frac{1}{JNR_m}+\frac{1}{JNR_a}}$$

$$\therefore |\rho|^2 \doteq \frac{1}{1+\frac{1}{JNR_E}} \doteq 1-\frac{1}{JNR_E}$$

LIMITING CASE FOR $|\rho|^2$ (CONT.)

$$\boxed{|\rho|^2 \doteq 1-\frac{1}{JNR_E}} \quad (1)$$

FOR $JNR_m \gg 1$

$JNR_a \gg 1$

WHERE

$$\boxed{JNR_E = \frac{1}{\frac{1}{JNR_m}+\frac{1}{JNR_a}}} \quad (2)$$

EX. $JNR_m = JNR_a = 27dB \Rightarrow JNR_E = 24dB$

$\Rightarrow |\rho| = 0.998$

OPTIMAL WEIGHT FOR SLC

(32)

$$\boxed{(W_s)_{OPT} = \frac{1}{k}\frac{\overline{V_m V_a^*}}{|V_a|^2}} \qquad (1)^*$$

NOTE:

$$W_s\Big|_{G_L=\infty} = (W_s)_{OPT} \qquad (2)$$

SEE (27-36) AND (27-3a)

TO PROVE (1) WE PROCEED AS FOLLOWS. FROM (27-1):

$$\overline{|V_r|^2} = \overline{|V_m - kW_sV_a|^2} = \overline{|V_m|^2} - \overline{V_m k W_s^* V_a^*} - \overline{V_m^* k W_s V_a} + k^2\overline{|W_s|^2|V_a|^2} \quad (3)$$

LET $(W_s)_{OPT} \equiv W_0$ (3a), AND $W_s = W_0 + \Delta W$ (3b)

THEN $$\overline{|V_r|^2} = \overline{|V_m|^2} - kW_0^*\overline{V_m V_a^*} - kW_0\overline{V_m^* V_a} + k^2|W_0|^2\overline{|V_a|^2} + |\Delta|^2\overline{|V_a|^2}k^2 \quad (4)$$

WHERE USE USE WAS MADE OF (1) $\neq f(G_a)$ IN OBTAINING (4).

FROM (4) IT FOLLOWS THAT $\overline{|V_r|^2}$ IS MINIMUM WHEN $|\Delta|^2 = 0$, HENCE W_0 IS THE OPTIMUM WEIGHT.

* NOTE THAT $1/k$ FACTOR NEEDED TO BALANCE OUT k FACTOR OF MIXER ON W_s.

(32a)

JAMMER CANCELLATION RATIO CR_0 FOR FEEDBACK LINEAR SINGLE-LOOP SLL (L/SSLC)

FROM (27-36)

$$W_s = \frac{\beta}{k}\frac{\overline{V_m V_a^*}}{|V_a|^2} = \frac{\beta}{k}\frac{\overline{E_{JM}E_{JA}^*}}{|E_{JA}|^2 + |E_{NA}|^2} = \frac{\beta}{k}\frac{k\overline{W}\,\overline{E_{JA}E_{JA}^*}}{|E_{JA}|^2 + |E_{NA}|^2} \qquad (1)$$

SEE (8)

$$= \beta\overline{W}\frac{1}{1+\frac{1}{JNR_a}} = \overline{W}\left(\frac{G_L}{1+G_L}\right)\frac{1}{1+\frac{1}{JNR_a}} = \overline{W}\left(\frac{1}{1+\frac{1}{G_L}}\right)\left(\frac{1}{1+\frac{1}{JNR_a}}\right) \qquad (2)$$

$$\doteq \overline{W}\left(1-\frac{1}{G_L}\right)\left(1-\frac{1}{JNR_a}\right) \doteq \overline{W}\left[1-\underbrace{\left(\frac{1}{G_L}+\frac{1}{JNR_a}\right)}_{\epsilon}\right] = \overline{W}[1-\epsilon] \qquad (3)$$

HENCE

$$E_{JR} = E_{JM} - k\overline{W}(1-\epsilon)E_{JA} = E_{JM} - E_{JM}(1-\epsilon) = \epsilon E_{JM} \qquad (4)$$

$$\therefore \quad CR_0 = \left|\frac{E_{JM}}{E_{JR}}\right|^2 = \frac{1}{\epsilon^2} = \left[\frac{1}{JNR_a}+\frac{1}{G_L}\right]^{-2} \qquad (5)$$

BUT $G_L \doteq JNR_a$ FOR $G_0 = 1$ AND $JNR_a \gg 1$, SEE (286-4). (6)

$$\therefore \quad \boxed{CR_0 = (JNR_a)^2/4} \quad \text{FOR } G_0 = 1 \text{ AND } JNR_a \gg 1. \qquad (7)$$

EX. $JNR_a = 40dB$, $CR_0 = 74dB$.

Note: USING $G_L = G_0(1+JNR_a)$ YIELDS FOR (5) $CR_0 = JNR_a^2\left(G_0/[1+G_0]\right)^2$ FOR $JNR_a \gg 1$ (8)

JAMMER CANCELLATION RATIO CR_0 FOR L/SSLC, CONT. (326)

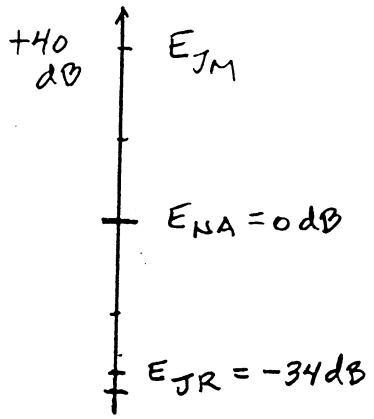

SUMMARY OF TRANSIENT RESPONSE OF SINGLE-LOOP FEEDBACK SLC (NO HARD LIMITING) (33)

τ_L = CLOSED LOOP TIME CONSTANT

τ_0 = OPEN LOOP TIME CONSTANT

G_L = LOOP GAIN

$$\boxed{\tau_L = \frac{\tau_0}{1+G_L}} \quad (1)$$

$$\tau_L \doteq \frac{\tau_0}{G_0\,JNR_a} \qquad \text{FOR } JNR_a \gg 1$$

$$\tau_L \gtrsim 3\tau_s \quad \text{WHERE} \quad \tau_s = \frac{1}{B_s}$$

$$\frac{\tau_0}{G_0\,JNR_a} \gtrsim 3\tau_s \qquad \tau_0 \gtrsim 3\tau_s\,G_0\,JNR_a$$

$$\text{FOR } G_0 = 1 \quad \frac{\tau_0}{JNR_a} \gtrsim 3\tau_s \qquad \tau_0 \gtrsim 3\tau_s\,JNR_a$$

TRANSIENT OUTPUT OF FEEDBACK SLC

(34)

FROM (25) and (26)

$$V_r = V_m - k\,W\,V_a = V_m - k\,W_s\left(1-e^{-t/\tau_L}\right)V_a \quad (1)$$

$$= V_m - k\,W_s V_a + k\,W_s V_a\, e^{-t/\tau_L} \quad (2)$$

BUT STEADY STATE V_r, CALLED V_{rs} IS

$$V_{rs} = V_m - k\,W_s\,V_a \quad (3)$$

HENCE:

$$\boxed{V_r = V_{rs} + k\,W_s\,V_a\,e^{-t/\tau_L}} \quad (4)$$

AND

$$\overline{|V_r|^2} = \overline{|V_{rs}|^2} + k^2\overline{|W_s|^2}\,\overline{|V_a|^2}\,e^{-2t/\tau_L} + 2\,\mathrm{Re}\left(V_{rs}\,k\,\overline{W_s^*}\,\overline{V_a^*}\,e^{-t/\tau_L}\right) \quad (5)$$

WHERE $\overline{|V_{rs}|^2}$ GIVEN BY (27-4).

(35)

LOOP NOISE

"LOOP NOISE" IS THE RANDOMNESS OF W DUE TO τ_L NOT BEING INFINITE. A LARGE RANDOMNESS IN W RESULTS IN CR BEING LESS THAN GIVEN BY (27-5) OR (28-4). IN ORDER FOR CR TO BE GIVEN BY (27-5) IT IS NECESSARY THAT τ_L BE LARGE ENOUGH, SPECIFICALLY THAT $\tau_L \geq 3\tau_s$, $\tau_s = \frac{1}{B_s}$

$$\boxed{2\omega_L \leq \frac{2\pi B_s}{10}} \Rightarrow \boxed{\frac{B_s}{2B_L} = H \geq 10} \quad (1)$$

(WHERE B_L = CLOSED LOOP BW IN HZ)

THAT IS:

2 × CLOSED LOOP BW, $B_L \leq \frac{1}{10}$th SIGNAL BW, B_s (1a)

($\frac{1}{10} \leftrightarrow H$)

WHERE

$$\boxed{\omega_L = \frac{1}{\tau_L} = \frac{1+G_L}{\tau_0}} \quad (2)$$

$\tau_0 = RC$

$G_L \doteq JNR_a$ FOR $G_0 = 1$ & $JNR_a \gg 1$

AND PHYSICALLY H = NUMBER OF INTERFERENCE SAMPLES AVERAGED.

(SEE BRENNAN, PUGH, REED, IEEE AES 3/71)

LOOP NOISE CONSTRAINT ON τ_0

FROM (35-1):

$$\tau_0 \gg \frac{10}{\pi B_s}\left[1 + \underbrace{G_0(1+JNR_a)}_{G_L}\right] \qquad (1)$$

WHERE: G_0 = LOOP GAIN WHEN NO JAMMER PRESENT

$$G_0 = G K^2 \overline{|V_{na}|^2} \qquad (2)$$

$$\tau_L = \frac{\tau_0}{1+G_L} \doteq \frac{\tau_0}{G_0 \cdot JNR_a}$$

DERIVATION:

SUBSTITUTING (35-2) INTO (35-1) YIELDS

$$\frac{1}{\tau_L} = \frac{1+G_L}{\tau_0} \leq \frac{\pi B_s}{10} \quad \text{or} \quad \tau_0 \gg (1+G_L)\frac{10}{\pi B_s} \qquad (3)$$

POWER

BUT $G_L = G K^2 \overline{|V_a|^2}$ SEE (26-1).

THUS FROM (29-1): $G_L = G K^2 \overline{|V_{ja} + V_{na}|^2} = \underbrace{G K^2 \overline{|V_{na}|^2}}_{G_0}\left[1 + JNR_a\right] = G_0\left[1+JNR_a\right]$ (4)

VOLTAGE

EX. $B_s = 5\,MHz$, $JNR_a = 10^4$, AND G PICKED SO THAT $G_0 = 1$,

THEN $\tau_0 = 6{,}370\,\mu s$, $B_0 = 25\,Hz$ = OPEN LOOP BW $= \frac{1}{2\pi\tau_0}$,

$\tau_L = 0.637\,\mu s$

HERE $\tau_0 = \frac{10}{\pi B_s}(1+G_0)$ $\quad \tau_L = \frac{\tau_0}{1+G_0} = \frac{10}{\pi B_s} \Rightarrow \tau_L \gg 3\tau_s$ $\quad \tau_s = 1/B_s$

$G_L = JNR_a$ FOR $G_0 = 1$, $JNR_a \gg 1$

$\tau_0 / JNR_a \cdot G_0 \geq 3\tau_s$

(36a)

VARIATION OF τ_L FOR FIXED τ_0 AND $G_0 = 1$ FOR L/SSCL

FROM (36-1)

$$\tau_0 \gg \frac{10}{\pi B_s}\left[1 + \underbrace{G_0(1+JNR_a)}_{G_L}\right] \qquad (1)$$

$$\tau_0 = \frac{10}{\pi B_s}\left[2 + (JNR_a)_{MX}\right] \quad \text{FOR } G_0 = 1 \qquad (2)$$

FROM (33-1)

$$\tau_L = \frac{\tau_0}{1+G_L} = \frac{10}{\pi B_s}\frac{\left[2+(JNR_a)_{MX}\right]}{\left[1+(1+JNR_a)\right]} \quad \text{FOR } G_0 = 1 \qquad (3)$$

$$\boxed{\tau_L \doteq \frac{10}{\pi B_s}\frac{(JNR_a)_{MX}}{JNR_a}} \quad \text{FOR } G_0 = 1,\ JNR_a \gg 1 \qquad (4)$$

ALTERNATELY

$$\boxed{\tau_L = \frac{\tau_0}{2 + JNR_a} \doteq \frac{\tau_0}{JNR_a}} \quad \text{FOR } G_0 = 1,\ JNR_a \gg 1 \qquad (5)$$

BROOKNER, E. 11/9/92

USE OF AGC CONTROL OF G_o TO SPEED UP τ_L FOR L/SSCL

FROM (33-1) AND (36-4)

$$\tau_L = \frac{\tau_o}{1+G_L} = \frac{\tau_o}{G_o[1+JNR_a]} \qquad (1)$$

IF VIA AGC WE MAKE

$$G_o = \frac{(JNR_a)_{MX}}{JNR_a} \qquad (2)$$

THE (1) BECOMES

$$\tau_L = \frac{\tau_o}{\frac{(JNR_a)_{MX}}{JNR_a}[1+JNR_a]} \doteq \frac{\tau_o}{(JNR_a)_{MX}} \quad \text{FOR } JNR_a \gg 1 \qquad (3)$$

USING (36a-2) YIELDS

$$\boxed{\tau_L \doteq \frac{10}{\pi B_s}\frac{2+(JNR_a)_{MX}}{(JNR_a)_{MX}} \doteq \frac{10}{\pi B_s}} \quad \text{FOR } JNR_a \gg 1 \qquad (4)$$

τ_L VERSUS JNR_a FOR LINEAR SINGLE-LOOP SLC (L/SSLC) (37)

USING EXAMPLE OF (36) τ_L VARIES AS SHOWN IN TABLE:

I.E. FOR $\tau_o = 6{,}370\,\mu s$, $G_o = 1$, $B_o \equiv \omega_o/2\pi = 25$ Hz, $H = 10$

JNR_a (dB)	τ_L (μs)	G_L (dB)	t_4 (μs)	CR_o (dB)	CR (dB)
40	0.637	80	3.38	74	37
30	6.36	60	26.4	54	27
20	62.5	40	187	34	17
10	531	20	979	16	7
0	2123	0	–	–	–

WHERE CR_o = CANCELLATION OF JAMMER IN MAIN CHANNEL.

$CR_o \doteq G_L^2/4$ (1) ; FOLLOWS FROM (28-4)

$t_A\big|_{A=4} = t_4$ = TIME FOR JAMMER TO BE SUPPRESSED A FACTOR OF 4 (6dB) BELOW THERMAL NOISE OF MAIN CHANNEL. NOISE OF AUXILIARY CHANNEL ASSUMED EQUAL TO THAT OF MAIN CHANNEL. THUS JAMMER A FACTOR A BELOW $\overline{|V_{nm}|^2} + \overline{|V_{na}|^2}$, THE TOTAL THERMAL NOISE IN MAIN CHANNEL.

$$\boxed{t_A = \tau_L \ln\sqrt{A\,JNR_m}} \quad (1) \qquad \text{BECAUSE } V_{jm}(t) = V_{jm}e^{-t/\tau_L}$$

WHERE A = FACTOR (AS POWER RATIO) THAT JAMMER IS TO BE SUPPRESSED BELOW $\overline{|V_{nm}|^2} = N_M$. HERE A = 4.

TRANSIENT RESPONSE FOR L/SSLC

(38)

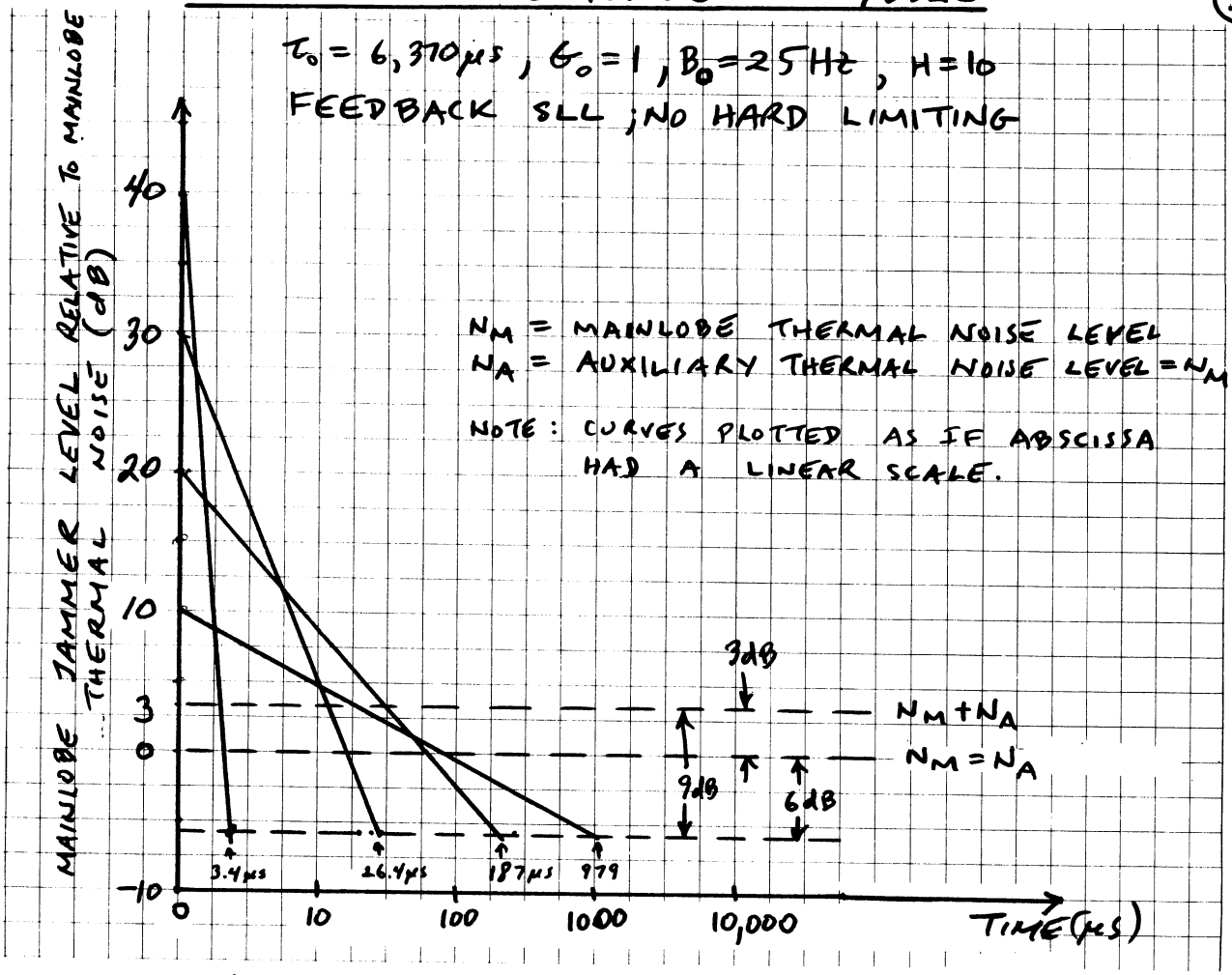

DYNAMIC RANGE PROBLEM

(39)

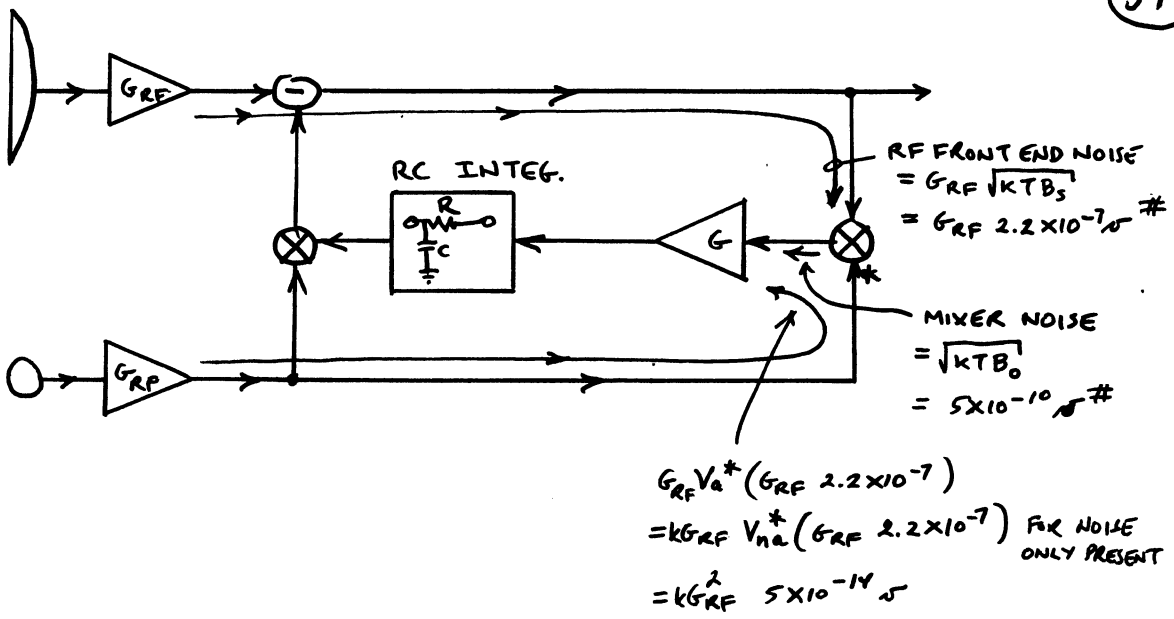

REQUIRE THAT FRONT END NOISE $\gg$ MIXER NOISE, I.E.,

$$kG_{RF}^2\ 5\times10^{-14} \gg 5\times10^{-10}$$

OR $$kG_{RF}^2 \gg 10^4 \qquad (1)$$

ASSUMED $T = 725^\circ K$, $B_0 = 25Hz$, $B_s = 5MHz$.

HARD-LIMITED (HL) SINGLE-LOOP SLC (SSLC)

(40)

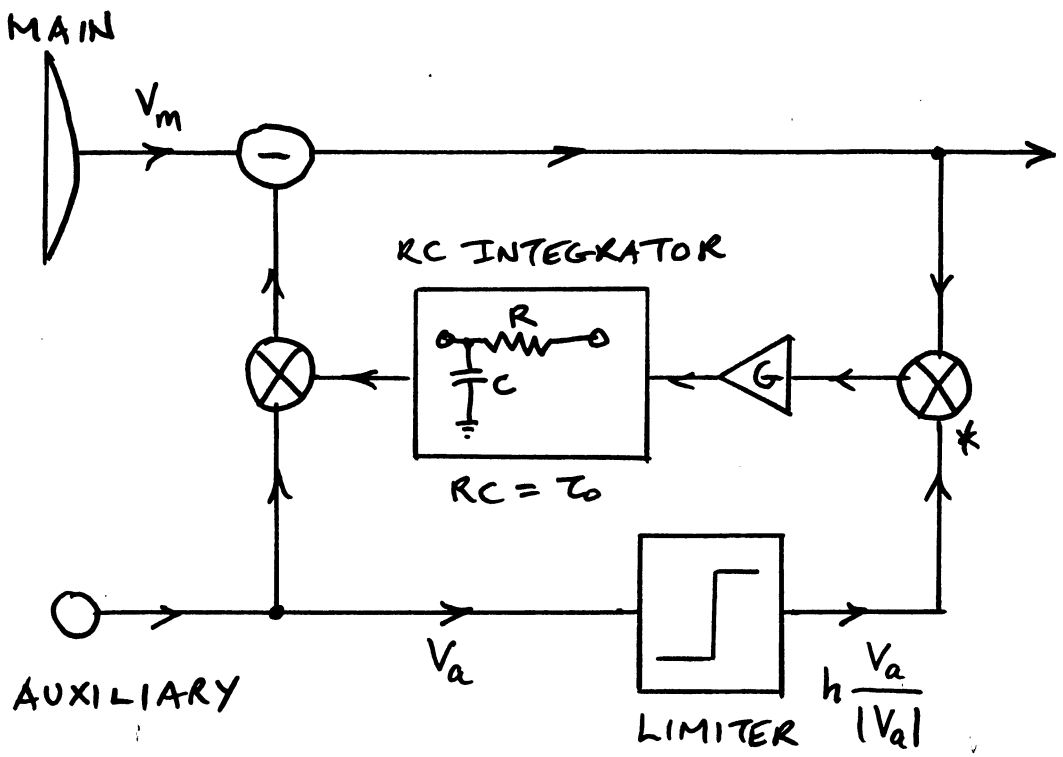

SIMPLE ANALYSIS OF SSLC WITH HARD LIMITING

(41)

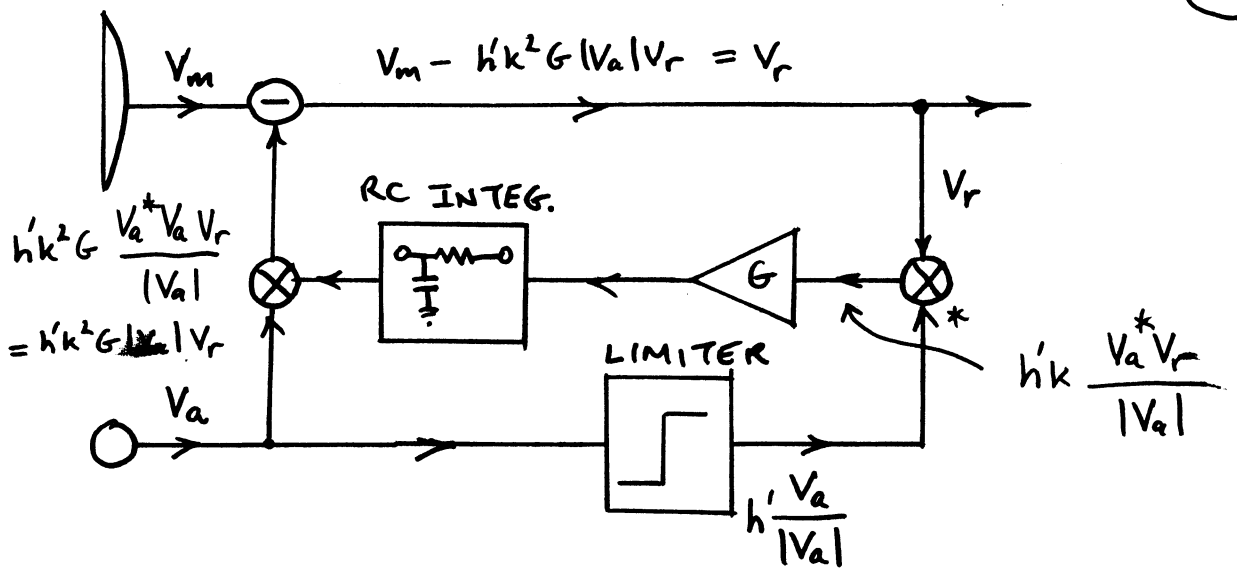

$$V_r = V_m - h'k^2G|V_a|V_r \qquad (1)$$

$$V_m = V_r\left(1 + \underbrace{h'k^2G|V_a|}_{G_L}\right) = V_r(1+G_L) \qquad (2)$$

$$\boxed{CR = \frac{|V_m|^2}{|V_r|^2} = (1+G_L)^2 \doteq G_L^2} \qquad (3)$$

COMPARE WITH (25-4).

TRANSIENT ANALYSIS FOR SSLC WITH HARD LIMITING (42)

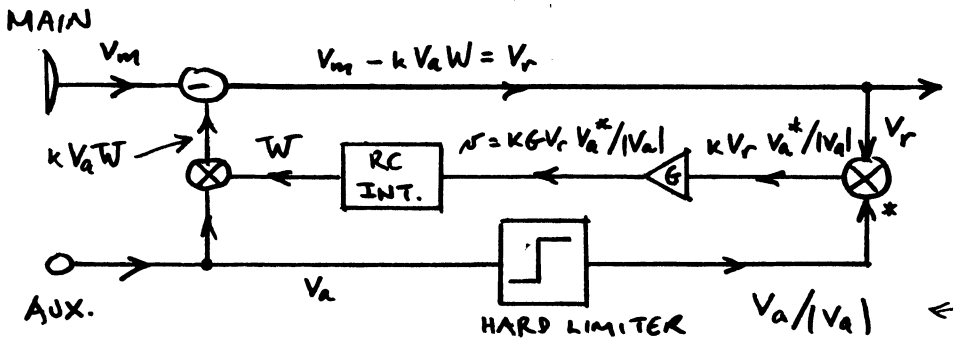

$$\tau_0 \frac{dW}{dt} + W = \bar{\nu} = KG\overline{V_r V_a^*/|V_a|} = KG\overline{(V_m - kV_aW)V_a^*/|V_a|} = KG\frac{\overline{V_m V_a^*}}{|V_a|} - \frac{\overline{KG|V_a|^2}}{|V_a|}W \quad (1)$$

$$\tau_0 \frac{dW}{dt} + W\underbrace{\left(1 + \underbrace{k^2G|V_a|}_{G_L}\right)}_{\alpha} = \underbrace{KG\overline{V_m V_a^*/|V_a|}}_{h} \quad (2) \qquad G_L = k^2G|V_a| = \text{LOOP GAIN} \quad (3)$$

$$G_L = k^2G|V_a| \quad (2a)$$

$$\frac{dW}{dt} + W\left(\frac{1+G_L}{\tau_0}\right) = \frac{h}{\tau_0} \quad (4) \qquad \alpha = \frac{1+G_L}{\tau_0} \quad (4a) \qquad h = KG\overline{V_m V_a^*/|V_a|} \quad (4b)$$

$$\boxed{W = W_S\left(1 - e^{-t/\tau_L}\right)} \quad (5), \qquad W_S = \text{STEADY STATE WEIGHT} = h/\alpha\tau_0 = h/(1+G_L) \quad (5a)$$

τ_L = LOOP TIME CONSTANT.

$$\boxed{\tau_L = \frac{\tau_0}{1+G_L} = \frac{1}{\alpha}} \quad (6)$$

$$\boxed{W_S = KG\overline{V_m V_a^*/[|V_a|(1+G_L)]}} \quad (7)$$

JAMMER CANCELLATION RATIO CR_0 FOR HL/SSLC (42a)

NEED TO CALCULATE ERROR ϵ IN W_S OF (42-7), I.E.,

$$W_S = W(1-\epsilon) \quad (1)$$

WHERE KW EQUALS CORRECT WEIGHT

$$KW = \frac{E_{JM}}{E_{JA}} \quad (2)$$

SEE (42) FOR EXAMPLE.

THEN FROM (3Ra-5)

$$\boxed{CR_0 = \frac{1}{\epsilon^2}} \quad (3)$$

JAMMER CANCELLATION RATIO CR_o FOR HL/SSLC (CONT.)

FROM (42-7)

$$W_s = kG\left[\frac{V_m V_a^*}{(1+G_L)|V_a|}\right] = \frac{kG}{1+G_L}\left[\frac{V_m V_a^*}{|V_a|}\right] = \frac{\overbrace{k^2 G|V_a|}^{G_L}}{1+G_L}\,\frac{1}{k|V_a|}\left[\frac{V_m V_a^*}{|V_a|}\right] \quad \text{SEE (42-2)} \qquad (1)$$

BUT

$$\left[\frac{V_m V_a^*}{|V_a|}\right] = \left[\frac{(E_{Jm}+E_{Nm})(E_{Ja}^*+E_{Na}^*)}{\sqrt{(E_{Ja}+E_{Na})(E_{Ja}^*+E_{Na}^*)}}\right] = \left[\frac{E_{Jm}E_{Ja}^* + E_{Jm}E_{Na}^* + E_{Nm}E_{Ja}^* + E_{Nm}E_{Na}^*}{\sqrt{|E_{Ja}|^2+|E_{Na}|^2+E_{Ja}E_{Na}^*+E_{Na}E_{Ja}^*}}\right] \qquad (2)$$

$$\doteq \left[\frac{E_{Jm}E_{Ja}^* + E_{Jm}E_{Na}^* + E_{Nm}E_{Ja}^* + E_{Nm}E_{Na}^*}{|E_{Ja}|\left[1+\frac{1}{2}\left|\frac{E_{Na}}{E_{Ja}}\right|^2 + \frac{E_{Ja}E_{Na}^*}{2|E_{Ja}|^2} + \frac{E_{Na}E_{Ja}^*}{2|E_{Ja}|^2}\right]}\right] \qquad (3)$$

$$\doteq \left[\frac{kW|E_{Ja}|^2}{|E_{Ja}|}\left[1 + \frac{E_{Jm}E_{Na}^*}{kW|E_{Ja}|^2} + \frac{E_{Nm}E_{Ja}^*}{kW|E_{Ja}|^2} + \frac{E_{Nm}E_{Na}^*}{kW|E_{Ja}|^2}\right]\left[1 - \frac{1}{2}\left|\frac{E_{Na}}{E_{Ja}}\right|^2 - \frac{E_{Ja}E_{Na}^*}{2|E_{Ja}|^2} - \frac{E_{Na}E_{Ja}^*}{2|E_{Ja}|^2}\right]\right] \qquad (4)$$

$$\doteq kW|E_{Ja}|\left[1 + \frac{E_{Na}^*}{E_{Ja}^*}\right]\left[1 - \frac{1}{2}\left|\frac{E_{Na}}{E_{Ja}}\right|^2 - \frac{E_{Na}^*}{2E_{Ja}^*} - \frac{E_{Na}}{2E_{Ja}}\right] \qquad (5)$$

JAMMER CANCELLATION RATIO CR_o FOR HL/SSLC (CONT.)

$$\left[\frac{V_m V_a^*}{|V_a|}\right] = kW|E_{Ja}|\left[1 - \frac{1}{2}\left|\frac{E_{Na}}{E_{Ja}}\right|^2 - \cancel{\frac{E_{Na}^*}{2E_{Ja}^*}} - \cancel{\frac{E_{Na}}{2E_{Ja}}} - \cancel{\frac{E_{Na}}{E_{Ja}^*}} - \frac{1}{2}\cancel{\frac{E_{Na}^*}{E_{Ja}^*}\left|\frac{E_{Na}}{E_{Ja}}\right|^2} - \cancel{\frac{(E_{Na}^*)^2}{2(E_{Ja}^*)^2}} - \frac{1}{2}\left|\frac{E_{Na}}{E_{Ja}}\right|^2\right] \qquad (6)$$

$$= kW|E_{Ja}|\left[1 - \left|\frac{E_{Na}}{E_{Ja}}\right|^2\right] = kW|E_{Ja}|\left[1 - \frac{1}{JNR_a}\right] \qquad (7)$$

FROM (42b-3)

$$|V_a| = |E_{Ja}|\left[1+\frac{1}{2}\left|\frac{E_{Na}}{E_{Ja}}\right|^2 + \cancel{\frac{E_{Na}^*}{2E_{Ja}^*}} + \cancel{\frac{E_{Na}}{2E_{Ja}}}\right] = |E_{Ja}|\left[1+\frac{1}{2}\frac{1}{JNR_a}\right] \qquad (8)$$

$$\frac{1}{|V_a|}\left[\frac{V_m V_a^*}{|V_a|}\right] = kW\left[1-\frac{1}{JNR_a}\right]\left[1-\frac{1}{2JNR_a}\right] = kW\left[1-\frac{3}{2JNR_a}\right] \qquad (9)$$

$$\therefore W_s = W\left(1-\frac{1}{G_L}\right)\left(1-\frac{3}{2JNR_a}\right) = W\left[1-\underbrace{\left(\frac{1}{G_L}+\frac{3}{2JNR_a}\right)}_{\epsilon}\right] \qquad (10)$$

BUT FROM (44-6)

$$G_L = 1+G_o\sqrt{1+JNR_a} \qquad (11)$$

$$= G_o\sqrt{JNR_a} \quad \text{FOR } JNR_a \gg,\ G_o \gg 1 \qquad (12)$$

JAMMER CANCELLATION RATIO CR_0 FOR HL/SSLC (CONT.)

$$\therefore \quad \epsilon = \frac{3}{2JNR_a} + \frac{1}{G_0\sqrt{JNR_a}} \qquad (13)$$

$$CR_0 = \left[\frac{3}{2JNR_a} + \frac{1}{G_0\sqrt{JNR_a}}\right]^{-2} \qquad (14)$$

* FOR $G_0 = 1$ AND $JNR_a \gg 1$

$$\boxed{CR_0 \doteq JNR_a} \quad \text{FOR } G_0 = 1,\ JNR_a \gg 1 \qquad (15)$$

EX. $G_0 = 1$, $JNR_a = 40$ dB $\quad CR_0 = 40$ dB

* FOR $G_0 = 10$ AND $JNR_a \geq 1000$

$$\boxed{CR_0 \doteq G_0^2 JNR_a} \quad \text{FOR } G_0 = 10,\ JNR_a \geq 1000$$

EX. $G_0 = 10$, $JNR_a = 40$ dB $\quad CR_0 \doteq 60$ dB

TRANSIENT OUTPUT OF FEEDBACK HL/SSLC

FROM (41) and (42)

$$V_r = V_m - kV_a\overline{W} = V_m - kV_a\overline{W}_s\left(1 - e^{-t/\tau_L}\right) \qquad (1)$$

$$= V_m - k\overline{W}_s + kV_a W_s e^{-t/\tau_L} \qquad (2)$$

BUT STEADY STATE $V_r = V_{rs}$ IS

$$V_{rs} = V_m - k\overline{W}_s\overline{V}_a \qquad (3)$$

HENCE

$$\boxed{V_r = V_{rs} + k\overline{W}_s V_a e^{-t/\tau_L}} \qquad (4)$$

$$\overline{|V_r|^2} = \overline{|V_{rs}|^2} + k^2|W_s|^2\overline{|V_a|^2}e^{-2t/\tau_L} + 2\,\mathrm{Re}\left[\overline{V_{rs}\,k\overline{W}_s^{*}V_a^{*}e^{-t/\tau_L}}\right] \qquad (5)$$

LOOP NOISE CONSTRAINT FOR HL/SSLC

36-3 STILL HOLDS, I.E.

$$\tau_0 \gg \frac{10}{\pi B_s}\left[1+G_L\right] \qquad (1)$$

WHERE NOW

$$G_L = G_0\sqrt{1+JNR_q} \qquad (2)$$

AND $G_0 = k^2 G\,\overline{|V_{nq}|}$ ← (3) = LOOP NOISE WHEN NO INTERFERENCE PRESENT.

DERIVATION: FROM (42-3):

$$G_L = 1+k^2G\overline{|V_q|} = 1+k^2G\sqrt{\left(\sigma_{JA}^2+\sigma_{NA}^2\right)\frac{2}{\pi}} = 1+\underbrace{k^2G\sqrt{\sigma_{NA}^2\frac{2}{\pi}}}_{G_0}\sqrt{1+JNR_q} \qquad (4)$$

WHERE $\sigma_{JA}^2 = \overline{|V_{Ja}|^2}$ $\sigma_{NA}^2 = \overline{|V_{na}|^2}$ (5)

THUS $G_L = 1+G_0\sqrt{1+JNR_q}$ QED. (6)

EX. $B_s = 5MH_z$, $JNR_q = 10^4 = 40dB$, AND $G_0 = 10^{\#}$

THEN $\tau_0 = 637\mu s$, $B_0 = 250\,H_z$, $\tau_L = 0.636\mu s$

G_0 SET TO 10 TO LOWER JAMMER STEADY STATE RESIDUAL. SEE NEXT FEW VUGRAPHS.

CLOSED LOOP TIME CONSTANT τ_L FOR HL/SSLC

FROM (42-6)

$$\tau_L = \frac{\tau_0}{1+G_L} \qquad (1)$$

BUT FROM (44-6)

$$G_L = 1+G_0\sqrt{1+JNR_q} \qquad (2)$$

$$\therefore \quad \boxed{\tau_L = \frac{\tau_0}{1+G_0\sqrt{1+JNR_q}}} \qquad (3)$$

$$\boxed{\tau_L \doteq \frac{\tau_0}{G_0\sqrt{JNR_q}}} \quad \text{FOR } JNR_q \gg 1 \qquad (4)$$

FOR FIXED τ_0 FROM (44-1) AND (44-6)

$$\tau_0 = \frac{10}{\pi B_s}(1+G_L) = \frac{10}{\pi B_s}\left[2+G_0\sqrt{1+(JNR_q)_{MX}}\right] \doteq \frac{10}{\pi B_s}\left[G_0\sqrt{(JNR_q)_{MX}}\right] \qquad (5)$$

$$\therefore \quad \boxed{\tau_L \doteq \frac{10}{\pi B_s}\sqrt{\frac{(JNR_q)_{MX}}{JNR_q}}} \quad \text{FOR } JNR_q \gg 1 \qquad (6)$$

USE OF AGC CONTROL OF G_0 TO SPEED UP τ_L FOR HL/SSLC

(44b)

FROM (42a-3)

$$\tau_L = \frac{\tau_0}{1+G_0\sqrt{1+JNR_a}} \qquad (1)$$

IF VIA AGC

$$G_0 = 10\sqrt{\frac{(JNR_a)_{MX}}{JNR_a}} \qquad (2)$$

THEN

$$\tau_L = \frac{\tau_0}{1+10\sqrt{\frac{(JNR_a)_{MX}}{JNR_a}}\sqrt{1+JNR_a}} \doteq \frac{\tau_0}{10\sqrt{(JNR_a)_{MX}}} \qquad \text{FOR } JNR_a >> 1 \qquad (3)$$

BUT FROM (44-1) AND (44-6)

$$\tau_0 = \frac{10}{\pi B_s}(1+G_L) = \frac{10}{\pi B_s}\left[2+G_0\sqrt{1+(JNR_a)_{MX}}\right] \doteq \frac{10}{\pi B_s}\left[G_0\sqrt{(JNR_a)_{MX}}\right] \qquad (4)$$

$$\therefore \quad \boxed{\tau_L = \frac{G_0}{\pi B_s}} \qquad (5)$$

EX. $G_0 = 10$, $B_s = 5\,MHz$; $\tau_L = 0.637\,\mu s$

(44c)

ADAPTIVE CONTROL OF τ_0 TO SPEED UP τ_L FOR HL/SSLC

1. MEASORE JNR_a

2. FROM (44-1) LET

$$\tau_0 = \frac{10}{\pi B_s}\left[1+\underbrace{G_0(1+JNR_a)}_{G_L}\right] = \frac{10}{\pi B_s}(1+G_L) \qquad (1)$$

BUT FROM (42-6)

$$\tau_L = \frac{\tau_0}{1+G_L} \qquad (2)$$

$$\therefore \quad \boxed{\tau_L = \frac{10}{\pi B_s}} \qquad (3)$$

INDEPENDENT OF JNR_a.

COMPARISON OF LINEAR AND HL SSLC RESIDUALS

FOR HL/SSLC, CR_o, REJECTION OF JAMMER SIGNAL, IS FROM (42d-14)

$$CR_o = \left[\frac{3}{2JNR_a} + \frac{1}{G_o\sqrt{JNR_a}}\right]^{-2} \doteq G_o^2 JNR_a \quad \text{FOR} \quad G_o \ll \sqrt{JNR_a} \qquad (1)$$

FOR L/SSLC (LINEAR SSLC) [FROM (32a-8)]:

$$CR_o \doteq JNR_a^2 (G_o/[1+G_o])^2 = JNR_a^2/4 \quad \text{FOR } G_o = 1 \qquad (2)$$

HENCE FOR HL/SSLC:

$$\overline{|V_{rs}|^2} \doteq \frac{\overline{|V_m|^2}}{CR_o} = \overline{|V_m|^2}\left[\frac{3}{2JNR_a} + \frac{1}{G_o\sqrt{JNR_a}}\right]^2 \doteq \overline{|V_m|^2}/(G_o^2 JNR_a) \quad \text{FOR} \quad G_o \ll \sqrt{JNR_a} \qquad (3)$$

FOR L/SSLC:

$$\overline{|V_{rs}|^2} \doteq \frac{\overline{|V_m|^2}}{CR_o} = \frac{\overline{|V_m|^2}}{(JNR_a)^2}\left(\frac{1+G_o}{G_o}\right)^2 \doteq \frac{4\overline{|V_m|^2}}{(JNR_a)^2} \quad \text{FOR } G_o = 1 \qquad (4)$$

FOR L/SSLC WHEN $G_o = 1$ $G_L \doteq JNR_a$ AND JAMMER, V_{jm}, SUPPRESSED G_L^2 OR AN AMOUNT G_L BELOW V_{nm}, THE THERMAL NOISE (IT BEING ASSUMED THAT $V_{nm} = V_{na}$). THUS FOR $JNR_a = 40dB$ $CR_o = 80dB$ AND RESIDUAL JAMMER IS 40dB BELOW THE MAIN CHANNEL THERMAL NOISE.

COMPARISON OF LINEAR AND HL SSLC RESIDUALS (CONT.) (46)

FOR HL/SSLC WHEN $G_0 = 1$, $G_L \doteq \sqrt{JNR_a}$. HENCE $JNR_a = 40dB$, $CR_0 \doteq 40dB$ AND RESIDUAL JAMMER IS EQUAL TO THE MAIN CHANNEL THERMAL NOISE. THIS RESULTS IN THE MAIN CHANNEL RESIDUAL V_{rs} BEING LARGER FOR THE HL/SSLC THAN FOR THE L/SSLC BY ABOUT 1.8dB. TO ELIMINATE THIS DEGRADATION CR HAS TO BE INCREASED FOR THE HL/SSLC SO THAT THE JAMMER IS SUPPRESSED BELOW THE MAIN CHANNEL THERMAL NOISE. THIS IS DONE BY CHOOSING G_0 TO BE >1.

FOR $G_0 = 10$, $JNR_a = 10^4$, $CR = 60dB$ (SEE 45-1 & 45-4). THUS THE JAMMER IS SUPPRESSED TO 20dB BELOW THE MAIN CHANNEL THERMAL NOISE.

COMPARISON OF LINEAR (L) AND HL SSLC RESIDUALS (CONT.) (47)

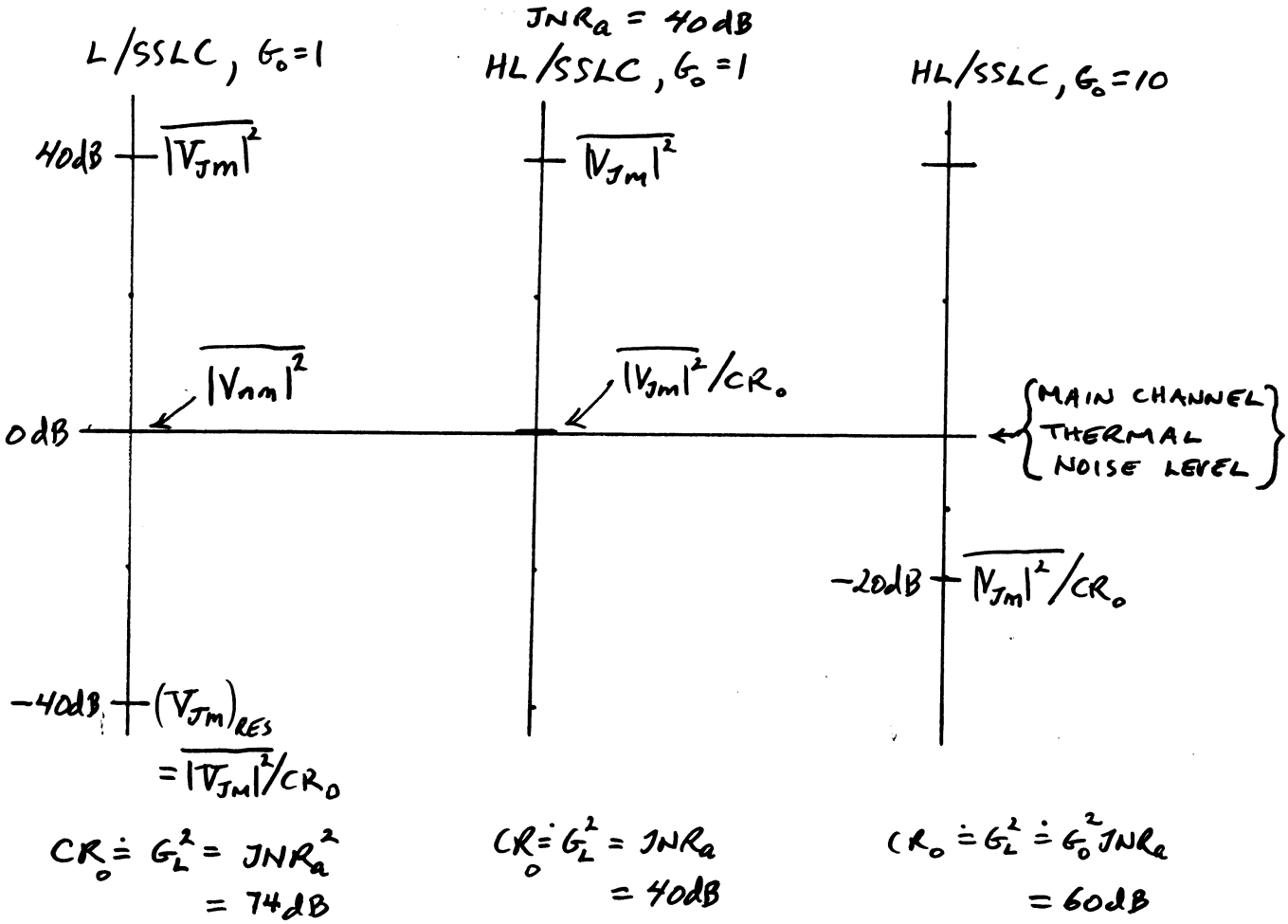

$CR_0 \doteq G_L^2 = JNR_a^2 = 74dB$

$CR_0 \doteq G_L^2 = JNR_a = 40dB$

$CR_0 \doteq G_L^2 \doteq G_0^2 JNR_a = 60dB$

T_L VERSUS JNRa FOR HL/SSLC

USING EXAMPLE OF (44) T_L VARIES AS SHOWN IN TABLE.
I.E. FOR $T_0 = 637\mu s$, $B_0 = 250\ Hz$, $G_0 = 10$, $H = 10$.

JNRa (dB)	T_L (μs)	G_L (dB)	t_4 (μs)
40	0.636	60	3.37
30	2.01	48	8.34
20	6.28	34	18.8
10	18.6	18	34.3

SEE (37) FOR DEFINITIONS.

TRANSIENT RESPONSE FOR HL/SSLC

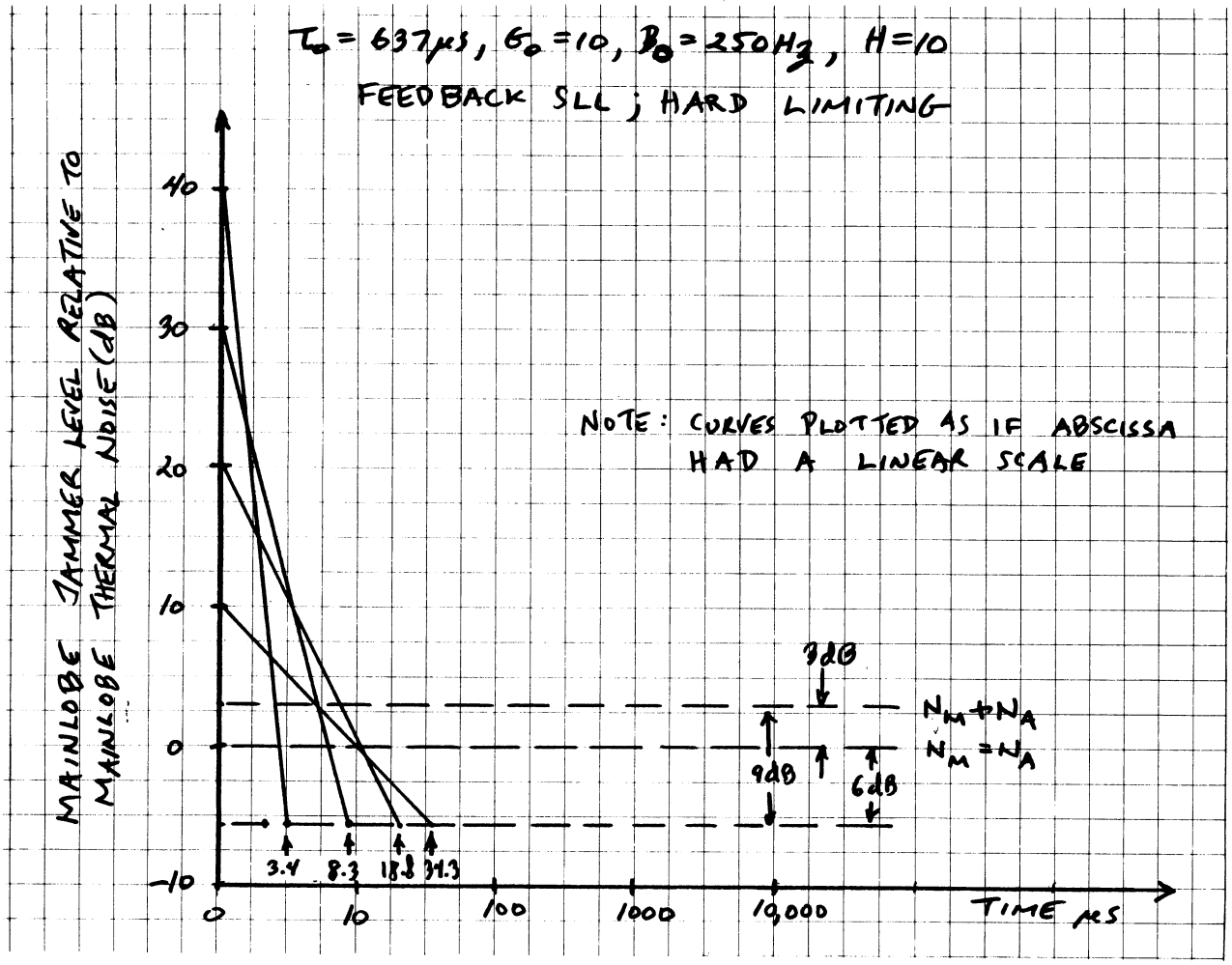

SIMULATION OF L/SSCL: CR VS $2B_L/B_S$ (49a)

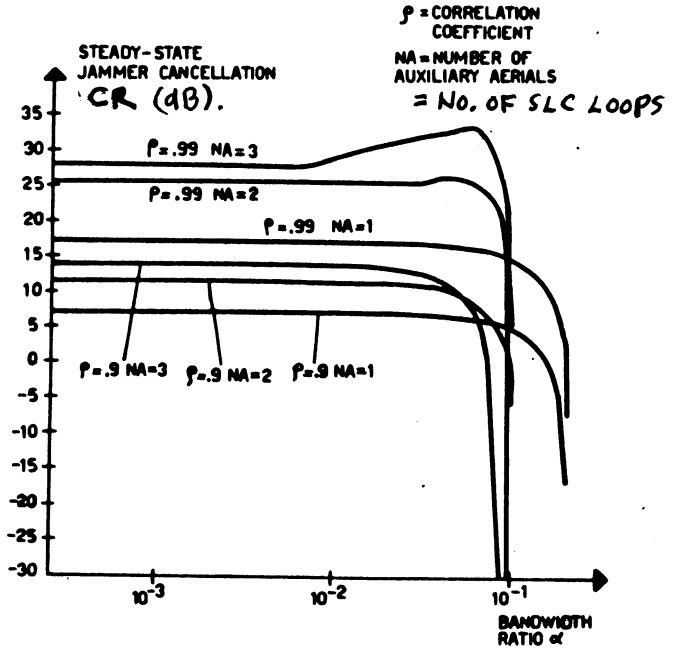

(FROM BUCCIARELLI, ESPOSITO, FARINA, LOSQUADRO, IEE RADAR-82)

LOOP NOISE (50)

FROM ANOTHER REFERENCE* THE FOLLOWING MORE STRINGENT CONDITION IS GIVEN FOR LOOP NOISE NOT TO DEGRADE CR#:

$$\frac{B_S}{2B_L} = H \geq 2CR \qquad (1)$$

THUS HERE $H = 2CR$

EX. $B_S = 5MHz$, $CR = 37dB^{\ddagger} \therefore H = 2CR = 40dB = 10{,}000.$

CASE	PARAMETER	H=10,000	H=10
L/SSLC	T_L (MS)	637	0.637
	B_L (Hz)	250	250K
HL/SSLC	T_L (MS)	637	0.636
	B_L (Hz)	250	250K

BY NOT MORE THAN 1.8 dB

‡ THIS IS THE CR OF EX. 1 OF VUGS. 36 & 44. FOR MAX. INR_A OF 40dB.

(* FARINA & STUDER, IEE PROC. 2/82)

CR VS $2B_L/B_S$

(51)

L/SSLC CASE

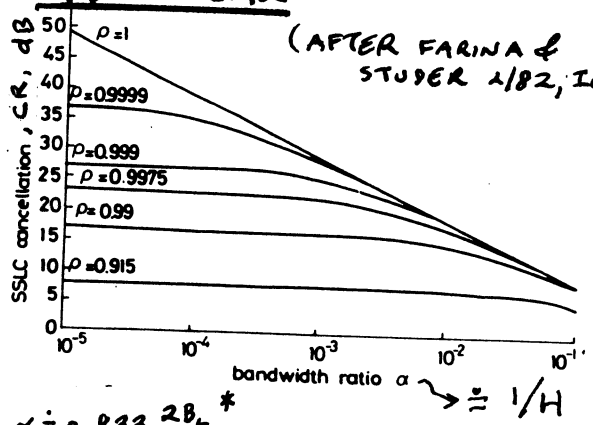

(AFTER FARINA & STUDER 1/82, IEE)

$\alpha \doteq 0.833 \frac{2B_L}{B_S}$ *, WHERE B_S = 3dB BW FOR GAUSSIAN INTERFERENCE SPECTRUM.

ρ = CORRELLATION BETWEEN V_m AND V_a

$= \exp\left[-(\Delta t/\tau_s)^2\right]$

WHERE τ_s IS CORRELLATION TIME OF INTERFERENCE, $\tau_s = 0.530/B_s$.
NO RECEIVER NOISE ASSUMED PRESENT.
Δt = DIFFERENCE IN ARRIVAL TIMES BETWEEN MAIN AND AUXILIARY CHANNELS.

NOTE $H = 0.833/\alpha$

PROBABILITY DENSITY FUNCTION FOR WEIGHT W; L/SSLC

(52)

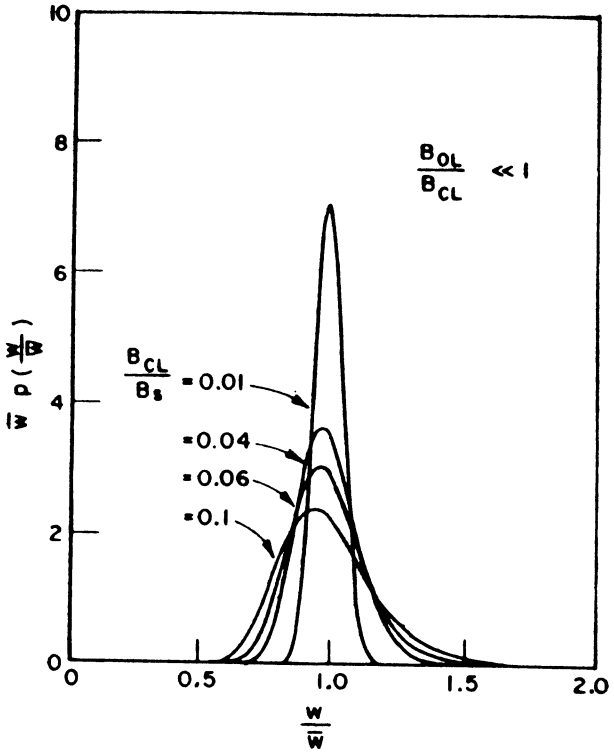

(FROM BERNI, IEEE AESS, 7/77, pp 355-61)

NORMALIZED VARIANCE OF WEIGHT FOR L/SSLC (53)

$$\sigma_W^2/\bar{W}^2 = \left[\frac{1}{\pi}\frac{B_L B_S}{(B_L - B_O)^2} - 1\right]^{-1} \doteq \frac{\pi}{2}\left(\frac{2B_L}{B_S}\right)^{1/H} \quad \text{FOR } B_L \gg B_O,\ B_S/\pi B_L \gg 1 \qquad (1)$$

WHERE B_L = CLOSED LOOP BW = $1/(2\pi\tau_L)$, B_O = OPEN LOOP BW = $1/(2\pi\tau_O)$

THUS FOR THE LOOP NOISE NOT TO DEGRADE CR*:

$$H = \frac{B_S}{2B_L} \geq \pi CR \qquad (2)$$

FOR EX. 1 OF (36),(37) $B_S = 5MHz$, $B_O = 25Hz$, $\tau_O = 6{,}370\mu s$, $JNR_a = 40dB$, $G_o = 1$, $H = 10$ (L/SSLC CASE)

JNR_a (dB)	τ_L (μs)	B_L (Hz)	$\sigma_W^2/\bar{W}^2$
40	0.637	250k	0.186
30	6.36	25k	0.016
20	62.5	2,550	0.0016
10	531	300	0.00016

EX. 2 (50) $B_S = 5MHz$, CR = 37dB, THEN $H = 15{,}700$, $\tau_L = 1000\mu s$ AND $B_L = 159Hz$. ALSO $\sigma_W^2/\bar{W}^2 = 0.000100$ (vs 0.186 ABOVE) (L/SSLC CASE)

(* FROM BERNI, IEEE AES 7/77.)

NULL DEPTH VS TIME (54)

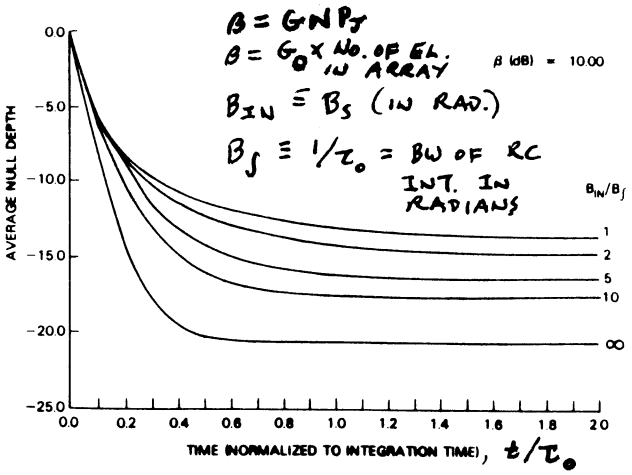

(AFTER GERLACH AND LANG, IEEE TRANS. ON ANT. AND PROP., 3/86.)

NULL DEPTH AND OUTPUT TIME CONSTANT VS RC INTEGRATION TIME τ_0

54a

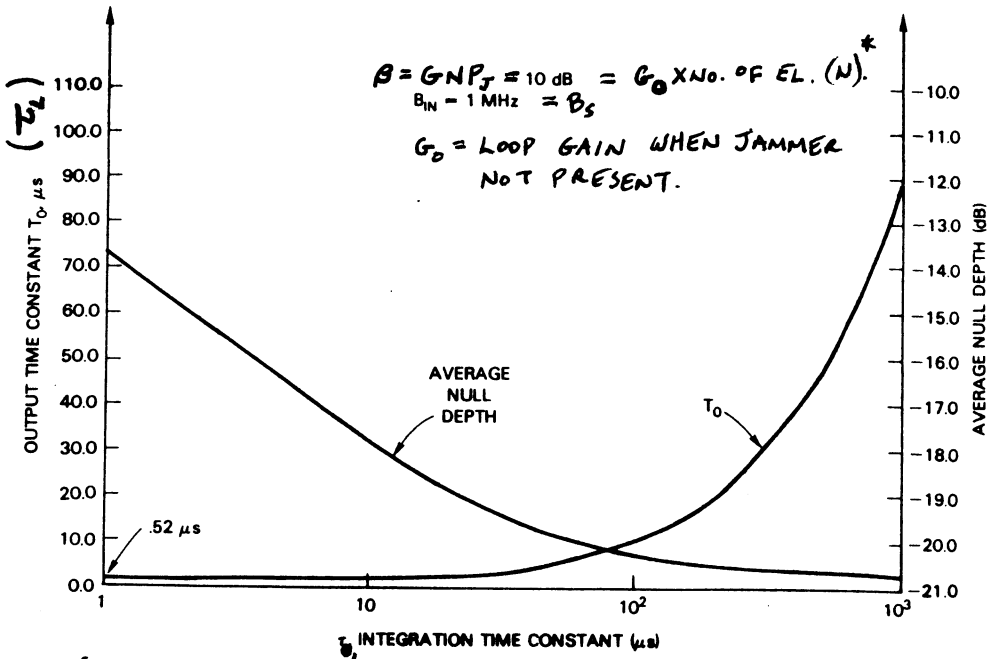

(AFTER GERLACH AND LANG, IEEE TRANS. ON ANT. AND PROP., 3/86)

54b

CLUTTER CANCELLATION VERSUS NORMALIZED JAMMER POWER

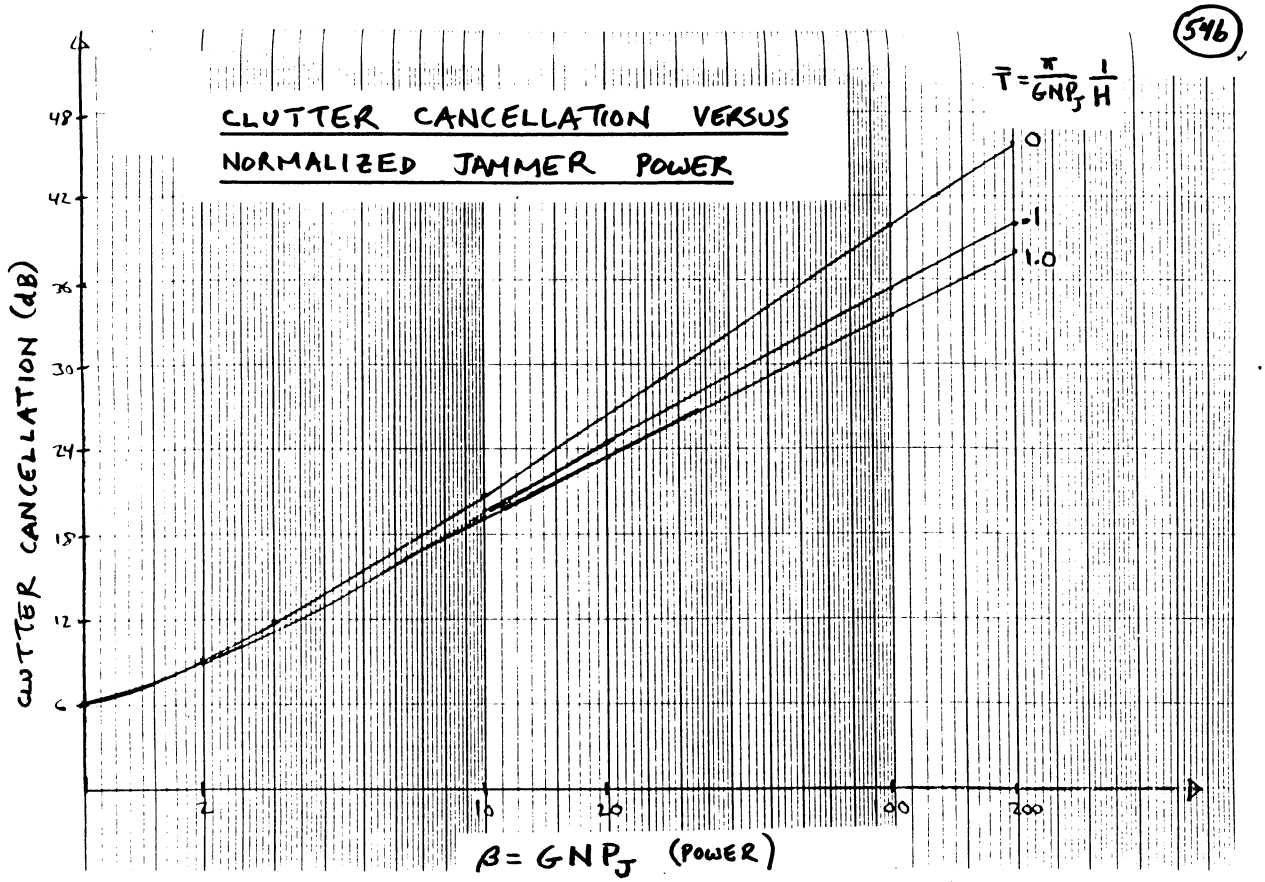

G = OPEN LOOP GAIN, N = NUMBER OF ELEMENTS IN FULLY ADAPTIVE ARRAY, P_J = JAMMER POWER

(GERLACH, FEB. 1981)

CR VS JAMMER DIRECTION, θ

(55)

$JNR_m = JNR_a = \infty$, PERFECT TRACKING BETWEEN CHANNELS.

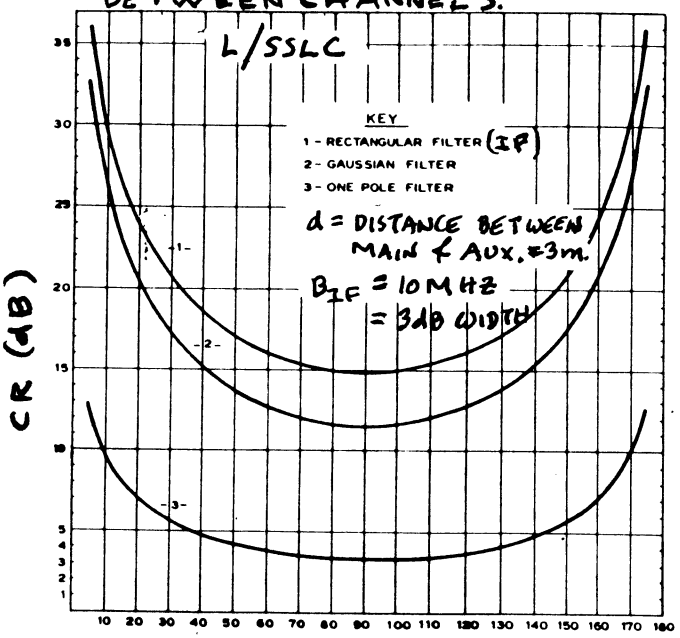

(FROM FARINA, IEEE AES, 11/77)

CR VS $(JNR_m)^{-1}$

(56)

PERFECT TRACKING BETWEEN CHANNELS.

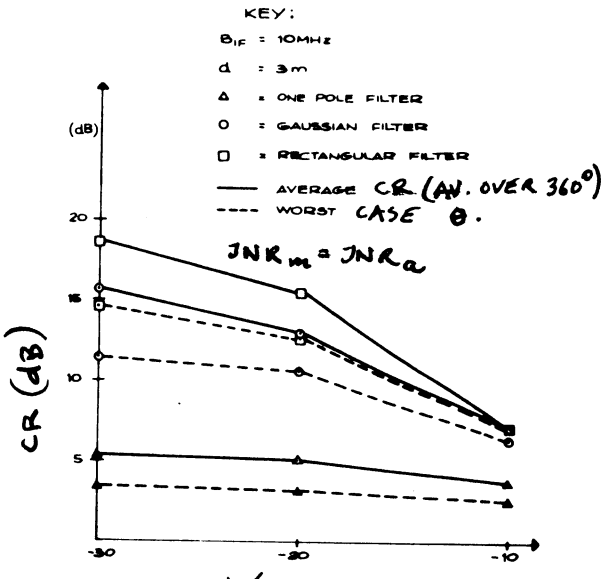

(FROM FARINA, IEEE AES, 11/7)

CR VS JAMMER DIRECTION θ FOR CASE OF NON-PERFECT TRACKING BETWEEN CHANNELS

(57)

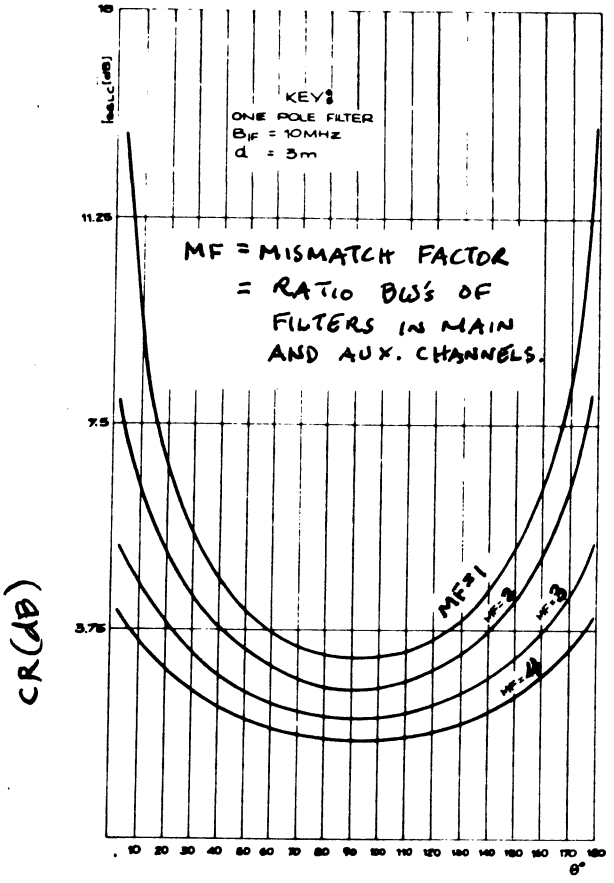

(FROM FARINA, IEEE AES, 11/77)

LINEAR DOUBLE-LOOP SLC (L/DSLC)

(58)

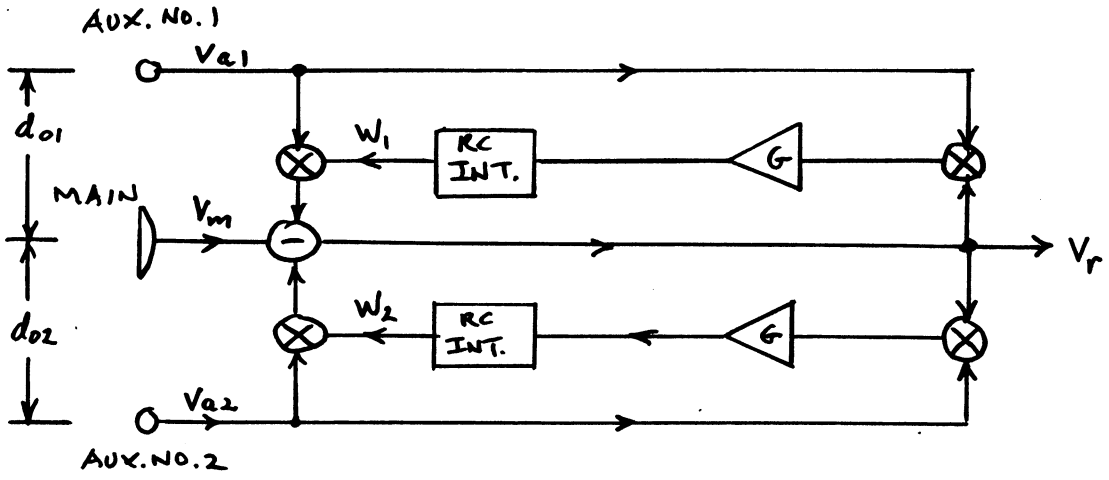

TRANSIENT RESPONSE OF L/DSLC (59)

THE L/DSLC OF (58) CAN BE SHOWN TO BE EQUIVALENT TO A L/DSLC FOR WHICH THE TWO LOOPS ACT INDEPENDENTLY AND HAVE TIME CONSTANTS GIVEN BY:

$$\tau_{L1} = \tau_0 / G_L(1-\rho^4) \quad (1)$$
$$\tau_{L2} = \tau_0 / G_L(1+\rho^4) \quad (2)$$

← (FROM FARINA AND STUDER, IEE PROC., Pt. F, 2/82)

WHERE ρ IS THE CORRELATIONS BETWEEN V_m AND V_{q1} AND V_m AND V_{q2}. IT IS ASSUMED HERE THAT $d_{01} = d_{02}$ IN (58), IN WHICH CASE ρ^4 IS THE CORRELATION BETWEEN V_{q1} AND V_{q2}. NO THERMAL NOISE IS ASSUMED TO BE PRESENT. G_L = CLOSED LOOP GAIN FOR EACH LOOP OF (58). ONLY ONE JAMMER ASSUMED PRESENT.

EX. 1: $G_L = 10^4$, $\tau_0 = 6{,}370\mu s$, $\rho = 0.99$ (SEE (37))

$\tau_{L1} = 16.2\mu s$, $\tau_{L2} = 0.325\mu s$ VERSUS $\tau_L = 0.637\mu s$ FOR L/SSLC; (SEE (37)).

2. $G_L = 10^4$, $\tau_0 = 6{,}370\mu s$, $\rho = 0.9999$ (SEE (37) & (28a)):

$\tau_{L1} = 1593\mu s$, $\tau_{L2} = 0.319\mu s$.

THE LONGER TIME CONSTANT DETERMINES THE SETTLING TIME OF THE L/DSLC SYSTEM BECAUSE BOTH LOOPS MUST REACH STEADY STATE.

CR FOR $G_L = \infty$, NO THERMAL NOISE CASE (L/DSLC) (60)

$$CR = \frac{(1+\rho^4)}{(1-\rho^2)^2} \quad (1)$$

← (FROM FARINA AND STUDER, IEE PROC., Pt. F, 2/82)

ONLY ONE JAMMER ASSUMED PRESENT.

EX. $\rho = 0.999$ $CR_{DSLC} \doteq \underline{57\,dB}$ VS. $CR_{SSLC} \doteq \underline{27dB}$ (SEE (28)).

THUS THE L/DSLC OFFERS BETTER CR THAN THE L/SSLC. FOR THIS EX. IT IS 30dB BETTER. THE L/DSLC IS BETTER THAN THE L/SSLC FOR $G_L = \infty$, OR EQUIVALENTLY, $\alpha = 0$, OR $2B_L/B_s = 0$. FOR $2B_L/B_s \neq 0$ THIS IS NOT ALWAYS TRUE, SEE (63). THIS IS BECAUSE TWO LOOP NOISES ARE THEN CONTRIBUTING TO OUTPUT RESIDUAL AND THEIR SUM CAN BE LARGER THAN FOR A SINGLE LOOP SYSTEM.

CR VS ρ FOR $G_L = \infty$
L/DSLC CASE

(61)

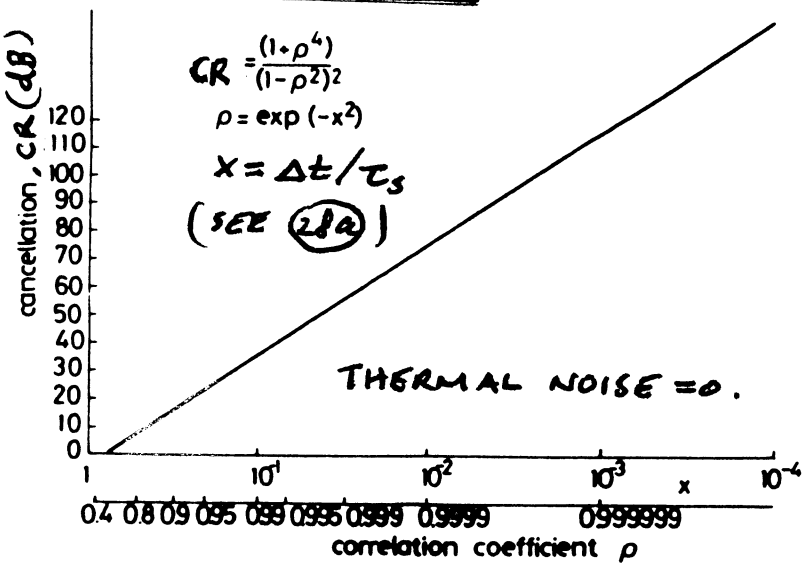

(AFTER FARINA AND STUDER, IEE PROC., Pt. F, 2/82)

CR VS $2B_L/B_s$
L/DSLC CASE

(62)

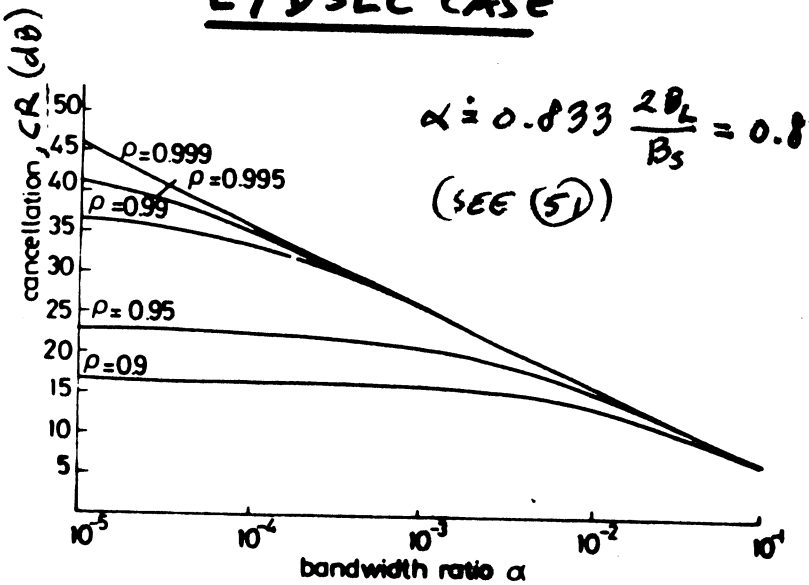

$\alpha \doteq 0.833 \frac{2B_L}{B_s} = 0.833 \frac{1}{H}$

(SEE (51))

(AFTER FARINA & STUDER, PROC. IEE, Pt. F, 2/82)

REGION WHERE CR FOR L/SSLC BETTER THAN FOR L/DSLC (63)

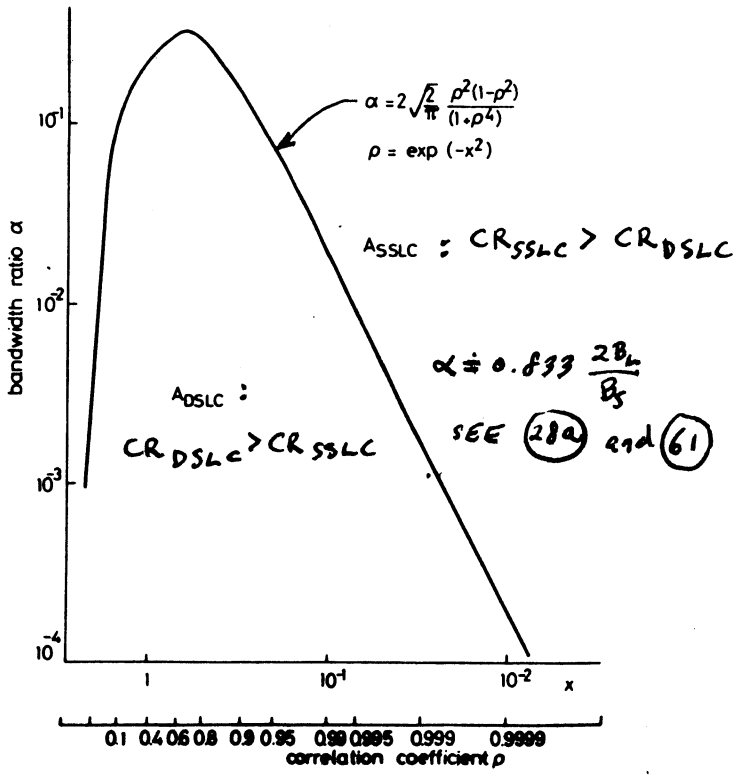

A_{SSLC} : $CR_{SSLC} > CR_{DSLC}$

A_{DSLC} : $CR_{DSLC} > CR_{SSLC}$

$\alpha \doteq 0.633\,\frac{2B_L}{B_S}$

SEE (28a) and (61)

MULTI-LOOP SIDELOBE CANCELLATION SYSTEM (MSLC) (64)

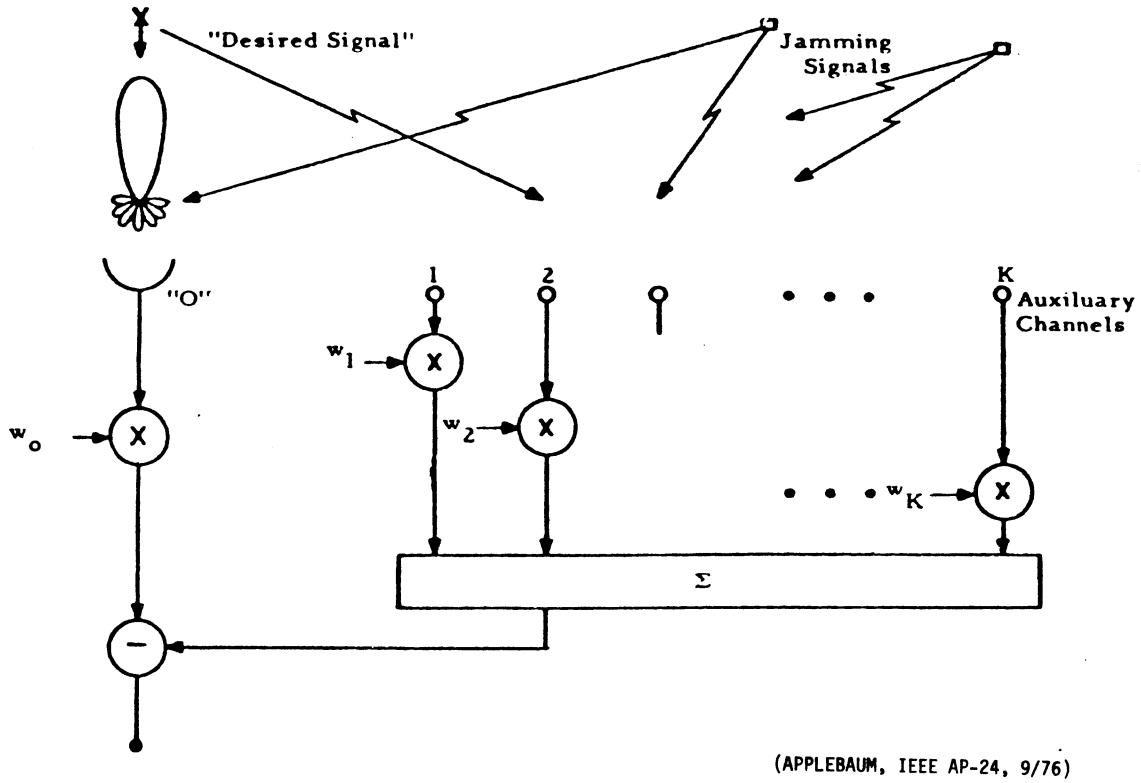

(APPLEBAUM, IEEE AP-24, 9/76)

CR VS NUMBER OF AUXILIARIES FOR MSLC (65)

IDEAL CASE OF $G_L = \infty$.

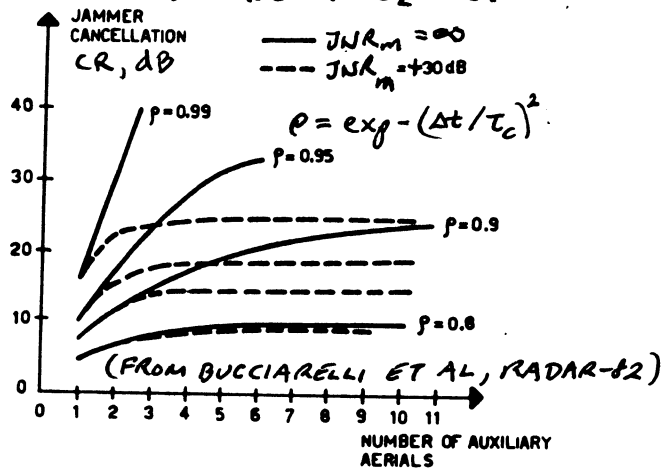

(FROM BUCCIARELLI ET AL, RADAR-82)

ρ = CORRELATION OF INTERENCE BETWEEN ADJACENT ANTENNAS. ANTENNAS ASSUMED EQUALLY SPACED.

FULLY ADAPTIVE ARRAY (66)

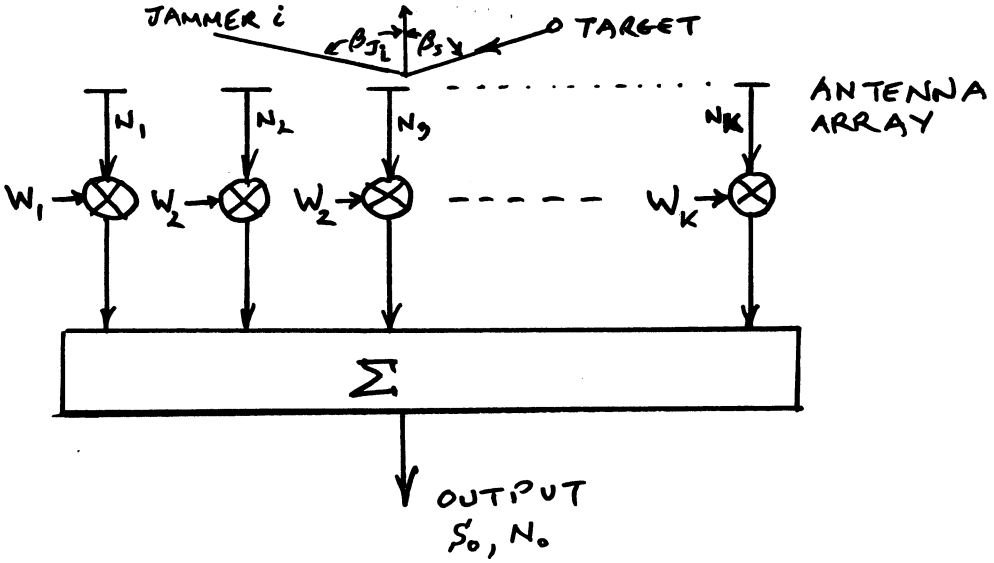

DESIRE TO FIND $W = [W_1, W_2, \cdots, W_K]^T$

WHICH MAXIMIZES OUTPUT SIR $= S_o/N_o$

SOLUTION#:

$$\boxed{W_{OPT} = W_o = M^{-1} S^*} \quad (1)$$

(#SEE APPLEBAUM IEEE AP 9/76)

PHASED ARRAY STEERED TO θ

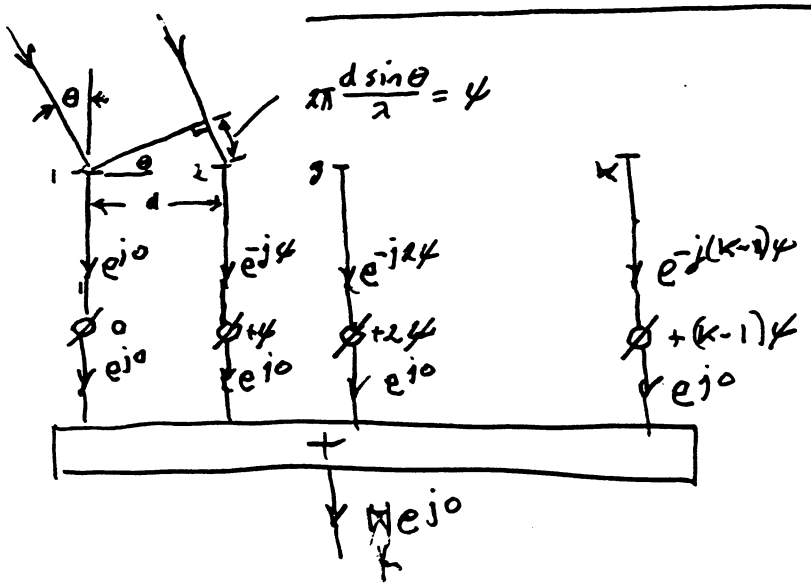

PHASED ARRAY STEERED TO θ (CONT.)

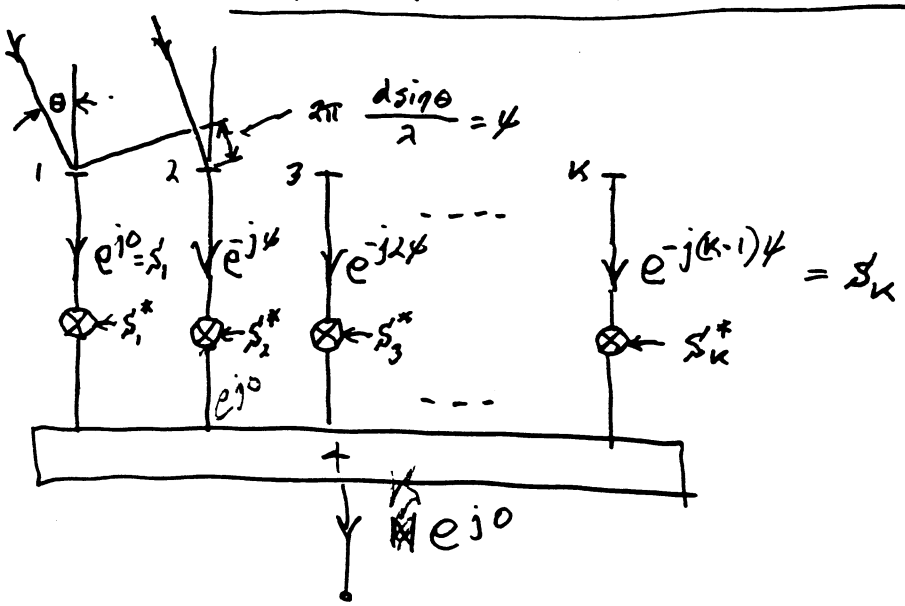

$$S = \begin{bmatrix} e^{j0} \\ e^{-j\psi} \\ e^{-j2\psi} \\ \vdots \\ e^{-j(K-1)\psi} \end{bmatrix} = \begin{bmatrix} S_1 \\ S_2 \\ S_3 \\ \vdots \\ S_K \end{bmatrix} \qquad S^* = \begin{bmatrix} e^{j0} \\ e^{j\psi} \\ e^{j2\psi} \\ \vdots \\ e^{j(K-1)\psi} \end{bmatrix} = \begin{bmatrix} S_1^* \\ S_2^* \\ S_3^* \\ \vdots \\ S_K^* \end{bmatrix}$$

EIGEN VECTOR e_i AND VALUE λ_i

EIGEN VECTOR IS SOLUTION OF :

$$M e_i = \lambda_i e_i$$

EIGEN VALUE IS SOLUTION OF :

$$\text{DET}\left[M - \lambda_i I\right] = 0$$ (SEE BROOKNER, TRACKING, WILEY, p. 279)

$$e_i^T = [e_{i1}\ e_{i2}\ \cdots\ e_{ik}]$$

$$\Phi = [e_1\ e_2\ \cdots\ e_k] = \text{MATRIX WHOSE COLOMNS ARE EIGEN VECTORS OF } M$$

$$\therefore\ M\Phi = [\lambda_1 e_1\ \lambda_2 e_2\ \cdots\ \lambda_k e_k] = \Phi\Lambda \qquad \Lambda = \text{DIAG}[\lambda_1\ \lambda_2 \cdots \lambda_k]$$

$$e_i^{*T} e_i = 1$$

$$\therefore\ \Phi^{*T}\Phi = I = \text{IDENTITY MATRIX}$$

WHERE

$$M = \begin{bmatrix} M_{11} & M_{12} & \cdots & M_{1K} \\ M_{21} & & & \vdots \\ \vdots & & & \\ M_{K1} & \cdots & & M_{KK} \end{bmatrix}$$

= COVARIANCE MATRIX OF INTERFERENCE ACROSS ANTENNA ARRAY (INCLUDES THERMAL NOISE)

$$M_{ij} = \overline{N_i N_j^*}$$

$$S'^* = \left[S_1'^*, S_2'^*, \cdots S_K'^*\right]^T$$

= SET OF WEIGHT WHICH STEER ANTENNA TO TARGET

NOTE: S' = RECEIVED SIGNAL IF TARGET PRESENT.

(SEE APPLEBAUM, AP 9/76)

QUIESCENT CONDITIONS, I.E., THERMAL NOISE ONLY PRESENT

$$N_i = n_i + J_i = n_i \qquad \text{SINCE } J_i = 0$$

$$\therefore \quad M_{ij} = \overline{n_i n_j^*} = \sigma^2 \text{ FOR } i=j$$
$$= 0 \text{ FOR } i \neq j$$

$$\therefore \quad M = M_{\text{g}} = \begin{bmatrix} \sigma^2 & & 0 \\ & \sigma^2 & \\ 0 & & \ddots \\ & & & \sigma^2 \end{bmatrix} = \sigma^2 \begin{bmatrix} 1 & & 0 \\ & 1 & \\ 0 & & \ddots \\ & & & 1 \end{bmatrix} = \sigma^2 I$$

AND $$\boxed{W_{OPT} = W_0 = M^{-1} S'^* = \frac{1}{\sigma^2} S'^*}$$

THIS IS THE MATCHED FILTER AS IT SHOULD BE.

PROOF OF OPTIMALITY (69)

$$SIR = \frac{|W^{T*} S'|^2}{W^{T*} M W} \quad * \quad (1)$$

($|W^{T*} S'|^2$: S_0; $W^{T*} M W$: N_0)

FOR GENERAL W

PROBLEM: TO FIND W WHICH MAXIMIZES SIR:

LET X AND Y BE K COMPONENT COLUMN VECTORS AND M BE POSITIVE DEFINITE HERMITIAN. DEFINE INNER PRODUCT OF X AND Y AS:

$$(X, Y) = X^{*T} M Y$$

THEN FROM SCHWARTZ INEQUALITY

$$(X, Y) \leq (X, X)(Y, Y)$$

EXPRESSING (1) IN TERMS OF INNER PRODUCTS YIELDS

$$SIR = |(W, M^{-1} S)|^2 / (W, W)$$

PROOF OF OPTIMALITY (CONT.) (70)

$$\therefore \quad SIR \leq [(W, W)(M^{-1} S, M^{-1} S)] / (W, W)$$

$$\leq (M^{-1} S', M^{-1} S') = S'^{*T} M^{-1*T} M M^{-1} S'$$

$$\therefore \quad \boxed{SIR \leq S'^{*T} M^{-1} S'} \quad (2)$$

BUT (1) ACHIEVE THE UPPER BOUND OF (2) WHEN

$$\boxed{W = M^{-1} S'} = W_{OPT} = W_0 \quad (3)$$

TO SEE THIS, SUBSTITUTE (3) IN (1) TO GET

$$SIR = |S'^{*T} M^{-1*T} S'|^2 / (S'^{*T} M^{-1*T} M M^{-1} S')$$

$$= (S'^{*T} M^{-1} S')^2 / (S'^{*T} M^{-1} S')$$

$$= S'^{*T} M^{-1} S' \quad \text{QED.}$$

NOTE: WHEN INTERFERENCE IS GAUSSIAN W_{OPT} ALSO MAXIMIZES DETECTION PROBABILITY. (SEE REED, ET AL, AESS 10/74)

METHODS FOR ESTIMATING W (71)

- SAMPLE MATRIX INVERSION (SMI) METHOD
- APPLEBAUM-HOWELLS ADAPTIVE FEEDBACK LOOPS
- RECURSIVE UPDATE OF ESTIMATE OF M^{-1}
- AN ORTHOGONALIZATION PROCEEDURE
  - ORTHOGONAL TRANSFORMATION
  - NOLEN TRANSFORMATION NETWORK
  - CASCADE PREPROCESSOR
  - GRAM-SCHMIDT ALGORITHM.
  - LATTICE FILTER
- KALMAN FILTER

SAMPLE MATRIX INVERSION (SMI) (72)

ADAPTIVE ARRAY

USE MAXIMUM LIKELIHOOD ESTIMATE OF M GIVEN BY

$$\hat{M} = \frac{1}{R} \sum_{j=1}^{R} X^{(j)} X^{(j)*T} \quad (1)$$

$X^{(j)T} = [N_1, N_2 \ldots N_K]_j$ FOR jth TIME SAMPLE.

(73)

ON SIGNAL-TO-INTERFERENCE RATIO (SIR)

DEGRADATION USING SMI

LET SIR_{SMI} = SIR OBTAINED USING

$$\boxed{W = W_{SMI} = \hat{M}^{-1} S^*} \quad * \quad (1)$$

LET

$$\rho = \frac{SIR_{SMI}}{SIR_A} \qquad (2) \qquad (SIR_A \equiv SNR_A)$$

THEN

$$\boxed{\rho = -3dB \quad FOR \quad R = 2K-3 \doteq 2K \text{ FOR } K \gg 1} \quad * \quad (3)$$

IN GENERAL

$$\rho = -10 \log_{10}[(R+2-k)/(R+1)] \qquad (4)$$

(SEE REED, MALLETT, & BRENNAN, IEEE AES, 11/74)

(74)

ON DETECTION LOSS DEGRADATION USING SMI

THE LOSS OF (73) IS A SIR LOSS. IF THE OUTPUT INTERFERENCE PLUS NOISE WAS GAUSSIAN IT WOULD GIVE THE DETETECTION LOSS. NITZBERG POINTS OUT IT IS NOT GAUSSIAN AND FINDS THAT THE DETECTION LOSS IS 3dB FOR R=2K ONLY FOR LARGE FALSE ALARM PROBABILITIES, P_{FA}.

FOR SMALL P_{FA} IT IS LARGER. SPECIFICALLY:

	Loss (dB)	
P_{fa}	K = 8	K = 16
10^{-4}	5.1	3.84
10^{-5}	5.84	4.09
10^{-6}	6.70	4.32

IN THIS TABLE R = 2K-3

(SEE NITZBERG, IEEE AES, 11/80)

APPLEBAUM ADAPTIVE ARRAY

(75)

(ALSO CALLED APPLEBAUM-HOWELLS ADAPIVE LOOP ARRAY)

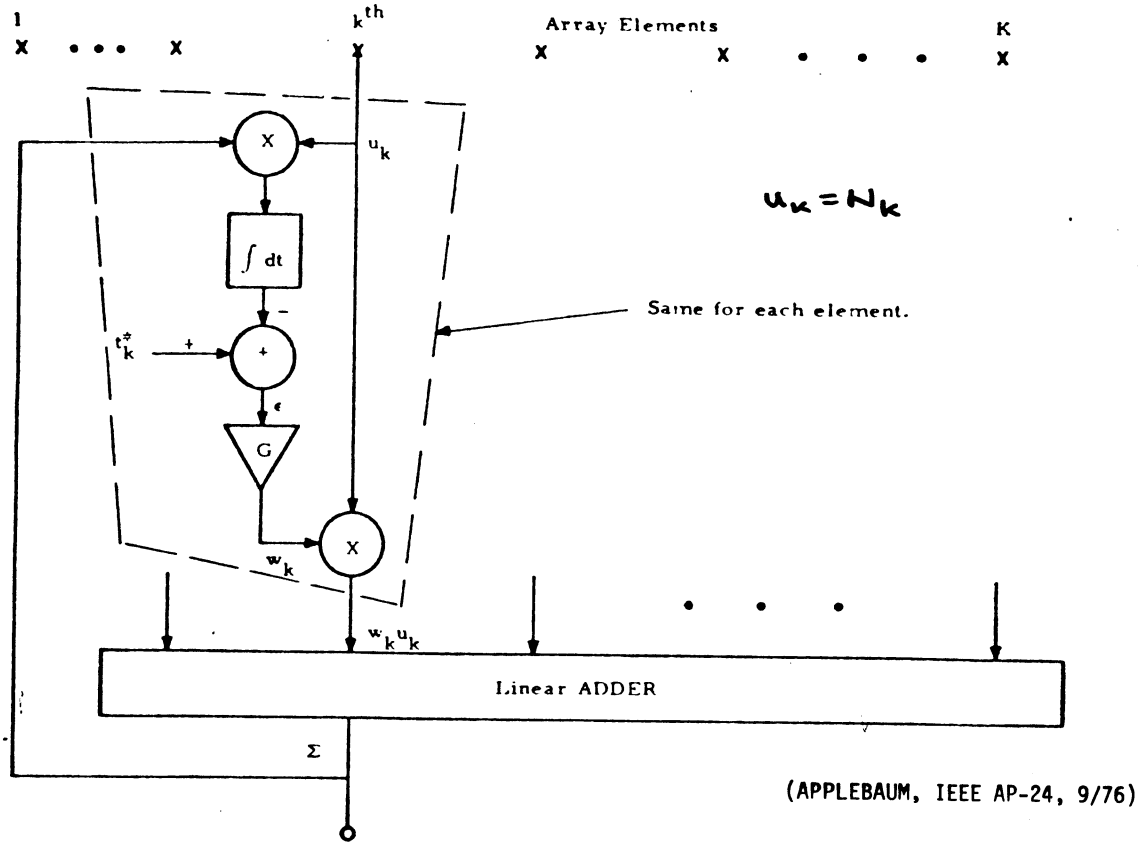

(APPLEBAUM, IEEE AP-24, 9/76)

APPLEBAUM ADAPTIVE ARRAY

(76)

(APPLEBAUM ADAPTIVE LOOPS)

$$w_k = G\left[t_k^* - u_k^* \sum_{\ell=1}^{k} w_\ell u_\ell\right] \qquad (1)$$

OR

$$\sum_{\ell=1}^{K} w_\ell \left[u_k^* u_\ell + \frac{\delta_{\ell k}}{G}\right] = t_k^* \qquad k = 1, \ldots, K$$

WHERE $\delta_{\ell k} = \begin{cases} 1 & k = \ell \\ 0 & k \neq \ell \end{cases}$

BUT $u_k^* u_\ell = k\ell$ element of M

HENCE (1) BECOMES

$$\left[M + \frac{I}{G}\right] W = T^* \qquad (2)$$

(NOTE: $T^* \equiv S^*$ HERE)

THUS FOR LARGE G (2) BECOMES

$$MW \doteq T^*$$

AND $$\boxed{W \doteq M^{-1} T^*} = W_{OPT,T}$$

UPDATED INVERSE ADAPTIVE ARRAY (77)

HERE A RECURSIVE PROCEDURE IS USED TO ESTMATE M. ASSUME $\hat{M}_J$ IS THE ESTIMATE OF M AFTER J-th DATA SAMPLE $X^{(J)}$ $J=1,2,\cdots,J$. THEN

$$\hat{M}_J = (1-\alpha)\hat{M}_{J-1} + \alpha X^{(J)*} X^{(J)} \quad * \quad (1)$$

ALSO:

$$\hat{M}_J^{-1} = \frac{1}{1-\alpha}\hat{M}_{J-1}^{-1} - \left(\frac{\alpha}{1-\alpha}\right)\frac{(M_{J-1}^{-1} X^{(J)*})(X^{(J)T}\hat{M}_{J-1}^{-1})}{(1-\alpha) + \alpha(X^{(J)T}\hat{M}_{J-1}^{-1} X^{(J)*})} \quad * \quad (2)$$

(SEE BRENNAN, MALLETT & REED, AES, 9/76)

ADAPTIVE AMTI RADAR (78)

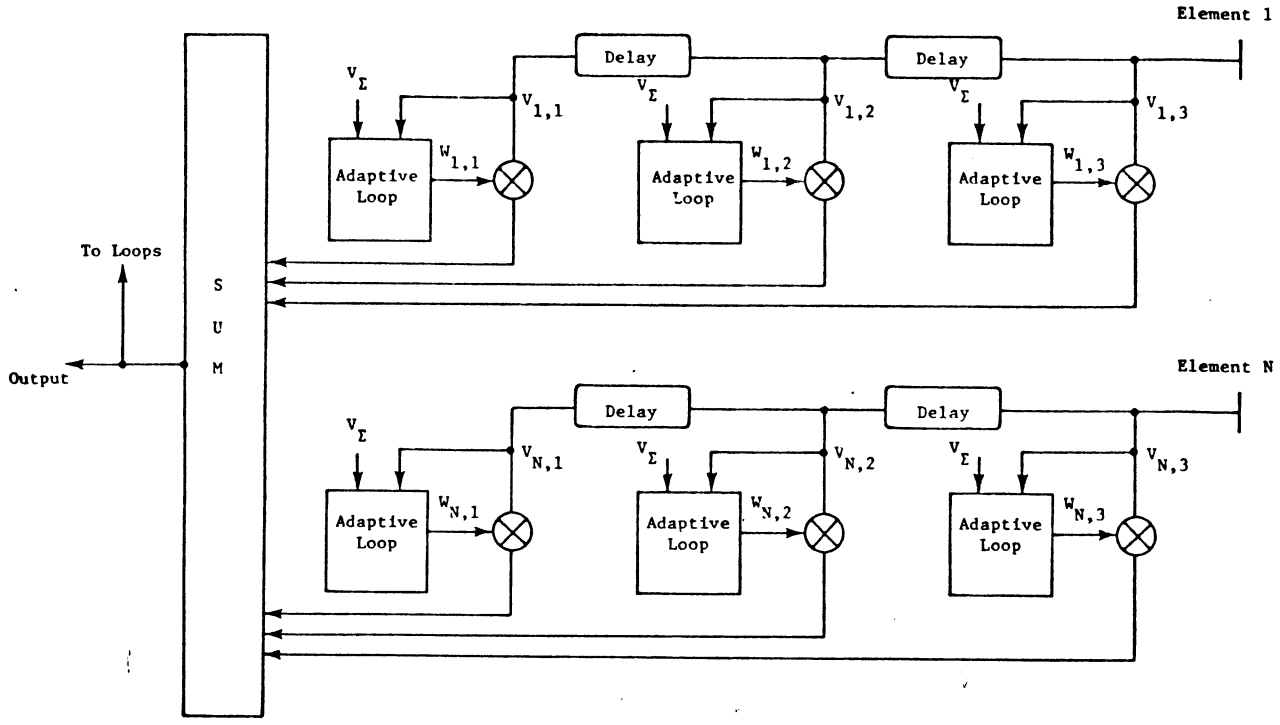

(BRENNAN, MALLETT AND REED, AP, 9/76)

(79)

ADAPTIVE PERFORMANCE VERSUS NUMBER OF SAMPLES. 8 ELEMENTS, 2 PULSES, ELEMENT SPACING = 0.5λ , INTERPULSE MOTION = 0.2λ , SCAN ANGLE = 90.0°, STEADY STATE GAIN = 125.5 dB. INITIAL CONDITIONS NEAR FINAL VALUES.

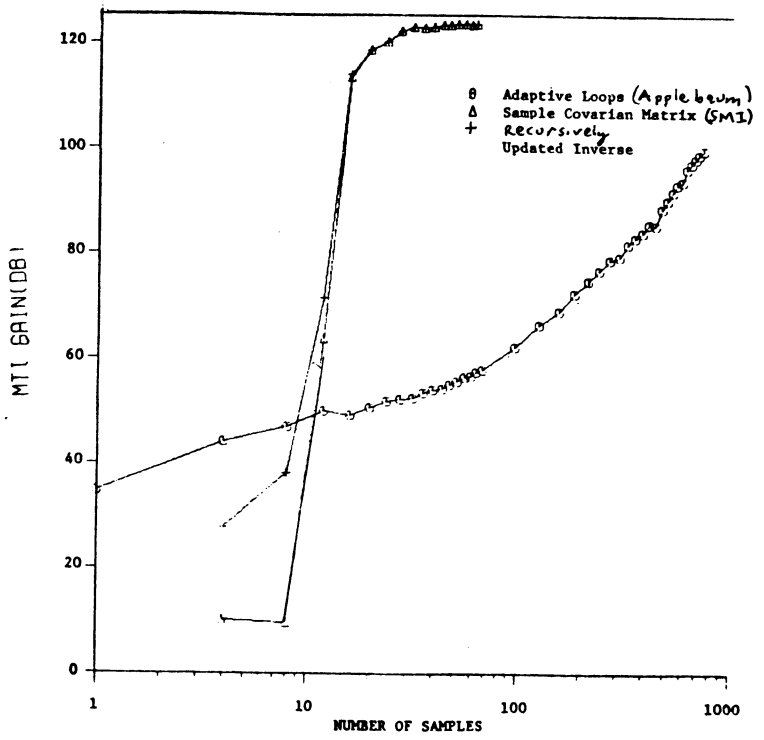

(BRENNAN, MALLETT AND REED, AP, 9/76)

(80)

ADAPTIVE PERFORMANCE VERSUS NUMBER OF SAMPLES. 8 ELEMENTS, 2 PULSES, ELEMENT SPACING = 0.5λ , INTERPULSE MOTION = 0.2λ , SCAN ANGLE = 0.0°, STEADY STATE GAIN = 108.1 dB. INITAL CONDITIONS FAR FROM FINAL VALUES.

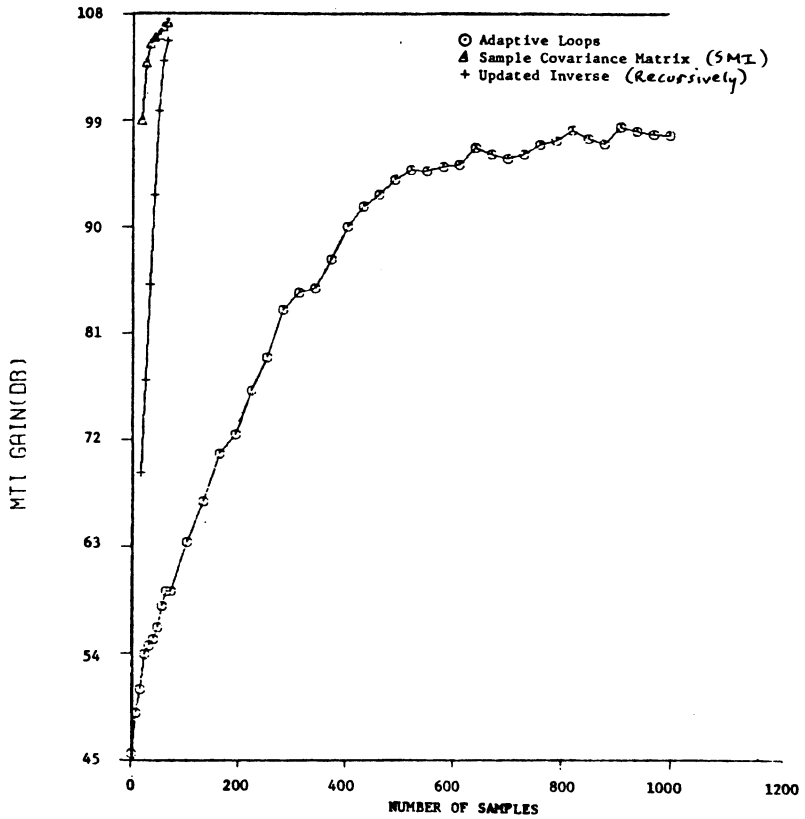

(BRENNAN, MALLETT AND REED, AP, 9/76)

CLUTTER REJECTION

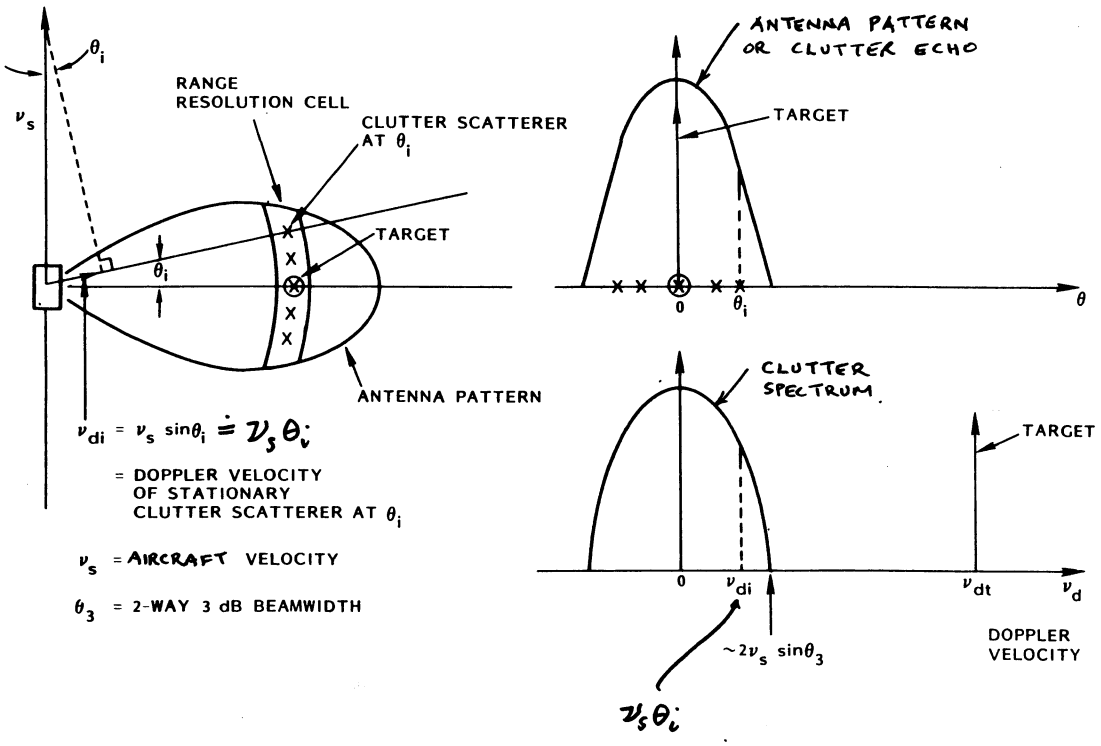

STOPPED ANTENNA

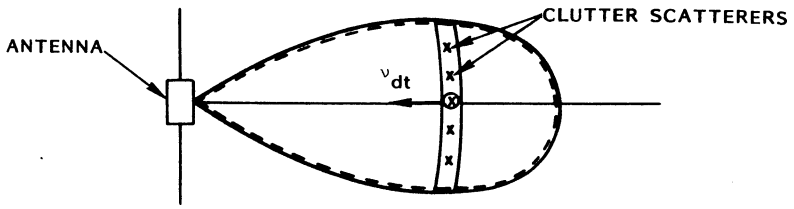

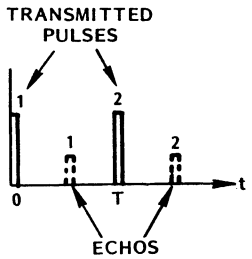

MOVING TARGET INDICATOR (MTI)

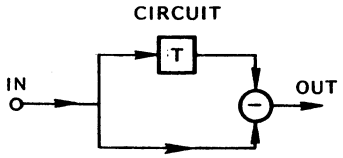

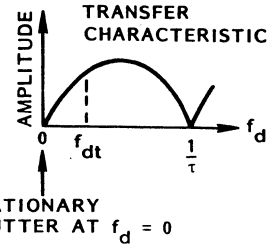

STOP THE ANTENNA

DISPLACED PHASE CENTER ANTENNA (DPCA) TECHNIQUE

MAKES ANTENNA STATIONARY

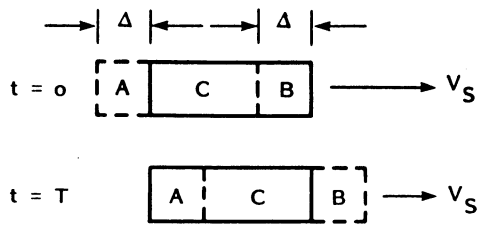

ALTHOUGH AIRCRAFT MOVED Δ IN TIME T THE ANTENNA EFFECTIVELY IS MADE STATIONARY BY SWITCHING OFF SECTION B AND SWITCHING ON SECTION A AT t=T.

TRANSMIT PATTERN

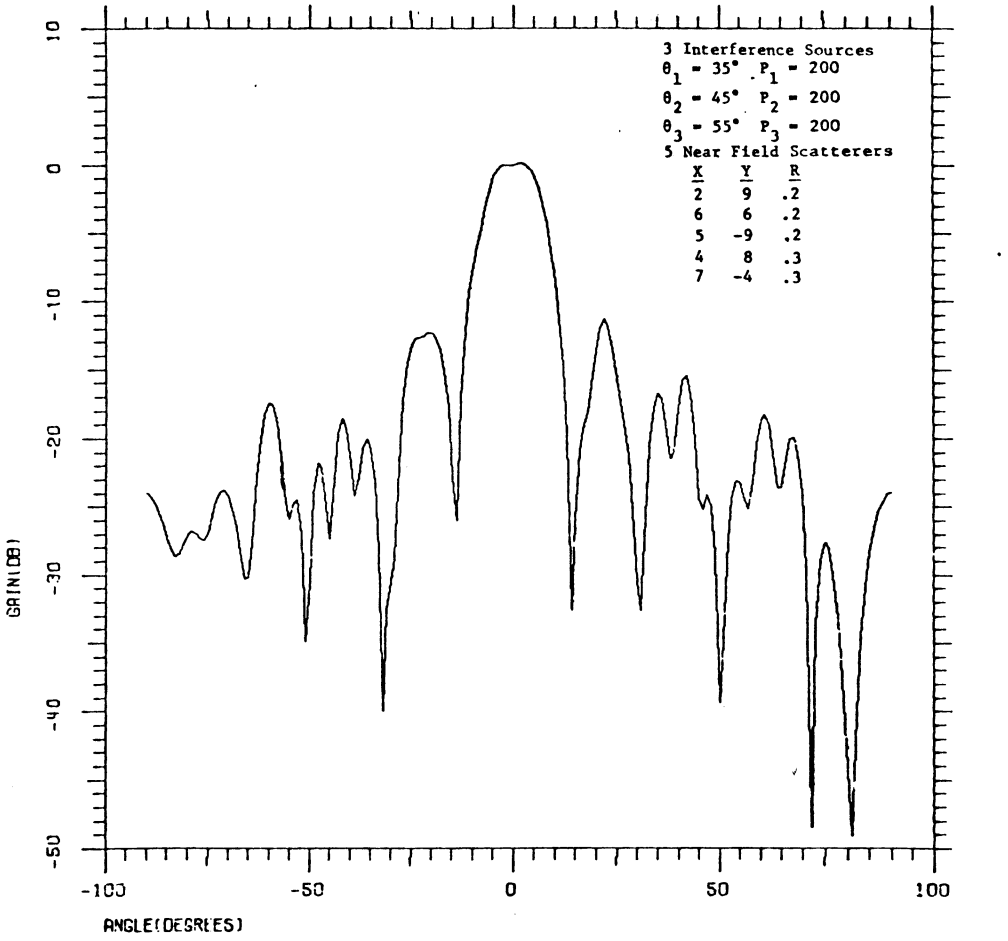

(BRENNAN, MALLETT AND REED, AP, 9/76)

(85)

RECEIVE PATTERN, PULSE 1.

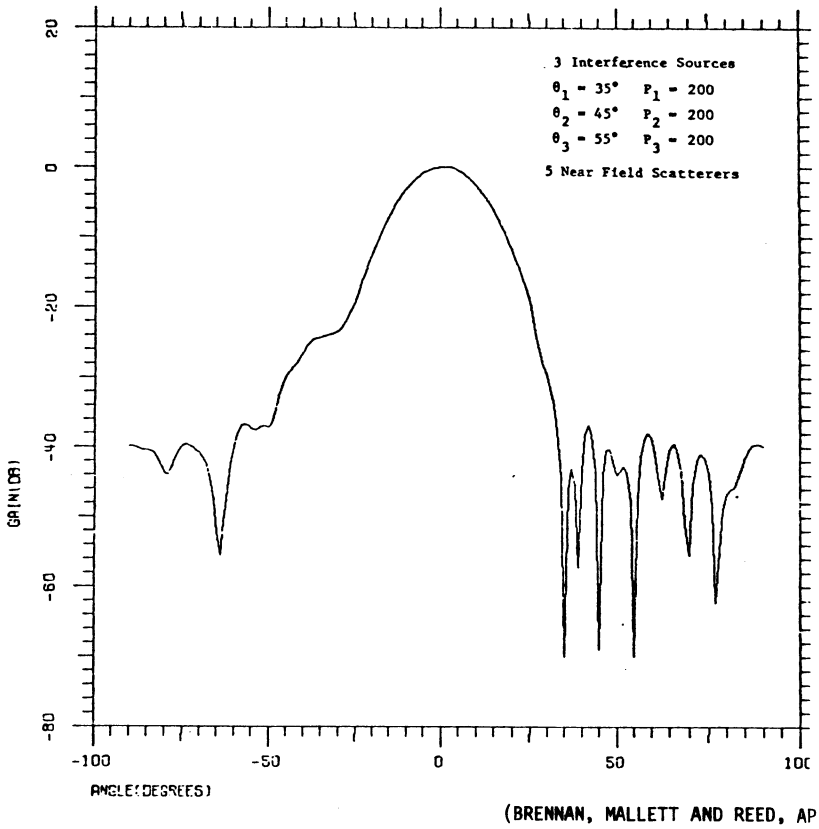

(BRENNAN, MALLETT AND REED, AP, 9/76)

(86)

RECEIVE PATTERN, PULSE 2.

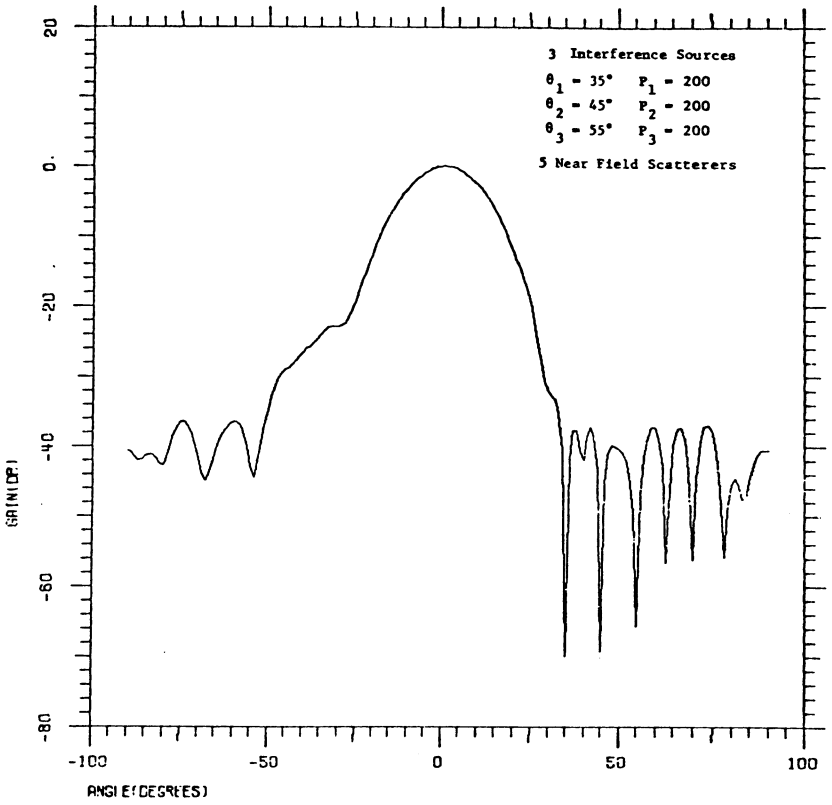

(BRENNAN, MALLETT AND REED, AP, 9/76)

ORTHOGONALIZATION

(P7)

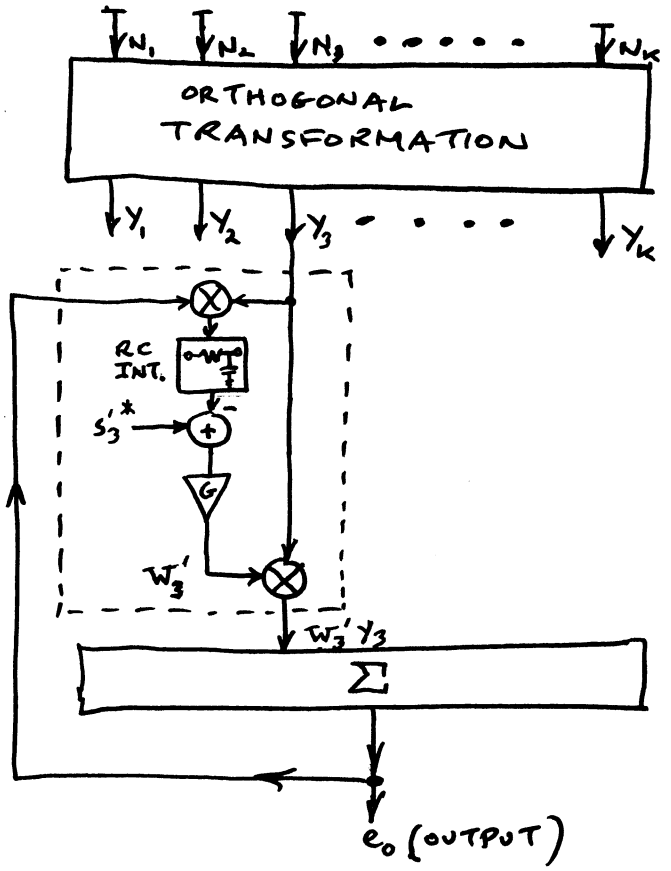

← Y_i INDEPENDENT

ORTHOGONAL APPLEBAUM LOOPS

NOTE: COULD USE SMI AFTER ORTHOGONAL TRANSFORMATION. INVERSION NOW BECOMES TRIVIAL.

(88)

ORTHOGONAL TRANSFORMATION

LET $N = [N_1, N_2, \ldots, N_K]^T$ (SEE P7)

Φ = ORTHOGONAL TRANSFORMATION MATRIX

IF

$$Y = \Phi^T N \qquad Y = [Y_1, Y_2, \ldots, Y_K]^T$$

AND

$$\overline{Y^T Y^*} = \Lambda = \begin{bmatrix} \lambda_1 & & 0 \\ & \lambda_2 & \\ & & \ddots \\ 0 & & \lambda_K \end{bmatrix}$$

λ_i ARE EIGENVALUES OF M. $\lambda_i = \overline{Y_i^* Y_i}$

Φ IS KxK MATRIX OF EIGENVECTORS OF M.

$\Phi^T \Phi = I$ = IDENTITY MATRIX.

OPTIMUM WEIGHTING (SEE (66)):

$$W_o' = \Phi^T W_o$$

$$S' = \Phi^T S \qquad S' = [S_1', S_2', \ldots, S_K']^T$$

TRANSIENT ANALYSIS FOR iTH LOOP (89)

$$\tau_o \frac{dW_i'}{dt} + W_i'(1+G_{Li}) = S_i'^* \quad (1)$$

WHERE $G_{Li} = k^2 G \lambda_i$ (2)

$$\therefore \quad \frac{dW_i'}{dt} + W_i' \underbrace{\left(\frac{1+G_{Li}}{\tau_o}\right)}_{\alpha_i} = \frac{S_i'^*}{\tau_o} \quad (3)$$

$$\therefore \quad W_i' = W_{Si}\left(1 - e^{-t/\tau_{Li}}\right) \quad (4)$$

τ_{Li} = iTH LOOP TIME CONSTANT

$$\tau_{Li} = \frac{\tau_o}{1+G_{Li}} = \frac{\tau_o}{1+k^2 G \lambda_i} \quad (5)$$

FOR $k^2 G \lambda_i^2 \gg 1$

$$\tau_{Li} \doteq \frac{\tau_o}{k^2 G \lambda_i} \quad (6)$$

TRANSIENT ANALYSIS FOR iTH LOOP (CONT.) (90)

$$\tau_{Li} \doteq \frac{\tau_o}{k^2 G \lambda_i} \quad (7)$$

THUS:

$$\tau_{Li} \propto \frac{1}{\lambda_i} \quad (8)$$

THUS SYSTEM SETTLING TIME DETERMINED BY SMALLEST λ_i.

TYPICALLY:

$$\lambda_i \tilde{\propto} \{\text{POWER OF iTH INTERFERER}\} \quad (9)$$

$$\therefore \quad \tau_{Li} \tilde{\propto} \frac{1}{\text{POWER OF iTH INTERFERER}} \quad (10)$$

ON REDUCING SETTLING TIME (91)

- WOULD LIKE ALL LOOPS TO HAVE SETTLING TIME OBTAINED FOR STRONGEST JAMMER.
- THIS IS ACHIEVED BY USING AGC FOR EACH Y_i SO AS TO MAKE THEM HAVE IDENTICAL POWERS AT OUTPUTS OF AGCs.

  THIS IS CALLED A WHITENING FILTER.

ORTHOGONALIZATION AND WHITENING (91a)

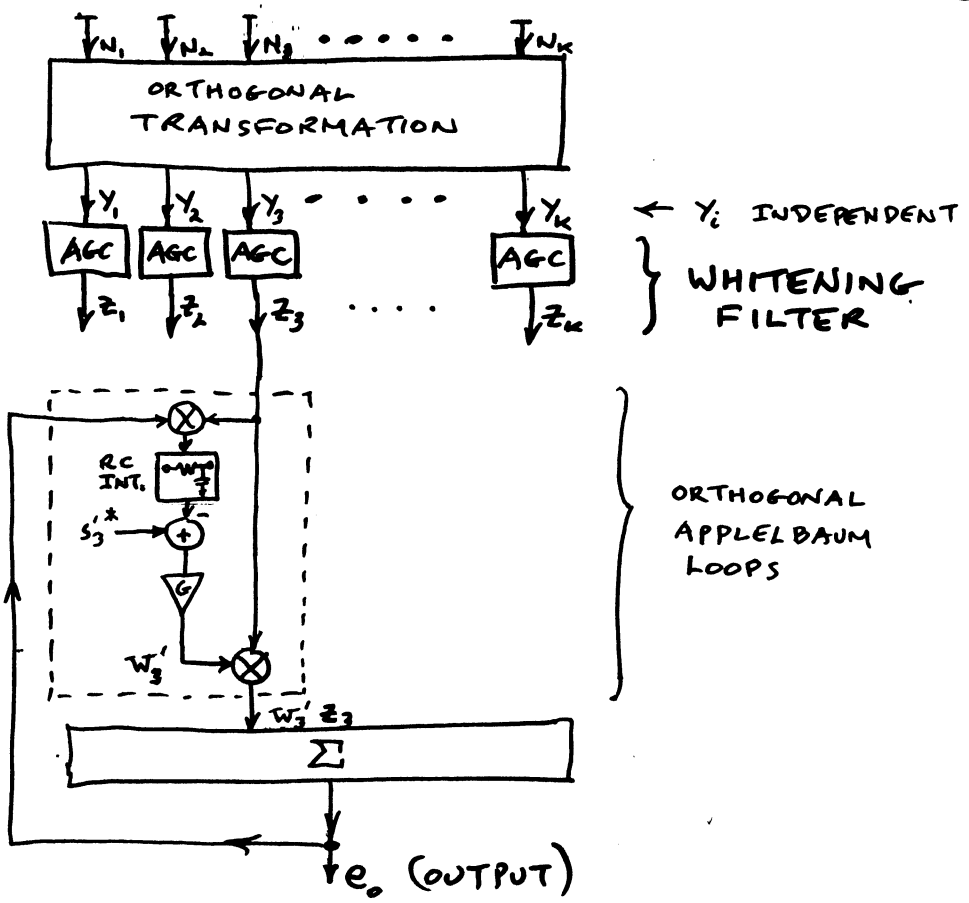

AGC (OR WHITENING FILTER) OUTPUT

AGC ADJUSTED SO THAT:

$$\overline{z_i^* z_i} = \lambda_{MAX} \text{ EXPECTED FOR "M"} \quad (1)$$

THEN

$$\tau_{Li} = \tau_{L,MIN} = \frac{\tau_o}{K^2 G \lambda_{MAX}} \quad (2)$$

ORTHOGONALIZATION AND WHITENING

FOLLOW ORTHOGONAL TRANSFORMATION Φ WITH WHITENING TRANSFORMATION $\Lambda^{-1/2}$ TO GET COMBINED TRANSFORMATION Φ'

$$\Phi' = \Lambda^{-1/2} \Phi$$

$$Y = \Phi^T N$$

$$Z = \Lambda^{-1/2} \Phi^T N = \Phi' N$$

THUS

$$\overline{z_i^* z_i} = 1$$

$$\overline{Z^* Z^T} = I = \text{IDENTITY MATIX} = \begin{bmatrix} 1 & & 0 \\ & 1 & \\ 0 & & \ddots & 1 \end{bmatrix}$$

$$= \Lambda^{-1/2} \Phi^{*T} N^* N^T \Phi \Lambda^{-1/2} = \Lambda^{-1/2} \Phi^{*T} M \Phi \Lambda^{-1/2}$$

$$= \Lambda^{-1/2} \Lambda \Lambda^{-1/2} = I$$

OPTIMUM WEIGHTING:

$$W_o' = \Phi'^T W_o = \Lambda^{-1/2} \Phi^T W_o$$

$$S' = \Phi'^T S$$

INDEPENDANCE OF Y_{1r} & Y_{2r}.

$$Y_{1r} = \frac{X_{1r}}{\sqrt{\overline{|X_{1r}|^2}}}$$

$$Y_{2r,\text{un}} = X_{2r} - \overline{X_{1r} Y_{1r}^*}\, Y_{1r}$$

$$Y_{2r,\text{un}}\, Y_{1r}^* = X_{2r} Y_{1r}^* - \overline{X_{1r} Y_{1r}^*}\, Y_{1r} Y_{1r}^*$$

$$\frac{1}{k}\sum_{\text{all } r}\left(Y_{2r,\text{un}}\, Y_{1r}^*\right) = \frac{1}{k}\sum_{\text{all } r}\left(X_{2r} Y_{1r}^*\right) - \overline{X_{1r} Y_{1r}^*}\,\underbrace{\frac{1}{k}\sum_{\text{all } r}\left(Y_{1r} Y_{1r}^*\right)}_{1}$$

$$= \overline{X_{1r} Y_{1r}^*} - \overline{X_{1r} Y_{1r}^*} = 0$$

GRAM-SCHMIDT ORTHOGONALIZATION

$$Y_1 = \frac{X_1}{\sqrt{|X_1|^2}} \qquad (1)$$

$$Y_i = \frac{X_i - \sum_{m=1}^{i-1} (\overline{X_i Y_m^*}) Y_m}{\left| X_i - \sum_{m=1}^{i-1} (\overline{X_i Y_m^*}) Y_m \right|^2} \qquad (2)$$

ORTHOGONALIZATION-WHITENING PROCESS

$X = [X_1, X_2, \cdots, X_K]^T$ $\qquad$ $Y = [Y_1, Y_2, \cdots, Y_K]^T$

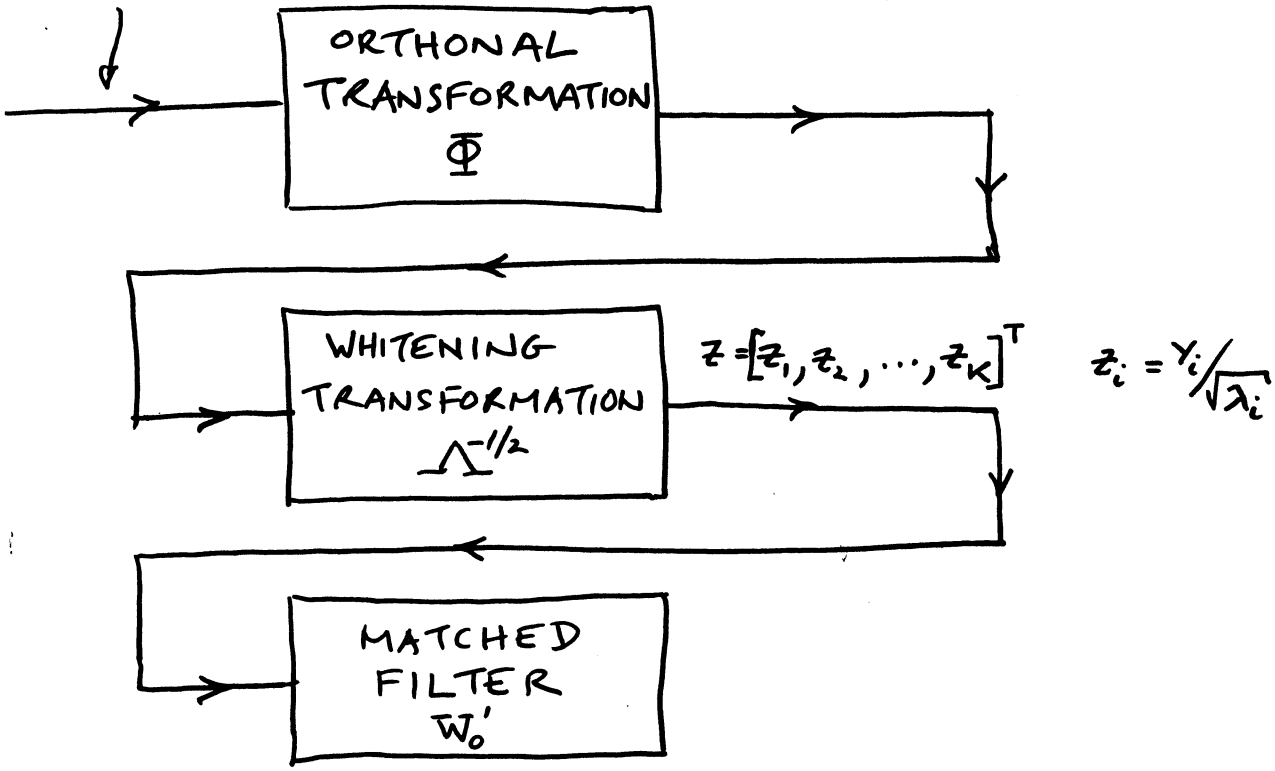

GRAM-SCHMIDT ORTHOGONALIZATION USING APPLEBAUM-HOWELLS LOOPS

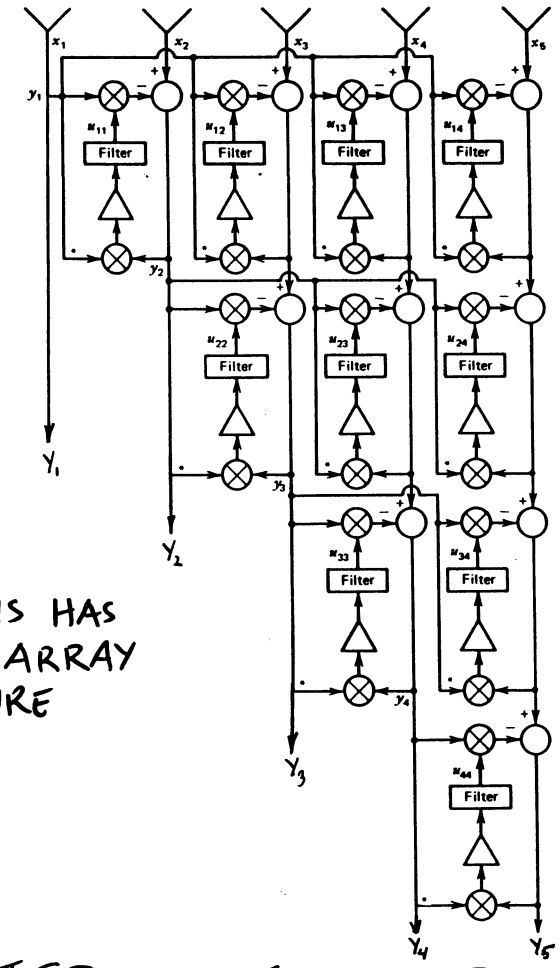

NOTE THAT THIS HAS A SYSTOLIC ARRAY ARCHITECTURE

(SEE MONZINGO AND MILLER, WILEY)

ADAPTED ANTENNA PATTERN AS UNADAPTED PATTERN MINUS AUXILIARY PATTERNS (EIGENVECTOR PATTERNS) AT JAMMER LOCATIONS

LEGEND

——— UNADAPTED MAIN BEAM PATTERN

••••••• AUXILIARY PATTERN (EIGENVECTOR PATTERN)

----- ADAPTIVED PATTERN

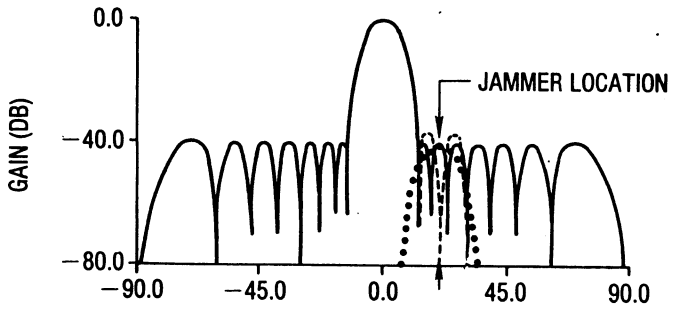

ADAPTED ANTENNA PATTERN AS UNADAPTED PATTERN MINUS AUXILIARY PATTERNS (EIGENVECTOR PATTERNS) AT JAMMER LOCATIONS

(97)

LET

$G_A(\theta)$ = ADAPTED PATTERN

$G_o(\theta)$ = UNADAPTED PATTERN

THEN

$$G_A(\theta) = G_o(\theta) - \sum_{i=1}^{K-1} g_i \phi_i(\theta)$$

WHERE

$\phi_i(\theta)$ = iTH EIGENVECTOR PATTERN

(SEE APPLEBAUM, IEEE AP 9/76)

ADAPTIVE ARRAY ANTENNA PATTERNS: WITH AND WITHOUT JAMMER

(98)

$\theta_S = 0^o$, $\theta_J = 21^o$, $P_J/P_N = 1250$

$\lambda_{MAX} = 10{,}001$

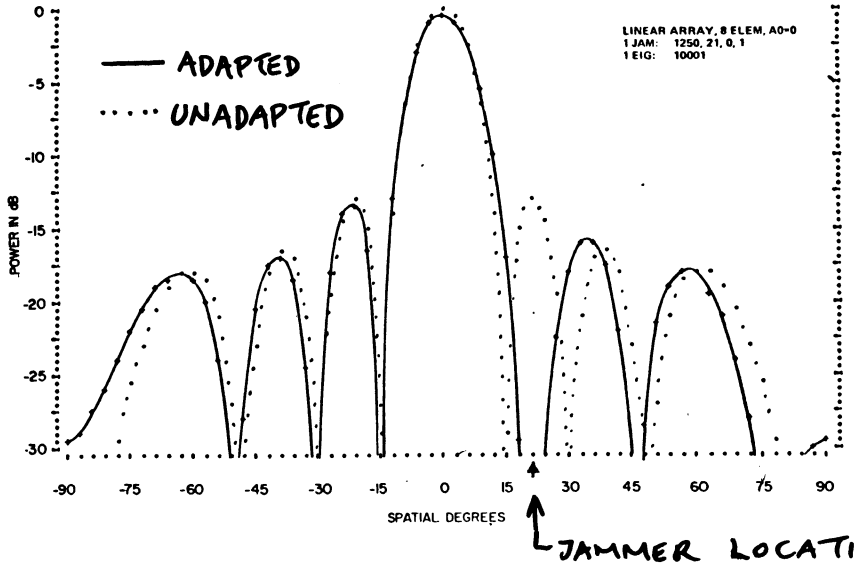

(AFTER GABRIEL, PROC. IEEE, FEB. '76, pp239-272)

EIGENVECTOR BEAM (RETRODIRECTIVE BEAM) FOR SINGLE JAMMER

$\theta_S = 0^0$, $\theta_J = 21^0$, $P_J/P_N = 1250$

$\lambda_{MAX} = 10{,}001$

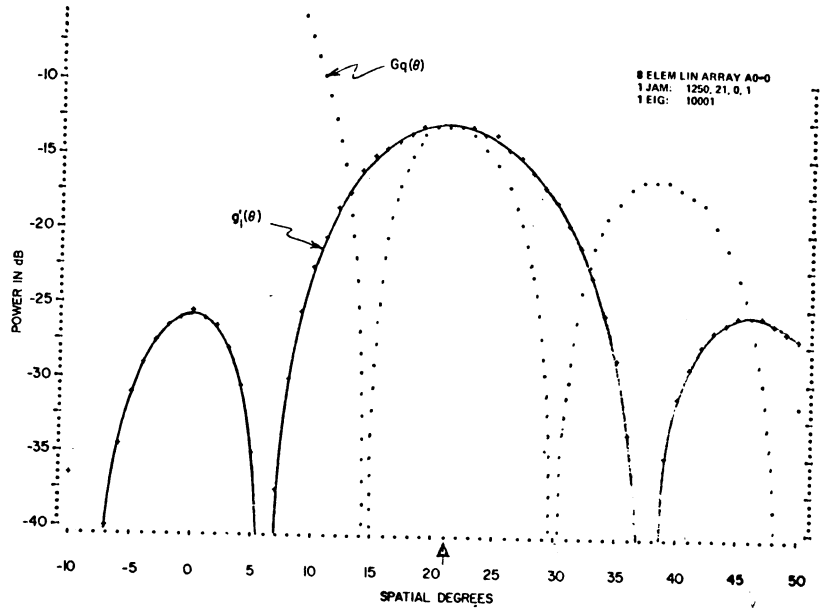

..... UNADAPTED MAINBEAM PATTERN

——— EIGENVECTOR PATTERN

(AFTER GABRIEL, PROC. IEEE, FEB. '76, pp239-272)

EIGENVECTOR BEAMS FOR TWO CLOSELY SPACED JAMMERS

$\theta_S = 0°$, $\theta_{J1} = 18°$, $\theta_{J2} = 22°$

$(P_J/P_N)_1 = 1250$, $(P_J/P_N)_2 = 1200$

$\lambda_1 = \lambda_{MAX} = 18{,}544$, $\lambda_2 = 1057$

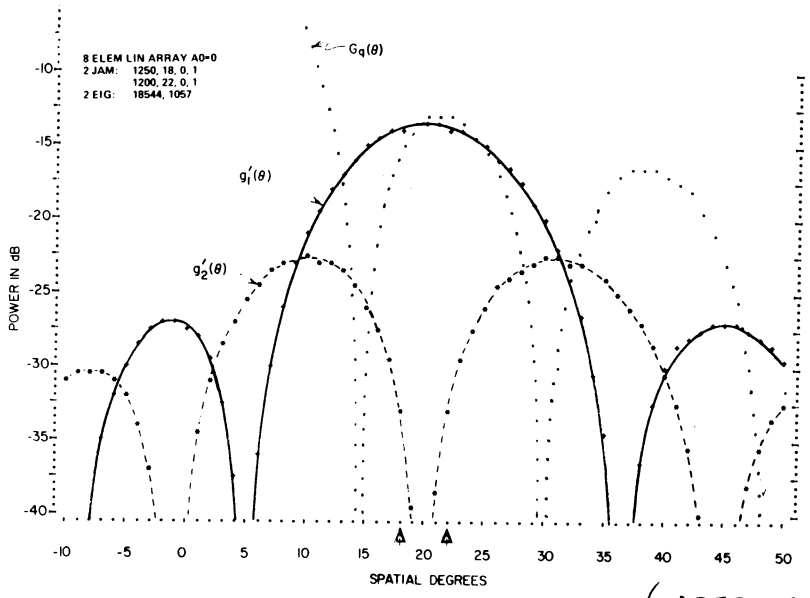

..... UNADAPTED MAINBEAM PATTERN

——— EIGENVECTOR PATTERN #1

——* EIGENVECTOR PATTERN #2

(AFTER GABRIEL, PROC. IEEE, FEB. '76)

UNADAPTED AND ADAPTED PATTERNS FOR TWO CLOSELY SPACED JAMMERS

$\theta_s = 0°$, $\theta_{J1} = 18°$, $\theta_{J2} = 22°$

$(P_J/P_N)_1 = 1250$, $(P_J/P_N)_2 = 1200$

$\lambda_1 = \lambda_{MAX} = 18,544$, $\lambda_2 = 1057$

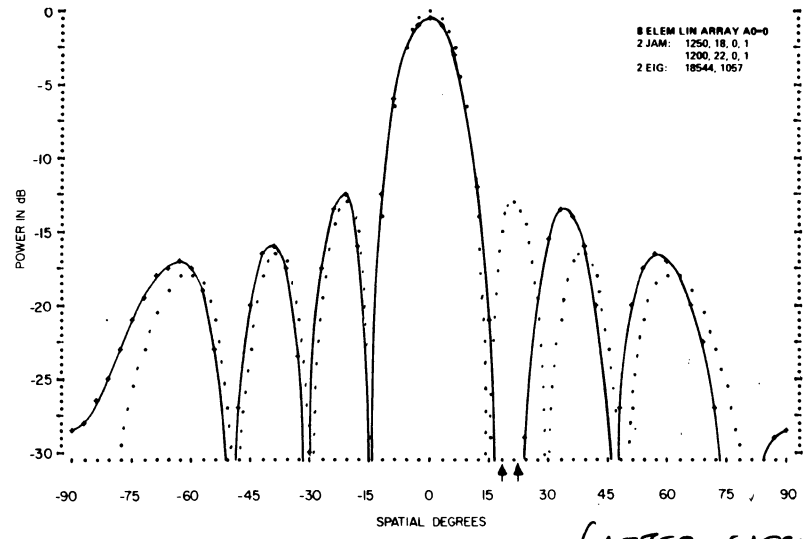

(AFTER GABRIEL, PROC. IEEE, FEB. '76)

LATTICE FILTER FOR ORTHOGONALIZATION

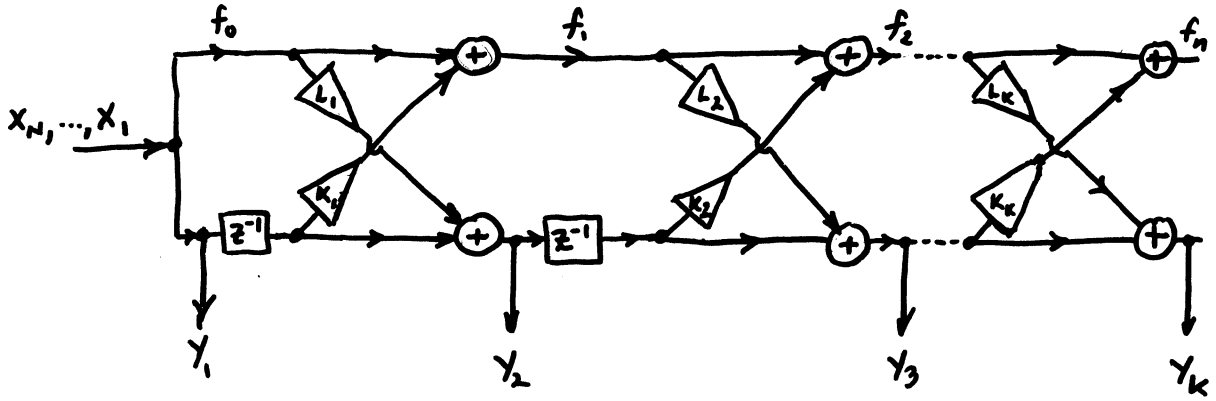

$$K_i(n) = -E[f_{i-1}(n)\, Y_{i-1}(n-1)] \,/\, E[Y^2_{i-1}(n-1)]$$

$$L_i(n) = -E[f_{i-1}(n)\, Y_{i-1}(n-1)] \,/\, E[f^2_{i-1}(n)]$$

n = nth time sample.

(McWhirter etal, IEE PROC., Pt.F, 2/83)

SYSTOLIC ADAPTIVE ARRAY JAMMER NULLING

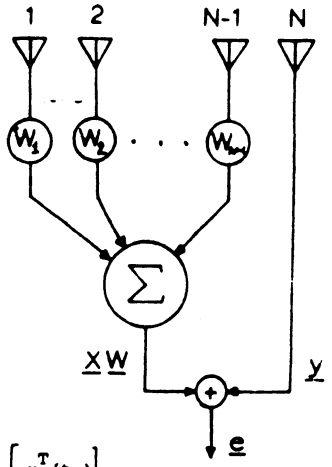

$$\underline{X}(k) = \begin{bmatrix} \underline{x}^T(t_1) \\ \underline{x}^T(t_2) \\ \vdots \\ \underline{x}^T(t_k) \end{bmatrix}$$

$$\phi = \underline{e}^H(k)\,\underline{e}(k) = \| \underline{X}\,\underline{W} + \underline{y} \|^2$$

$$= \underline{W}^H \underline{X}^H \underline{X}\,\underline{W} + \underline{W}^H \underline{X}^H \underline{y} + \underline{y}^H \underline{X}\,\underline{W} + \underline{y}^H \underline{y}$$

$$\bar{\nabla}\phi = 2\,|\underline{X}^H \underline{X}\,\underline{W} + \underline{X}^H \underline{y}|$$

Complex gradient, $\bar{\nabla}\phi$, is zero when

$$\underline{X}^H \underline{X}\,\underline{W} = -\underline{X}^H \underline{y}$$

FIGURE 1 : The Least Squares Solution *

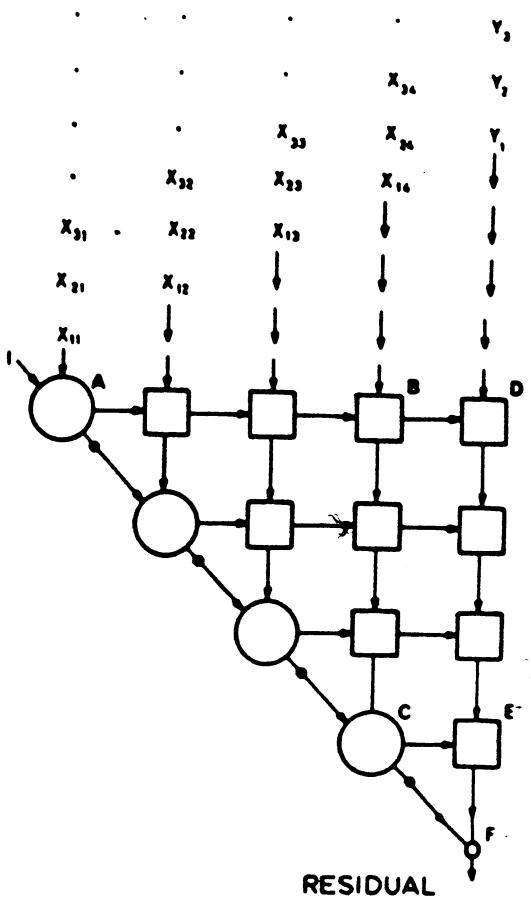

Figure 1. Systolic array for recursive least-squares minimization#

(a) BOUNDARY CELL

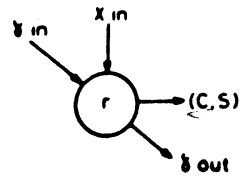

If $x_{in} = 0$ then
$(c \leftarrow 1;\ s \leftarrow 0$
$y_{out} \leftarrow y_{in})$ otherwise
$(r' \leftarrow (\beta^2 r^2 + x_{in}^2)^{\frac{1}{2}}$
$c \leftarrow \beta r/r';\ s \leftarrow x_{in}/r'$
$r \leftarrow r';\ y_{out} \leftarrow c\, y_{in})$

(b) INTERNAL CELL

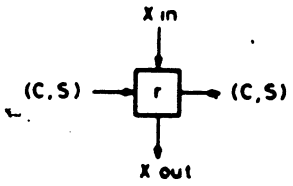

$x_{out} \leftarrow c\, x_{in} - s\, \beta r$

$r \leftarrow s\, x_{in} + c\, \beta r$

(c) FINAL CELL

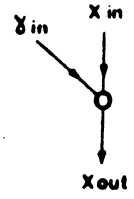

$x_{out} \leftarrow y_{in}\, x_{in}$

Figure 2. Cells required for the basic Givens rotation algorithm#

(* WARD ET AL., ICASSP-84)

(# McWHIRTER, SPIE VOL. 431, 1983)

WORDLENGTH DEPENDENCE ON ALGORITHM

102a

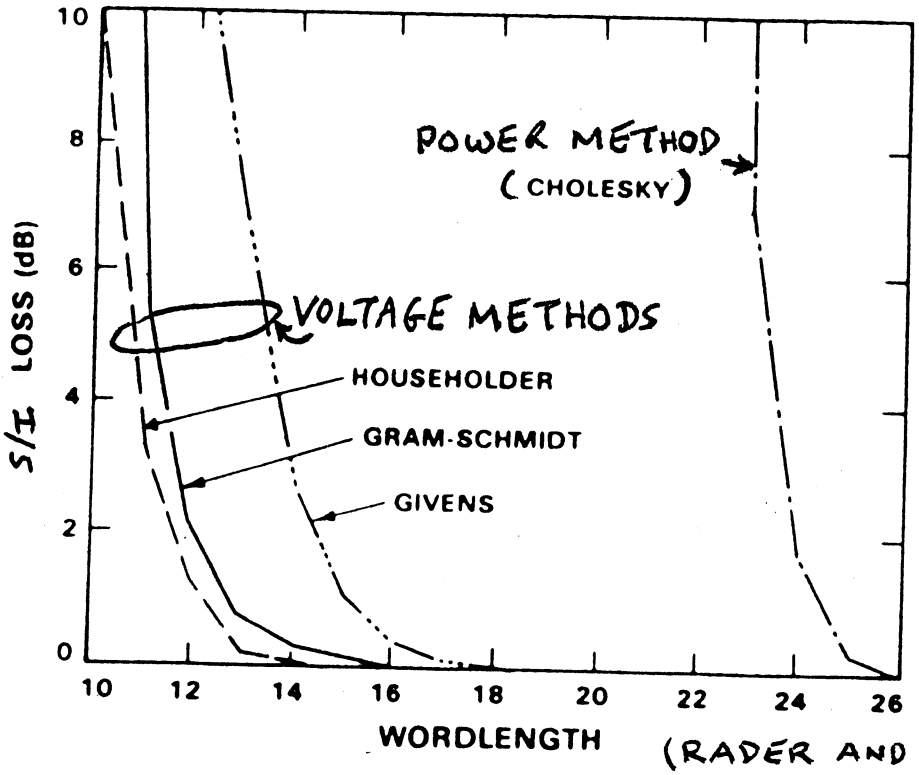

(RADER AND STEINHARDT, IEEE ASSP-34, 12/86)

PERFORMANCE OF VOLTAGE (GIVENS) VERSUS POWER (SMI) METHODS

102e

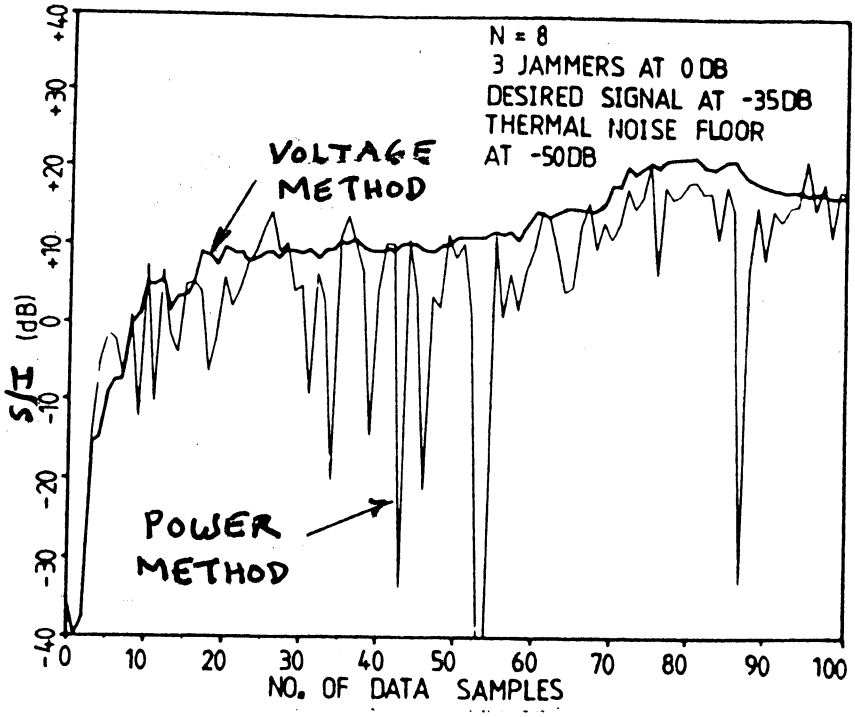

(WARD ET AL IEEE AP-34 3/86)

WIDROW MINIMUM MEAN SQUARE ERROR (MSE) ADAPTIVE ARRAY

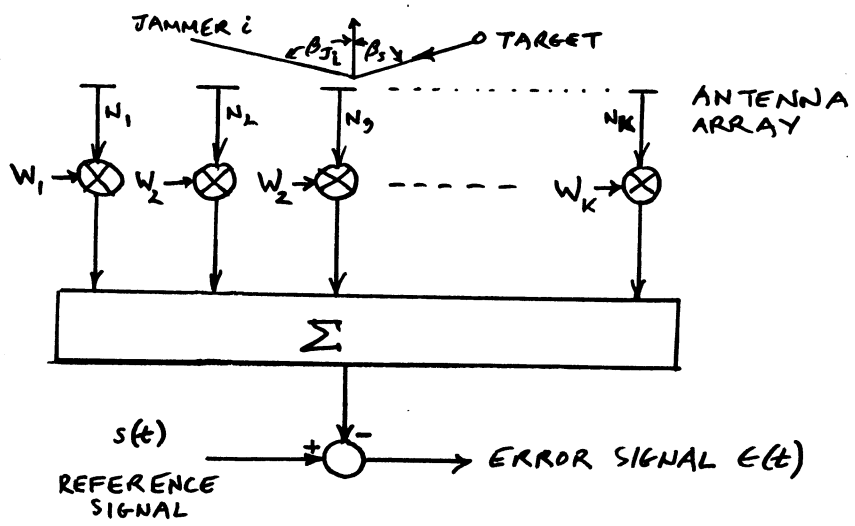

$$\epsilon(t) = s(t) - W^T N \qquad (1)$$

OPTIMUM WEIGHT W IS ONE THAT MINIMIZES $\overline{|\epsilon(t)|^2}$

WHICH IS

$$\boxed{W_{OPT} = M^{-1} m_{NS}^*} \qquad (2)$$

(WEINER-HOPF EQ. IN MATRIX FORM, THIS IS WEINER SOL.)

$$m_{Nd} = \left[\overline{N_1 s^*(t)}, \overline{N_2 s^*(t)}, \cdots \overline{N_K s^*(t)}\right]^T \qquad (3)$$

RELATIONSHIP OF MIN. MSE TO MAX. SIR SOLUTION

$$N = s(t)\,S + N_{TH} + J \qquad (1)$$

WHERE $N_{TH} = \left[N_{TH1}, N_{TH2}, \cdots, N_{THK}\right]^T \qquad (2)$

N_{THi} = THERMAL NOISE AT iTH ELEMENT

$J = \left[J_1, J_2, \cdots, J_K\right] \qquad (3)$

J_i = INTERFERENCE AT iTH ELEMENT

S = NORMALIZED RECEIVED SIGNAL FROM DIRECTION β_s

$S = \left[1, \exp j\xi, \exp j2\xi, \cdots, \exp j(k-1)\xi\right]^T \qquad (4)$

$\xi = \frac{2\pi d}{\lambda} \sin\beta_s$, d = SPACING BETWEEN ARRAY ELEMENTS

THEN $m_{NS} = P_s S$ WHERE $P_s = \overline{s(t)s^*(t)}$ = AV. SIG. POWER

AND

$$\boxed{W_{MSE} = P_s M^{-1} S^*} \qquad (5)$$

WHICH IS MAX. SIR SOL.

SEE (66).

DERIVATION OF MIN. MSE SOLUTION (105)

ASSUME REAL VARIABLES FOR SIMPLICITY. THEN:

$$\epsilon(t) = s(t) - W^T N \quad (1)$$

$$\overline{\epsilon^2(t)} = \overline{s^2(t)} - 2s(t)W^T N + \overline{(W^T N)^2} \quad (2)$$

$$= P_s - 2W^T m_{NS} + W^T N W \quad (3)^*$$

GRADIENT OF $\overline{\epsilon^2(t)} = \nabla_W[\overline{\epsilon^2}]$ IS GIVEN BY $^\#$

$$\nabla_W[\overline{\epsilon^2}] = -2m_{NS} + 2MW \quad (4)$$

SETTING $\nabla_W[\overline{\epsilon^2}] = 0$ TO SOLVE FOR MIN. $\overline{\epsilon^2}$ YIELDS

$$\boxed{MW = m_{NS}} \quad (5)$$

OR $$\boxed{W_{MSE} = M^{-1} m_{NS}} \quad (6) \quad \text{QED.}$$

---

* NOTE: $\overline{(W^T N)^2} = \overline{(W^T N)(W^T N)^T} = W^T \overline{N N^T} W = W^T M W$

$^\#$ $\nabla_W(\xi) = \frac{\partial \xi}{\partial W_1} e_1 + \frac{\partial \xi}{\partial W_2} e_2 + \cdots + \frac{\partial \xi}{\partial W_K} e_K$ WHERE $e_1, \ldots, e_K$ ARE UNIT BASIS VECTORS OF VECTOR W.

LEAST MEAN SQUARE (LMS) STEEPEST DESCENT ALGORITHM (106)

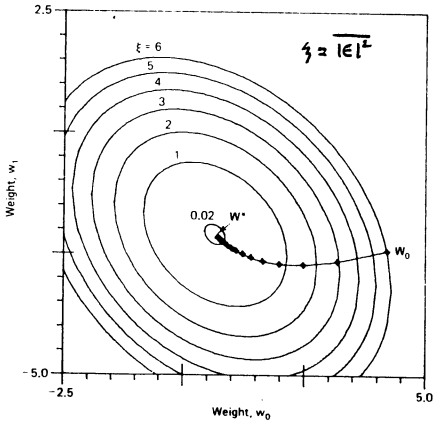

$$\boxed{W_{j+1} = W_j + \mu \epsilon_j N(j)} \quad (1)$$

WHERE W_j = jTH ITERATION ESTIMATE OF W.

$N(j)$ = jTH TIME SAMPLE OF N_j

$\epsilon_j = s(t_j) - W_j^T N_j$

μ = A CONST. THAT DETERMINES CONVERGENCE RATE.

ANALOG REALIZATION OF LMS ALGORITHM (107)

$$W_{j+1} = W_j + \mu \epsilon_j N(j)$$

$$\frac{W_{j+1} - W_j}{\Delta t} = a \epsilon_j N^*(j) \qquad \text{(IN COMPLEX NOTATION.)}$$

$$\frac{dW(t)}{dt} = a \epsilon(t) N^*(t)$$

$$W(t) = a \int_0^t \epsilon(t) N^*(t)\, dt + W(0)$$

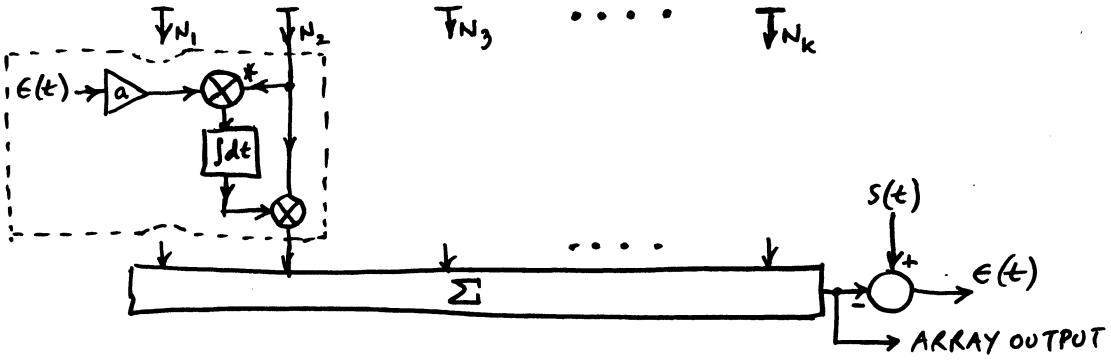

(107a)

DERIVATION OF NEWTON ALGORITHM

LET $$\boxed{\xi = \overline{|\epsilon(t)|^2}} \qquad (1)$$

THIS CAN BE WRITTEN AS

$$\boxed{\xi = \xi_{MIN} + (W - W_0)^T M (W - W_0)} \qquad (2)$$

WHERE $W_0 = W_{OPT} = W_{MSE}$ (3)

OR $$\boxed{\xi = \xi_{MIN} + V^T M V} \qquad (4)$$

WHERE $V = W - W_0$ (5)

$\therefore$ $$\boxed{\nabla_V \xi = 2MV = 2M(W - W_0)} \qquad (6)$$

$$\boxed{W - W_0 = \tfrac{1}{2} M^{-1} \nabla_V \xi} \qquad (7)$$

$$\boxed{W_{k+1} = W_k + \tfrac{1}{2} M^{-1} \nabla_V \xi} \qquad (8)$$

FULLY ADAPTIVE ARRAY AS MULTI-LOOP SLC (MSLC)

FOR FULLY ADAPTIVE ARRAY

$$W_o = M^{-1} S^* \quad (1) \quad (\text{SEE } 66)$$

FOR MSLC

$$S^* = [1, 0, 0, \ldots, 0]^T \quad (2) \quad (\text{SEE } 64)$$

REWRITE (1) AS

$$M W_o = S^* \quad (3)$$

LET

$$M = \left[\begin{array}{c|c} P_o & \Psi^{T*} \\ \hline \Psi & M_a \end{array}\right] \quad (4), \qquad W_o = \left[\begin{array}{c} 1 \\ \hline W_1 \\ \vdots \\ W_k \end{array}\right] = \left[\begin{array}{c} 1 \\ \hline W_a \end{array}\right] \quad (5) \quad (\text{SEE } 64)$$

WHERE W_o = WEIGHT ON MAIN CHANNEL WHICH WAS WITHOUT LOSS OF GENERALITY SET AT "1".

W_a = WEIGHTS FOR AUXILIARY ANTENNAS (SEE 64)

THEN (3) BECOMES

FULLY ADAPTIVE ARRAY AS MSLC (CONT.)

$$P_o + \Psi^{T*} W_a = 1 \quad (6)$$

$$\Psi + M_a W_a = 0 \quad (7)$$

$$\therefore \quad \boxed{W_{a,OPT} = M_a^{-1} \Psi} \quad (8)$$

WHERE

$$\Psi = \begin{bmatrix} \overline{N_1^* N_o} \\ \overline{N_2^* N_o} \\ \vdots \\ \overline{N_k^* N_o} \end{bmatrix} \quad (9)$$

N_o = SIGNAL + INTERFENCE RECEIVED IN MAIN CHANNEL

N_i = " " " " " iTH AUXILIARY.

METHODS FOR ESTIMATING W_a FOR MSLC

SAME AS FOR

FULLY

ADAPTIVE

ARRAY

SEE (71)

GRAM-SCHMIDT IMPLEMENTATION OF TWO AUXILIARY SLC

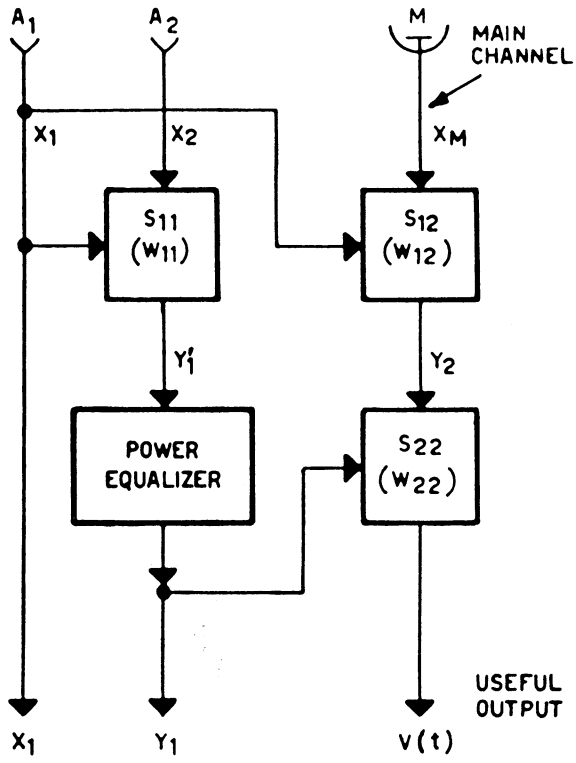

(FROM BUCCIARELLI ET AL, RADAR-82)

DIGITAL GRAM-SCHIDT CANCELLER: (112)

SINGLE AD AND ALU TIME SHARED

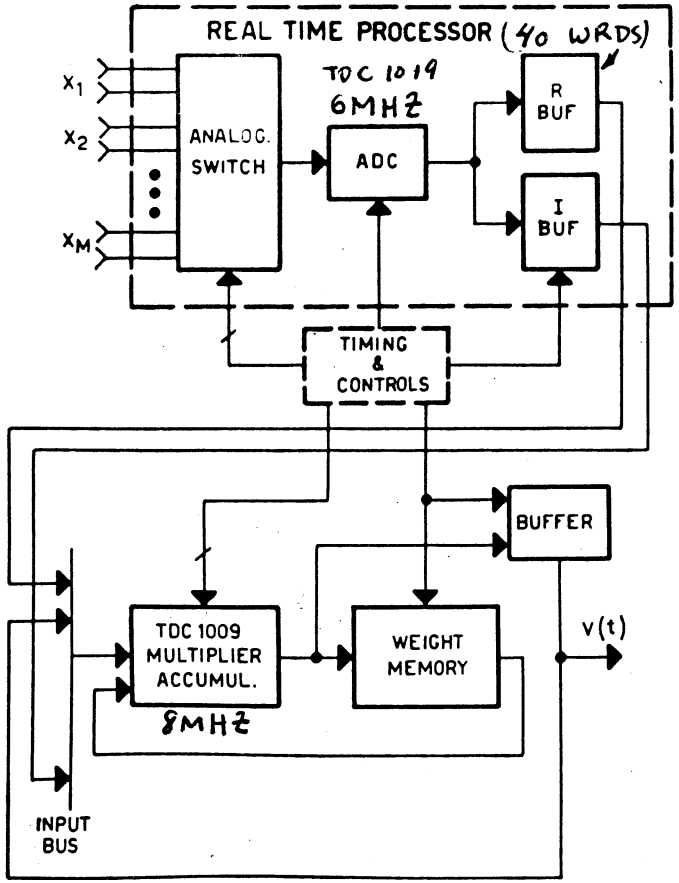

(AFTER BUCCIARELLI ET AL, RADAR-82)

TRANSIENT RESPONSE OF GRAM-SCHMIDT (GS) TWO AUX. SLC (113)

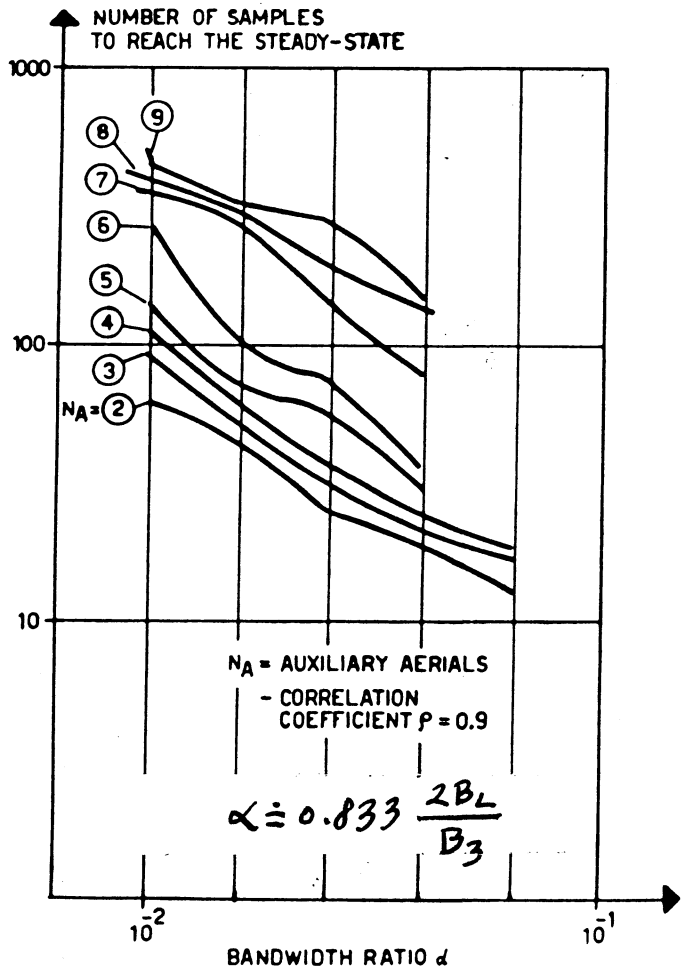

(AFTER BUCCIARELLI ET AL RADAR-82)

NOTE: STEADY STATE CR GIVEN BY (54) FOR HOWELLS-APPLEBAUM SYSTEM APPLY FOR GS CASE AS WELL.

TRANSIENT RESPONSE OF HOWELLS-APPLEBAUM (L/MSLC) TWO AUX. SLC

(114)

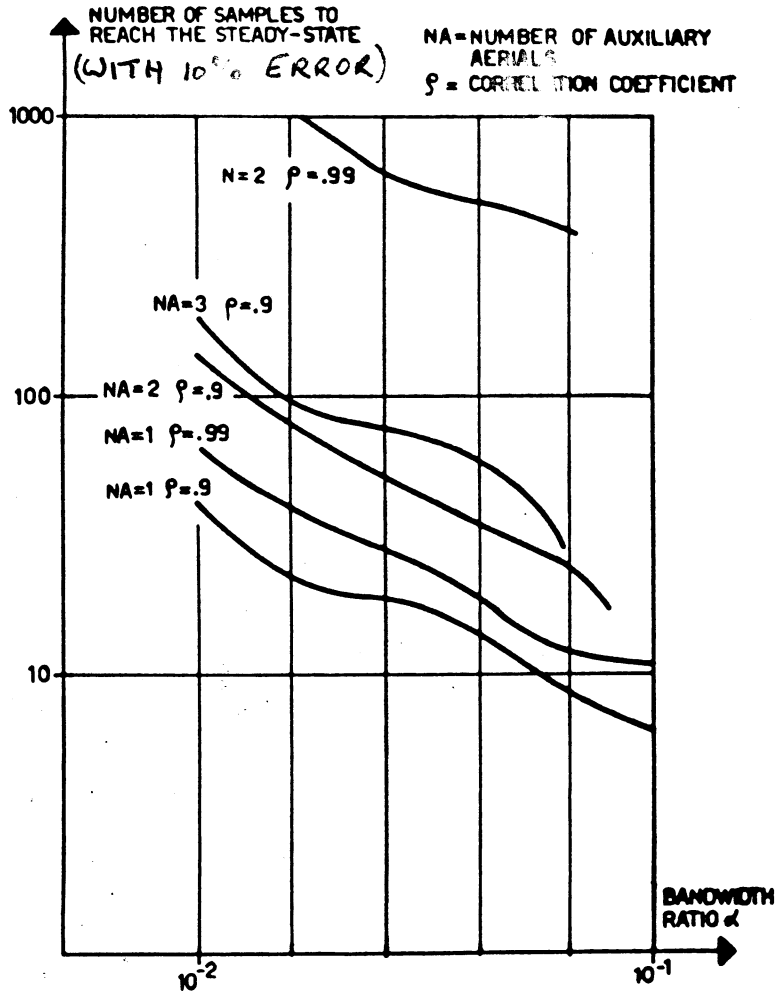

(AFTER BUCCIARELLI ET AL RADAR-82)

CANCELLATION LOSS VS NUMBER OF BITS FOR GRAM-SCHMIDT CANCELLER

(115)

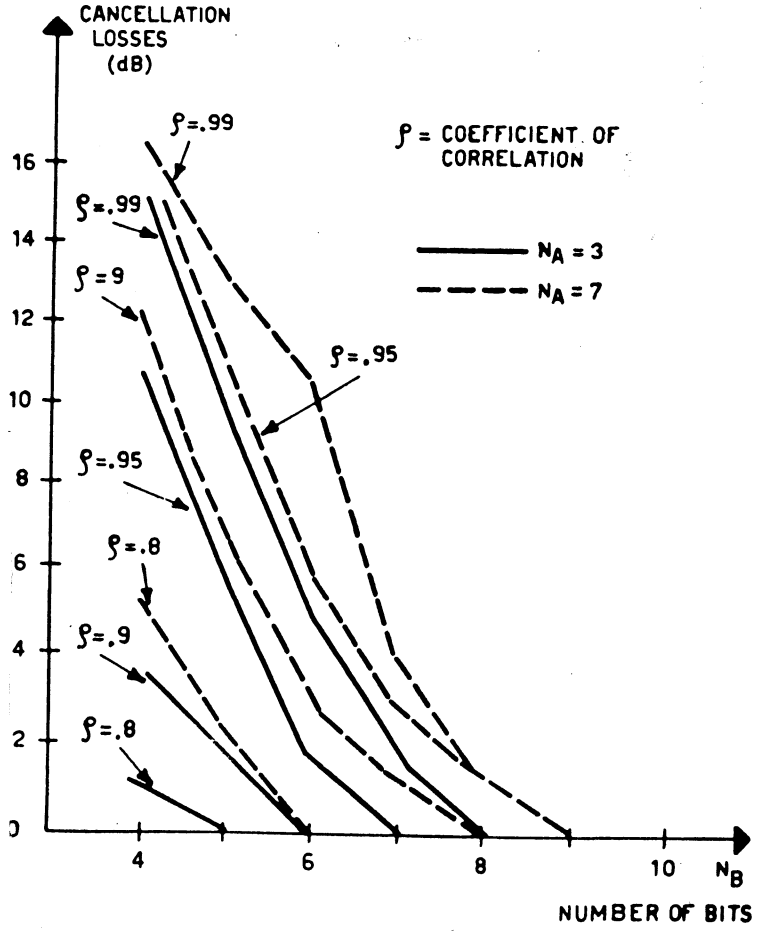

(AFTER BUCCIARELLI ET AL, RADAR-82)

MSLC USING ONE-STEP KALMAN PREDICTOR

(116)

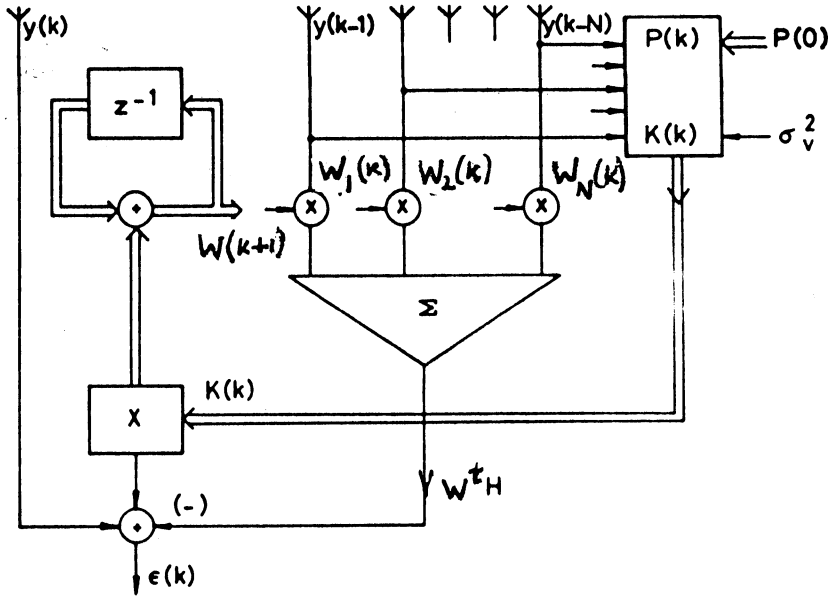

(AFTER KRÜKER, IEE PROC. Pt. F, 2/83)

KALMAN UPDATE EQUATIONS FOR WEIGHTS

(117)

$$W(k) = W(k-1)\,K(k)\left[Y(k) - H^T(k)\,W(k-1)\right]$$

WHERE

$$K(k) = P(k,k-1)\,H^*(k)\left[H^T(k)\,P(k,k-1)\,H^*(k) + \sigma_v^2\right]^{-1}$$

$$P(k+1,k) = \Phi(k+1,k)\left[(I - K(k)\,H^T(k))\,P(k,k-1)\right] \times \Phi^T(k+1,k)$$

$\Phi(k+1,k)$ = NXN TRANSITION MATRIX
(ASSUMED = I = IDENTITY MATRIX FOR (116))

σ_v^2 = VARIANCE OF OBSERVATION MODEL NOISE $v(k)$, SEE (11f).

(SEE KRÜKER, IEE PROC. Pt. F, 2/83)

INTERFERENCE MODELED AS ALL POLE FILTER DRIVEN BY WHITE NOISE

(118)

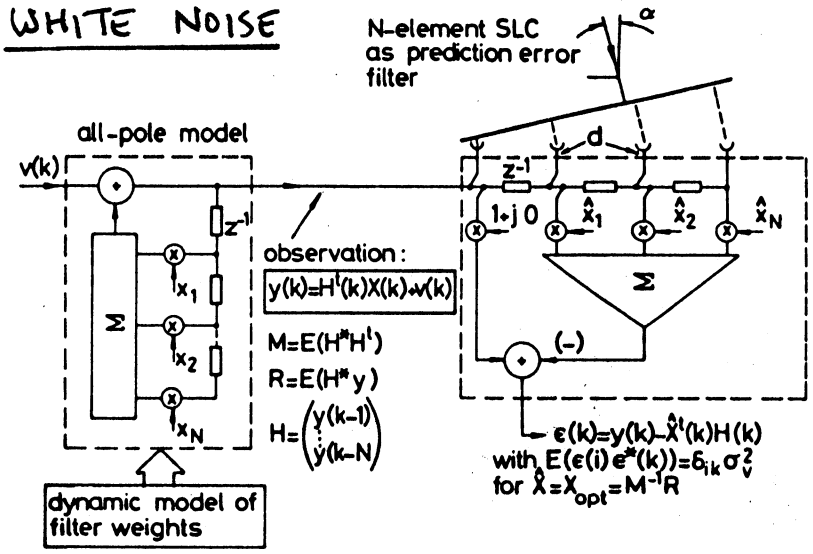

TRANSIENT RESPONSE OF ONE-STEP KALMAN MSLC

(119)

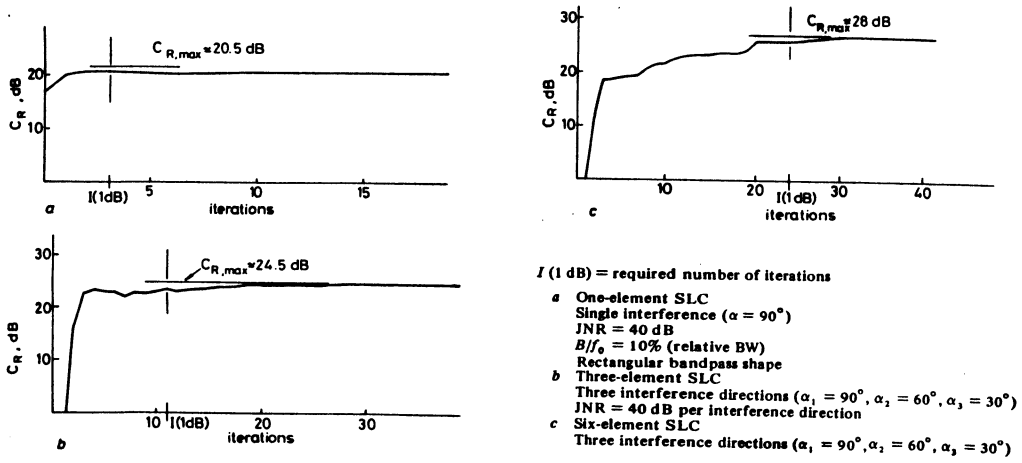

I (1 dB) = required number of iterations

a One-element SLC
Single interference ($\alpha = 90°$)
JNR = 40 dB
B/f_0 = 10% (relative BW)
Rectangular bandpass shape

b Three-element SLC
Three interference directions ($\alpha_1 = 90°, \alpha_2 = 60°, \alpha_3 = 30°$)
JNR = 40 dB per interference direction

c Six-element SLC
Three interference directions ($\alpha_1 = 90°, \alpha_2 = 60°, \alpha_3 = 30°$)

(FROM KRÜKER, IEE PROC. Pt. F, 2/83)

NUMBER OF BITS REQUIRED FOR WEIGHTS OF L/MSLC (120)

(WORST CASE ERRORS)

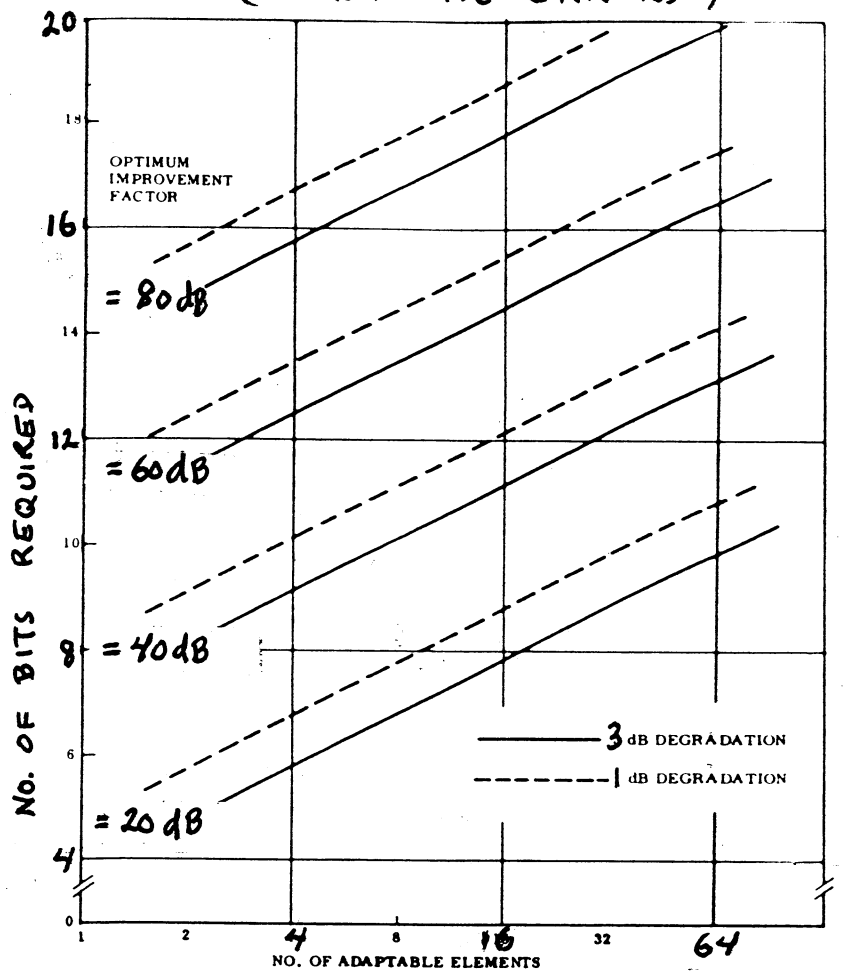

NITZBERG, IEEE AES 5/76

NUMBER OF BITS REQUIRED FOR WEIGHTS OF L/MSLC (121)

Optimum Adaptive Rejection = 37.4 dB 12 Auxiliary Elements; 24 Vector Measurements			
No. Quantization Bits	Adaptive Rejection - dB		
	Simulation	Worst Case Computation	Mean Square Computation
Infinite	34.5	37.4	-
15	34.5	37.4	-
13	34.4	37.3	-
11	34.3	36.0	-
9	31.3	28.9	-
7	23.2	17.5	25.3
5	10.9	5.5	13.3
3	-1.0	-6.5	1.3

(NITZBERG, IEEE AES 5/76)

122

NUMBER OF BITS REQUIRED FOR MATRIX INVERSION FOR L/MSLC

(WELL-RESOLVED INTERFERERS)

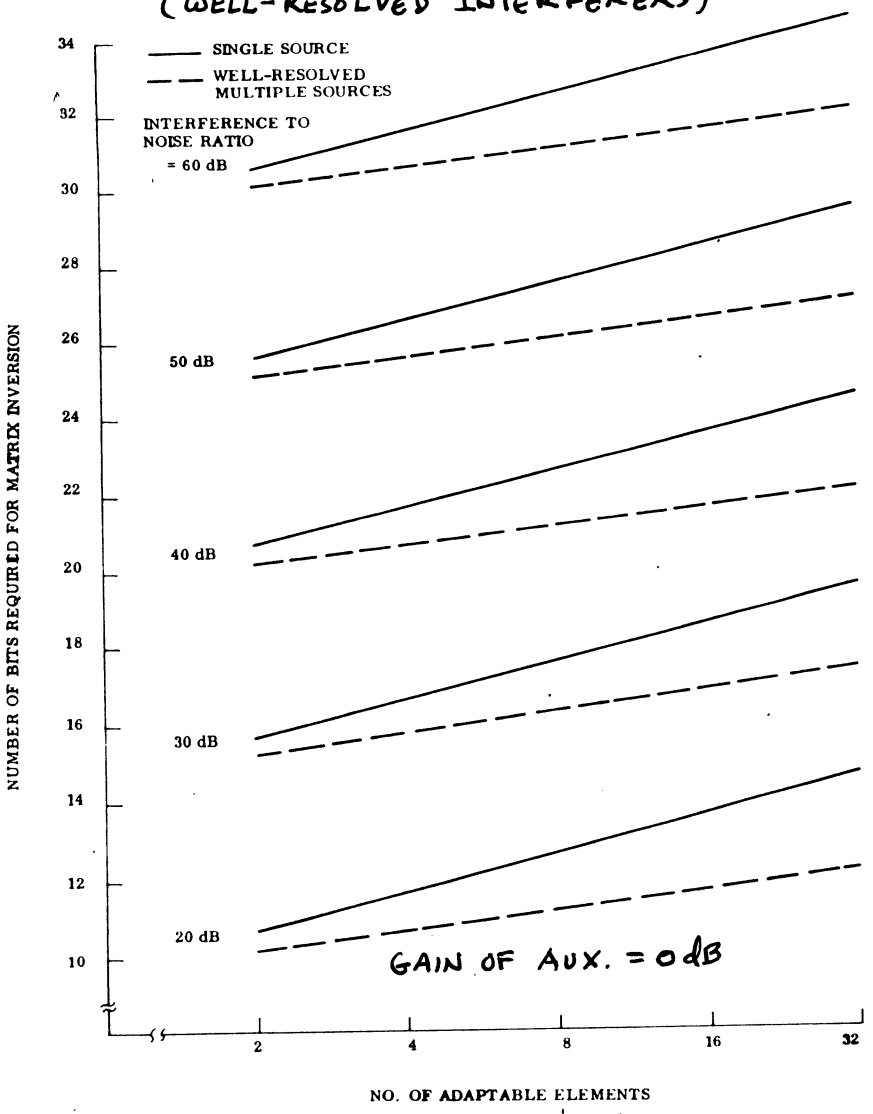

(NITZBERG, IEEE AES, 7/80)

123

NUMBER OF BITS REQUIRED FOR MATRIX INVERSION FOR L/MSLC

(COMPLICATED MULTIPLE INTERFERENCE GEOMETRY)

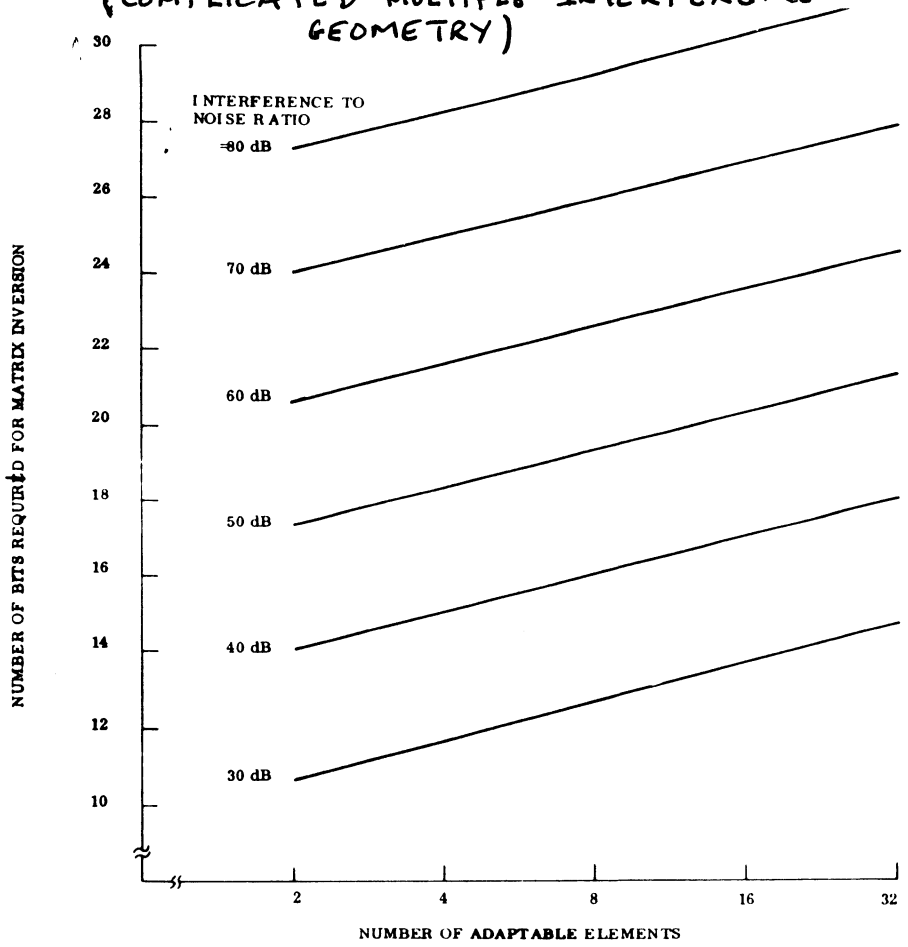

(NITZBERG, IEEE AES, 7/80)

(124)

STRUT SUPPORTED MULTIPLE-BEAM ANTENNA (MBA)

SEVEN BEAMS OFF REFLECTOR;
$\theta_3 = 5.75^\circ$, $f_o = 1550$ MHz, $D/\lambda = 10.7$

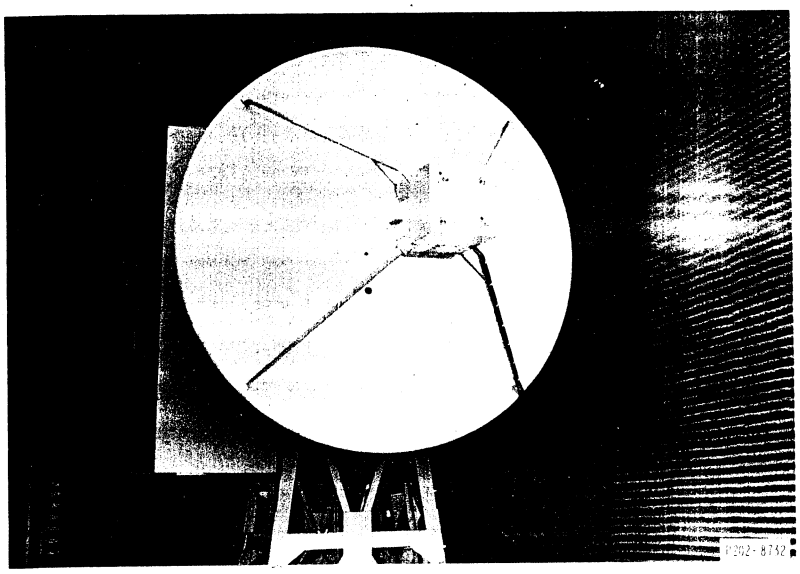

MAYHAN, LINCOLN LAB.
REPORT 1978-1
FEB. 17, 1978

(125)

STRUT SUPPORTED MULTIPLE BEAM ANTENNA

WITH GROUND PLANE FOR ISOLATION

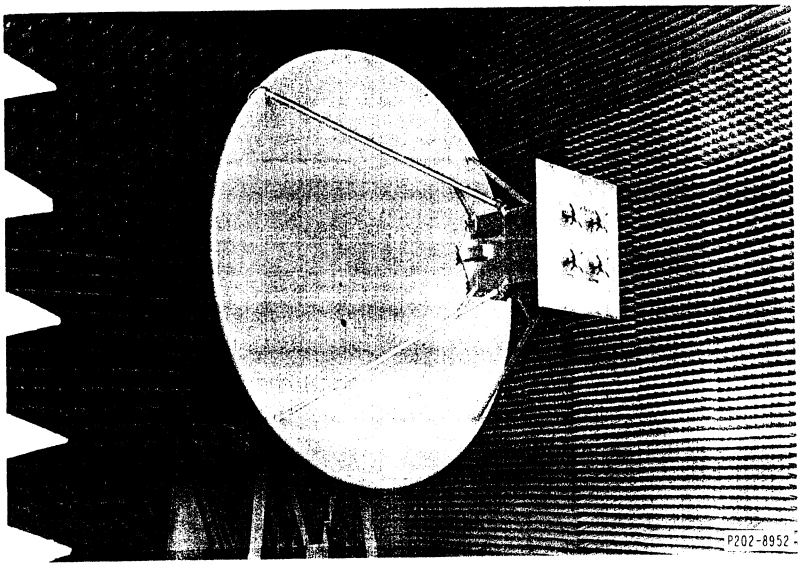

MAYHAN, LINCOLN LAB.
REPORT 1978-1
FEB. 17, 1978

(126)

MULTIPLE BEAM ANTENNA 3dB CONTOURS OF 7 BEAM CLUSTER

EARTH COVERAGE (FROM SYNCHRONOUS ALTITUDE)

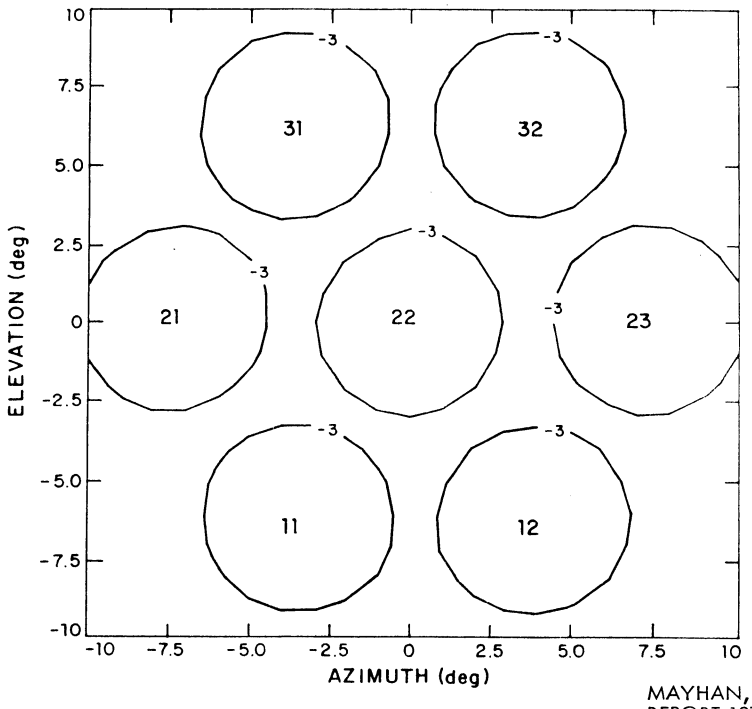

MAYHAN, LINCOLN LAB.
REPORT 1978-1
FEB 17, 1978

(127)

MBA AVERAGE CANCELLATION AS A FUNCTION OF BANDWIDTH

EARTH COVERAGE (FROM SYNCHRONOUS ALTITUDE)
ONE JAMMER (AZ = 4°, EL = 2°)

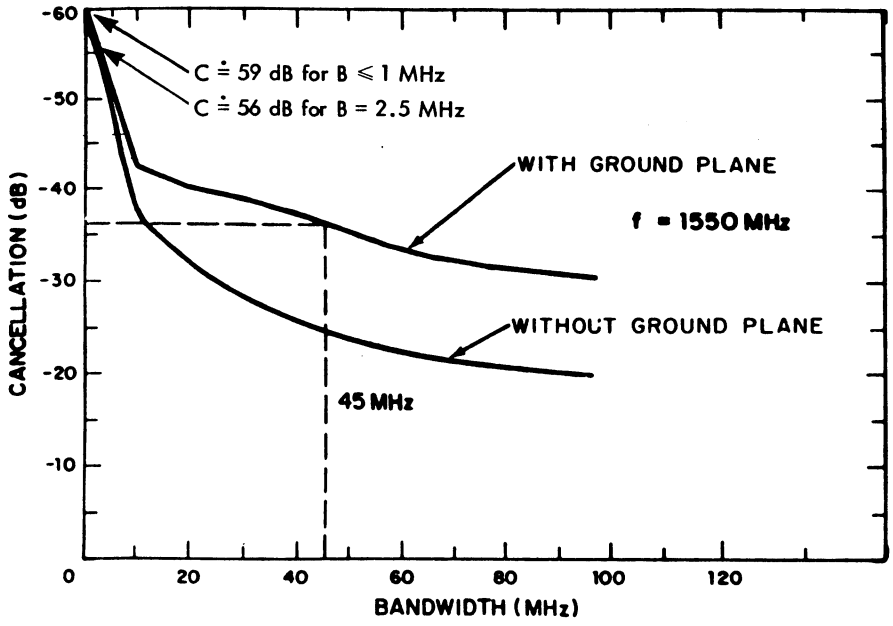

MAYHAN, LINCOLN LAB.
REPORT 1978-1
FEB. 17, 1978

(128)

POWER OF INTERFERERS FOR ADAPTIVE ARRAY SYSTEM

NOTE: S_j ALSO JTH EIGENVALUE OF M, THE COVARIANCE MATRIX OF INTERFERENCE FOR N ELEMENT ADAPTIVE ARRAY

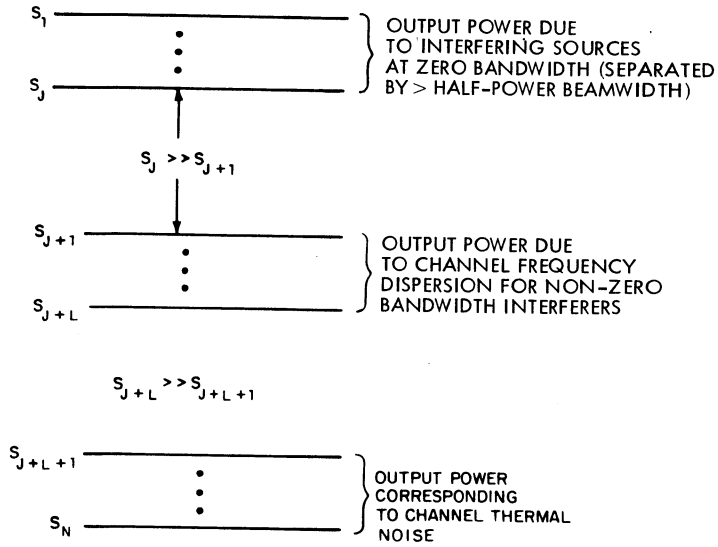

MAYHAN, LINCOLN LAB.
REPORT 1978-1
FEB. 17, 1978

(129)

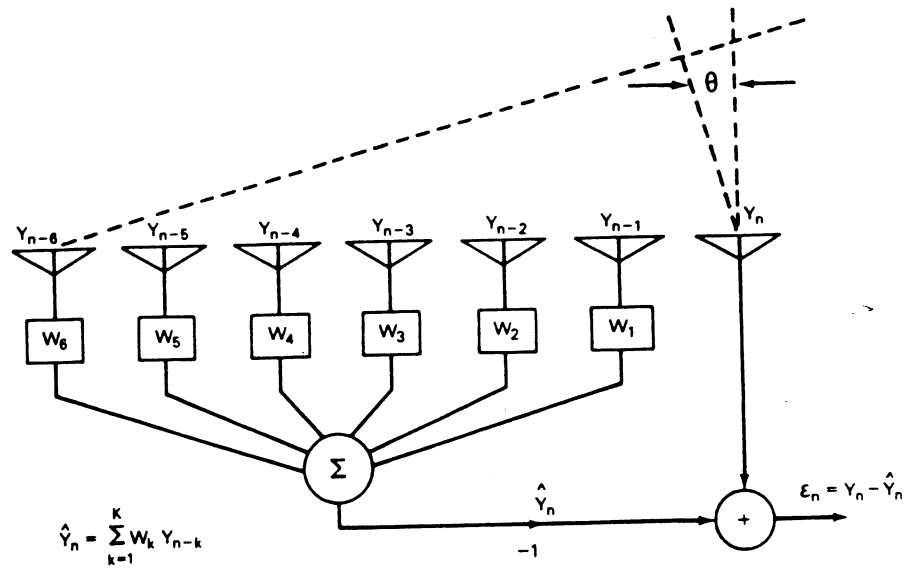

Fig. 3—Array aperture linear prediction spatial filter model

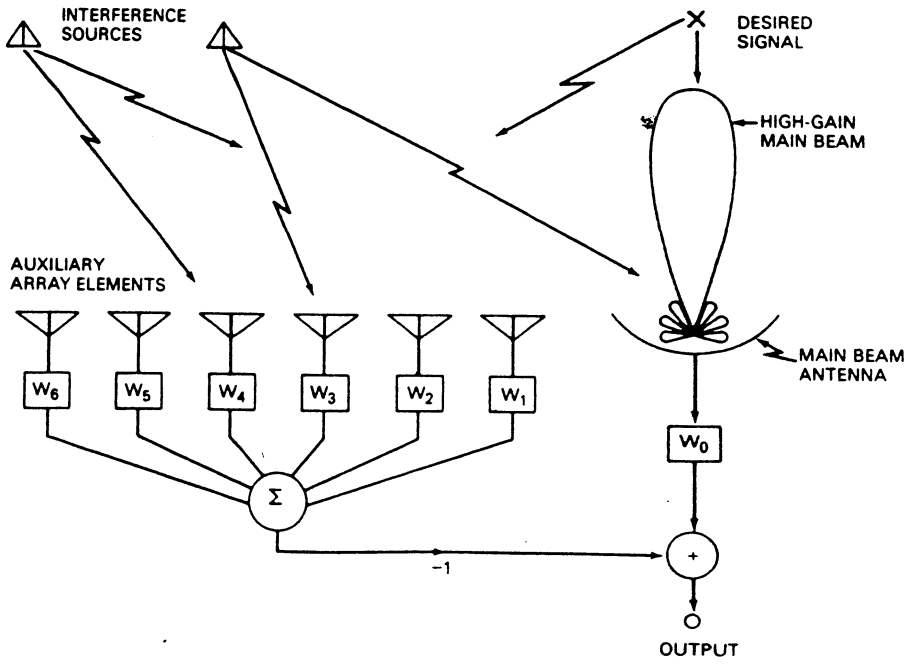

Fig. 4—Typical adaptive array sidelobe canceller configuration

(GABRIEL, 2/1/80, NRL RPT 8345 or IEEE Proc. 6/80)

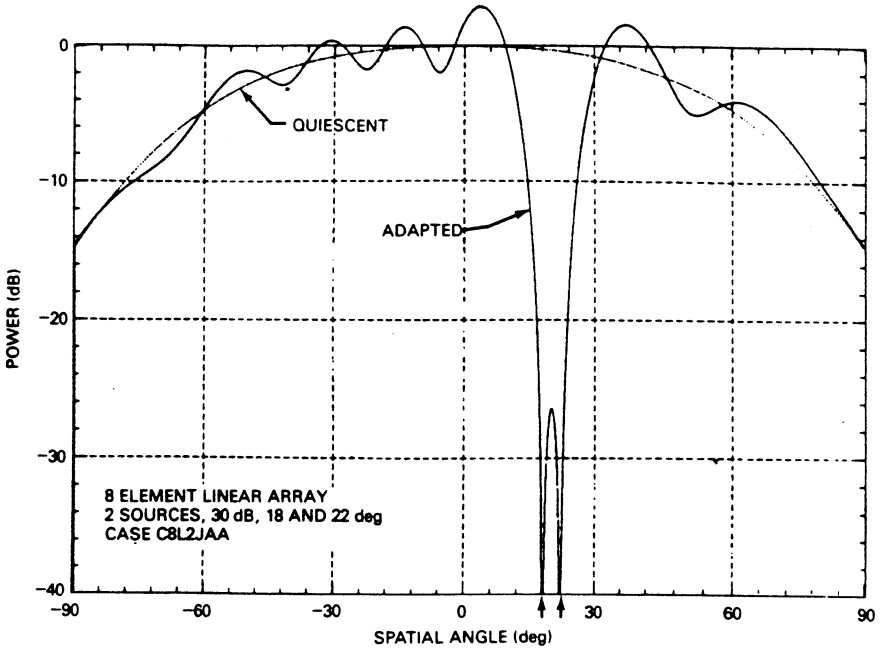

Fig. 5—Quiescent (single-element) and adapted patterns for two-source case, covariance matrix inverse algorithm, 1024 datasnaps

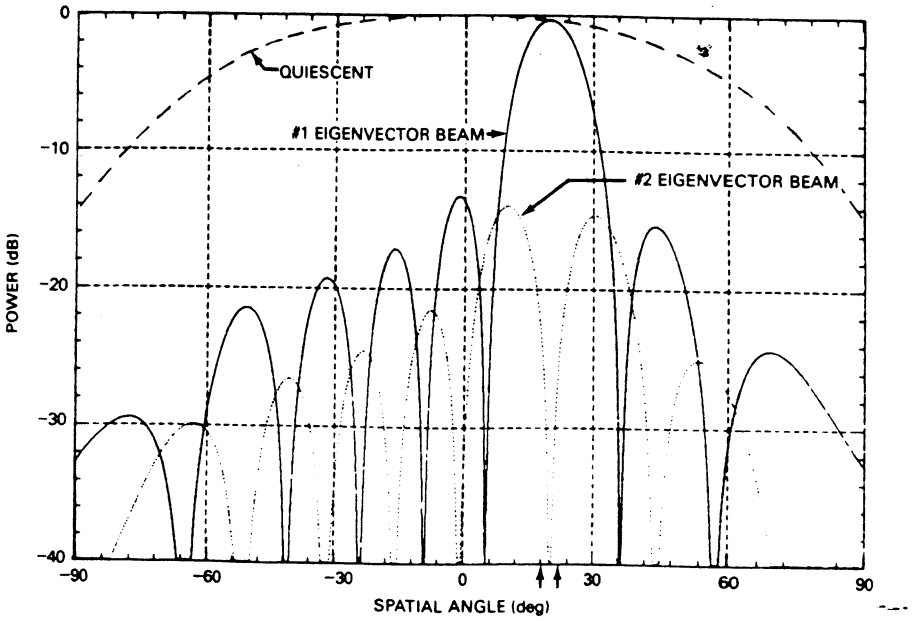

Fig. 6—Eigenvector component beam patterns for the two-source case of Fig. 5

(GABRIEL, NRL RPT 8345, 2/1/80)

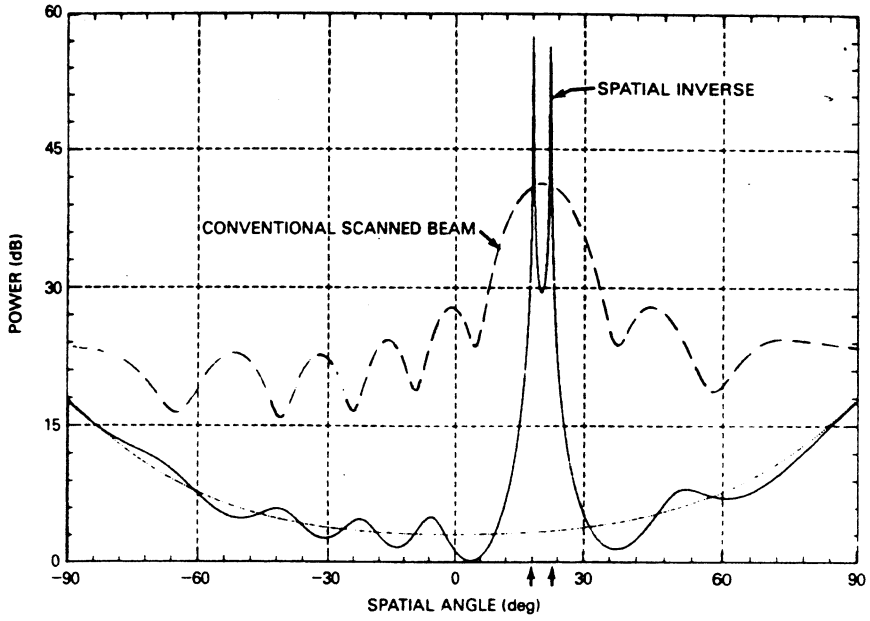

Fig. 7—Spatial spectrum inverse pattern for the two-source case of Fig. 5, and comparison with output of conventional scanned beam

(GABRIEL, NRL REP. 8345)

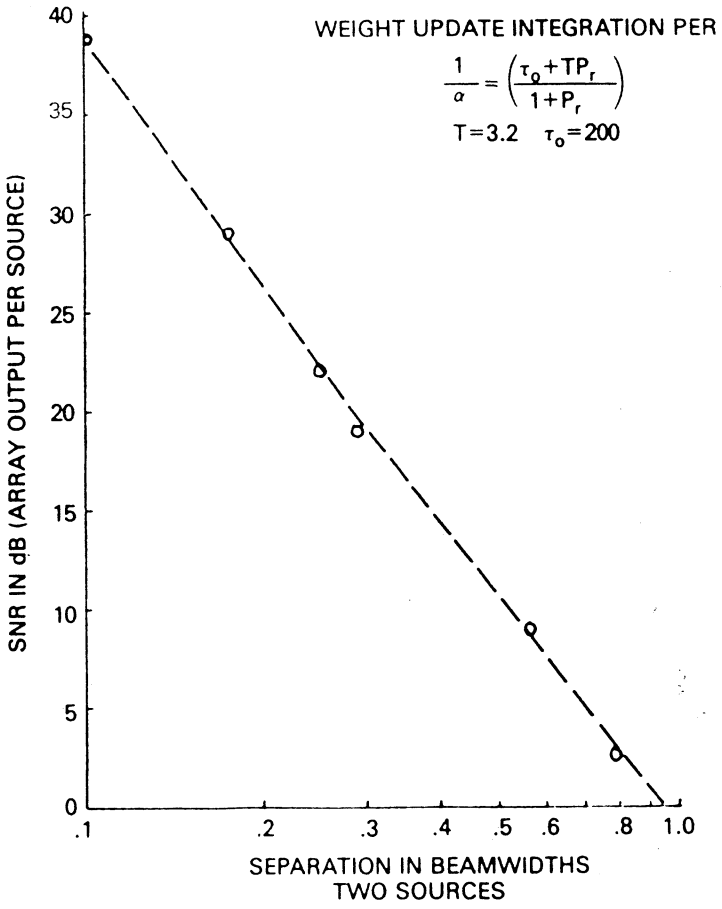

Fig. 12—Universal approximate resolution limit for two incoherent sources. Simulation conditions: narrowband, no array errors, $\lambda/2$ element spacing, linear array, Gaussian receiver noise.

(GABRIEL, NRL REP. 8345)
2/1/80

MAXIMUM LIKELIHOOD METHOD (MLM) ESTIMATE

$$H(\theta)_{MLM} = \frac{1}{S^T M^{-1} S^*}$$

(134a)

(134b)

MUSIC ESTIMATE

$$H(\theta)_{MUS} = \frac{1}{S^T R_N^{-1} S^*}$$

WHERE

$$R_N^{-1} = \sum_{i=q+1}^{K} \lambda_i \Phi_i \Phi_i^{*T}$$

& Φ_i $i = q+1$ to K ARE NOISE EIGENVECTORS OF R

(134c)

COMPARISON OF FOUR METHODS FOR ESTIMATING LOCATION OF INTERFERING SOURCES

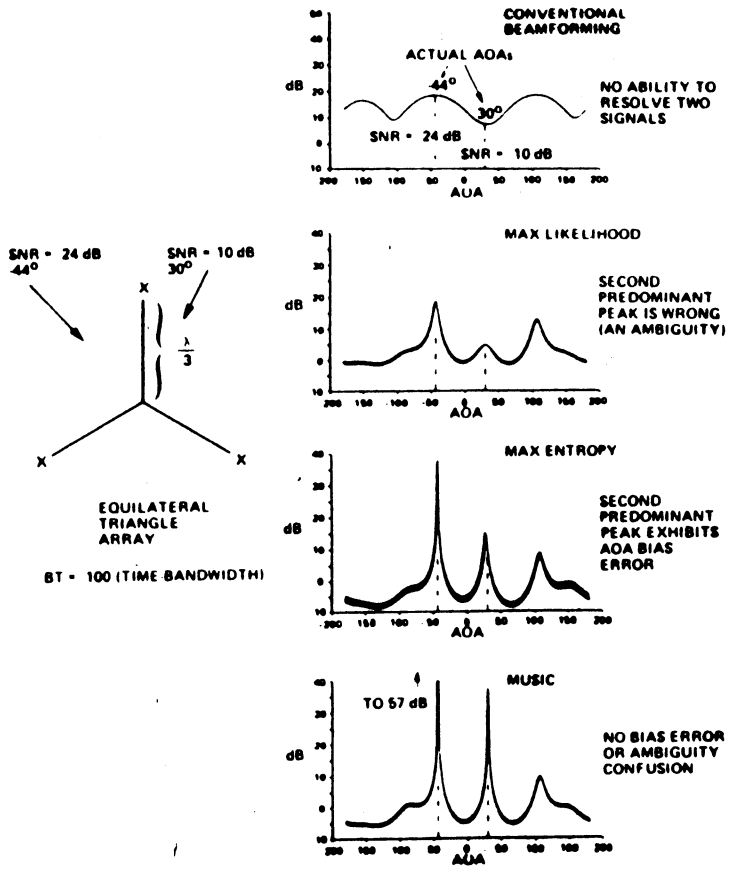

(SCHMIDT, IEEE AP 3/86)

9501

(134d)

COMPARISON OF THREE METHODS FOR ESTIMATING LOCATION OF INTERFERING SOURCES

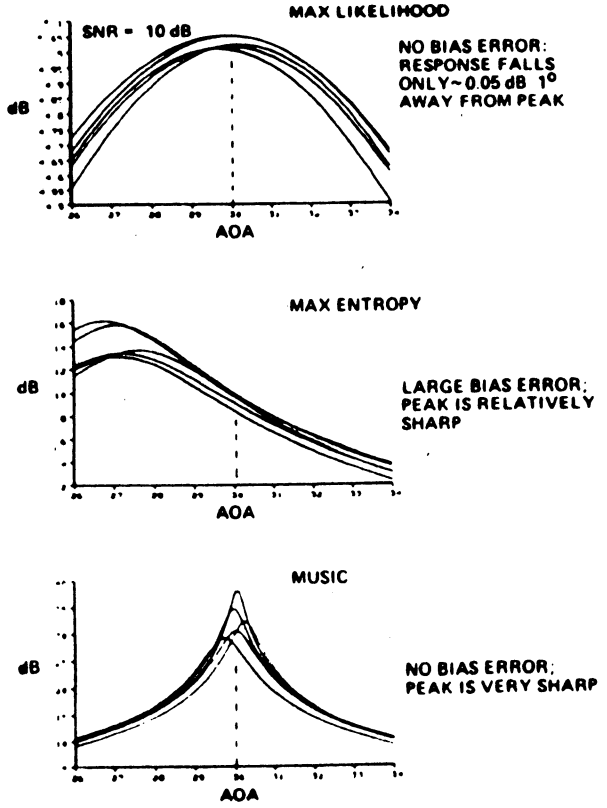

(SCHMIDT, IEEE AP 3/86)

SHIPBOARD UHF ULTRA LOW SIDELOBE ANTENNA

S12-1

135

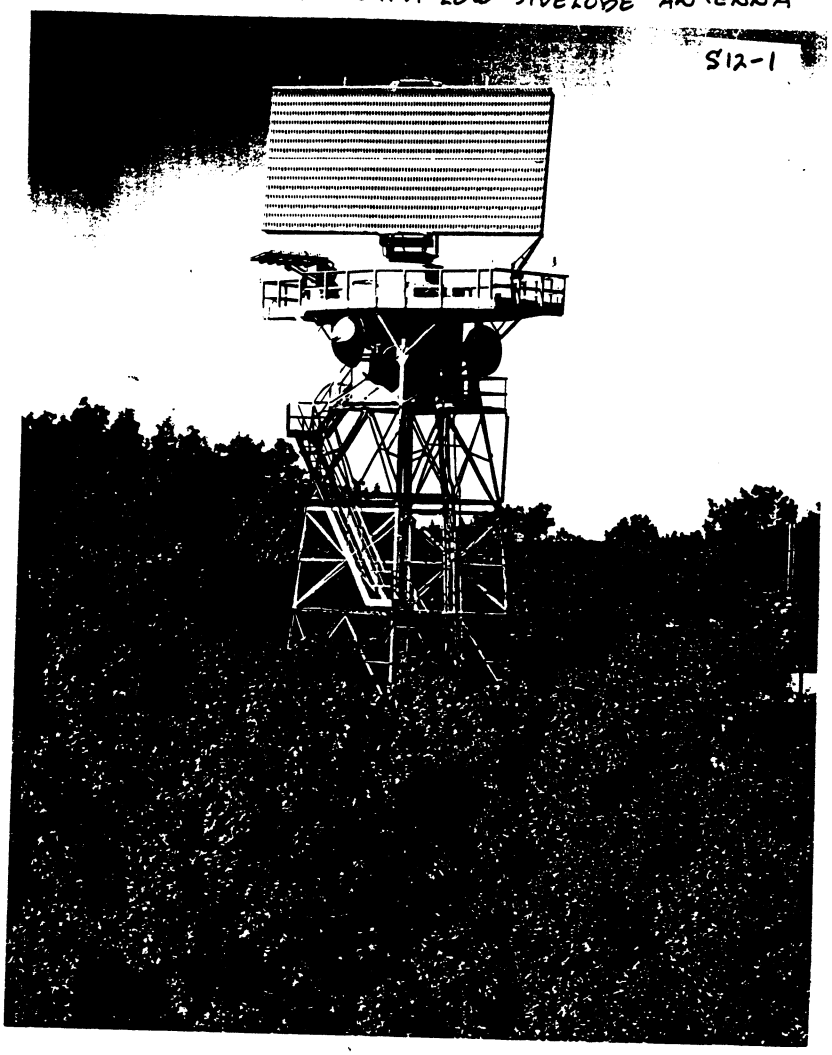

(CARLSON ET AL., LIN. LAB J., SUMMER '90)

S12-2

136

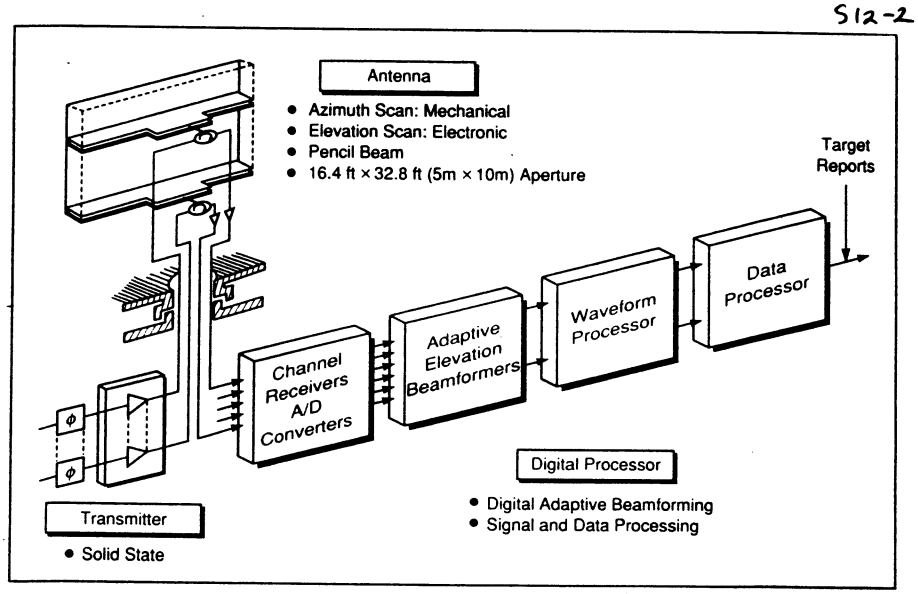

Fig. 2—Radar configuration.

Carlson et al., Lincoln Lab. J
Summer, '90

S12-3 (137)

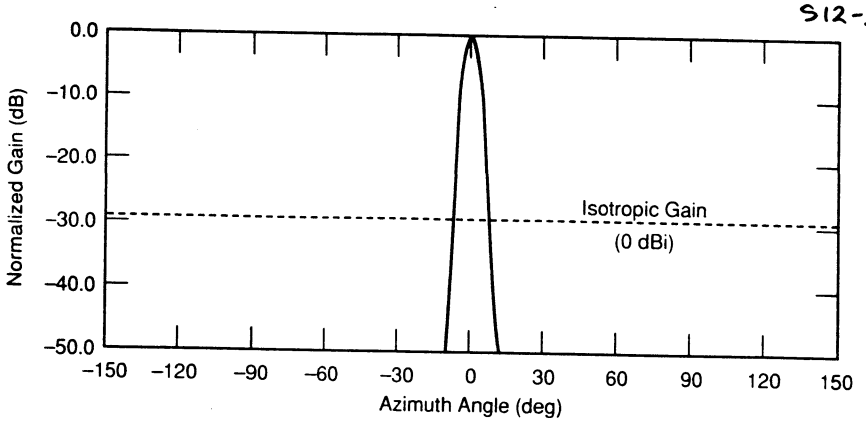

Fig. 8—Azimuth pattern for 14-row array averaged over 410 to 460 MHz.

(138)
S12-4

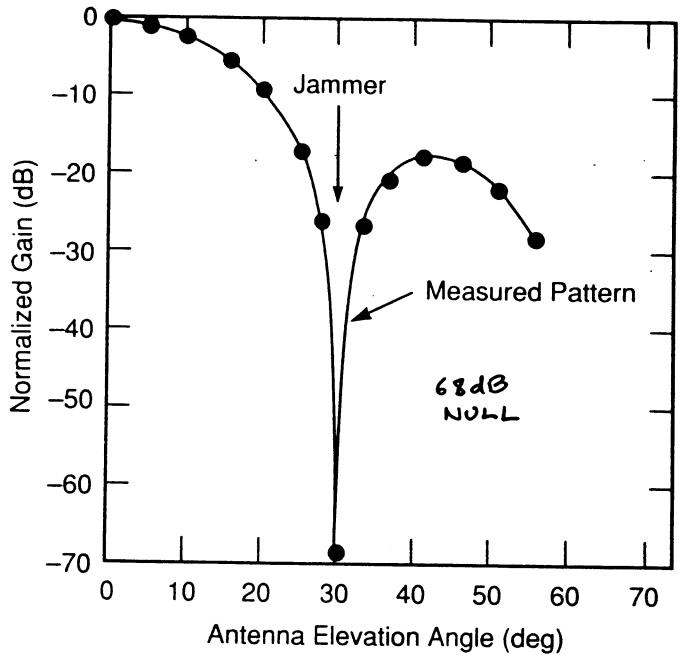

Fig. 18—Experimentally measured elevation pattern for the four-row array antenna at 445 MHz. Note that a null depth of –68 dB was obtained.

Adaptive - Adaptive Array Processing

by

Eli Brookner

and

James M. Howell

Raytheon Company

Wayland, MA

(1) IEEE PROC. OF IEEE, April 1986 and
(2) PHASED ARRAYS 1985 SYMP. PROC. Oct. 15-18, 1985, The Mitre Corp., RADC Rept. RADC-TR-85-171 8/85.

A-1

Fully Adaptive Array

SMI Algorithm Used

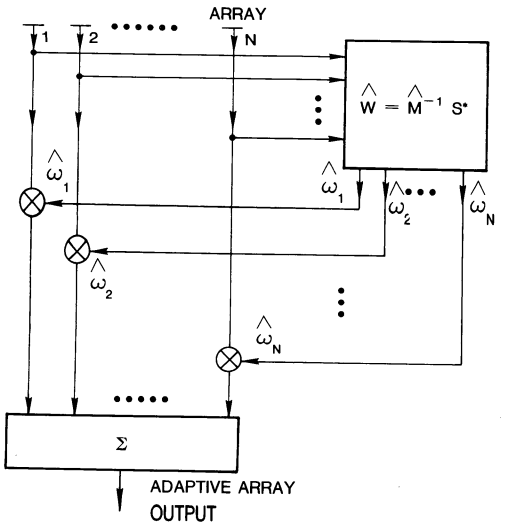

A-3

Background

- Applebaum Developed Method for Archieving Fully Adaptive Array Processing (1966).
  Signal-to-Interference Maximized.
- Reed, Mallett and Brennan provide
  Fast Convergence Method for Fully Adaptive Array (1974).

A-2

Fully Adaptive Array Sidelobe Level:

SMI Algorithm

14 Element Array
15 Time Samples used for estimation of weights

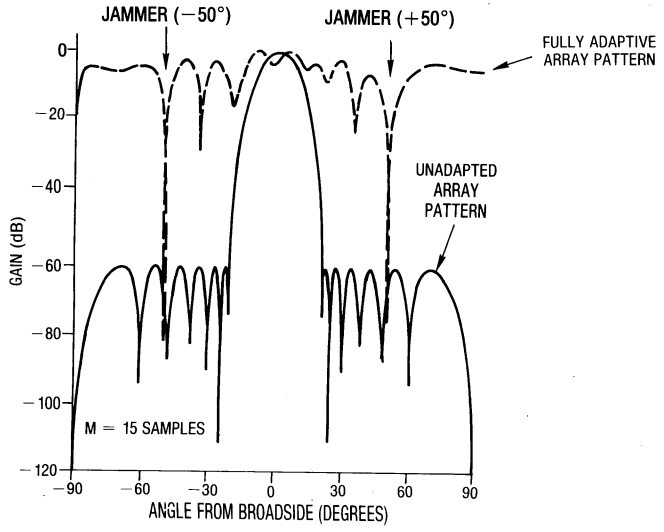

A-4

Fully Adaptive Array Sidelobe Level:

SMI Algorithm

3000 Time Samples used for estimation of weights

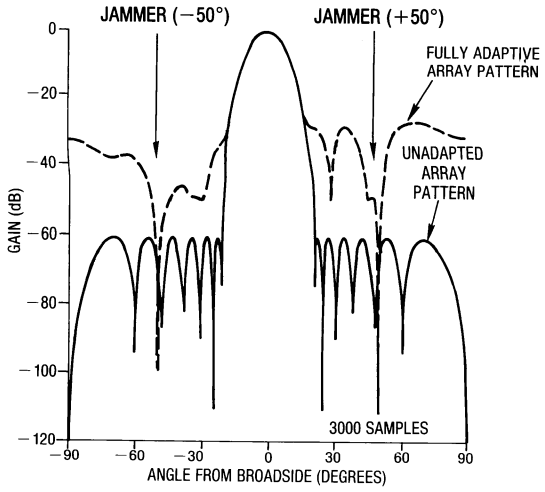

A-5

Comparison Of Antenna Patterns

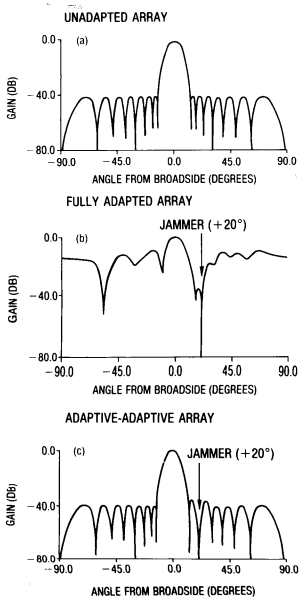

A-7

Principle of Fully Adaptive Array

14 Element Array

15 Time Samples

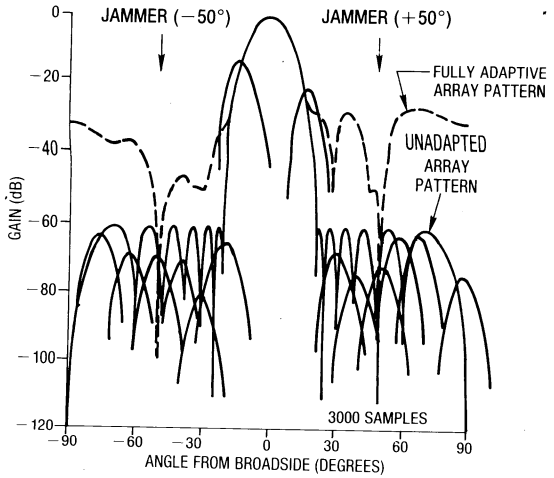

A-6

Adaptive-Adaptive Array Approach

- Only put nulls where jammers exist
- Procedure:
  1. Locate jammers
  2. Place high gain beams in direction of jammers
  3. Apply standard fully adaptive array processing to outputs of main (signal) beam and jammer beams

A-8

Adaptive-Adaptive Array System

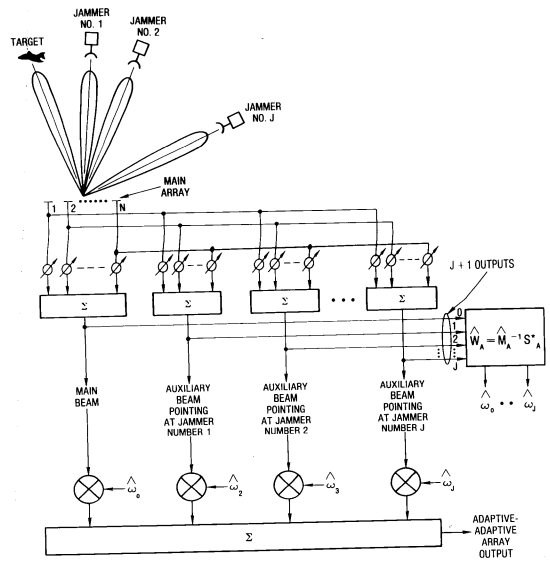

A-9

Methods for Locating Jammer

- DFT of first row of $\hat{M}$
- Search with main beam
- Maximum entropy method (MEM) or some other super resolution technique
- MOSAR
- Butler matrix
- Rotman lens

A-11

Standard Fully Adaptive Array Versus Adaptive-Adaptive Array Processing

	Standard	Adaptive-Adaptive
Sidelobe Level	Severely Degraded	Minor Degradation
Computation Complexity	Invert NXN Matrix Ex. N = 100 × 100 Array = 10^4 Elements Invert 10,000 × 10,000	Invert (J+1) × (J+1) Matrix Ex. J = 10 Jammers Invert 11 × 11 Reduction of ~ 2 × 10^7 in Computation
Transient Time, τ	τ = 2N Above Ex. τ = 20,000	τ = 2 (J + 1) Above Ex. τ = 22 Reduction of ~ 1000

A-10

Location of Jammer

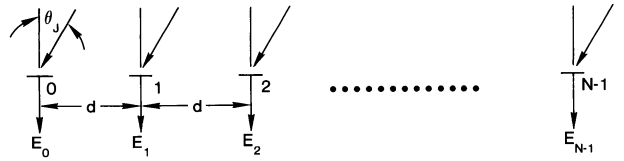

$$E_0 = J \exp(o) = J$$

$$E_1 = J \exp\left(j\frac{2\pi d \sin\theta_J}{\lambda}\right)$$

$$E_n = J \exp\left(j\frac{n2\pi d \sin\theta_J}{\lambda}\right)$$

$$E_O E^*_n = |J|^2 \exp\left(-j\frac{n2\pi d \sin\theta_J}{\lambda}\right) \equiv |J|^2 \sin\left[\frac{n2\pi d \sin\theta_J}{\lambda}\right]$$

$$= |J|^2 \sin nU_J$$

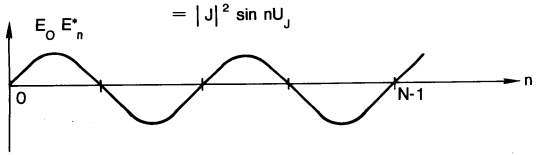

A-12

Location of Jammers Using DFT of First Row of $\hat{M}$

$$\hat{M} = \begin{bmatrix} \hat{M}_{11} & \hat{M}_{12} & \cdots & \hat{M}_{1N} \\ M_{21} & M_{22} & \cdots & \\ \vdots & & & \vdots \\ M_{N1} & & \cdots & M_{NN} \end{bmatrix}$$

$$\hat{U}(s) = \frac{1}{N} \sum_{n=1}^{N} \hat{M}_{in} \exp\left(-j \frac{2\pi ns}{N}\right)$$

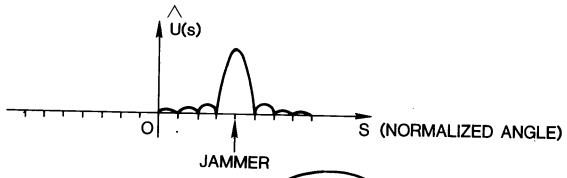

A-13

Time Multiplexed Configuration

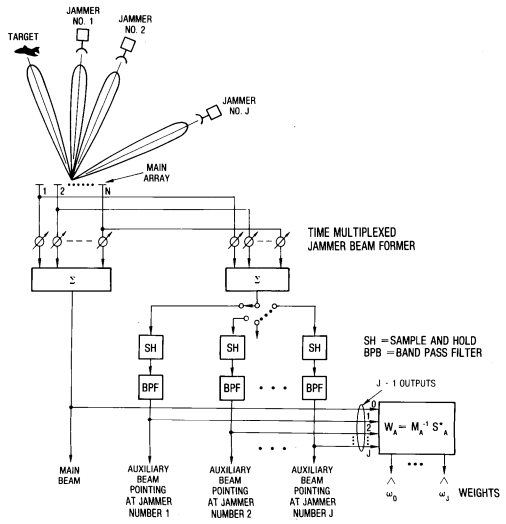

A-15

Adaptive - Adaptive Processing

LEGEND

——— UNADAPTED MAIN BEAM PATTERN

••••••• AUXILIARY PATTERN

– – – – – ADAPTIVE-ADAPTIVE PATTERN

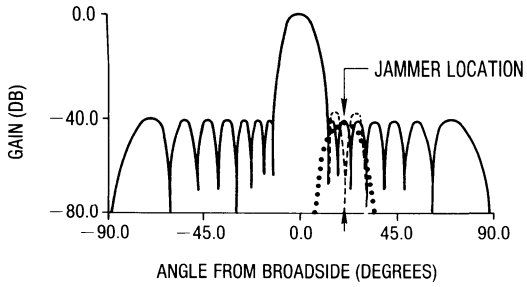

A-14

Conclusions Relative To Adaptive - Adaptive Array Processing

- Provides better sidelobe level
- Reduces computation complexity
  - — Up to many orders of magnitude
- Reduces transient time
  - — Up to orders of magnitude
- Provides essentially same optimum S/I performance as standard fully adaptive array

A-16

(C-1)

PREDICTION THEORY

AND

MAXIMUM ENTROPY METHOD (MEM)

ALL-POLE MODEL FOR PROCESS

(C-2)

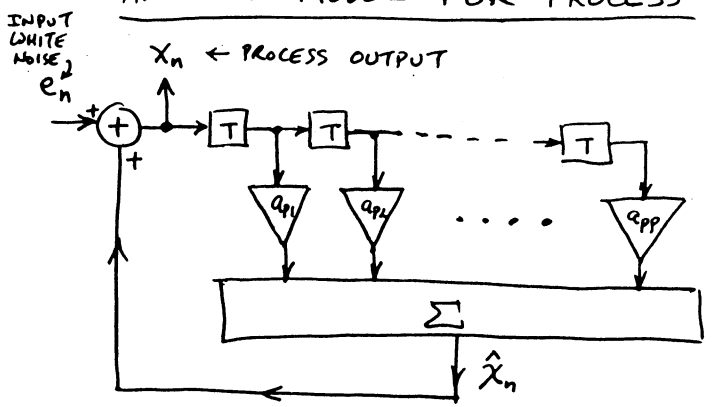

$$x_n = \hat{x}_n + e_n = \sum_{i=1}^{p} x_{n-i}\, a_{pi} + e_n \quad (1)$$

$$X = \sum_{i=1}^{p} X z^{-i} a_{pi} + E \quad (2), \qquad E = X - \sum_{i=1}^{p} X z^{-i} a_{pi} \quad (3)$$

$$E = X\underbrace{\left[1 - \sum_{i=1}^{p} z^{-i} a_{pi}\right]}_{H_p(z) \,\equiv\, \text{WHITENING FILTER}}, \quad (4) \qquad E = H_p(z)\,X \quad (5)$$

ALL-POLE MODEL FOR PROCESS (CONT.)

(C-3)

$$X = \frac{E}{H_p(z)} = \frac{E}{\left[1 - \sum_{i=1}^{p} z^{-i} a_{pi}\right]} \quad (6)$$

LET $\overline{|e_n|^2} = \sigma^2/T = P_p$ (7)

THEN SPECTRUM OF x_n IS:

$$|X(f)|^2 = \frac{\sigma^2}{\left|\underbrace{\left[1 - \sum_{k=1}^{p} a_{pi} \exp -jk\omega T\right]}_{H_p(\omega),\ \omega = 2\pi f}\right|^2} \quad (8)$$

SINCE $z = \exp j\omega T$

T = SAMPLING PERIOD

RELATIONSHIP BETWEEN COVARIANCE MATRIX OF x_n AND WEIGHTS a_{pi}

(C-4)

$$\underbrace{\begin{bmatrix} M(0) & M(1) & \cdots & M(p) \\ M(1) & M(0) & \cdots & \vdots \\ \vdots & & & \\ M(p) & M(p-1) & \cdots & M(0) \end{bmatrix}}_{M = \text{COVARIANCE MATRIX OF } [x_1, \ldots, x_n]} \begin{bmatrix} 1 \\ a_{p1} \\ \vdots \\ a_{pp} \end{bmatrix} = \begin{bmatrix} P_p \\ 0 \\ \vdots \\ 0 \end{bmatrix} \quad (1)$$

P_p = Average Mean Square Error $\overline{|e_n|^2}$ for prediction filter; See previous and next Vugraphs.

OPTIMUM PREDICTOR FOR ALL-POLE PROCESS

(C-5)

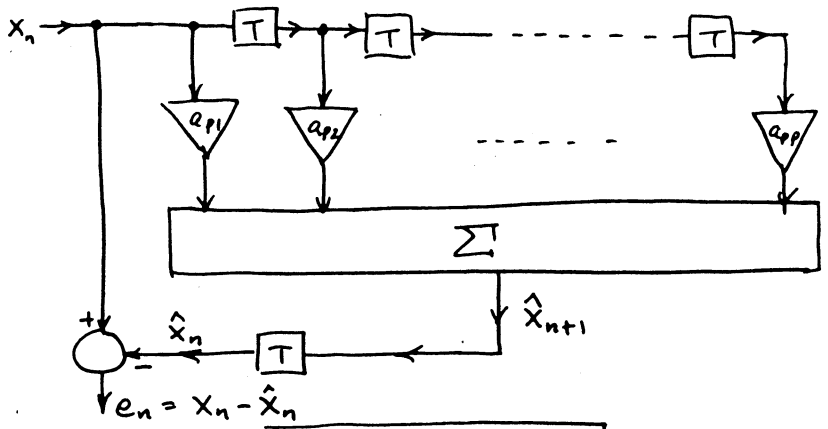

$$\hat{x}_{n+1} = \sum_{i=1}^{p} a_{pi}\, x_{n-i+1} \qquad (1)$$

OPTIMUM PREDICTOR FOR ALL-POLE PROCESS (CONT.)

(C-6)

OPTIMUM FILTER MINIMIZES THE SQUARE OF THE PREDICTION ERROR e_n, I.E.,

$$\overline{|e_n|^2}$$

OPTIMUM PREDICTOR FOR ALL-POLE PROCESS (CONT.)

(C-7)

$$e_n = x_n - \hat{x}_n$$

$$E = x - \sum_{i=1}^{p} a_{pi}\, x\, z^{-i+1} z^{-1}$$

$$E = x\left[1 - \sum_{i=1}^{p} z^{-i} a_{pi}\right]$$

$$E = x\, \underbrace{H_p(z)}_{\text{WHITENING FILTER}}$$

APP. B

Proceedings Letters

This section is intended primarily for rapid dissemination of brief reports on new research results within the scope of the IEEE members. Contributions are reviewed immediately, and acceptance is determined by timeliness and importance of the subject, and brevity and clarity of the presentation. Research letters must contain a clear concise statement of the problem studied, identify new results, and make evident their utility, importance, or relevance to electrical engineering and science. Key references to related literature must be given.

Contributions should be submitted in triplicate to the Editor, PROCEEDINGS OF THE IEEE, *345 East 47th Street, New York, NY 10017-2394. The length should be limited to five double-spaced typewritten pages, counting each illustration (whether labeled as a figure or part of a figure) as a half page. An abstract of 50 words or less and the original figures should be included. Instructions covering abbreviations, the form for references, general style, and preparation of figures are found in "Information for IEEE Authors," available on request from the IEEE Publishing Services Department. Authors are invited to suggest the categories in the table of contents under which their letters best fit.*

After a letter has been accepted, the author's company or institution will be requested to pay a voluntary charge of $110 per printed page, calculated to the nearest whole page and with a $110 minimum to cover part of the cost of publication.

Adaptive–Adaptive Array Processing

ELI BROOKNER AND JAMES M. HOWELL

A technique is described which provides the jammer cancellation advantages of a fully adaptive array without its many disadvantages such as an excessively large number of computations, poor sidelobes in the directions other than the jammer locations, and poor transient response. This is done at the expense of the hardware complexity. The technique involves transforming a large array of N elements into an equivalent small array of J + 1 elements, where J is the number of jammers present. The technique involves estimating the number and locations of the jammers by a discrete Fourier transform of the array element outputs or by the use of standard maximum entropy methods (MEM) or by other super-resolution techniques. Once the number and locations of the jammers have been determined, beams are formed in the direction of the jammers using the whole array. The outputs of these jammer beams together with the output of the main signal beam from the transformed array now consist of J + 1 ports instead of N ports. The standard sample matrix inversion (SMI) or the Applebaum algorithm can be applied to the J + 1 ports of the equivalent adaptive–adaptive array. Whereas N may be very large, like 10000 for large arrays, J + 1 for the equivalent array could be very small. For example, if there are only 10 jammers then J + 1 becomes 11. The total of multiplies needed to do the adaptive array processing reduces from something of the order of $2N^3 = 2\,(10000^3) = 2 \times 10^{12}$ to about 10^5 a reduction in the computation complexity by seven orders of magnitude. In addition, the settling time for the adaptive–adaptive array is much faster. For the above example, the settling time for the full array is about 20000 samples, whereas for the adaptive–adaptive array it is only 22 time samples, for an improvement of three orders of magnitude.

Manuscript received January 3, 1985; revised April 15, 1985.
The authors are with the Raytheon Company, Wayland, MA 01778.

SUMMARY

A technique is described for adaptive array processing which eliminates the complex computation problem (see Table 1) of a large fully adaptive array while at the same time provides the same optimum performance as obtained for the fully adaptive array in [1]. The technique also has the advantage of not significantly degrading the antenna sidelobe levels at angles where the jammers are not present; see Fig. 1. This feature is important in the presence of intermittent short pulse interference coming through the radar sidelobes and for ground radars which have clutter in the sidelobes

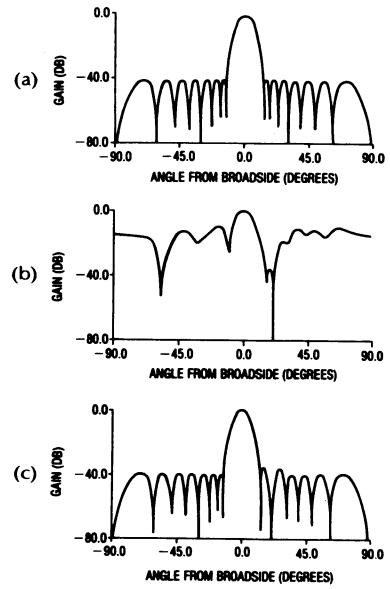

Fig. 1. Sixteen-element array having 40-dB antenna sidelobes (Chebyshev weighting). Jammer at 20° (peak of second sidelobe). (a) Unadapted antenna pattern. (b) Antenna pattern for fully adaptive array (SMI algorithm). $M = 2N = 32$ (M equals the number of time samples used to estimate the adaptive antenna weights). For the fully adaptive array, not only is there a degradation of the antenna sidelobes, there is also a degradation in the antenna main lobe peak gain. The peak gain degradation was found to be as much as 5 dB in the simulation carried out. (c) Antenna pattern for adaptive–adaptive array processing. $M = 2(J+1) = 4$.

0018-9219/86/0400-0602$01.00 ©1986 IEEE

Table 1 Comparison of Computations Required (Assumption: J = number of jammers = 10.)

Type Array Antenna	Jammer Cancellation Technique	Number of Complex Multiples to Calculate Weights	Complex Multiplies to Form Array Output per Signal Time Sample#	Transient Time (Units of Signal Time Samples)
One-Dimensional (N Elements = 100)	Fully Adaptive	$2N^3 = 2 \times 10^6$	$N = 10^2$	$2N = 200$
	Adaptive–Adaptive	$2(J+1)^3 + 7NJ^* \doteq 10^4$	$J + 1 = 11 \doteq 10$	$2(J+1) = 22$
	(Improvement)	200	10	~ 10
Square Two-Dimensional (N Elements = 10^4)	Fully Adaptive	$2N^3 = 2 \times 10^{12}$	$N = 10^4$	$2N = 2 \times 10^4$
	Adaptive–Adaptive	$2(J+1)^3 + N\log_2\sqrt{N}^{**} \doteq 7 \times 10^4 \doteq 10^5$	$J + 1 = 11 \doteq 10$	$2(J+1) = 22$
	(Improvement)	$\sim 2 \times 10^7$	10^3	$\sim 10^3$

#Does not include computations of column three.

*Second term assumes MEM algorithm used to locate jammer. This term drops out if jammers located using search beam. For this case number of multiplies $\doteq 2(J+1)^3 \doteq 2 \times 10^3$ and improvement becomes $\sim 10^3$.

**Second term assumes fast Fourier transform (FFT) algorithm used to locate jammer. Term drops out if jammer located using search beam (or beams). In this case number of multiplies $\doteq 2(J+1)^3 \doteq 2 \times 10^3$ and improvement becomes $\sim 10^9$.

and the mainlobe. The adaptive–adaptive array also has the advantage of a much faster settling time; see Table 1.

The technique uses a two-step process. First the number of interfering jammers and their locations are estimated by such techniques as a spatial discrete Fourier transform of the array outputs (digitally or by use of a Butler matrix or Rotman lens), by maximum entropy method spectral estimation techniques [2], [3], or just by a search in angle with an auxiliary beam. Once the number of jammers and their locations have been determined, auxiliary beams are formed pointing at these jammers, with one beam being pointed at each jammer; see Fig. 2. These beams are formed using

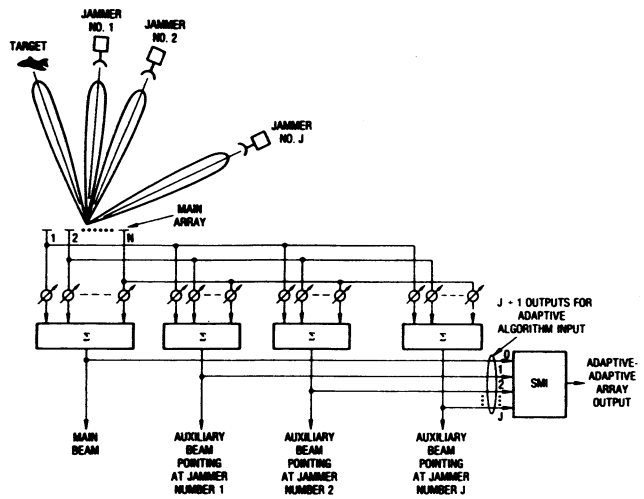

Fig. 2. Adaptive–adaptive array configuration. N-element array is reduced to $J+1$ element array where J is equal to the number of jammers.

the whole array. They are formed using beam-forming networks parallel to the main signal beam network. The number of beams formed is equal to the number of jammers. These beams could be formed using amplitude weighting to achieve low sidelobe levels if desirable. The outputs of the auxiliary jammer beam ports together with the main signal beam port form the adaptive–adaptive transformed array. The number of degrees of freedom in this transformed array is reduced from N, the number of elements in the original array, to one plus the number of jammers J. Thus for the adaptive–adaptive array a $(J+1)$ $(J+1)$ matrix has to be inverted instead of an $N \times N$ matrix. Furthermore, the conversion time for the adaptive–adaptive array is much faster than for the full array. For the SMI algorithm, the number of time samples needed to form the weights is equal to two times the number of degrees of freedom in order to obtain cancellation within 3 dB of the optimum [4]. Thus for the adaptive–adaptive array $2(J+1)$ time samples are needed instead of the $2N$ required for the full array; see Table 1.

It is useful to physically understand why the adaptive–adaptive array does not degrade the antenna sidelobes. The adaptive–adaptive array subtracts one auxiliary beam pointed at the jammer and containing the jammer signal from the main signal channel beam as illustrated in Fig. 3. The gain of the auxiliary beam in the direction

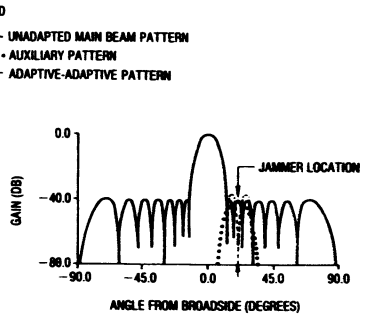

Fig. 3. Main unadapted array pattern, the auxiliary jammer beam pointed at the jammer that is subtracted from the main beam at the jammer location, and the resultant adaptive–adaptive pattern.

of the jammer is made to equal the gain of the main channel beam sidelobe in the direction of the jammer. As a result, the subtraction produces a null at the angle of the jammer in the main channel sidelobe. It is apparent from Fig. 3 that the auxiliary antenna pattern subtraction does not significantly degrade the main antenna beam sidelobe levels. For the fully adaptive array, N retrodirective beams are formed based on the eigenvalues and eigenvectors of the fully adaptive array covariance matrix [5]. Because of the presence of thermal noise in the array elements the estimates of the covariance matrix of the fully adaptive array and, in turn, the retrodirective beams are poor for $M = 2N$. Instead of forming only one retrodirective beam as desired when one jammer is present, N retrodirective beams are formed for the fully adaptive array. The $N-1$ retrodirective beams for which there are no jammers are the ones which degrade the antenna sidelobe levels at the angles where no jammers exist. It is found that even if 3000 time samples are used, the sidelobe levels are still severely degraded for the fully adaptive array system although considerably improved. The adaptive–adaptive array technique first determines what jammers are present which will degrade the system performance. Once the locations of these jammers are determined the array adapts to the situation by only placing retrodirective beams at these angles. Consequently, the beams at other angles where there are no jammers are not formed and do not, as a result, degrade the antenna sidelobes at these angles.

A number of variations are possible on the above adaptive–adap-

tive array system. First, the MOSAR method of [6] can be used to locate the jammer positions based on a single time sample. Second, it is not necessary to use the whole array to locate the jammers. Third, if the jammers can be located so as to come through the backlobes, then an auxiliary array (or arrays) is needed which covers the backlobes or whatever angles are not covered by the main array. Finally, it is possible to use only one parallel beam-forming network instead of J with this beam-forming network being time multiplexed so as to produce the J beams pointed at the J jammers and in this way reduce the hardware complexity of the adaptive–adaptive array processor.

The physical explanation given above together with Fig. 3 helps in understanding the performance of the adaptive–adaptive algorithm for nonperfect conditions and leads to the following insights. Even if the jammer location is in error by plus and minus a half beamwidth, jammer cancellation results similar to those in Fig. 1(c) will still be obtained. There will only be a degradation of the sidelobe to the right or left of the null by about 3 dB. Furthermore, if the cancelor weights calculated using the SMI (or some other adaptive algorithm) is inexact, the null depth will be degraded but it is apparent from Fig. 3 that the sidelobe level will be unaffected except for a small amount for the sidelobes just to the right and left of the null. Increasing M for the SMI computation will increase the null depth. If a jammer is not detected than it will not be canceled out. This, however, will tend to occur only if the jammer is weak, a case not of as much concern because the jammer will then only cause a small degradation in signal-to-interference ratio. If a jammer is estimated to be present when in fact it is not, the system will incur very little degradation in signal-to-interference ratio and in antenna sidelobe level because the SMI weights for the channel pointing in the direction where no jammer actually exists will be very low, the weight being established by the correlation between the noise in the main channel and the noise in the auxiliary channel pointing at no jammer with these noises being independent so that the correlation on the average is zero. If there are a large number of jammers then there can be antenna sidelobe level degradation if the auxiliary jammer beams have sidelobe levels that are not low enough. If J jammers are present then, in order to avoid sidelobe level degradation in the main channel, the auxiliary channel antenna sidelobe levels should be greater than 10 ($\log_{10} J$) decibels down, a condition that can generally be met.

Acknowledgment

The idea of pointing high-gain auxiliary antenna beams in the direction of the jammers appears to have first been suggested by P. W. Howells, the inventor of the IF sidelobe cancelor [7]. He did not, however, form multiple auxiliary high-gain beams in an array to achieve jammer nulling performance essentially that of a fully adaptive array while avoiding the associated sidelobe degradation problem as done in this letter. W. F. Gabriel of NRL has independently done this. Fig. 1 was obtained using a simulation written by C. D. Brommer (Raytheon).

References

[1] S. P. Applebaum, "Adaptive arrays," *IEEE Trans. Antennas Propagat.*, vol. AP-24, no. 5, pp. 585–598, Sept. 1976.

[2] S. M. Key and S. L. Marple, Jr., "Spectrum analysis—A modern perspective," *Proc. IEEE*, vol. 69, no. 11, pp. 1380–1418, Nov. 1981.

[3] J. P. Burg, "Maximum entropy spectral analysis," Ph.D. dissertation, Dept. Geophysics, Stanford U., Stanford, CA, May 1975.

[4] I. S. Reed, J. D. Mallett, and L. E. Brennan, "Rapid convergence rate in adaptive arrays," *IEEE Trans. Aerosp. Electron. Syst.*, vol. AES-10, no. 6, pp. 853–863, Nov. 1974.

[5] W. F. Gabriel, "Adaptive arrays–An introduction," *Proc. IEEE*, vol. 64, no. 2, pp. 239–272, Feb. 1976.

[6] M. A. Johnson, "Phased-array beam steering by multiplex sampling," *Proc. IEEE*, vol. 56, pp. 1801–1811, Nov. 1968.

[7] P. W. Howells, "Explorations in fixed and adaptive resolution at GE and SURC," *IEEE Trans. Antennas Propagat.*, vol. AP-24, no. 5, pp. 575–584, Sept. 1976.

APP. C

THE UBIQUITOUS ORTHORNOMAL TRANSFORMATION — IN SIDELOBE CANCELLING, ADAPTIVE ARRAYS, AND TRACKING

by

Eli Brookner
Raytheon Company
Wayland, Massachusetts 01778

Abstract

Orthonormal transformations provide a powerful method for solving the sidelobe cancellation problem and the least squares tracking filter problem. A simple tutorial is given on the application of these transformations to these two vastly different physical problems showing how very much they are mathematically similar. Covered are the classical and modified Gram-Schmidt orthonormal transformations including how they are related to each other, to geometric projection theory and to coordinate transformations theory. Also covered is the relationship of these transformations to the Gauss elimination method, the use of a systolic implementation of the Givens transformation and the relationship to Gauss' original least-squares estimation work.

1) Sidelobe Cancelling Problem

Figure 1-1 shows the sidelobe cancelling problem. For simplicity we will consider the case of two auxiliary antennas (m = 2) and three time samples (s = 3). It is simple to extend the results to the general case. In matrix form the output of the sidelobe canceller is given by

$$\begin{bmatrix} \varepsilon_1 \\ \varepsilon_2 \\ \varepsilon_3 \end{bmatrix} = \begin{bmatrix} s_1 \\ s_2 \\ s_3 \end{bmatrix} - \begin{bmatrix} v_{11} & v_{12} \\ v_{21} & v_{22} \\ v_{31} & v_{32} \end{bmatrix} \begin{bmatrix} w_1 \\ w_2 \end{bmatrix} \tag{1-1}$$

or

$$E = S - VW \tag{1-1a}$$

where

$$E = \begin{bmatrix} \varepsilon_1 \\ \varepsilon_2 \\ \varepsilon_3 \end{bmatrix} \quad S = \begin{bmatrix} s_1 \\ s_2 \\ s_3 \end{bmatrix} \quad V = \begin{bmatrix} v_{11} & v_{12} \\ v_{21} & v_{22} \\ v_{31} & v_{32} \end{bmatrix} \quad W = \begin{bmatrix} w_1 \\ w_2 \end{bmatrix} \tag{1-1b}$$

We want to find weights w_1 and w_2 that minimize the interference signal at the output of the canceller. This is achieved by minimizing the sum of the squares of the canceller output signals, i.e., by minimizing

$$e_n = \sum_{i=1}^{3} \varepsilon_i^2 \tag{1-2}$$

This minimization gives us the least-squares solution. Let us view the columns of the matrices of E, S and V as vectors in 3-dimensional orthonormal x, y, z space. In this space s_1 is the "x" coordinate of the vector S, s_2 the y coordinate, and s_3 the z coordinate. The first and second columns of V form the vectors v_1 and v_2 given by

$$v_1 = [v_{11} \; v_{21} \; v_{31}]^T \tag{1-3a}$$

$$v_2 = [v_{12} \; v_{22} \; v_{32}]^T \tag{1-3b}$$

where the superscript "T" stands for matrix transpose. Figure 1-2 illustrates this 3-dimensional space. The optimum weight matrix W is that which causes the magnitude of the vector E to be minimum. Equivalently, it is that W which causes the Euclidean norm squared of E to be minimum. The Euclidian squared of E is given by

$$\|E\|^2 = e_n^2 = E^T E = (S - VW)^T (S - VW) \tag{1-4}$$
$$= \|S - VW\|^2$$

From simple geometry we know that $\|E\|^2$ is minimized when the vector E is perpendicular to the 2-dimensional plane determined by the column vectors v_1 and v_2 of V. When E is perpendicular to the plane V_p, the vector VW (which is the weighted sum of v_1 and v_2) becomes the projection of S onto the V_p plane. We now show how to determine this projection and in effect the optimum weight vector.

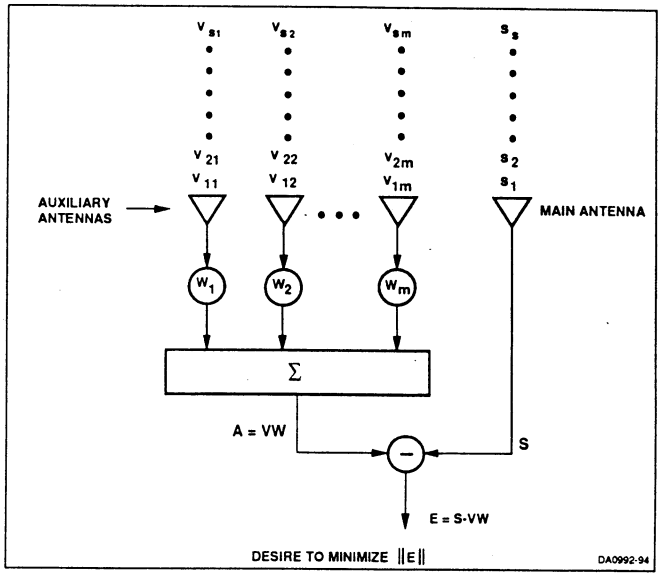

Figure 1-1. Sidelobe Canceller (SLC)

2) Projection Theory and Orthonormal Transformation

Assume we had two orthonormal unit vectors q_1 and q_2 in the plane V_p as indicated in Figure 2-1. The projection of S is simply obtained by projecting S onto q_1 and q_2 and then adding these projections. The magnitude of the projection of a vector S onto the unit vector q_i is given by the dot product of these vectors. Designate this magnitude as s_i'. Then

$$s_i' = q_i^T S \quad \text{for i=1 and 2} \tag{2-1}$$

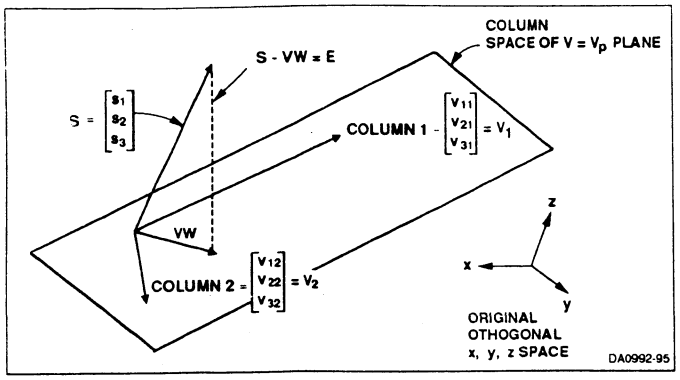

Figure 1-2. Three-Dimensional Space of Data Vectors (after Strang [20])

Hence the vector component of S along q_i is

$$p_i = s_i' q_i = (q_i^T S)\, q_i \tag{2-2}$$

Then the projection of S onto V_p is given by

$$p_v = s_1' q_1 + s_2' q_2.$$

$$= (q_1^T S)\, q_1 + (q_2^T S) q_2 \tag{2-3}$$

This projection vector gives the optimum VW so we replace W by W* to indicate that W is the optimum in that it minimizes (1-2) or equivalently (1-4).

Note that by picking a unit vector q_3 perpendicular to both q_1 and q_2 we form a new orthogonal 3-dimensional coordinate system different from the original x, y, z system; see Figure 2-1. Note that s_1' and s_2' represent respectively the q_1 and q_2 coordinates of S in this new coordinate system. Let s_3' be the third coordinate of S. It is given by

$$s_3' = q_3^T S \tag{2-4}$$

Let the vector S when represented in the q_1, q_2, q_3 coordinate system be called S'. Then

$$S' = [s_1' \;\; s_2' \;\; s_3']^T \tag{2-5}$$

and from (2-1) and (2-4) we see that

$$S' = Q^T S \tag{2-6}$$

where

$$Q^T = [q_1 \;\; q_2 \;\; q_3]^T \tag{2-6a}$$

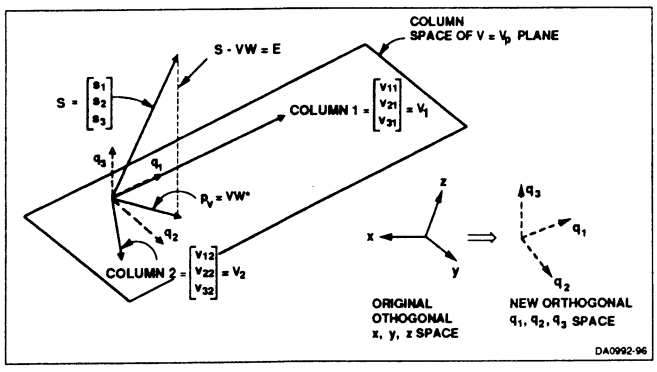

Figure 2-1. Projection onto V_p Plane

In the original x, y, z coordinate system the unit vectors along x, y, z are designated as i, j, k and represented in matrix form by

$$i = \begin{bmatrix}1\\0\\0\end{bmatrix} \quad j = \begin{bmatrix}0\\1\\0\end{bmatrix} \quad k = \begin{bmatrix}0\\0\\1\end{bmatrix} \tag{2-7}$$

In the original coordinate system

$$q_i = [q_{1i} \;\; q_{2i} \;\; q_{3i}]^T, \; i=1,2,3 \tag{2-8}$$

From (2-6) we see that premultiplying the vector S by Q^T transforms S from a vector expressed in the x, y, z coordinate system to the q_1, q_2, q_3 coordinate system. This is true for any vector.

For convenience replace Q^T by the matrix F, i.e., let

$$F = Q^T \tag{2-9}$$

Then

$$S' = FS \tag{2-10}$$

Because the q_i are orthonormal vectors it follows that

$$F^T F = F F^T = I \tag{2-11}$$

and

$$F^T = F^{-1} \tag{2-12}$$

A matrix satisfying (2-11) and (2-12) is called an orthonormal transformation matrix.

It now remains to show how we select the orthonormal unit vectors q_1 and q_2 and in turn q_3.

3) On Finding A New Orthonormal Coordinate System - Classical Gram-Schmidt (CGS) Orthogonalization

How do we pick q_1, q_2, q_3? We pick the unit vector q_1 to lie along v_1 and then pick q_2 to be perpendicular to q_1 but in the plane V_p. The unit vector q_3 is finally picked to be orthogonal to q_1 and q_2. This procedure amounts to a Gram-Schmidt orthogonalization of the augmented matrix V_o obtained by adding the column vector S to V. Thus

$$V_o = [v_1 \;\; v_2 \;\; v_3] \tag{3-1}$$

where v_3 is the column vector S. Carrying out a Gram-Schmidt orthogonalization of the column vectors of V_o to produce the column vectors q_1', q_2', q_3' and then normalizing these vectors to unity produces the desired unitary orthogonal vectors q_1, q_2, q_3 for the columns. We shall now carry out this orthogonalization.

First we pick q_1' to equal v_1, i.e.,

$$q_1' = v_1 \tag{3-2}$$

Next q_2' is picked perpendicular to q_1', but in the V_p plane, by setting it equal to v_2 minus its component parallel to v_1, the latter being the projection of v_2 onto q_1, which in turn is q_1' normalized to unity. Thus

$$q_2' = v_2 - r_{12}' q_1' \tag{3-3}$$

where

$$r'_{12} = \frac{q'^T_1 v_2}{q'^T_1 q'_1} \tag{3-4}$$

Finally q'_3 is picked to equal v_3 minus its components parallel to q'_1 and q'_2, i.e.,

$$q'_3 = v_3 - r'_{13}\, q'_1 - r'_{23}\, q'_2 \tag{3-5}$$

where

$$r'_{13} = \frac{q'^T_1 v_3}{q'^T_1 q'_1} \tag{3-6}$$

$$r'_{23} = \frac{q'^T_2 v_3}{q'^T_2 q'_2} \tag{3-7}$$

The desired unitary vectors q_1, q_2, q_3 are obtained from q'_1, q'_2, q'_3 by normalizing. Thus

$$q_i = q'_i / \|q'_i\| \tag{3-8}$$

Having obtained q_1, q_2, q_3 gives the matrix Q and in turn the orthonormal matrix F; see (2-9).

From the above expressions for q'_i it follows that

$$v_1 = \quad q'_1 \tag{3-9a}$$

$$v_2 = r'_{12}\, q'_1 + \quad q'_2 \tag{3-9b}$$

$$v_3 = r'_{13}\, q'_1 + r'_{23}\, q'_2 + q'_3 \tag{3-9c}$$

It readily follows that in terms of q_1, q_2, q_3 (3-9a to 3-9c) become

$$v_1 = u_{11}\, q_1 + 0 \cdot \quad q_2 \quad + 0 \cdot \quad q_3 \tag{3-10a}$$

$$v_2 = u_{12}\, q_1 + u_{22}\, q_2 \quad + 0 \cdot \quad q_3 \tag{3-10b}$$

$$v_3 = u_{13}\, q_1 + u_{23}\, q_2 \quad + u_{33}\, q_3 \tag{3-10c}$$

where

$$u_{ij} = r'_{ij}\, \|q'_i\| \quad \text{for } i<j \tag{3-10d}$$

$$u_{ii} = \|q'_i\| \tag{3-10e}$$

Physically the values of u_{ij} are the amplitudes of the unit vectors q_1, q_2, q_3 into which v_j is composed in the new coordinate system.

We will now apply F to the vectors of (1-1) and in so doing transform (1-1) into a simpler set of equations from which the optimum weight vector W* can easily be obtained. In Section 2 we pointed out that applying the orthonormal transformation F to any vector S in the x, y, z coordinate system gives us S expressed in the q_1, q_2, q_3 coordinate system. From (3-10a to 10d) we see that v_1, v_2 and v_3 expressed in the q_1, q_2, q_3 space are given by

$$Fv_1 = \begin{bmatrix} u_{11} \\ 0 \\ 0 \end{bmatrix} \quad Fv_2 = \begin{bmatrix} u_{12} \\ u_{22} \\ 0 \end{bmatrix} \quad Fv_3 = \begin{bmatrix} u_{13} \\ u_{23} \\ u_{33} \end{bmatrix} \tag{3-11}$$

But $v_3 = S$, hence we also have from (2-10)

$$Fv_3 = FS = S' = \begin{bmatrix} s'_1 \\ s'_2 \\ s'_3 \end{bmatrix} \tag{3-12}$$

so that $s'_i = u_{i3}$. Let

$$FE = E' = \begin{bmatrix} \varepsilon'_1 \\ \varepsilon'_2 \\ \varepsilon'_3 \end{bmatrix} \tag{3-13}$$

Applying F to (1-1) and using (3-11 to -13), yields

$$\begin{bmatrix} \varepsilon'_1 \\ \varepsilon'_2 \\ \varepsilon'_3 \end{bmatrix} = \begin{bmatrix} s'_1 \\ s'_2 \\ s'_3 \end{bmatrix} - \begin{bmatrix} u_{11} & u_{12} \\ 0 & u_{22} \\ 0 & 0 \end{bmatrix} \begin{bmatrix} w_1 \\ w_2 \end{bmatrix} \tag{3-14}$$

Writing this out yields

$$\varepsilon'_1 = -u_{11}\, w_1 - u_{12}\, w'_2 + s'_1 \tag{3-15a}$$

$$\varepsilon'_2 = \quad 0 \quad - u_{22}\, w'_2 + s'_2 \tag{3-15b}$$

$$\varepsilon'_3 = \quad 0 \quad - \quad 0 \quad + s'_3 \tag{3-15c}$$

The optimum W is obtained when $\|E\|$ is minimized in (1-1a). We now show that this is equivalent to minimizing the transformed E, i.e., $E' = FE$ because, as expected, the Euclidean norm of E is not changed by the transformation F. From (1-4) and (2-11)

$$\|E'\| = \|FE\|^2 = (FE)^T FE = EF^T FE = \|E\| \tag{3-16}$$

as we desired to show. Hence minimizing $\|E\|^2$ is equivalent to minimizing $\|E'\|^2$ given by

$$\|E'\|^2 = \varepsilon'^2_1 + \varepsilon'^2_2 + \varepsilon'^2_3 \tag{3-17}$$

But ε'^2_3 is equal to s'^2_3 which is dependent on the S and is not variable, i.e., it is a constant. Thus only ε'_1 and ε'_2 are at our control and the optimum W is obtained by minimizing

$$\varepsilon'^2_1 + \varepsilon'^2_2$$

Only the top two equations of (3-15), (3-15a) and (3-15b), contain ε'_1 and ε'_2 and enter into the determination of W. Because we now have only two equations with only two unknowns w_1 and w_2 to solve for, ε'_1 and ε'_2 can be forced to be zero. When doing this we get

$$s'_1 = u_{11} w^*_1 + u_{12} w^*_2 \tag{3-18a}$$

$$s'_2 = \quad u_{22} w^*_2 \tag{3-18b}$$

where we have replaced w_1 and w_2 by their least-squares estimate values w^*_1 and w^*_2, because the solution of (3-18a and 3-18b) gives us our desired least-squares solution. Since (3-18a and 3-18b) consists of two equations with only two unknowns it can be solved easily for w^*_1 and w^*_2. This is in contrast to (1-1) which is overdeterministic; it consisting of two unknowns, w_1 and w_2, and three equations. What we want to call attention to is that (3-18a and 3-18b) are in the very convenient Gauss elimination form. The bottom equation only contains the unknown w^*_2, the next upper equation, the top one in this

case, w_2^* and w_1^*. Hence we solve the bottom equation easily for w_2^* and then use the next upper equation to find w_1^*. Although the above Gauss elimination form was obtained for the case where we had only two auxiliary antennas (m=2) with weights w_1 and w_2 to determine, the Gauss elimination form is obtained for the general case where we have m auxiliaries and obtain m equations for (3-18). Having (3-18) in the Gauss elimination form in the general case avoids the need to do a matrix inversion to solve for W*.

Equations (3-18a and 3-18b) in matrix form becomes

$$(S_1')= UW^* \tag{3-19}$$

where

$$S_1' = \begin{bmatrix} s_1' \\ s_2' \end{bmatrix} \quad W^* = \begin{bmatrix} w_1^* \\ w_2^* \end{bmatrix} \tag{3-20}$$

and U is the upper triangular matrix

$$U = \begin{bmatrix} u_{11} & u_{12} \\ 0 & u_{22} \end{bmatrix} \tag{3-21}$$

If (3-19) were not in the Gauss elimination form, it would be solved by multiplying both sides by the inverse of U to obtain

$$W^* = U^{-1}(S_1') \tag{3-22}$$

It is no accident that (3-18) is in the Gauss elimination form. This results directly from the application of the Gram-Schmidt orthogonalization to column vectors of V_0 of (3-1). This causes the matrix

$$FV_0 = U_0 \tag{3-23}$$

where the columns of U_0 are given by the column vectors of (3-11), to be upper triangular and hence in turn cause U to be upper triangular. This is true for the general case of m auxiliary antennas in Fig. 1-1

The above procedure for obtaining W* using the Gram-Schmidt orthogonalization procedure is referred to as the voltage-processing procedure or square-root procedure [1, 2]. This procedure is less sensitive to computer round-off errors than what is called the power method. With the power method procedure W* is obtained using the equation [3-7].

$$W^* = \hat{M}^{-1}\hat{\rho} \tag{3-24}$$

where $\hat{M}$ is the estimate of the spatial covariance matrix M of the voltages v_{ij} across the array and $\hat{\rho}$ is an estimate of the cross correlation ρ between the main antenna output s_i and the auxiliary channel outputs v_{ij}. (Explicit expressions for $\hat{M}$ and $\hat{\rho}$ are given in Section 8.) The use of (3-24) is called the power method because the elements of $\hat{M}$ are obtained by averaging the product of the voltages v_{ij} to yield power terms; to be shown in Section 8. The voltage-processing method only involves additions and subtractions of voltage terms and does not involve power term calculations. It is this difference that makes the voltage-processing method less sensitive to computer round-off errors. As a result of this difference the computer dynamic range required for the power method is larger. For example, if the range of voltages is 1 to 10^4 for the voltage method it will be 1 to $(10^4)^2 = 10^8$ for the power method. Hence more bits are required in the computer computation when using the power method. Fortunately more bits are becoming available at a lower cost with future computers.

4) Modified Gram-Schmidt (MGS) Orthogonalization

There is an improvement of the Gram-Schmidt orthogonalization voltage-processing method that makes it still less sensitive to computer round-off errors. This is the Modified Gram-Schmidt (MGS) orthogonalization procedure. For both the CGS and MGS orthogalization procedures q_3' is formed from v_3 by subtracting from it the components of v_3 parallel to q_1 and q_2. The difference between the CGS and MGS methods arises in how the component of v_3 parallel to q_2 is calculated. For the CGS method the magnitude of the projection of v_3 onto q_2 is calculated; see (3-7). For the MGS method instead of projecting v_3 onto q_2, v_3 without the component parallel to q_1, designated as $v_3^{(2)}$ and equal to $v_3 - (v_3^T q_1)q_1$, is projected onto q_2. Physically this gives the same q_3, if there were no computer round-off error. But because of round-off errors the MGS orthonormalization procedure is more accurate. The reason for this is that $v_3^{(2)}$ is smaller than v_3 and hence using $v_3^{(2)}$ in the computation in place of v_3 leads to a more accurate answer [8]. The above described difference between the CGS and MGS methods applies for the general case of arbitrary m and s. For the general case, to calculate the component of v_j parallel to q_i ($j > i$), $v_j^{(i)}$ is used instead of v_j where $v_j^{(i)}$ is v_j with the components parallel to q_1 to q_{i-1} removed. These components are removed sequentially — first q_1 is removed from v_j to form $v_j^{(2)}$, then q_2 from $v_j^{(2)}$ to form $v_j^{(3)}$, etc.; see Reference 9.

5) The Givens Orthonormalization Procedure

The Givens orthonormalization procedure is like the standard step-by-step Gauss elimination procedure. With the standard Gauss elimination procedure we operate on two equations of (1-1) at a time to eliminate one term at a time until finally we have the Gauss elimination form. This is equivalent to working with the augmented matrix V_0 to achieve an upper triangular form, only two rows being processed at any one time or step. Three steps are needed to triangularize our 3x3 V_0 as indicated below:

$$V_0 = \begin{bmatrix} X & X & X \\ X & X & X \\ X & X & X \end{bmatrix} \xrightarrow{1} \begin{bmatrix} X & X & X \\ O & X & X \\ X & X & X \end{bmatrix} \xrightarrow{2} \begin{bmatrix} X & X & X \\ O & X & X \\ O & X & X \end{bmatrix} \xrightarrow{3} \begin{bmatrix} X & X & X \\ O & X & X \\ O & O & X \end{bmatrix} \tag{5-1}$$

The difference between the Givens method from the standard Gauss elimination procedure is that with the former the Euclidean norm for the columns of transformed V_0's are unchanged after each transformation of the V_0 matrix. Doing this has the advantage of making the computations less sensitive to computer round-off errors [10].

The process of going from one transformed V_0 form to the next in (5-1) above can be thought of as resulting from a change in the 3-dimensional coordinate system. The ith transformation is achieved by premultiplying the ith V_0 by a Givens orthonormal transformation G_i. The orthonormal transformation F of (2-9) is obtained after all three Givens transformations have been carried out, i.e.,

$$F = G_3\, G_2\, G_1 \tag{5-2}$$

The first Givens transformation G_1 is expressed by

$$G_1 = \begin{bmatrix} c_1 & s_1 & 0 \\ -s_1 & c_1 & 0 \\ 0 & 0 & 1 \end{bmatrix} \tag{5-3}$$

where

$$c_1 = \cos\theta_1 = v_{11}/(v_{11}^2 + v_{21}^2)^{1/2} \quad (5\text{-}3a)$$

$$s_1 = \sin\theta_1 = v_{21}/(v_{11}^2 + v_{21}^2)^{1/2} \quad (5\text{-}3b)$$

The Givens G_1 transformation transforms the columns expressed in the original x, y, z coordinate system to a coordinate system in which only two coordinates of x, y, z are altered, those of x, y, with z being left unchanged. Specifically, the new x coordinate, call it x_1, is arranged to line up with the vector formed by the x and y components of v_1, while the new y_1, coordinate, call it y_1, is chosen to be perpendicular to these two components but in the plane of the original x, y coordinates. Doing this forces the second coordinate of the transformed v_1, to be zero as indicated in (5-1). The other Givens transformations likewise only alter two coordinates at a time with the final coordinates x_3, y_3 and z_3, being actually our former coordinates q_1, q_2, q_3; see Ref. [9].

The Givens transformation can be carried out using a systolic array as shown in Figure 5-1 for arbitrary [11]. The circular boxes determine the rotation θ_1 to be done by the ith Givens transformation, see (5-3 to 3b), while the square boxes perform these rotations. The CORDIC algorithm can be used to carry out these trignometric operations. Rader [12] of Lincoln Laboratory has implemented such a systolic array for the case of 63 auxiliary elements, i.e., m=63. The processor can fit in a compact disc size package requiring only 20W and performing 2000 MROPS [12,13].

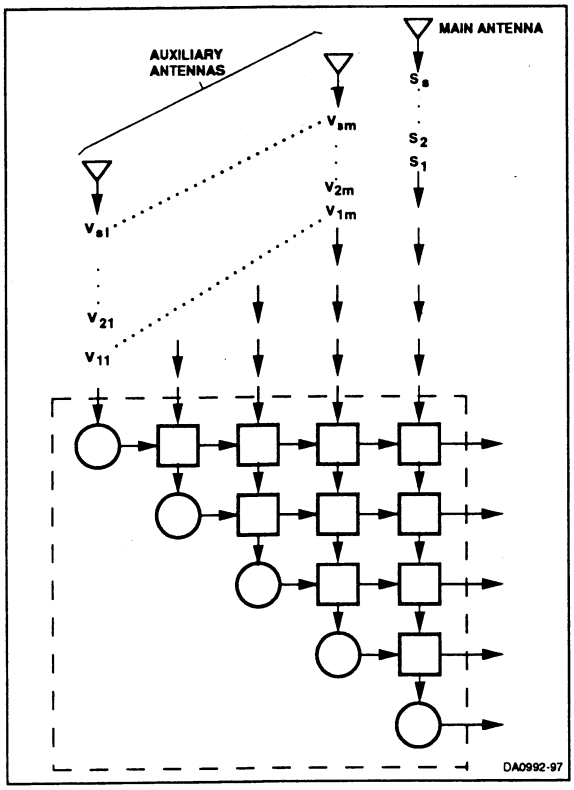

Figure 5-1. Systolic Array Implementation of Givens Transformations for SLC

6) The Householder Orthonormalization Procedure

The Householder orthonormalization achieves the triangularization of V_0 with a number of Householder orthonormal transformations. Here two transformations H_i are needed with the V_0 taking the following forms after each transformation:

$$V_0 = \begin{bmatrix} X & X & X \\ X & X & X \\ X & X & X \end{bmatrix} \xrightarrow{1} \begin{bmatrix} X & X & X \\ O & X & X \\ O & X & X \end{bmatrix} \xrightarrow{2} \begin{bmatrix} X & X & X \\ O & X & X \\ O & O & X \end{bmatrix} \quad (6\text{-}1)$$

We see that the Housholder transformation does with one transformation H_1 what the Givens did with two, G_1 and G_2, at the first step. Specifically,

$$H_1 = G_2 G_1 \quad (6\text{-}2)$$

H_2 is equal to G_3. For the general case of arbitrary m and s, the ith Householder transformation zeros out all the elements of V_0 below the ith column diagonal element. The Householder transformation H_1 is actually not obtained using (6-2). Instead, what is called a reflection transformation is used. How the Householder reflection transformation is obtained is illustrated in Figure 6-1.

The Householder transformation can not be implemented using a systolic array. It requires a general purpose processor. However, it requires fewer computations as shall be indicated later.

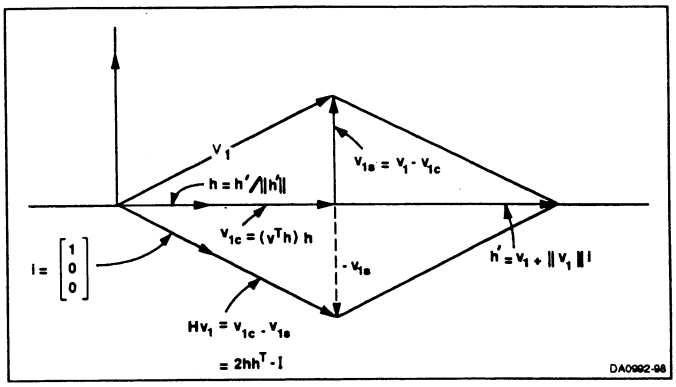

Figure 6-1. Householder Reflection Transformation H

7) Application of Orthonormal Transformation to Fully Adaptive Arrays

The above orthonormal transformations can be applied to the fully adaptive array problem of Figure 7-1. One way is to transform the fully adaptive array problem to the sidelobe canceller problem of Figure 1-1. There are two methods to do this. The first method is to apply the McWhirter preprocessor [1] to transform the fully adaptive array problem to the sidelobe canceller problem. The preprocessor and the resulting sidelobe canceller are shown in Figure 7-2.

The second method is to go to beam space by the use of a beamformer which for an M + 1 element array forms M + 1 beams, beams in all directions. One of the beams points in the target direction and becomes the sidelobe canceller main beam. The other m beams become the auxiliary beams. Actually it is not necessary to use all the m auxiliary beams. Only the auxiliary beams which have jammers, or other interference, need be used. This reduces the computation complexity enormously. It also reduces the transient time for the array adaption [14]. The use of beam space without using all the auxiliary beams has been referred to as adaptive-adaptive array processing [14].

The above orthgonal transformations can also be used to orthogonalize the signals of the different elements of the array of Figure 7-1 [15, 16]. This also can provide an improvement of the transient response of a fully adaptive array.

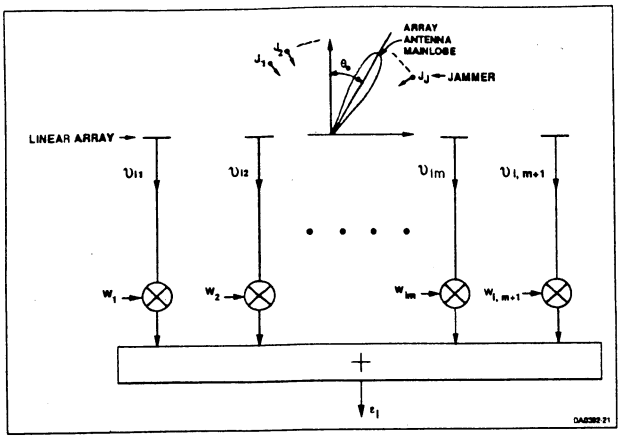

Figure 7-1. Fully Adaptive Phased Array

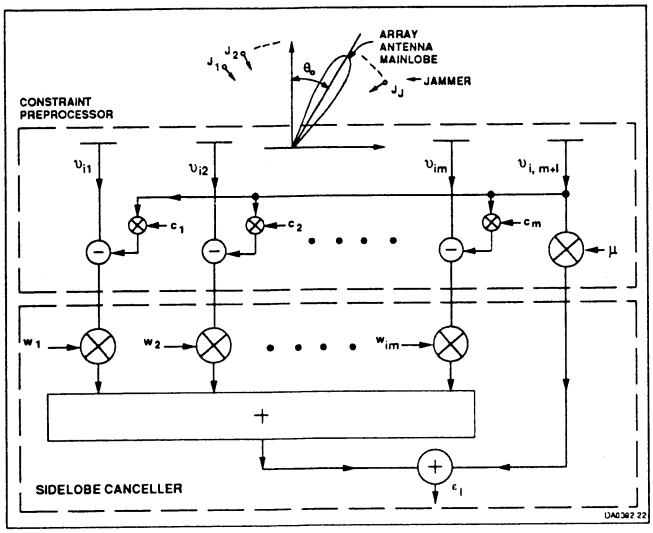

Figure 7-2. Transformation of Fully Adaptive Array to Sidelobe Canceller

8) Application of Orthogonal Transformations to Tracking Problems.

Assume a radar which is tracking a target only in range. You have heard of flatland -- well this is linland, one-dimensional space, range only. Let x_n be the target range at time n. Let $\dot{x}_n$ be the target velocity at time n, i.e., the derivative of x_n with respect to time. Assume we are only measuring the target range, not its Doppler velocity. Let the measurement of the target range at time n be y_n. Assume measurements are made at times n=1 to n as shown in Figure 8-1 for n=6. For the radar tracking problem we are trying to obtain a best estimate of the target position and velocity at time n based on the n measurements made up to and including that at time n. Designate the estimate of the position and velocity at time n as, respectively, x_n^* and $\dot{x}_n^*$. These estimates are used to estimate where the target will be in the future. This information is needed in commercial air traffic control radars to avoid collision and in military radars for target interception.

Assume the target has a constant velocity. This implies that the target trajectory is given by a straight line in Figure 8-1. The estimate of the target position and velocity at any time i can be expressed in terms of its values at time n using the following equation for a constant velocity target

$$x_i^* = \dot{x}_n^* - (n-i)\,T\,\dot{x}_n^* \qquad (8\text{-}1)$$

where T is the time between measurements. What we are looking for is the best fitting straight trajectory to the data in Figure 8-1. The least squares fitting line is that for which the sum of the squared deviations $y_i - x_i^*$ is minimized. Stated mathematically, it is that line for which the following sum of the squared errors

$$e_n = \sum_{i=1}^{n} (y_i - x_i^*)^2 \qquad (8\text{-}2)$$

is minimized. Let

$$\epsilon_i = y_i - x_i^* \qquad (8\text{-}3)$$

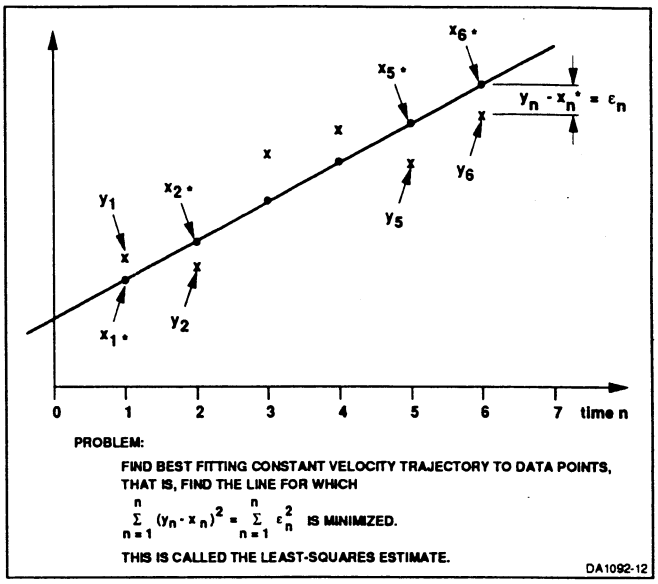

Figure 8-1. Least-Squares Tracking Filter Problem

Substituting (8-1) into (8-3) yields

$$\epsilon_i = y_i - x_n^* + (n-i)\,T\dot{x}_n^* \qquad (8\text{-}4)$$

Assume n=3. Writing (8-4) in matrix form for i=1 to 3 yields

$$\begin{bmatrix} \epsilon_1 \\ \epsilon_2 \\ \epsilon_3 \end{bmatrix} = \begin{bmatrix} y_1 \\ y_2 \\ y_3 \end{bmatrix} - \begin{bmatrix} 1 & -2T \\ 1 & -T \\ 1 & 0 \end{bmatrix} \begin{bmatrix} x_3^* \\ \dot{x}_3^* \end{bmatrix} \qquad (8\text{-}5)$$

or

$$E = Y - T_t\,X_n^* \qquad (8\text{-}5a)$$

where

$$E = \begin{bmatrix} \epsilon_1 \\ \epsilon_2 \\ \epsilon_3 \end{bmatrix} \quad Y = \begin{bmatrix} y_1 \\ y_2 \\ y_3 \end{bmatrix} \quad X_n^* = \begin{bmatrix} x_n^* \\ \dot{x}_n^* \end{bmatrix} \qquad (8\text{-}5b)$$

$$T_t = \begin{bmatrix} 1 & -2T \\ 1 & -T \\ 1 & 0 \end{bmatrix} \qquad (8\text{-}5c)$$

Comparing (8-5) and (8-5a) with (1-1) and (1-1a) we see that they are identical. Hence the least-squares estimate problem being considered here is identical to the sidelobe cancelling problem of Section 1. For both cases we are trying to minimize $\|E\|^2$. Here Y, X_n^* and T_t replace, respectively, S, W and V. Hence, all the orthonormal transformations results applied to the sidelobe canceller problem can be applied to obtain the solution of the least-squares tracking problem. One difference that exists is that T_t is not composed of random entries. As a consequence, T_t is known in advance in many situations and can be triangularized off-line in advance. However, the appropriate triangularization operations still have to be applied to Y to obtain the least-squares solution.

The use of the above orthonormal transformation gives us the voltage-processing solutions to the least-squares tracking problem. There is also a power method solution equivalent to (3-24) for the sidelobe canceller problem. This solution is obtained by writing (8-2) as

$$e_n = \sum_{i=1}^{n} (y_i - x_i^*)^2 = \|E\|^2 = E^T E = (Y - T_t X_n^*)^T (Y - T_t X_n^*) \tag{8-6}$$

where use was made of (8-3) and (8-5b). Equation (8-6) is equivalent to (1-4) obtained for the sidelobe canceller problem. Differentiating (8-6) with respect to X_n^* and setting the result equal to zero yields

$$\frac{de_n}{dX_n^*} = T_t^T (Y - T_t X_n^*) = 0 \tag{8-7}$$

or

$$T_t^T T_t X_n^* = T_t^T Y \tag{8-7a}$$

The above is known as the normal equal solution to the least-squares problem. Solving for X_n^* yields

$$X_n^* = (T_t^T T_t)^{-1} T_t^T Y \tag{8-8}$$

For the sidelobe canceller problem on replacing X_n, T_t and Y by respectively W^*, V and S, we get for (8-8)

$$W^* = (V^H V)^{-1} V^H S \tag{8-9}$$

where T has been replaced by H indicating Hermitian transposition, i.e., the complex conjugate of the transpose of the matrix. H is needed in place of T because the matrices V and S have complex entries.

On comparing (8-9) with (3-24) we find that

$$\hat{M} = \frac{1}{s} V^H V \tag{8-10a}$$

$$\hat{\rho} = \frac{1}{s} V^H S \tag{8-10b}$$

Division by the factor s is needed to have (8-10a and -10b) physically be estimates of the entries of M and ρ.

The least-squares filter described above for a constant velocity target is identical to the well known g-h filter (also known as the α-β filter). The least-squares g-h filter equations are given by the following simple recursive equations

$$\dot{x}_{n,n}^* = \dot{x}_{n,n-1}^* + h_n (y_n - x_{n,n-1}^*)/T \tag{8-11a}$$

$$x_{n,n}^* = x_{n,n-1}^* + g_n (y_n - x_{n,n-1}^*) \tag{8-11b}$$

where $x_{n,n}^*$ and $\dot{x}_{n,n}^*$ are the estimates of the target range and velocity, respectively, at time n (the first subscript) based on the measurements made up to and including time n (the second subscript) and $x_{n,n-1}^*$ and $\dot{x}_{n,n-1}^*$ are the predicted position and velocity estimates at time n (the first subscript) based on the measurements made up to and including time n-1 (the second subscript). The first subscript indicates for what time the range or velocity estimate applies, the second subscript indicates the last time a measurement was made that contributed to this estimate. For the least-squares filter (also called the growing-memory or expanding-memory filter)

$$g_n = \frac{2(2n+1)}{(n+2)(n+1)} \tag{8-12a}$$

$$h_n = \frac{6}{(n+2)(n+1)} \tag{8-12b}$$

where n is the number of measurements made, which we here assumed to go from time n=1 to n=n. (Note that the variable s was used in Section 1 for the number of measurements. We shifted to n here because that is the variable often used in the literature for the tracking problem.)

The above growing-memory filter is used for track initiation. In steady state the discounted least-squares filter, or similar filter, is used. For this filter the old errors ϵ_i of (8-3) are not weighted as much in the sum of errors expression given by (8-2) or (8-6). Specifically, the weighted sum to be minimized in the following semi-infinite sum

$$e_n = \theta^0 (y_n - x_n^*)^2 + \theta^1 (y_{n-1} - x_{n-1}^*)^2 + \theta^2 (y_{n-2} - x_{n-2}^*)^2 + \ldots \tag{8-13}$$

where $0 \le \theta \le 1$. Here g_n and h_n are constants given by

$$g = 1 - \theta^2 \tag{8-14a}$$

$$h = (1-\theta)^2 \tag{8-14b}$$

9) Gauss and the Least-Squares Filter.

Gauss in developing his least-squares filter took into account the possibility that the measurements y_n may have different variances. Let σ_n^2 be the variance of y_n. Gauss then went one step better than to find the x_n^* that minimizes (8-6). Instead he minimized a weighted sum of the errors with the weighting being done according to the importance of a measurement, ϵ_i for an accurate y_i measurement being given more weight. Specifically he found the X_n^* which minimized

$$e_n = (Y - T_t X_n^*)^T R_d^{-1} (Y - T_t X_n^*) \tag{8-15}$$

where R_d is the diagonal matrix

$$R_d = \text{Diag}\,[\sigma_1^2, \sigma_2^2, \ldots, \sigma_n^2] \tag{8-15a}$$

Gauss did this work at the ripe old age of 19 in 1795 while still a teenager. They do not grow teenagers like they used to!

If the errors in the measurements y_n are correlated, then to obtain the optimum X_n^* the following should be minimized

$$e_n = (Y - T_t X_n^*)^T R^{-1} (Y - T_t X_n^*) \tag{8-16}$$

where R is the nondiagonal covariance matrix of the y_n measurements. Aitken suggested the minimization of (8-16) in 1934 [17]. The estimate obtained by minimizing (8-16) is called the minimum variance estimate [18]. It can be easily obtained by differentiating (8-16) with respect to X_n^*, setting the result to zero and then solving for X_n^*.

10) Comparison of Various Least-Squares Algorithms

Table 10-1 compares the computational complexity of the various algorithms for the case where T_t is real. The normal equations (power method) require the fewest computations but puts the greatest accuracy requirements on the computer. With 32 and 64 floating point processors becoming more available at lower cost this will be less of a problem in the future. However, where a high throughput is needed, the systolic architecture offered by the Givens approach may be preferred.

Table 10-1. OPERATION COUNTS FOR VARIOUS LEAST SQUARES COMPUTATIONAL METHODS[19]

Method	Asymptotic Number of Operations Where an Operation Is a Multiply or Divide Plus and Add		
Normal Equations (Power Method)	$nm^2/2$	+	$m^3/6$
Householder Othogonalization	nm^2	--	$m^3/3$
Modified Gram-Schmidt	nm^2		
Givens Othogonalization	$2nm^2$	--	$2m^3/3$

11) Acknowledge

The material given here is extracted from a copyrighted book being prepared by the author [9].

References

[1] Hargrave, C. R., J.G. McWhirter, and C. R. Ward, "A Novel Algorithm and Architecture for Adaptive Digital Beamforming," IEEE Transactions on Antennas and Propogation, vol. AP-34, no. 3, 1986, pp 338-346.

[2] Bierman, G.J., "Factorization Methods for Discrete Sequential Esimation," Academic Press, Inc., 1977.

[3] Monzingo, R. A. and Miller, T.W., "Introduction to Adapative Arrays," John Wiley and Sons, New York, 1980.

[4] Farina, A., "Antenna-Based Signal Processing Techniques for Radar Systems," Artech House, Norwood, MA 1992.

[5] McWhirter, J.G., "Adaptive Antenna Array Signal Processing," in Tutorial Seminar on "Adaptive Radar Processing," sponsored by IEEE, October, 22-23, 1987.

[6] Nitzberg, R., "Adaptive Signal Processing," Artech House, Norwood, MA 1992.

[7] Brookner, E., "Sidelobe Cancelling and Adaptive Array Processing," in Tutoral Seminar on "Adaptive Radar Processing," sponsored by IEEE, October 22-23, 1987.

[8] Lawson, C.L. and R.J. Hanson, "Solving Least-Squares Problems," Prentice Hall, Inc., 1974.

[9] Brookner, Eli, "Tracking and Kalman Filters as Friends," to be published.

[10] Charles Rader, Lincoln Laboratory, Private Communication

[11] Haykin, S., "Adaptive Filter Theory," Prentice-Hall, 2nd Edition, 1991.

[12] Rader, C.M., "Wafer-Scale Integration of a Large Systolic Array for Adaptive Nulling," Lincoln Laboratory Journal, Spring 1991, Vol. 4, No. 1, pp. 3-30.

[13] Rader, C. "MUSE. . . A Compact Architecture for Antenna Nulling computations," Adaptive Antenna Systems Symposium and Electronic Hardware and Software Exhibition, IEEE Long Island Section, November 19, 1992.

[14] Brookner, E. and J.M. Howell, "Adaptive-Adaptive Array Processing," Phased Arrays Symp. Proc., The Mitre Corp., Bedford, MA, October 15-18, 1985, pp. 133-146. See also: RADC Rep. No. RADC, Hanscom AFB, Bedford, MA, Air Force Systems Command, August 1985; IEEE Int. Conf. Radar-87, London, October 19-21, 1987; Proc. IEEE< Vol. 74.

[15] White, W. D., "Cascade Preprocessors for Adaptive Antennas," IEEE Trans. on Antennas and Propagation, Vol. AP-24, No. 5, Sept. 1976, pp. 670-684.

[16] Gabriel, W.F., "Adaptive Arrays - An Introduction," Proc. IEEE, Vol. 64, No. 2, February 1976, pp. 239-272.

[17] Aitken, A.C., "On Least-Squares and Linear Combinations of Observations," Proc. Roy. Soc. Edinb. A, 55, 42-7, 1934.

[18] Morrison, N., "Introduction to Sequential Smoothing and Prediction", McGraw-Hill Book Company, N.Y., N.Y., 1969.

[19] Golub, G.H. (1965), Numerical Methods for Solving Linear Least-Squares Problems, Num, Math 7, 206-216.

[20] Strang, G., "Linear Algebra and Its Applications," Academic Press, 1980.

(38a)

ADAPTIVEL CONTROL τ_o TO SPEED UP CLOSED-LOOP TRANSIENT TIME

(1) MEASURE JNR_a

(2) FOR $JNR_a = 30dB$ INSTEAD OF 40dB RESET τ_o USING (36-1):

$$\tau_o \geq \frac{10}{\pi B_s}\left[1 + \frac{G_o(1+JNR_a)}{G_L}\right] \qquad (1)$$

FOR $G_o = 1$, $JNR_a = 30dB$, $B_s = 5MHz$

$\tau_o \geq 638\mu s$

SET $\tau_o = 638\mu s$

THEN FROM (33-1)

$$\tau_L = \frac{\tau_o}{1+G_L} = 0.637\mu s \quad (2)$$

SAME AS WHEN $JNR_a = 40dB$; SEE (37).

(3) IN GENERAL FROM (2) AND (1) FOR $G_o = 1$:

$$\tau_L = \frac{10}{\pi B_s}\left(\frac{2+JNR_a}{1+JNR_a}\right) \doteq \frac{10}{\pi B_s} = 0.637\mu s$$

INDEPENDENT OF JNR_a. IF τ_o SET USING (1) FOR VARYING JNR_a.

(102 bq)

CORDIC SUBSYSTEM

(1 Of 96)

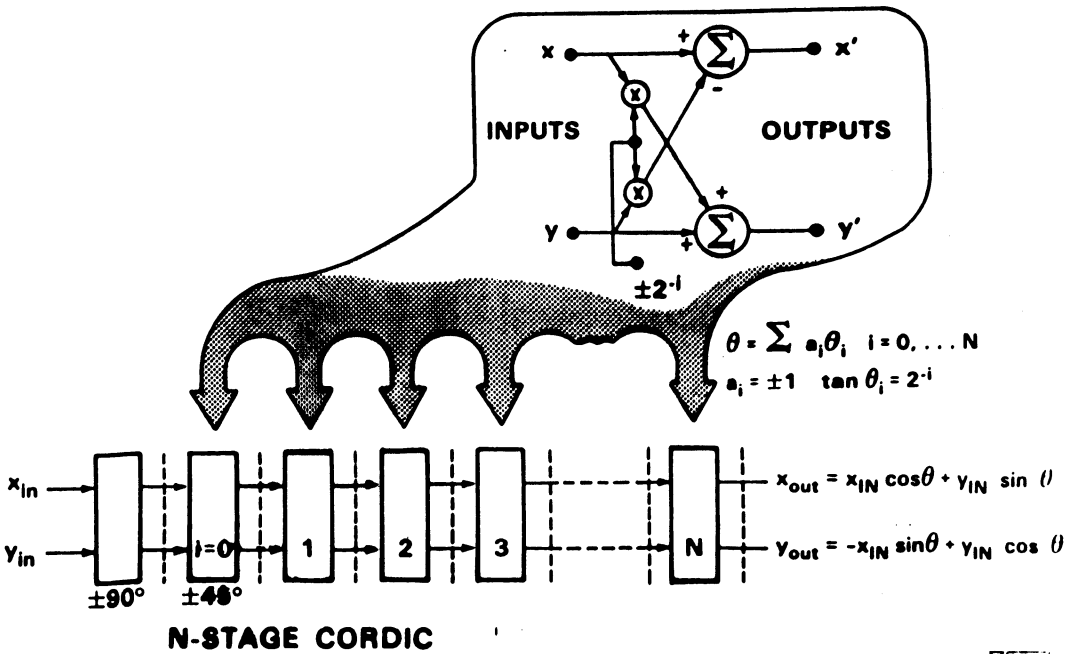

N-STAGE CORDIC

101777-2